

# City Research Online

## City St George's, University of London

**Citation:** South, R. (1973). An investigation of the structures of laminar diffusion flames. (Unpublished Doctoral thesis, The City University)

This is the accepted version of the paper.

This version of the publication may differ from the final published version. To cite this item please consult the publisher's version.

**Permanent repository link:** https://openaccess.city.ac.uk/id/eprint/38676/

**Copyright and Reuse:** Copyright and Moral Rights remain with the author(s) and/or copyright holders. Copies of full items can be used for personal research or study, educational, or not-for-profit purposes without prior permission or charge, unless otherwise indicated, provided that the authors, title and full bibliographic details are credited, a hyperlink and/or URL is given for the original metadata page and the content is not changed in any way. For full details of reuse please refer to City Research Online policy.

City Research Online: http://openaccess.city.ac.uk/ publications@citystgeorges.ac.uk

# AN INVESTIGATION OF THE STRUCTURES OF LAMINAR DIFFUSION FLAMES

by

ROBERT SOUTH

B.Sc. (LONDON), A.R.C.S.

A Thesis Submitted for the Degree of Doctor of Philosophy at the City University, London.

Department of Mechanical Engineering

March 1973

THE CITY UNIVERSITY LIBRARY,
ST. JOHN STREET, LONDON, E.C.1.

ACKNOWLEDGEMENTS

I should like to extend my sincere thanks to [redacted] for suggesting the problem and for his encouragement during the course of the work and to Mr. B.M. Hayward for his guidance and supervision throughout the duration of the project.

I should like to thank also [redacted] for assistance in part of the experimental aspects of part 1 of this thesis and my colleagues at Watson House for valuable discussion during the work.

The research presented in this thesis was carried out by permission of the Gas Council to whom I am indebted. In particular I should like to thank [redacted], Assistant Director, and [redacted], Research Manager, of Watson House for providing me with this opportunity.

[redacted]

Robert South

March 1973

CONTENTS

Part I.

FLAME STRUCTURE STUDY OF LAMINAR DIFFUSION FLAMES OF METHANE


| | | Page |
|---|---|---|
| 1.1. | INTRODUCTION | 3 |
| 1.2. | SURVEY OF PREVIOUS FLAME STUDIES | 8 |
| 1.2.1. | Diffusion Flames | 8 |
| 1.2.2. | Pre-mixed Flames | 19 |
| 1.3. | DETAILS OF APPARATUS AND EXPERIMENTAL PROCEDURES | 24 |
| 1.3.1. | Burner and Flow System | 25 |
| 1.3.2. | Measurement of Temperature Profiles | 27 |
| 1.3.3. | Measurement of Velocity Profiles | 32 |
| 1.3.4. | Measurement of Species Profiles | 35 |
| 1.4. | ANALYSIS OF EXPERIMENTAL DATA | 38 |
| 1.4.1. | Generalised Continuity Equation | 38 |
| 1.4.2. | Continuity of Species | 40 |
| 1.4.3. | Continuity of Heat Energy | 41 |
| 1.4.4. | Calculation of Transport Properties | 41 |
| 1.4.5. | Organisation of Programs for Computing Transport Properties and Fluxes | 48 |
| 1.4.6. | Estimation of Reaction Rates and Heat Release Rates | 52 |

| | | |
|---|---|---|
| 1.5. | RESULTS AND DISCUSSION | 54 |
| 1.5.1. | Temperature Profiles | 54 |
| 1.5.2. | Velocity Profiles | 56 |
| 1.5.3. | Species Profiles | 62 |
| 1.5.4. | Species Fluxes | 74 |
| 1.5.5. | Heat Energy Fluxes | 80 |
| 1.5.6. | Reaction Rates | 89 |
| 1.5.7. | Heat Release Rates | 92 |
| 1.5.8. | Accuracy of Results | 104 |
| 1.6. | CONCLUSIONS | 108 |

## Part II.

## OPTICAL STUDY OF LAMINAR DIFFUSION FLAMES OF METHANE


| | | Page |
|---|---|---|
| 2.1. | INTRODUCTION | 112 |
| 2.2. | OPTICAL METHODS OF MEASURING TEMPERATURE | 115 |
| 2.2.1. | Introduction | 115 |
| 2.2.2. | Radiation Thermometry Methods | 115 |
| 2.2.3. | Methods of Geometrical Optics | 118 |
| 2.2.4. | Methods of Physical Optics | 121 |
| 2.2.5. | Conclusions | 124 |
| 2.3. | DETAILS OF APPARATUS | 126 |
| 2.3.1. | Burner and Flow System | 128 |
| 2.4. | DEVELOPMENT OF AN INTERFEROMETRIC METHOD | 130 |
| 2.4.1. | Choice of Interferometer | 130 |
| 2.4.2. | Principle of Single Beam Interferometer | 133 |
| 2.4.3. | Construction of Interferometer | 136 |
| 2.4.4. | Experimental Procedure | 137 |
| 2.4.5. | Diffusion Flame Interferograms | 138 |

| | | |
|---|---|---|
| 2.5. | ANALYSIS OF A DIFFUSION FLAME INTERFEROGRAM | 140 |
| 2.5.1. | Existing Methods of Analysis | 140 |
| 2.5.2. | Extension to Existing Methods | 145 |
| 2.5.3. | Final Flame Temperature | 147 |
| 2.5.4. | Analysis Procedure | 154 |
| 2.5.5. | Organisation of Programs for Computing Refractivity and Final Flame Temperature | 156 |
| 2.5.6. | Assessment of Method of Analysis | 159 |
| 2.5.7. | Estimation of Conductive Heat Energy Fluxes and Heat Release Rates | 162 |
| 2.6. | RESULTS AND DISCUSSION | 164 |
| 2.6.1. | Diffusion Flame Interferograms | 164 |
| 2.6.2. | Temperature Profiles | 167 |
| 2.6.3. | Conductive Heat Energy Fluxes | 170 |
| 2.6.4. | Heat Release Rates | 172 |
| 2.7. | CONCLUSIONS | 176 |
| 2.8. | FUTURE WORK | 177 |
| REFERENCES | | 179 |

## NOMENCLATURE

| | |
|---|---|
| A | Lindsey Bromley coefficient |
| a | Polarizability |
| | Optical thickness |
| $a^*$ | Reduced polarizability |
| $C_i$ | Coefficient of Spline cubic |
| $C_p$ | True specific heat |
| $\overline{C_p}$ | Mean specific heat |
| d | Diameter of thermocouple bead |
| | Diameter of light beam |
| D | Multicomponent diffusion coefficient |
| $\mathscr{D}$ | Binary diffusion coefficient |
| eps | Force constant |
| $\underline{F}$ | Vector flux of a property |
| $\underline{F}_M$ | Species flux |
| $\underline{F}_H$ | Heat Energy flux |
| H | Relative humidity |
| K | Boltzmann's constant |
| k | Gladstone-Dale constant |
| m | Molecular weight |
| N | Molar density, Refractive index |
| n | Parameter denoting overlap of light beams |

| | |
|---|---|
| $P$ | Pressure |
| $P_v$ | Pressure of water vapour in air |
| $q$ | Rate of creation of a property or reaction rate |
| $Q$ | Volumetric heat release rate |
| $r$ | Radius |
| $R_o$ | Radius of Refractive index disturbance |
| $S$ | Sutherland constant |
| | Fringe shift |
| $T$ | Temperature |
| $T_b$ | Maximum flame temperature |
| $T_u$ | Temperature uncorrected for radiation losses |
| $T_w$ | Wire temperature |
| $V$ | Velocity |
| $W$ | Diameter of light beam |
| $w$ | Mass fraction |
| $X$ | Mole fraction |
| $\alpha$ | Degree of imperfection of a gas |
| $\beta$ | Angle of incidence |
| $\varrho$ | Density |
| $\eta$ | Viscosity |
| $\lambda$ | Thermal conductivity |
| | Vacuum wavelength of light |

| | |
|---|---|
| $\sigma_s$ | Stefan - Boltzmann constant |
| $\sigma$ | Force constant |
| $\mu$ | Dipole moment |
| $\mu^*$ | Reduced dipole moment |
| $f_{ij}$ | Collision number |
| $\Omega^{(1,1)*}$ | Collision integral of type (1,1) |
| $\omega$ | Reduced mass |
| $\epsilon$ | Emissivity of thermocouple coating |

Subscripts

| | |
|---|---|
| CND | Contribution due to thermal conduction |
| CNV | Contribution due to convection |
| DIF | Contribution due to molecular diffusion |
| TOT | Total Contribution |
| i,j,k | Component indices |
| n | Non-polar molecule |
| o | Subscript denoting ambient conditions |
| P | Polar molecule |
| | Spline boundary or knot |
| x,y,z | Cartesian co-ordinates |

# AN INVESTIGATION OF THE STRUCTURES OF LAMINAR DIFFUSION FLAMES


## SUMMARY

Flame structure analyses have been carried out on the stabilising region of two laminar diffusion flames of methane; one close to the blow-off limit and the second a stable flame for reference. The flames were formed on a slot-type burner to provide an effectively two-dimensional flame system. The experimental study involved the determination of sets of interrelated profiles - aerodynamic, thermal and compositional - using the techniques of stroboscopic particle-tracking, fine-wire thermocouple thermometry and micro-probe sampling followed by gas chromatographic analysis. The experimental data were combined with the conservation equations of species and heat energy to yield fluxes and rates of creation of material species and heat energy.

Results have shown that, for diffusion flames, the limiting rate of supply of oxidant into the stabilising region is governed, not by the mass flow, as in pre-mixed flames, by predominantly by diffusive flow across the stream tubes. Contrary to the recent suggestions of Robson and Wilson, and Bellis, the flame structure analyses carried out here strongly

suggest that the magnitude of velocity at the flame base is incidental to the phenomenon of flame lift, extinction being limited by chemical reaction rate and mass diffusion rather than by the bulk flow. A picture emerges of a maximum fuel consumption rate of the same order as that in a laminar stoichiometric premixed flame. Analysis of the thermal structure shows that the major proportion of the heat liberated in the reaction zone arises, in mathematical terms, from changes in the conduction flux profile which, in turn, depend primarily on changes in the temperature profile. In order to fully exploit this result an attempt is made to develop a sufficiently rapid and accurate method for measuring flame temperature.

It is shown that the technique of laser interferometry is capable of providing the resolution and precision compatible with the more conventional probe methods that are normally associated with flame structure studies. An extended spline fit technique has been successfully adapted for the quantitative interpretation of conical flame interferograms. Finally, the results offer encouragement that a method similar to the one described can provide a complete picture of the thermal structure (temperature, fluxes of heat energy and rates of heat release) of laminar diffusion flames.

# PART I

# FLAME STRUCTURE STUDY OF LAMINAR DIFFUSION FLAMES OF METHANE

## 1.1. INTRODUCTION

The discovery of natural gas in the North Sea has very rapidly led to its use directly as a fuel in both industrial and domestic appliances. This has necessitated the conversion of a wide range of equipment previously fuelled by town gas and the process of appliance conversion revealed a number of combustion problems. Several have been overcome, largely on an ad hoc basis, but many factors, governing the combustion of methane are not understood in any detail, especially those of flame stability. The reasons are not hard to see since even the simplest combustion problems are relatively complex involving simultaneous chemical reactions as well as aspects of convection, thermal conduction and molecular diffusion. Yet it is perhaps somewhat surprising to find that only comparatively recently has technology begun to provide a quantitative understanding of the process of combustion - a process which man has utilised as a basic source of energy for some tens of thousands of years.

Early attempts to determine stability mechanisms of laminar flames were confined almost exclusively to carrying out macroscopic measurements under a wide variety of flame conditions. These measurements largely centred on the conventional flame stability limits (blow-off and flash-back) and although they provided some insight into the reasons for the instability of flames of stoichiometric, fuel-lean, or fuel-rich mixtures burning in an inert atmosphere, they contributed relatively little to the understanding of the stability mechanisms of fuel-rich flames in which there is a secondary combustion surface.

In the last twenty years or so not only has our understanding of the individual physical processes pertaining to flames improved but also dramatic improvements in experimental and computational techniques have rendered accessible the field of microscopic flame structure, a field which had previously remained unexplored. Despite these improvements in microscopic technology, many of the recent studies have been applied only to one-dimensional and relatively thick flame systems. These simplifications make it easier to achieve the necessary degree of experimental precision, reduce unwanted disturbances by probes to a

minimum and decrease both the number and density of measurements and computations that are otherwise necessary. Only very recently has it been adequately demonstrated that the methods of microscopic flame-structure can provide worthwhile additions to our knowledge and understanding of flames more closely related to those encountered in practice.

The work presented in this thesis embodies a microscopic examination of the structures of laminar flames closely related to those encountered in practice. The investigation has been confined to flames of initially separated reactants, i.e. diffusion flames, since for these flames the stabilising mechanism is not well established. Particular emphasis has been placed on elucidating the mechanism that leads to the phenomenon of flame lift. The work is presented in two separate but closely interrelated parts.

The first part is exclusively concerned with the micro-structure of laminar diffusion flames of methane. Structural analyses have been carried out on two flames; one close to the blow-off limit and the second a stable flame for reference. The flames were formed on a slot-type burner to provide a relatively simple two-dimensional flame system. The experimental study involved the determination of sets of interrelated

characteristic profiles - aerodynamic, thermal and compositional - throughout the stabilising region of each flame. These pointwise aerodynamic, thermal and compositional properties of the gas were determined using the techniques of stroboscopic particle-tracking, fine-wire thermocouple thermometry and micro-probe sampling followed by gas chromatographic analysis respectively. Formal equations relating conservation of heat energy, mass and species with the differential equations of diffusion, conduction and species production have provided the basis for interpretation of the experimental data in terms of two types of information. First, the determination of the relative importance of the various physical processes that occur in the stabilising region of diffusion flames, i.e. principally, thermal convection, molecular diffusion and thermal conduction. Second, the quantitative evaluation of the rates of reaction of the major initial, intermediate and final stable species together with the associated volumetric rates of heat release. It was concluded that both types of information were a necessary prelude to a further understanding of

the mechanism of flame stability. However, the analysis involved, even for a single flame condition was extremely lengthy and as such impracticable as regards the study of the wide variety of flame systems that are currently of interest to the Gas Industry.

The second part of this thesis attempts, therefore, to develop a suitable experimental technique for estimating the structure of flames over a wide range of fuel flow rates by applying some of the results and conclusions obtained in part 1 of this thesis. Temperature profiles, alone, have been used to derive, approximately, the rates of heat release throughout the stabilising region of each flame system.

Laser Interferometry was chosen for the measurement of flame temperature, this being the only technique suitable for processing the large quantity of data that was necessary. Unavoidably, this necessitated the use of a burner of axial symmetry since, only for this geometry could the optical path equations involved in interferometry lead to unambiguous solutions for flame temperature.

The presentation of experimental work and conclusions are given separately for the two parts of the thesis.

## 1.2. SURVEY OF PREVIOUS FLAME STUDIES

### 1.2.1. Diffusion Flames

In the past, chemists have been little interested in flames of initially separated reactants (i.e. diffusion flames) because these flames involved the additional complexities, compared with pre-mixed flames, of diffusion and aerodynamic processes. Physicists were similarly unable to measure any fundamental parameters that would characterise diffusion flames. Hence early work on laminar diffusion flames, pioneered by Burke and Schumann in 1928, attempted to predict gross flame parameters such as shape and height. In order to permit mathematical treatment of the problem Burke and Schumann had to make certain simplifying assumptions which, although not wholly justifiable, succeeded in giving a formal picture of the diffusion flame as far as shape and height were concerned. Principally their assumptions were:

(i) Mixing occurs by radial diffusion only

(ii) The velocities of fuel and oxidant in the region of the flame are constant and equal to that of the approach flow

(iii) The coefficient of molecular diffusion is the same in the two gas streams and independent of flame temperature and composition

(iv) Combustion occurs at an infinitesimally thin zone where the rate of diffusion of combustible gas outward and the rate of diffusion of oxygen inward are in stoichiometric proportions

The first assumption restricts the analysis to fairly tall flames. The second and third were advanced as heuristic and possibly legitmate when considered in conjunction with each other. However the use of a diffusion coefficient which is independent of flame temperature and composition has been widely criticised. As the gases heat up, the diffusion coefficient increases roughly as $T^{1.75}$ and this is only partly compensated for by an increase in the velocity of the gas stream which only increases in direct proportion to T. The change of diffusion coefficient in the horizontal direction may, for flames burning in oxygen, be greater by a factor of 30 at the hottest part of the flame and this may lead to an

nitrogen). These flames were of interest because of recirculation of products of combustion in gas turbines. Barr and Mullins were able to express flame height in terms of the rates of flow of reactant and oxidant, mixture composition and the degree of vitiation. However, it is difficult to make reliable calculations for different velocities of reactant and oxidant because to formulate a rational mathematical solution requires that no transfer of momentum takes place, i.e. that reactant and oxidant retain their separate velocities.

Hottel and Hawthorne (1949), Wohl, Gasley and Kapp (1949), Barr (1953,1954) and Fay (1954) extended these theories to flames supported by unequal fuel and air velocities.

Whilst the ideas of Burke and Schumann and subsequent workers are useful in predicting gross flame parameters, they are ineffective when considering the phenomenon of flame lift for diffusion flames. It is well known that on increasing the rate of reactant supply a flame will eventually move downstream of a burner. The potentially infinite reaction rate employed by Burke and Schumann would evidently hold its own against any rate of reactant supply. Clearly, the ensuing theories on diffusion flames had, unlike

the formal ideas of Burke and Schumann, to recognise the existence of finite reaction rates extending over zones of finite thickness.

Zeldovich (1949) and Spalding (1950 to 1955) attempted to combine mass transfer theory with considerations of chemical kinetics. Using an overall reaction rate scheme, extinction is considered in relation to the maximum intensity of reaction, called the flame strength, which is permitted in the flame. When the supply of reactants into the flame exceeds this maximum, flame temperature begins to fall, engendering a reduction of reaction rate that leads to extinction. Potter and Butler (1959) and Potter, Heimel and Butler (1960) attempted to verify the concepts of Spalding by using an experimental flame strength defined as the mass average flow rate of fuel and oxidant necessary to extinguish the flame. Their results, however, agreed only roughly with theory principally because of the low flow rates employed in their early experiments. Later experiments (Anagostou and Potter) at higher Reynolds numbers ($> 1000$) showed better consistency with the Spalding theory (Spalding (1961)).

In order to develop a more rigorous theory of diffusion flames, Wolfhard and Parker in 1952 attempted

with the aid of new spectroscopic methods what was probably the first structural analysis of a reaction zone. Flames of hydrogen, ammonia and ethylene, each supported by oxygen, were stabilised above the common interface of two rectangular ducts. A flow of nitrogen surrounded the flames affording protection from the atmosphere. Structurally, each flame consisted of a main reaction zone where temperature is a maximum and the component gases are in chemical equilibrium. This region is surrounded by pre-heating zones where reactants and oxidants undergo chemical changes. Together with qualitative observations, the results of Wolfhard and Parker showed clearly that diffusion flames supported by pure oxygen have, at atmospheric pressure, a structure characteristic of flames in which diffusion is the rate controlling process, an assumption previously employed more generally by Burke and Schumann. Any changes in the concentrations of species and flame temperature engendered by diffusion processes are rapidly brought back into equilibrium by the high rate of chemical reaction. However, flames supported by air, as opposed to pure oxygen, may not obey this rather ideal concept of a diffusion flame.

In the case of flames supported by ammonia and ethylene, the chemical changes on the fuel side of the main reaction zone were considered to be principally pyrolytic, the main reaction zone presenting a barrier to oxygen penetration. The conclusion that the reactant is pyrolised before coming into contact with the oxidant is supported by the sampling studies carried out by Smith and Gordon (1956) on methane-air flames. Various pyrolysis products were detected using a small quartz probe together with subsequent analysis of the sample by mass spectrometry but apart from a rather uncertain trace of formaldehyde no sign of intermediate oxidation products was detected. Since it is well known that trace quantities of molecular oxygen strongly enhance the rate of thermal decomposition of hydrocarbons, the existence of these small concentrations of oxygen would seem to suggest that chemical breakdown of hydrocarbon - air diffusion flames may be pyrolytic. Of course, not only are spatially extended reactions responsible for the structure of diffusion flames but also such aspects as thermal convection, molecular diffusion and thermal conduction. Moreover, the structure of laminar diffusion flames can be studied in depth only by an

analysis that includes these physical aspects as well as the usual chemical considerations.

The first attempt at a full structural analysis of a diffusion flame was made by Pandya and Weinberg in 1963. The main prerequisite of such an investigation is that the flame shall afford a structure that would make a detailed analysis worthwhile. For this reason Pandya and Weinberg carried out their analysis on an approximately flat flame stabilised in the counter-flow régime of opposed jets of ethylene and air. Three complementary methods were employed for the measurement of flame temperature; interferometry, line reversal and fine-wire thermocouples. Additionally, the velocity and species profiles were measured using the techniques of particle-track flow-visualization and gas chromatography respectively. The aerodynamic and thermal structures were then analysed to yield the distribution of heat release per unit volume of the flame. A rather unexpected feature of the heat release rate profiles was the appearance of small endothermic regions on both sides of the main reaction peak. Whilst it did not seem unlikely that pyrolysis would give rise to such a phenomenon on the fuel side, the appearance of an endothermic region on the oxidant side

was rather surprising. Other than this, the most significant observation made by Pandya and Weinberg concerned the width of the reaction zone - an order of magnitude greater than the equivalent pre-mixed flame. Clearly, it had been demonstrated that flame structure techniques could provide a very convenient tool for the study of fast burning mixtures at high temperatures and at atmospheric pressure.

In recent years both Tsuji and Yamaoka (1970) and Thomas (1968) have shown that structural techniques could, with some care, be usefully applied to approximately one-dimensional flame systems. The counter-flow methane-air diffusion flame of Tsuji and Yamaoka, stabilised in the forward stagnation region of a porous cylinder, again showed a small endothermic valley on the fuel side of the main reaction peak and this was attributed to pyrolysis-type reactions. Yet, unlike the previous studies, the temperature profile measured by these workers showed a curious change of gradient that would perhaps account for the small region of absorption. In the work of Thomas (1968), an attempt was made to examine the internal structure and reaction rates of $H_2$-$O_2$-$N_2$-air flames produced this

time from two parallel reactant streams on a modified burner of a type previously employed by Parker and Wolfhard. Thomas examined the distributions of stable species in some depth as well as molar rates of disappearance of hydrogen and oxygen and the associated rates of heat release. He found the heat release profiles to be totally exothermic within a factor of two accuracy. The thermal picture emerging from Thomas's work is that heat liberated by combustion leaves the reaction zone mainly by conduction while only a small part is conveyed by diffusion processes. The analysis shows, in addition, that reaction occurs over a relatively wide proportion of the available mixing zone between the two combustible streams showing that the reaction zone could not be regarded, as thought by Linan (1961), as a comparatively minor variation in the separation region between the two streams of combustibles.

Recently Robson and Wilson (1969) have employed structural techniques in considering the phenomenon of flame lift for diffusion flames of methane on small tubular burners. However, only an approximate analysis

of the structure was carried out. The accessible flame parameters - temperature, velocity and composition of stable species - were mapped out over a small region of the flame base to yield fluxes of heat, energy and oxygen. The former showed that the flame base loses considerable heat to the central stream whilst the latter showed that considerable amounts of heat are generated below the visible zone of the flame. The mechanism of lift was considered by Robson and Wilson to be predominantly due to a velocity effect. Increasing the reactant flow causes an increase in the inward horizontal flux of oxygen at the flame base whilst the vertical component remains fairly constant. The resulting increasing oxygen flux requires a corresponding increase in the reactant flux and since the reactant is transferred only by diffusion processes this compels the concentration gradient to steepen and the flame to contract. In this way, two interrelated effects combine to cause flame lift; increasing the reactant flow rate increases the velocity even at constant radius, and stoichiometry necessitates that the flame moves inwards to a position where the velocity is higher still. Eventually, in the picture presented by Robson and Wilson, the flow velocity exceeds the local burning velocity

and the flame moves downstream to extinction. Of course, although velocity might well be expected to be an important factor in determining flame lift, a further limitation on stability may well be imposed by the composition of the flame gases and their associated rates of reaction. This point is not well established.

The general findings of Robson and Wilson are supported by Bellis (1968) who carried out a study of the mixing region of flames of methane and ethylene in air. In addition, Bellis found the mixture at the flame base to be leaner than the conventional limits of inflammability and suggested that the conventional limits of inflammability as defined by Linnet and Simpson (1957) are modified in the mixing region of diffusion flames. Bellis did not attempt a full structural analysis in his studies.

1.2.2. Pre-mixed Flames

It was mentioned in the previous section that much of the early work on diffusion flames considered combustion to take place where admixture of the combustibles occurs in stoichiometric proportions. For this reason a brief summary of previous structural studies of stoichiometric and pre-mixed combustion is relevant also to the present study.

The most extensive of the early structural studies was carried out on an approximately one-dimensional fuel-lean methane-oxygen flame at reduced pressure (Fristrom and Westenberg, 1965). Measurements of the accessible flame parameters (temperature, velocity and species concentrations) were combined with the conservation equations for matter and heat energy to yield approximate profiles of rates of reaction and heat release. One of the most interesting features of the results was that the flame could be considered as comprising three spatially distinct regions; a transport region, or pre-reaction zone, where almost no reaction takes place, a main exothermic combustion zone where methane reacts to form the intermediate products of combustion (carbon monoxide and hydrogen), and a secondary reaction zone, of considerable spatial extent, where carbon monoxide is oxidised to carbon dioxide. The rates of reaction were considered to be accurate to $\pm$ 10%.

More recently Tewari and Weinberg (1967) have applied the techniques, developed for flame structure studies, to an inter-flame/heat sink region associated with a flat pre-mixed lean ethylene-air flame. Detailed structural measurements combined with analysis

involving conservation of heat energy showed that a cooled metallic surface quenches the second stage of reaction but has little effect upon the maximum rate of heat release. In this way the reaction zone narrows only slightly towards the heat sink.

Perhaps the most relevant of the structural studies on pre-mixed flames, to the present study, are those of Datta, Hayward and Reed (1971) and Datta and Reed (1972). Structural analyses, carried out on near-stoichiometric (9.9%) and moderately fuel-rich (14%) methane-air flames, illustrated a fundamental change in the stabilising mechanism when the mixture becomes fuel-rich. The maximum rate of heat release associated with the near-stoichiometric burner flame was found to be about 160cals $cm^{-3}s^{-1}$ whereas that for the moderately fuel-rich flame was significantly lower at 88 cal $cm^{-3}s^{-1}$. Nevertheless a 50% decrease in the maximum heat release rate was associated with a 50% increase in stability of the latter compared with the former. The conclusion that the maximum heat release rate in the stabilising region of moderately fuel-rich flames is much less than for a stoichiometric flame is

not in accord with the classical view (Lewis and Von-Elbe, and Wohl, Kapp and Gasley) that pre-mixed flames are stabilised by a stoichiometric mixture formed by intermixing with the ambient atmosphere. Indeed, it has been shown, conclusively, that little or no intermixing at the flame base takes place for mixture compositions ranging from stoichiometric to 13% methane (Smith 1971). However, it is clear that, for the type of flame considered in this thesis, pre-mixing at the flame base is a necessary prerequisite for combustion.

The foregoing discussion highlights two important points. First, the micro-structure of the stabilising region of diffusion flames, and particularly the relative importance of aerodynamic and diffusive mixing processes at the base of these flames is not well understood. Second, the exact mechanism that leads to the phenomenon of flame lift of diffusion flames is not well established since the flow situation at the base of these flames is clearly quite different from that for the pre-mixed flames studied so far. These questions are of particular interest at the present

time because of the desirability of achieving simple, compact, high thermal loading burners in the field of natural gas utilisation.

With these objectives in mind, the present thesis attempts to apply the detailed structural techniques, developed for approximately one-dimensional studies, to two-dimensional burner flames commonly encountered in practice. This would seem feasible provided these flames can be stabilised with an extremely high degree of spatial stability.

## 1.3. DETAILS OF APPARATUS AND EXPERIMENTAL PROCEDURE

In order to ascertain the most suitable flame systems that would afford a worthwhile analysis of diffusion flame structure and elucidate the mechanism that leads to flame lift, a few preliminary observations and temperature measurements were carried out on flames of pure methane at various fuel flow rates. The nature and volume of experimental data that was to be obtained restricted analysis to two flame systems only. It was felt that the two flame systems selected should indicate the changes in flame structure on approaching the lift stability limit and at the same time should allow the use of experimental techniques normally associated with studies of flames of relatively low momenta. With these aims in mind, the flames selected for study were

(1) A relatively stable flame (reactant supply 142 mls $^{-1}$) burning well away from the lift stability limit. This flame fulfilled the role of a reference condition.

(ii) A flame operating close to the lift stability limit (reactant supply 650 mls$^{-1}$), yet remaining sufficiently stable that the probes used in the investigation produced no visible signs of interfering with the normal structure of the flame.

1.3.1. Burner and Flow System

The flames were supported on a long slot-type burner made of steel and housed in a vertical wind tunnel. Fig. 1 shows the burner supporting a flame burning 142 mls $^{-1}$. The dimensions of the burner slot (8.3 cm by 0.1 cm) were chosen to give an effectively two-dimensional laminar flame region. Air for combustion entered through flow-straightening honeycomb providing an essentially streamline flow.

An essential requirement of any burner system affording a detailed structural analysis is to ensure an extremely high degree of spatial stability in the flame region being studied. However, the system described above was not capable, in its basic form, of providing the degree of spatial stability compatible with a flame structure study. Indeed, this was only to be expected from the photographs of a similar

system published by Simmonds and Wilson (1948), the problem being that eddies shed from the upper part of the flame sheet fed perturbations back to the flame base. Two remedies were tried. The first employed two slotted air injectors, of similar slot dimensions to those of the burner, situated well downstream of the stabilising region of the flame. These were orientated along each side of the burner with their long sides parallel to those of the burner such that the air jets formed the sides of a triangle whose apex lay on the burner axis. Air flow through the injectors was sufficient to prevent eddies, shed in the mixing region in the uppermost parts of the flame, from reaching the flame base. However, despite a satisfactory degree of spatial stability a major disadvantage was that the peripheral flow system associated with the air injectors impeded access to the base regions of the flame where measurements were to be taken. Hence an alternative remedy had to be tried. This employed an extractor hood, the base of which was a sintered metal plate. The hood was situated 43 mm above the flame base (Fig.1) and connected through a heat exchanger to an extractor unit (Type Noo horizontal discharge blower, manufactured

by K. Blackman Ltd.) fitted with a variable control on the air inlet. A constant pressure drop, just sufficient to prevent eddies from reaching the flame base, was maintained across the hood. In order to establish the effect, on the base regions of the flame, of this mild form of extraction, a number of particle-track flow-visualization photographs were taken. These showed that no discernable changes in the aerodynamic pattern and hence flame structure were brought about by this mild form of extraction which provided an extremely high degree of spatial stability.

Pure methane for combustion was taken from a high pressure cylinder, through a rotameter at constant pressure and thence to the base of the burner. A photograph of the entire experimental rig is shown in Fig. 2.

1.3.2. Measurement of Temperature Profiles

In the case of flame fronts there has been some debate as to whether it is meaningful to speak of a single temperature profile. Temperature, of course, is a parameter characteristic of a system at equilibrium whereas a system like a laminar flame is, to a certain extent, a non-equilibrium system, chemically. Nevertheless the accepted opinion is that although the internal degrees of freedom of species in flames have on occasion been observed to be in a non-equilibrium

state, it is still valid to measure a local translational temperature.

Although there are many ways of measuring flame temperature (e.g. probe thermometry, radiation thermometry and thermometry by measuring gas density) only a few possess sufficient reliability and spatial resolution to be of use for the local measurements required for a detailed structural study. Each, of course, has its particular advantages and disadvantages and the final choice therefore depends on the range of temperature and temperature gradient to be measured as well as considerations such as ease and rapidity of measurement. On this basis the method of probe thermometry, employing fine-wire thermocouples, was considered the most suitable.

In this study the materials chosen were Pt 20% Rh and Pt 40% Rh. This choice was preferred to the normally used Pt and Pt 10% Rh combination in order to raise the melting point of the junction above the peak flame temperatures. At the same time, drift due to rhodium migration is reduced.

To make precise temperature measurements in flames requires the use of extremely small thermocouples and for this study wires of diameter 0.0025 cm were used.

The fabrication of these fine-wire couples involved two operations; first, welding the junction and second, coating the final couple. Welding was carried out using a micro-flame-torch and the final operation of coating consisted of passing the couple several times through a flame, containing vapour of silicon fluid, at a sufficiently high temperature (about 1800°K) to produce a homogeneous coating. The junction was mounted on support wires of the same materials of diameter 0.05cm held in twin-bore quartz tubing. The measuring technique consisted of passing the thermocouple through the flame using a mechanised micro-manipulator and recording the potential developed on a chart recorder.

Despite the high precision and good spatial resolution of thermocouples the main disadvantages, in common with all probe methods, are the effects of the probe on the flame. These fall into three categories; chemical, thermal and aerodynamic.

The main chemical disturbance is the promotion of catalytic reactions on the probe surface. This causes spuriously high temperatures and hysteresis in the temperature profile. This effect was minimised, in this study, by using the standard method of coating

with non catalytic silica.

Second, even when coated wires are used the temperature measured is still that of the junction. The gas temperature is different by an amount depending on the heat balance between the flame gases and the thermocouple. Losses by conduction along the wires were minimised by positioning the thermocouple along an isotherm. In order to take into account losses by radiation, the equation derived by Kaskan was used:

$$\Delta T_{RADIATION} = \frac{1.25\,\epsilon\,\sigma_s}{\lambda}\left(T_w^4 - T_o^4\right) d^{0.75}\left(\frac{h}{ev}\right)^{0.25} \quad (2)$$

The emissivity of thermocouples coated with silica varies both with the thickness of the coating and flame temperature. Bradley and Entwistle, working on Pt/Pt 10% Rh wires, have shown that at lower temperatures the effect of the silica is to increase $\epsilon$ whereas at higher temperatures there is a decrease in $\epsilon$, which, for thicker coatings, may even be less than the value of $\epsilon$ for an uncoated wire. For the purpose of this thesis, however, in the absence of corresponding data for Pt20% Rh/Pt 40% Rh wires, a constant value of $\epsilon = 0.22$ was employed which, at an overall diameter of 0.0075 cm on a core of diameter 0.0025 cm, gives the

correct spectral emission at about 1300°K. At temperatures less than 1300°K an error in $\epsilon$ would be offset by the decreased dependence of $\Delta T$ on $T_w$ whereas at higher temperatures any error in $\epsilon$ would give, at worst, an error of about 18% in $\Delta T$ or only about 1% in T itself. To a first approximation it can be seen from equation (2) that the magnitude of the radiation correction depends on $d^{0.75}$ and hence very fine thermocouples were used to minimise this effect.

Finally, a thermocouple of finite diameter perturbs the flame, to some degree, and causes a viscous velocity wake downstream which is roughly similar in magnitude to the thermal wake. This means that the thermocouple will tend to sample a temperature downstream of its apparent position. A rigorous treatment of the coupling between the velocity and the thermal wakes would be difficult and has not been attempted. The problem has been treated approximately however (Westenberg and de Haas) by adjusting the final temperature profiles four bead diameters downstream along the flow streamlines (Friedman, Fristrom and Westenberg). The significance of this correction on the resulting heat flux profiles etc. will be discussed fully in section 1.5.8.

1.3.3. Measurement of Velocity Profiles

Several techniques exist for making flame aerodynamic measurements. The most versatile of these is the particle-tracking method in which microscopic dust particles are introduced into the relevant gas streams and their paths are recorded photographically using a high intensity illumination system. If a repetitive source, of known frequency, is used velocity profiles can be measured directly. However, because of the small size of particles, the brevity of the interruptions and the high resolution required, experimental techniques are difficult. In addition it is necessary to have an injection system that supplies an extremely low density of particles, since in an extreme case the flame could be disturbed (Anderson and Fein). Nevertheless despite the intricacies involved, the method of particle tracking was considered the most suitable for a detailed structural study.

The introduction of particles will, to some extent, disturb the flame under study. The main physical effect is that of heat abstraction by the particles but, in the case of an extremely low particle density,

this amounts to only a small fraction of a percent of the heat liberated at the reaction zone. Chemical effects are harder to establish but were minimised by using an extremely low density of chemically non-reactive magnesium-oxide particles. At the reaction zone these particles undergo rapid accelerations, the force due to acceleration being balanced by the aero-dynamic drag caused by particle slippage relative to the flame gases. Another source of error, important in flame front particle-track studies, is the thermo-mechanical effect, the force which a particle experiences in a strong temperature gradient (Fristrom and Westenberg). In order to minimise these effects particles were elutriated to a mean diameter of approximately 5$\mu$ prior to the experiments. A low density of these was then vibrated into both the air and methane streams.

Repetitive illumination was provided by a 500 watt high pressure mercury vapour lamp in series with a chopper disc mounted on a synchronous motor. A series of different discs were employed giving frequencies in the range 100 to 5000 $S^{-1}$. Accurate calibration was carried out using a tachometer. The

light scattered by the particles was viewed at right angles to the plane of illumination using a high precision 150 mm lens connected via an extension tube to a Hasselblad 500 C camera body. A check on lens performance was made by using a standard precision grid which also provided an accurate scaling factor for the photographs. These were enlarged, on average to a magnification of X 35, on high contrast, high stability, lithographic film (Agfa-Gevaert type R1pM).

Processing of the data, presented on film, was carried out using a Pencil Follower (d-Mac Ltd.) and a simple computer program. The Pencil Follower rapidly translates graphic data into a digital form, suitable for subsequent computer processing, using an inductively coupled "free pencil" to record data co-ordinates on to computer compatible punched cards. A simple computer program was written to calculate, from measurements of the co-ordinates of successive particle tracks, velocities in the component directions y and z. Finally, in conjunction with a plotter (type I.B.M. 1627) the position and magnitude of the two components of velocity were drawn up on a rectangular grid. In this way the aerodynamic pattern was built up track by track.

1.3.4. Measurement of Species Profiles

Two experimental techniques are available for measuring the concentrations of species in flames; direct spectral analysis and sample withdrawal followed by analysis. Both methods have their advantages but the second has been particularly successful for measuring the concentrations of stable species and hence was the method chosen for this study.

Taking a sample from a reaction zone, rapidly quenching it and then analysing it is a classical method of reaction kinetics. Analysis by gas chromatography is relatively straight forward. The sample under investigation is injected into a stream of carrier gas at the head of a column of separating material. The sample is then swept by the carrier gas on to the column where the individual species are absorbed and resorbed at different rates and thus separated. The presence of the component species in the carrier is then detected using a suitable physical property of a gas such as thermal conductivity. Although analysis by chromatography is relatively straight forward the application of probe sampling

techniques to flame reaction zones gives rise to a number of difficulties. In particular these concern the effects of the probe on the flame, spatial resolution and the interpretation of the sample obtained. In order to minimise flame disturbance, the sampling rate must be small whilst at the same time the pressure in the sampling line must be sufficiently low to quench any chemical reactions. However, the problem can be minimised by introducing the sampling probe along a flow streamline. The limitations and justifications of the technique of probe sampling have been discussed in some detail (Fristrom, Prescott and Grunfelder) with the conclusion that, with care, reasonably self-consistent data can be obtained.

In the present study these difficulties were minimised by constructing microprobes of quartz drawn down to a fine orofice (40 - 80$\mu$). The samples were withdrawn at sonic velocities prior to chromatographic analysis. The sampling line was constructed of P.T.F.E. tubing and heated to prevent any water vapour present in the sample from condensing out.

A Pye 104 series Gas Chromatograph, incorporating two columns, was used to separate the component species

and a hot-wire thermal conductivity cell used as a detector. Samples were withdrawn from the flame using a batchwise process. Initially the sampling line was evacuated to a small fraction of a cm of mercury using a vacuum pump. The pump was then isolated and the sample injected on to a column of the chromatograph at a pressure of 150 mm of mercury. The sample was then swept on to a column using helium as the carrier gas flowing at 80 ml $min^{-1}$ at a column temperature of 50°C. Separation of the permanent gases, i.e. hydrogen, oxygen, nitrogen, methane and carbon monoxide was carried out on a "Molecular Sieve" type of column and carbon dioxide, higher hydrocarbons and water vapour on a "Porapak-q" column. The response from the hot-wire thermal conductivity cell was integrated using a "Chromalog 2" integrator (Kent Instruments Ltd.) and a direct indication of the output was provided by a potentiometric chart recorder. Finally the concentrations of the stable species were calculated using previously calibrated response factors of each species relative to pure nitrogen. Nitrogen samples were injected and analysed both before and after each sample withdrawal and analysis.

## 1.4. ANALYSIS OF EXPERIMENTAL DATA

It has already been mentioned that processes occurring in flowing reaction systems are relatively complex involving simultaneous chemical reactions as well as aspects of convection, thermal conduction and molecular diffusion. These interrelated effects tend to make mathematical analysis of such systems rather complex. Nevertheless, structural parameters, such as fluxes of material species and heat energy and also the rates of creation of chemical species and heat energy, may be formally related with the experimentally accessible flame parameters - temperature, velocity and material species. These structural parameters provide a sound basis for interpreting the experimental data.

### 1.4.1. Generalised Continuity Equation

For the purpose of this thesis the flames are assumed to fulfil the following conditions:-

(i) The flames are steady-state so that all macroscopic variables are independent of time

(ii) The flames are essentially constant pressure systems so that the equation of motion may be neglected as well as the effects of pressure gradients

(iii) Effects arising from viscosity, radiation and external forces are negligible and

(iv) Effects arising from thermal diffusion and its reciprocal effect (Dufour) are negligible.

The latter assumption is true only for mixtures deficient in large concentrations of a mobile constituent such as hydrogen.

With these simplifying assumptions the generalised continuity equation, describing any property of a gas, may be expressed in cartesian co-ordinates (x,y,z) by

$$\text{div } F_i = \frac{\partial}{\partial x}F_{i,x} + \frac{\partial}{\partial y}F_{i,y} + \frac{\partial}{\partial z}F_{i,z} = q_i \qquad (3)$$

Where F is the flow rate of the property per unit area and q is the rate of creation per unit volume. Equation (3) may be simplified to fit any two-dimensional flow régime and in particular the flame systems studied in this thesis

$$\text{div } F_i = \frac{\partial}{\partial x}F_{i,x} + \frac{\partial}{\partial y}F_{i,y} = q_i \qquad (4)$$

This generalised form of the continuity equation for a two-dimensional flow régime may then be usefully applied to flame properties such as the flow of material species and the flow of heat energy. In these cases

contributions to the flux term F may arise from convection and a transport term involving thermal conductivity and/or molecular diffusion.

1.4.2. Continuity of Species

The fluxes of material species i may be expressed in terms of the component contributions from convection and molecular diffusion.

$$\text{i.e. } \underline{F}_{M,i} = w_i \rho \underline{V} + \frac{N m_i}{\sum_k m_k X_k} \sum_{\substack{j \\ j \neq i}} m_j D_{ij} \text{ grad } X_j \qquad (5)$$

In equation (5) $w_i$ is the mass fraction of species i, $\rho$ is the density of the mixture of gases and V is the flow velocity. N is the molar density of the mixture, $X_k$ and $X_j$ are the mole fractions of species k and j respectively whilst $m_i$, $m_j$ and $m_k$ are the molecular weights of species i, j and k respectively. $D_{ij}$ denotes the multicomponent diffusion coefficient of the gas pair i, j.

From equation (4) continuity of species i yields

$$\text{div} \left( w_i \rho \underline{V} + \frac{N m_i}{\sum_k m_k X_k} \sum_{\substack{j \\ j \neq i}} m_j D_{ij} \text{ grad } X_j \right) = q_i \qquad (6)$$

In equation (6) $q_i$ is the rate of creation of species i by chemical reaction, normally termed the

reaction rate of species i.

1.4.3. Continuity of Heat Energy

Similarly, the fluxes of heat energy may be expressed in terms of the component contributions from convection, molecular diffusion and thermal conduction

$$\text{i.e. } \underline{F}_H = \sum_i \left( w_i \rho \underline{V} + \frac{N m_i}{\sum_k m_k X_k} \sum_{j \neq i} m_j D_{ij} \text{ grad } X_j \right) h_i - \lambda \text{ grad } T \qquad (7)$$

In equation (7) $h_i$ denotes the specific enthalpy of species i, T the mixture temperature and $\lambda$ the thermal conductivity of the mixture.

From equation (4) continuity of heat energy yields

$$\text{div} \left\{ \sum_i \left( w_i \rho \underline{V} + \frac{N m_i}{\sum_k m_k X_k} \sum_{j \neq i} m_j D_{ij} \text{ grad } X_j \right) h_i - \lambda \text{ grad } T \right\} = Q \qquad (8)$$

In equation (8) Q is the volumetric rate of production of heat energy or heat release rate.

1.4.4. Calculation of Transport Properties

The experimentally accessible parameters in a flame are of course the temperature of the flame gases (T), the flow velocity (V), and the mole fractions of the stable species ($X_i$). But in order to solve both for continuity of material species and continuity of

heat energy it is first necessary to derive the transport properties involved in equations (5) - (8). The methods of calculation employed and the sources of data, as appropriate, are given below for each of the relevant properties.

Mass Fraction

The mass fraction of each species, $w_i$, required for calculating the convective contributions to the fluxes of material species and heat energy, is simply related to the experimentally accessible mole fraction $X_i$ through

$$w_i = X_i m_i \Big/ \sum_i X_i m_i \qquad (9)$$

Mass Density

The mass density of a mixture of gases, $\rho$, again required for calculating the convective contributions to the fluxes of material species and heat energy was calculated from the pure component values through

$$\rho = \sum_i X_i \rho_i \qquad (10)$$

The pure component values at N.T.P. were taken from Spiers and conversion to the temperature of the flame gases was effected using the perfect gas law.

Molar Density

The molar density of a mixture of gases, N, required for calculating the contribution from molecular diffusion to the fluxes of material species and heat energy was calculated from

$$N = \rho / \Sigma_i m_i x_i \qquad (11)$$

Specific Enthalpy

In order to calculate the fluxes of heat energy and subsequently the rates of heat release, the specific enthalpy of each species was derived from

$$h_i = \overline{C_{p,i}} \, (T - T_o) \qquad (12)$$

In equation (12) T is the gas temperature, $T_o$ the ambient temperature whilst $\overline{C_{p,i}}$ denotes the mean specific heat at constant pressure of species i between $T_o$ and T.

The mean specific heat $\overline{C_{p,i}}$ was then related to the true component values $C_{p,i}$, tabulated by Svehla, through

$$\overline{C_{p,i}} = \frac{1}{T - T_o} \int_{T_o}^{T} C_{p,i} \, dt \qquad (13)$$

The integral in equation (13) was carried out using an orthogonal polynomial fit (Forsythe) of $C_{p,i}$ against T.

Viscosity

For the purpose of compensating for heat losses by radiation from a silica coated thermocouple (equation (2)) the viscosity of a mixture of gases, $\eta$, was calculated in an approximate form from

$$\eta = 1 \Big/ \sum_i X_i/\eta_i \qquad (14)$$

Here $\eta_i$ denotes the viscosity of the pure component taken from Svehla.

Thermal Conductivity

The thermal conductivity of a mixture of gases, $\lambda$, required for calculating the fluxes of heat energy and subsequently the rates of heat release, was calculated from the expression suggested by Wassiljewa

$$\text{i.e. } \lambda = \sum_i \frac{\lambda_i}{1 + \sum_{\substack{j \\ j \neq i}} A_{ij} X_j / X_i} \qquad (15)$$

In equation (15) $\lambda_i$ denotes the viscosity of the pure component and $A_{ij}$ the coefficient due to Lindsay and Bromley. Values of $\lambda_i$ were, for the most part, taken from the experimental work of Johnston and Grilly except at high temperatures where they were complemented by the estimated values of Svehla. The coefficient, $A_{ij}$, was calculated from the formula of Lindsay and Bromley

$$\text{i.e. } A_{ij} = \frac{1}{4}\left\{1+\left[\frac{\eta_i}{\eta_j}\left(\frac{m_j}{m_i}\right)^{\frac{3}{4}}\left(\frac{1+S_i/T}{1+S_j/T}\right)\right]^{\frac{1}{2}}\right\}^2\left[\frac{1+S_{ij}/T}{1+S_i/T}\right] \quad (16)$$

In equation (16) S denotes the Sutherland constant. The Sutherland constants of the pure components were calculated from

$$\eta_i = bT^{\frac{3}{2}}/T+S_i \quad (17)$$

by considering two temperatures, above and below the mixture temperature, and eliminating the constant b in equation (17). Further, $S_{ij}$, the Sutherland constant for the gas pair i, j, was calculated from

$$S_{ij} = (S_i S_j)^{\frac{1}{2}} \quad (18)$$

Multicomponent Diffusion Coefficient

In order to make reliable estimates of all the structural parameters considered in this thesis, an accurate knowledge of the transport property relating to the process of concentration diffusion is essential. Since the flame system under study contains many species, multicomponent diffusion must be considered for a rigorous analysis of the problem.

In this thesis the values of the multicomponent diffusion coefficient, $D_{ij}$, of each gas pair i, j have been calculated along the lines set out by Hirshfelder et al and more recently employed by Dixon-Lewis. To a first approximation $D_{ij}$ was calculated from

$$D_{ij}\Big|_1 = X_i \frac{16T}{25P} \sum_k \frac{m_k X_k}{mj} \left[\frac{L^{j,i} - L^{i,i}}{|L|}\right] \qquad (19)$$

In equation (19) P denotes the pressure of the flame system (atmospheric) and $|L|$ is the determinant of the matrix $L_{ij}$ in which $L^{j,i}$ are the minors. The elements of L were calculated from

$$L_{ij} = \frac{16T}{25P} \sum_k \frac{Xk}{m_i \mathcal{D}_{ik}|_1} \left[ m_j X_j (1-\delta_{i,k}) - m_i X_i (\delta_{i,j} - \delta_{j,k}) \right] \qquad (20)$$

Here $\mathcal{D}_{ik}$ denotes the binary diffusion coefficient of the gas pair i, k and the coefficients $\delta$ take the values:-

$$\delta_{i,j} = 0, \quad i \neq j$$
$$\delta_{i,i} = 1, \quad i = j$$

The first approximation to the binary diffusion coefficient $\mathcal{D}_{ij}$ was calculated from

$$\mathcal{D}_{ij}\Big|_1 = \frac{0.002628 \left[T^3/2\omega_{ij}\right]^{\frac{1}{2}}}{P \sigma_{ij}^2 \Omega_{ij}^{(1,1)*}} \qquad (21)$$

Here, T denotes the temperature and P the pressure of the gases. $\omega_{ij}$ is the reduced mass for the gas pair i,j ($= m_i m_j / m_i + m_j$) and $\Omega_{ij}^{(1,1)*}$ is the reduced collision integral for the gas pair i,j. Values of $\Omega_{ij}(1,1)*$ were interpolated from the values tabulated by Hirshfelder et al as a function of reduced

temperature $T^{*}$ (= $KT/eps_{ij}$) where K is Boltzmann's constant. The parameters $\sigma_{ij}$ and $eps_{ij}$ are force constants characteristic of the chemical species of of colliding molecules. These were estimated using the following combining rules based on the Lennard-Jones potential energy model for colliding molecules

$$\sigma_{ij} = \tfrac{1}{2} (\sigma_i + \sigma_j) \xi^{-1/6} \qquad (22)$$

$$eps_{i,j} = (eps_i \times eps_j)^{\frac{1}{2}} \xi^{2} \qquad (23)$$

Equations (22) and (23) are suitable for interactions between pairs of non-polar molecules as well as interactions between a polar and non-polar molecule . $\xi$ is a collision number which takes the value unity except for interactions between a polar and non-polar molecule in which case

$$\xi = 1 + a_n^{*} t_p^{*} \left[ eps_p / 2 eps_n \right]^{\frac{1}{2}} \qquad (24)$$

where $a_n^{*}$ is the reduced polarizability of the non-polar molecule (= $a_n/\sigma_n^3$) and $t_p^{*} = \mu_p^{*2}/(8)^{\frac{1}{2}}$ where $\mu_p^{*}$ is the reduced dipole moment of the polar molecule (= $\mu_p/eps_p \sigma_p^3$). The values of $a_n$ and $\mu_p$ were taken from Hirshfelder et al and $t_{H_2O}^{*}$ was taken as 1.225.

Finally, in choosing values of the force constants, $\sigma$ and eps, some care is necessary to ensure that suitably matched pairs are used. In this work the values for $O_2$ were taken from Svehla whilst the remaining values were calculated from the experimental data of Walker and Westenberg for gas pairs. Thus the complete list of values is as tabulated below:

| SPECIES | $\sigma$ ($A^o$) | $\frac{eps}{K}$ ($^oK$) |
|---|---|---|
| $H_2O$ | 3.229 | 54.6 |
| $CH_4$ | 3.267 | 310.4 |
| $O_2$ | 3.467 | 106.7 |
| $N_2$ | 3.796 | 57.9 |
| $H_2$ | 2.183 | 216.4 |
| $CO_2$ | 3.263 | 425.2 |
| CO | 3.495 | 77.6 |

1.4.5. Organisation of Programs for Computing Transport Properties and Fluxes

The evaluation of the expressions given in the preceding sections, for estimating the fluxes of material species and heat energy, involves numerous repetitive calculations. For this reason some considerable time

was spent in evolving a network of computer programs. A rectangular right handed system of axes was set up with the x axis along the line of symmetry of the burner, the y axis perpendicular to the burner and the z axis vertically upwards. Experimental data are accepted from a matrix in the y - z plane, having spatial intervals of 0.01 cm in the component directions y and z. The stages involved may be set out as follows:-

(i) Input of tables of the pure component properties $\eta_i$ and $\lambda_i$ as a function of T and input of the coefficients of the orthogonal polynomial fits of $C_{p,i}$ as a function of T.

(ii) Input of $m_i$, $\rho_i$ (N.T.P.), $\sigma_i$, $eps_i/K$, $a_i$, $t^*$ and $\mu$ for the polar molecule, water.

(iii) Input of table of $\Omega_{ij}^{(1,1)*}$ as a function of reduced temperature $T^*$.

(iv) Input of tables of e.m.f. as a function of T for Pt 20%Rh/Pt 40%Rh thermocouples in the temperature range 0-1890°C.

(v) Input of experimental data - e.m.f.($T_w$), $V_y$, $V_z$ and $X_i$ at each point of a matrix encompassing the stabilising region of the flame. The values of e.m.f.($T_w$) are converted by linear interpolation into thermocouple bead temperature, $T_w$.

(vi) Calculation of approximate values of the transport properties of the flame gases $\lambda(T_w)$, $\mu(T_w)$ and $\rho(T_w)$. The program then calculates values of flame temperature, T, using equation (2).

(vii) Calculation, at the corrected flame temperature - (T), of $w_i$, $\rho$, N, $h_i$, $C_{p,i}$, $\lambda$ and $D_{ij}$, using equations (9) - (24).

(viii) Calculation of the derivatives - grad X and grad T - at each point in the matrix. The component derivatives $\frac{\partial X}{\partial y}$ and $\frac{\partial X}{\partial z}$ etc. are calculated using fitting of experimental data by an extension of the spline fit technique (Klaus and Van Ness (1967), South (1970)).

(ix) Calculation of the component contributions to the fluxes of material species, $\underline{F}_{M,i}$ and the fluxes of heat energy, $\underline{F}_{H,i}$, at each point in the matrix, using equations (5) and (7).

(x) Output, at each point in the matrix, of tables of

1. Experimental Data - T, $V_y$, $V_z$ and $X_i$
2. Transport Properties - $w_i$, $\rho$, N, $h_i$, $C_{p,i}$, $\lambda$ and $D_{ij}$
3. Material Fluxes - $\underline{F}_{M,i}$
4. Heat Energy Fluxes - $\underline{F}_{H,i}$

The derivative terms (grad X and grad T) for evaluating the fluxes ($\underline{F}_{M,i}$ and $\underline{F}_{H,i}$) are the most difficult to determine quantitatively and, as mentioned above, an extension of the spline fit technique was used for this purpose. This is a relatively little known, but extremely useful, technique which employs local cubic interpolating polynomials between consecutive values of the experimental data. By requiring continuity in the first and second derivatives at the junction points, or knots, and thus

effecting an overall fit of the data, this approximation becomes remarkably superior to other approximation techniques applied over a given interval. The result is a zone-wise analytic curve rather than a single overall analytic fit and this preserves the differentiation advantages of spline fitting over those of a single polynomial. In this thesis, these differentiation advantages have been utilised in evaluating the derivative terms, grad X and grad T.

The advantages are best demonstrated by contrasting the derivatives evaluated from spline fitting with those from a simple graphical method. This comparison is demonstrated later in the text in section 1.5.5.

1.4.6. Estimation of Reaction Rates and Heat Release Rates

Whilst the smoothing spline fit technique provides an accurate method of evaluating the flux profiles from the derivative terms, grad X and grad T, the task of evaluating the rates of reaction and heat release, from the associated flux profiles, is more difficult. Here, the derivatives of the fluxes are often rapidly changing within very small linear distances such that

a careful choice of the interval boundaries, involved in spline fitting, would not preclude unwarranted inflection points in the resulting rate profiles. For this reason it was necessary to employ a simple, but time consuming, graphical method for evaluating the rates of reaction and heat release.

## 1.5. RESULTS AND DISCUSSION

### 1.5.1. Temperature Profiles

The distributions of temperature for the two flames examined, namely a reference flame burning 142 $mls^{-1}$ and a flame operating closer to the lift stability limit, burning 650 $mls^{-1}$, were obtained using the method of thermocouple probe thermometry as outlined in Section 1.3.2.

Traverses were carried out at nine levels both above and below the burner port and the results plotted out in the form of isotherms (Figs. 3 and 4). Superimposed on the isotherms are the approximate positions of the visible flame sheet. Of course measurements of the extent of the visible flame sheet are partly subjective but the inward and upward movement of the flame sheet, with increasing reactant supply, is quite apparent.

The shape of the temperature pattern for the two flames is much as expected. Both flames assume a shape such that combustion takes place over a broad flame sheet which is inclined away from the axis of the flame with increasing distance above the burner part. It would seem, from evidence provided by the

temperature profiles alone, that combustion occurs over a relatively wide proportion of the available mixing zone between the two combustible streams.

For both flames, the locus of the points of maximum temperature lies towards the unburnt-fuel side of the centre of the flame sheet. The maximum temperatures themselves are similar for the two flame systems - about 1950°K. The most significant difference, however, between the temperature patterns of the two flames is the steepening of the gradients of temperature at the base of the flame with increasing supply of reactant. Not only is there an upward and inward movement of the flame sheet with increasing supply of reactant, but also a general contraction of the combustion zone. It can be seen from Figs. 3 and 4 that as the supply of reactant is increased from 142 $mls^{-1}$ to 650 $mls^{-1}$ the maximum gradient of temperature at the base of the flame increases from 13,400°K $cm^{-1}$ to 20,500°K $cm^{-1}$. Thus, it would be expected that significantly more heat is lost from the base of the flame towards the burner and surroundings in the case of the flame burning 650 $mls^{-1}$ than the flame burning 142 $mls^{-1}$. In addition, Figs. 3 and 4 indicate that the gradient of temperature decreases

rapidly with increasing vertical height above the base of the flame sheet. Within a vertical distance of less than 3 mm from the flame base, the temperature has reached its maximum value. If one accepts, at this stage, that the stabilising region lies at the base of the flame sheet, then the anchoring point of the flame is confined to a very small zone at the base of the flame.

Beneath the flame sheet, both flames exhibit fairly high temperatures lending some support to the observations of Robson and Wilson that appreciable amounts of heat energy may be generated in this region. This is particularly likely for the flame burning 650 $mls^{-1}$ where temperatures up to 1400$^{o}$K prevail beneath the visible flame zone. But of course it is the change of gradient of temperature that really indicates a region of heat release. This aspect is discussed later in the text in section 1.5.7.

1.5.2. Velocity Profiles

The distributions of velocity, for the two flames examined, were obtained using the method of particle tracking as outlined in section 1.3.3. By using a

simple computer program the positions and magnitudes of the two components of flow velocity, $V_y$ and $V_z$, were drawn up over a matrix encompassing the stabilising region of each flame. The results are shown in Figs. 5 to 8 in the form of isovels of the components $V_y$ and $V_z$. In addition, the results of the particle tracking are shown in Fig. 9 in the form of flow streamlines superimposed on which are shown the magnitudes of velocity over the region at the base of each flame sheet.

It can be seen from Figs. 5 to 8 that, in each case, the flame takes up a position such that combustion occurs over a broad flame sheet in a region of relatively low mixture velocity. The isovels of component $V_y$ assume a shape not unlike that of the isotherms (Figs. 3 and 4). The locus of the points of maximum component $V_y$ lies towards the unburnt-fuel side of the flame sheet. This would seem to indicate that the maximum inward flux of oxidant and hence the maximum rate of combustion takes place towards the unburnt-fuel side of the observed flame sheet, thus confirming the structure indicated by the temperature

profiles. The isovels of component $V_z$, on the other hand, show clearly the very different velocities between the entraining reactant stream and the refracted oxidant stream. In the mixing region between these streams very large gradients of velocity prevail but in the stabilising region at the base of the flame sheet the magnitudes of velocity are similar to those associated with the pre-mixed flame concept of normal burning velocity, $S_u$ ($S_{u,max}$ = 42 $cms^{-1}$ for a methane-air mixture - Gunther and Janisch (1972)). The gradients of velocity in this latter region do not vary much with distance up the flame sheet.

The dividing streamline between the entraining reactant stream and the refracted oxygen stream, as shown in Fig. 9, lies well towards the unburnt-fuel side of the observed flame sheet. Admixture of the two streams therefore occurs by molecular diffusion of the reactant across the stream tubes and thermal convection and molecular diffusion of the oxidant stream towards the flame sheet. This is in marked contrast to the situation for fuel-lean and stoichiometric flames where the strong back pressure of the flame causes the dividing stream line to lie well towards the

secondary-air side of the base of the flame sheet (Fristrom and Westenberg). The general behaviour of flow fields under various mixture compositions has been discussed recently by Melvin, Moss and Clarke. Their observation of increasing displacement of the dividing streamline away from the flame sheet towards the unburnt mixture with increasing richness of the fuel gas is supported by the work of this thesis. It is interesting, if not unexpected, to note that the limiting fuel-gas composition above which the oxidant emanates predominantly from the refracted ambient stream (e.g. neat gas flames) and below which the oxidant emanates predominantly from the fuel stream (e.g. stoichiometric flames) occurs around the upper limit of inflammability. Thus the oxidant stream is refracted only when the fuel-mixture contains insufficient oxygen for combustion and this situation strongly obtains in the flames of initially separated reactants studied in this thesis.

But, perhaps the most significant result, shown in Fig. 9, concerns the magnitude of the velocity at the base of the flame sheet. Increasing the supply of reactant from 142 $mls^{-1}$ to 650 $mls^{-1}$ causes the magnitude of the resultant velocity at the base of the

flame sheet to increase from 23.5 $cms^{-1}$ to only 33.5 $cms^{-1}$. The low power dependence, here, of velocity on flow rate of approximately $\frac{1}{4}$, has been similarly observed by others where convection is the dominant physical process. Clearly, very small changes in the aerodynamic pattern at the base of the flame sheet may greatly enhance the upper stability limit of diffusion flames.

Although convection would seem to account quite well for the magnitude of the velocity at the base of the flame sheet, the direction of flow is strongly influenced by the entraining reactant stream. Increasing the supply of reactant causes an increase in the amount of refraction of the oxidant stream with respect to the flame sheet. Clearly, this engenders an increase in the flux of oxidant into the base of the flame sheet.

Thus, the effect of increasing the supply of reactant is seen as increasing both the magnitude of the velocity and the inward flux of oxidant at the base of the flame sheet. These two effects lend support to the phenomenological picture of lift put forward by Robson and Wilson. With increasing supply

of reactant, the increase in the inward flux of oxidant requires a similar increase in the flux of reactant to maintain stoichiometry. Since the dividing streamline between the entraining reactant stream and the refracted oxygen stream lies well towards the unburnt-fuel side of the observed flame sheet (Fig. 9), an increase in the flux of reactant requires a steepening of the concentration gradient of the reactant and this compels the flame to contract. Thus, there are two inter-related effects both of which can be seen as creating an unfavourably high velocity field at the base of the flame. Increasing the supply of reactant increases the velocity at the base of the flame sheet and stoichiometry necessitates that the flame moves inwards to a position where the velocity is higher still. On this basis many previous workers (e.g. Robson and Wilson, Bellis) have cited velocity as the controlling parameter affecting the phenomenon of lift of diffusion flames. Certainly, it is well understood that in pre-mixed flames the reactants can be supplied only at a limited rate which is expressed by the burning velocity. Clearly, for these flames, since the reactant supply emanates totally from the

mass flow (Smith), stability is predominantly controlled by the velocity at the flame base. But in the case of the diffusion flames, studied in this thesis, the reactant and oxidant interdiffuse to form the reaction zone and again, as suggested by Spalding, there should be a limit to the rate at which they can be supplied without extinguishing the flame. Thus, for diffusion flames, the rate of supply of reactant and oxidant is governed not only be the mass flow but also the diffusive flow. Clearly whether or not the mechanism of flame lift can be considered as predominantly due to a velocity effect will depend on the relative contributions to the supply of reactant and oxidant from the mass flow and the diffusive flow. These aspects are discussed later in the thesis in section 1.5.4.

1.5.3. Species Profiles

The distributions of species, for the two flames, were obtained using micro-probe sampling and analysis by gas chromotography as outlined in section 1.3.4. Samples were taken from seven levels enclosing an area both below and above the burner port and the results plotted out in the form of isopleths of each of the

major stable species. Those for the flame burning 142 $mls^{-1}$ are shown in Figs. 10 to 16 whilst those for the flame burning 650 $mls^{-1}$ are shown in Figs. 17 to 23.

The patterns for methane (Figs. 11 and 18) show that combustion takes place over a broad flame sheet in a region of extremely low fuel concentration. For both flames, the concentration, by volume, of methane at the extreme base of the flame sheet is around 2%. The significance of this point will be discussed later in the thesis. Figs. 11 and 18 show also the existence of substantial concentrations of methane at levels well below the burner port. Thus, not only is methane transferred, by molecular diffusion, in a radially outward direction, but also vertically downwards towards the inward convected oxidant stream. The isopleths of oxygen (Figs. 12 and 19) show the inner edge of the observed flame sheet as a sink for oxygen in an oxygen field that penetrates well to the unburnt-fuel-side of the flame sheet. Clearly, oxygen reaches the flame sheet both from the low temperature region between the base of the flame sheet

and the burner wall as well as from the oxidant side. The isopleths show a weak gradient of concentration towards the flame sheet from the inside as well as a strong gradient from the outside. Similar patterns for diffusion flames of methane have been reported both by Smith and Gordon and by Robson and Wilson. The isopleths for the intermediate species, hydrogen and carbon monoxide, (Figs. 14, 16, 21 and 23) are much as expected. Both show loci of the points of maximum concentration well to the unburnt-fuel side of the inner edge of the visible flame sheet. On the other hand, those for the final products, water vapour and carbon dioxide, (Figs. 10, 15, 17 and 22) show loci of points of maximum concentration within the visible flame sheet itself. For both flames examined, results show that the inward refracted oxidant stream is considerably diluted by the outward diffusion of final products, water vapour and carbon monoxide. This point will be examined in a subsequent section.

The discovery of extremely low fuel concentrations at the base of a diffusion flame sheet is not new. Bellis, working on laminar flames of methane and ethylene,

found concentrations of fuel as low as 2% by volume whilst Robson and Wilson, working on methane flames have reported concentrations of fuel of 2.1% by volume. Although such low concentrations lie well below the conventional lower limit of inflammability (5% by volume of methane in air), this applies only to a static binary mixture at room temperature. The base of a laminar flame is a relatively complex multi-component mixture of inerts and reacting species at high temperatures. On the one hand, the presence of inerts - nitrogen, water vapour and carbon dioxide - would be expected to reduce the inflammability range whilst on the other, the presence of intermediate species - hydrogen and carbon monoxide - and unstable species - free radicals and ions - would be expected to extend the lower limit of inflammability. Additionally, high temperatures would be expected to extend the lower conventional limit of inflammability (Craven and Foster). Nevertheless, the effects discussed above are somewhat difficult to quantify and whilst there is some evidence to suggest that ratios of oxidant to reactant in excess of the conventional lower limit of inflammability would be capable of supporting

combustion, the extent to which this reasoning applies is not at all clear. Equally, it could be argued that the ratios of oxidant to reactant at the base of the flame sheet are so lean that they would not be expected to support combustion without some additional factor coming into play.

In an attempt to shed some light on this uncertainty, the relative proportions of reactant, oxidant and inerts, along the inner edge of the visible flame sheet, have been examined in some detail. The results, given in table 1, show clearly that, for the flame burning 142 $mls^{-1}$, with increasing distance above the visible base of the flame sheet, the ratio of oxidant to reactant changes rapidly from a fuel-lean value of 4.1 at the base to what is almost certainly a fuel-rich value of 0.1 at a level 2 mm above the burner port. Between these extremes the ratio of oxidant to reactant would seem to pass through a value close to stoichiometric proportions at a level of approximately 0.1 mm. A similar pattern is observed for the flame burning 650 $mls^{-1}$. In this case the ratio of oxidant to reactant passes through a value close to stoichiometric proportions at a level approximately 0.6 mm above the

| REACTANT SUPPLY $ml s^{-1}$ | LEVEL W.R.T. BURNER PORT mm | SPECIES CONCENTRATION (mole %) | | | | | | | | | RATIO OF OXIDANT TO REACTANT | $\sum x_i$ TOTAL |
|---|---|---|---|---|---|---|---|---|---|---|---|---|
| | | $CH_4$ | CO | $H_2$ | $\sum x_i$ REACT-ANTS | $N_2$ | $H_2O$ | $CO_2$ | $\sum x_i$ INERTS | $O_2$ | | |
| 142 | VISIBLE FLAME BASE | 2·0 | 1·0 | 0·3 | 3·3 | 73 | 7·5 | 2·5 | 83·0 | 13·5 | 4·1 | 99·8 |
| 142 | 0 | 4·5 | 2·1 | 1·1 | 7·7 | 68 | 15·5 | 5·0 | 88·5 | 5·0 | 0·7 | 101·2 |
| 142 | 1 | 4·8 | 3·2 | 2·3 | 10·3 | 65 | 18·2 | 6·4 | 89·6 | 0·8 | 0·1 | 100·7 |
| 142 | 2 | 5·0 | 3·2 | 2·8 | 11·0 | 64 | 18·2 | 6·5 | 88·7 | 0·8 | 0·1 | 100·5 |
| 650 | VISIBLE FLAME BASE | 2·0 | 2·0 | 0·5 | 3·5 | 74·5 | 9·0 | 3·2 | 86·7 | 11·0 | 3·4 | 101·2 |
| 650 | 1 | 4·0 | 2·8 | 2·0 | 8·8 | 69 | 15·2 | 6·1 | 90·3 | 1·8 | 0·5 | 100·9 |
| 650 | 2 | 4·5 | 3·4 | 3·0 | 10·9 | 66 | 17·2 | 6·5 | 89·7 | 0·8 | 0·4 | 101·4 |

TABLE 1. DISTRIBUTION OF SPECIES ALONG INNER EDGE OF VISIBLE FLAME SHEET

burner port. The reactant, here, is considered as comprising the species carbon monoxide, hydrogen and methane whilst the oxidant comprises oxygen only. Depending on the relative proportions of the individual reacting species the ratio of oxidant to reactant for complete combustion would be expected to lie between the extremes for the individual species, i.e. 0.5 and 2.0. Although the above analysis is clearly a gross simplification, it would suggest that the anchoring point is not, as is widely held (Bellis, Robson and Wilson), at the extreme base of the flame sheet, but at a distance somewhat above the base region. Indeed, whether or not the phenomenon of flame lift is reaction rate limited or mass flow limited, a stoichiometric region would conceivably act as the anchoring point of the flame. In the case of a reaction rate limitation, Spalding has suggested that the maximum permitted fuel consumption rate per unit area should approximate to that obtaining in a pre-mixed stoichiometric flame. Any other mixture composition would tend to lower flame temperature thereby engendering a rapid reduction in reaction rate. In the case of a mass flow limitation, the high

reaction rate associated with stoichiometric mixtures would allow the flame to hold its own against greater mass flows than other mixture compositions. Thus, in diffusion flames where the diffusive flux of reactant remains relatively invariant with distance above the flame base, a region of stoichiometric mixture composition would be expected to be the anchoring point of these flames. Furthermore, such a stabilising region could conceivably be thought of as a continuous ignition source providing a diffusive flux of highly reactive active species to regions both above and below the anchoring point. The diffusive flux of active species to the base region of the flame sheet would thus account for combustion well below the conventional lower limit of inflammability. Whether or not the above mechanism is likely to predominate may be indicated by the distributions of rate of reaction and rate of heat release that will be evaluated shortly.

The effect, on the distribution of species, of increasing the supply of reactant to the burner can be seen from Table 1. Whilst the concentrations of methane, at the extreme base of the flame sheet, are similar for both the flames examined (2% by volume),

increasing the supply of reactant causes a marked fall in the concentration of oxidant and a corresponding rise in the concentration of inerts. There is, therefore, a progressive dilution of the extreme base of the flame sheet by inert products of combustion. This would absorb heat, otherwise available for combustion, and reduce the local rate of reaction. Clearly, this would be expected to adversely affect local flame stability. On the other hand, the ratio of oxidant to reactant decreases from 4.1 to 3.4, with increasing supply of reactant to the burner, and is evidently tending towards stoichiometric proportions. This latter effect would be expected to increase the local rate of reaction, thereby enhancing flame stability. However, since the flame temperature at the extreme base of the flame burning 650 $mls^{-1}$ is higher by some 300°K than that at the base of the flame burning 142 $mls^{-1}$ (Figs. 3 and 4), it would seem that the effect, on stability, of progressive dilution by products of combustion is more than offset by the increasing richness of the mixture towards stoichiometric proportions. Further support to the trend of increasing richness of the combustible mixture at the extreme base of the

flame sheet, with increasing supply of reactant, is provided by the data reported by Robson and Wilson. These workers studied a laminar diffusion flame of methane burning extremely close to the lift stability limit which understandably restricted their detailed analysis of flame structure. Sampling of the flame gases at the extreme base of the flame sheet yielded concentrations of methane and oxygen of 2.1% and 5.3% by volume, respectively. Although analyses for carbon monoxide and hydrogen were not carried out by Robson and Wilson, the detected ratio of oxidant to reactant of 2.6, for a flame close to the lift stability limit, is evidently close to stoichiometric propertions. Had concentrations of carbon monoxide and hydrogen been analysed, the above figure would have been even lower. Thus, there seems little doubt that, with increasing supply of reactant to the burner, the extreme base of the flame sheet becomes progressively fuel-rich and tends increasingly towards stoichiometric proportions. Clearly, this would be expected to enhance localised flame stability.

But perhaps more important are the effects of increasing the supply of reactant on the probable

anchoring point of the flame. Here, a rather different pattern emerges. From table 1 it can be shown that the stoichiometric stabilising point lies at a level approximately 0.1 mm above the burner port for the flame burning 142 $mls^{-1}$ and at a level of approximately 0.6 mm for the flame burning 650 $mls^{-1}$. The concentration of inerts, i.e. nitrogen, water vapour and carbon dioxide, is seen to vary little between these levels remaining at around 88% by volume. In contrast to the extreme base of the flame sheet, at the probable anchoring point of the flame there is little increased dilution with increasing supply of reactant. Here, mixtures of roughly stoichiometric proportions are consumed in concentrations of inerts which are roughly similar for the two flames. But, as was shown in section 1.5.2., the velocity fields in this region are markedly different. Thus, in considering the phenomenon of flame lift, the anchoring point, which, as established earlier, lies somewhat above the flame base, may be considered as a stoichiometric zone which moves progressively inwards and upwards into regions of higher mixture velocity, as

the supply of reactant is increased, until finally the flame moves downstream to extinction. The results of probe sampling of the stable species would seem to confirm the earlier picture that the phenomenon of flame lift is associated with an increase in velocity at the flame base. However, at this stage, it is not at all clear whether the mechanism that leads to flame lift is mass flow limited or diffusive flow limited.

The previous discussion has shown that the accessible parameters themselves - namely temperature, velocity and material species - provide a valuable picture of the structure of the stabilising region of laminar diffusion flames as well as elucidating the phenomenon of flame lift. However, in order to exploit fully the large volume of experimental data, a full structural analysis in terms of the fluxes of heat energy and material species and the rates of creation of heat energy and material species has been carried out. The formal equations relating these structural parameters with the accessible flame parameters were set out in section 1.4.

1.5.4. Species Fluxes

Species fluxes were estimated in terms of the individual contributions from convection and molecular diffusion according to equation (5). The derivative terms associated with the diffusive flux contributions were evaluated using the numerical technique of spline fitting. The application of this technique to the method of calculating the flux terms is discussed more fully in section 1.5.5. Fluxes of the six stable species were estimated at two levels in each flame as a preliminary to evaluating rates of reaction. Typical results for oxygen are shown in Figs. 24 and 25 for the flame burning 142 $mls^{-1}$, and in Figs. 26 and 27 for the flame burning 650 $mls^{-1}$. Figs. 24 and 26 give the flux profiles at a level which cuts the stabilising region whilst Figs. 25 and 27 give corresponding profiles at a level somewhat above the flame base.

Considering first the relative contributions of the individual terms, it can be seen that on the oxidant side of the flame sheet the contributions from thermal convection and molecular diffusion, in each of the component directions, combine rather than compete,

to provide the total flux of oxidant. On the extreme unburnt-fuel side of the flame sheet the dominant feature is the strong vertical convective term associated with the entraining methane stream. But perhaps the most significant feature of the results concerns the relative contributions of convection and molecular diffusion in the visible flame sheet itself where the fluxes of the various species are rapidly changing. For the flame burning 142 $mls^{-1}$, at z=0, y=2 mm, which corresponds closely to the location of the stoichiometric stabilising region, the flux of oxygen, estimated as the summation of the bulk flow and diffusion terms, is 13.5 x $10^{-4}$ g $cm^{-2}s^{-1}$ of which 9.3 x $10^{-4}$g $cm^{-2}s^{-1}$ originates from the diffusion term. Thus, at the probable anchoring point of the flame, the process of molecular diffusion supplies not only the total flux of methane but also 69% or more of the flux of oxygen. A similar picture emerges from the base of the flame burning 650 $mls^{-1}$ except that the percentage contribution is even greater. At z=0.5 mm, y=1.7 mm, which corresponds closely to the location of the stoichiometric region, 75% of a total flux of

oxygen of 21.8 x $10^{-4}$ g $cm^{-2}s^{-1}$ originates from the contribution of molecular diffusion. Thus, the results of this thesis would suggest that, for diffusion flames, the limiting rate of supply of reactant and oxidant into the stabilising region is governed not be the mass flow, as in pre-mixed flames, but predominantly by mass transfer by molecular diffusion across the stream tube boundaries.

The foregoing discussion suggests strongly that the increase in velocity at the flame base, associated with an increasing supply of reactant, (Fig. 9) is to some extent incidental to the phenomenon of flame lift, extinction being limited by chemical reaction rate rather than by the mass flow. The evidence provided by this thesis, as to the stabilising mechanism of diffusion flames, is, therefore, in contradiction of the mechanisms proposed by recent investigators (Robson and Wilson, Bellis) in which the mass flow at the flame base was considered to be the limiting factor in controlling the phenomenon of flame lift. It should be pointed out also that although in the structure of an established diffusion flame the rate of diffusion is the rate determining process

(Gaydon and Wolfhard) the phenomenon of extinction is limited by chemical reaction rate.

It is interesting also to contrast the oxygen fluxes of the flames of this thesis against those of earlier investigators. In the case of the flame burning 142 $mls^{-1}$ the total oxygen flux into the stoichiometric region of the flame was $13.5 \times 10^{-4}$ g $cm^{-2}s^{-1}$ or 0.15 g mol $cm^{-2}h^{-1}$ whereas the corresponding flux for the flame burning 650 $mls^{-1}$ was $21.8 \times 10^{-4}$ g $cm^{-2}s^{-1}$ or 0.25 g mol $cm^{-2}h^{-1}$. However, in order to permit full use of the experimental techniques associated with a flame structure study the flame burning 650 $mls^{-1}$ was stabilised some way from the lift stability limit and hence the figure of 0.25 g mol $cm^{-2}h^{-1}$ in no way represents a limiting factor. However, Robson and Wilson have estimated the total oxygen flux into the base of a methane diffusion flame operating somewhat closer to the lift stability limit as 0.36 g mol $cm^{-2}h^{-1}$. Clearly, there would seem to be not only a reasonable degree of consistency between these investigations but also a very definite trend towards a limiting flux beyond which chemical reaction cannot keep pace with the supply of fuel and oxidant and the reaction abruptly ceases. According

to Spalding and Jain the maximum fuel consumption rate per unit area of a counterflow diffusion flame should be equal to 0.89 times the rate in a laminar stoichiometric pre-mixed flame. This would represent a limiting oxygen flux of 0.66 g mol $cm^{-2} h^{-1}$, although this figure should be treated with some caution since in a counter-flow diffusion flame on which this calculation was based the oxygen flux originates not only from molecular diffusion but also, to some extent, from forced convection. Nevertheless, although the flame structure studies carried out in this thesis have, of necessity, been restricted to flames operating some way from the lift stability limit, when taken in conjunction with earlier work, a picture emerges of a maximum fuel consumption rate for diffusion flames dependent predominantly on mass diffusion rather than mass flow, and equal approximately to the rate in a laminar stoichiometric pre-mixed flame.

With increasing distance above the stabilising region the results, given in Figs. 24 to 27, indicate that the gradients of the oxygen flux become somewhat shallower. This is shown also in Figs. 28 and 29 where the results for the diffusive flux contribution have been plotted, throughout the stabilising region, as

species flux vectors. Each vector represents, in addition to the direction of material flow, the magnitude of the flux at the end of its tail according to the scale shown. Figs. 28 and 29 show also that molecular diffusion would appear to contribute to a localised region of favourable mixture composition situated just above the flame base, supporting the concept, discussed in section 1.5.3., of a localised stoichiometric stabilising region. Moreover, it would be expected also, from the results of this section, that the rates of reaction, evaluated from the species flux profiles, will decrease with increasing distance above the stabilising region.

1.5.5. Heat Energy Fluxes

The fluxes of heat energy, for the two flames, were calculated in terms of the individual contributions from convection, molecular diffusion and thermal conduction, in the component directions y and z, according to equation (7). Results for seven levels, encompassing the stabilising region of the flame, are shown in Figs. 30 to 36 for the flame burning 142 $mls^{-1}$ and in Figs. 37 to 43 for the flame burning 650 $mls^{-1}$.

It was mentioned earlier that fluxes of material species or of heat energy are difficult to evaluate quantitatively since they involve a number of derivative terms. For this reason some considerable time was spent in cross-checking the results obtained from the numerical technique of spline fitting with those from a simple graphical method. A typical example of the cross-checking analysis for the conductive heat flux terms is shown in table 2 at a level z=1.0 mm in the flame burning 650 $mls^{-1}$. Intercomparison of the fluxes evaluated graphically with those from spline fitting shows, in general, good agreement demonstrating the advantageous differentiation characteristics of spline fitting. Corresponding analyses were carried

out also for the diffusive fluxes of material and heat energy and again surprisingly good agreement was found between the two methods. A typical example of the method of evaluating the diffusive fluxes is shown in table 3 for a single species, water vapour. The analysis was repeated for the remaining species in order to evaluate the total heat flux. The whole process was then repeated at 28 points throughout the stabilising region of the flame.

The results, given in Figs. 30 to 43, illustrate the relative importance of the three physical processes - convection, molecular diffusion and thermal conduction - in determining the resultant heat transfer pattern in the stabilising region of each flame. Considering first the y-flux components, it can be seen that, on the unburnt-fuel side of the flame sheet, the contribution from conduction represents a negative (inward) flux whilst the contribution from molecular diffusion represents a positive (outward) flux. In this latter case, methane, of relatively high enthalpy, is diffusing outwards against the inward diffusive flow of low enthalpy oxygen and products of combustion, the net effect being a positive flux from the unburnt-gas

| $y$ | T | $\lambda \times 10^6$ | $-\frac{\partial T}{\partial y}$ | $-\frac{\partial T}{\partial z}$ | $-\lambda\frac{\partial T}{\partial y}$ | | $-\lambda\frac{\partial T}{\partial z}$ | |
|---|---|---|---|---|---|---|---|---|
| mm | °k | cal $cm^{-1}$ $s^{-1}$°$k^{-1}$ | °k $cm^{-1}$ GRAPHICALLY | °k $cm^{-1}$ | cal $cm^{-2}s^{-1}$ GRAPH | SPLINE | cal $cm^{-2}s^{-1}$ GRAPH | SPLINE |
| 0·4 | 393·5 | 108·3 | −5,750 | −0,650 | −0·62 | −0·64 | −0·07 | −0·11 |
| 0·8 | 866·2 | 210·2 | −18,200 | 0 | −3·83 | −3·85 | 0·00 | −0·03 |
| 1·2 | 1526·5 | 310·7 | −11,100 | −0,350 | −3·45 | −3·47 | −0·11 | −0·20 |
| 1·6 | 1837·2 | 326·7 | −3,100 | −2,200 | −1·01 | −1·03 | −0·72 | −0·81 |
| 2·0 | 1744·3 | 289·2 | 7,100 | −4,900 | 2·05 | 2·06 | −1·42 | −1·48 |
| 2·4 | 1369·1 | 225·2 | 10,050 | −6,050 | 2·26 | 2·25 | −1·36 | −1·34 |
| 2·8 | 956·6 | 161·5 | 10,450 | −6,600 | 1·67 | 1·73 | −1·01 | −1·09 |
| 3·2 | 614·6 | 110·5 | 7,300 | −5,100 | 0·81 | 0·85 | −0·56 | −0·53 |
| 3·6 | 371·4 | 74·7 | 3,300 | −2,100 | 0·25 | 0·24 | −0·16 | −0·16 |
| 4·0 | 301·0 | 63·4 | 0,500 | −0,200 | 0·03 | 0·04 | −0·01 | −0·01 |

TABLE 2. INTERCOMPARISON OF CONDUCTIVE HEAT FLUXES EVALUATED GRAPHICALLY AND FROM SPLINE FITTING

(METHANE FLOW RATE 650 $mls^{-1}$, LEVEL Z = 1·0 mm.)

| i | j | $m_j$ | $D_{\ddot{u}}$ | $\frac{\partial x}{\partial y}_{\ddot{u}}$ | $\frac{\partial x}{\partial z}_j$ | $m_j D_{\ddot{u}} \frac{\partial x}{\partial y}_j$ | $m_j D_{\ddot{u}} \frac{\partial x}{\partial z}_j$ | $\frac{Nm_i}{\sum_k m_k X_k}$ | $\bar{C}_p(T-T_o)$ | $F_{H,DIF_y,i}$ | $F_{H,DIF_z,i}$ |
|---|---|---|---|---|---|---|---|---|---|---|---|
| | | g | $cm^2 s^{-1}$ | $cm^{-1}$ | $cm^{-1}$ | g cm $s^{-1}$ | g cm $s^{-1}$ | $cm^{-3}$ | cal $g^{-1}$ | cal $cm^{-2} s^{-1}$ | cal $cm^{-2} s^{-1}$ |
| $H_2O$ | $CH_4$ | 16·04 | 3·339 | 0·00 | 0·00 | 0·000 | 0·000 | $7·991 \times 10^{-5}$ | 343·1 | 0·86 | −1·31 |
| | $O_2$ | 32·00 | 1·703 | 0·68 | −1·07 | 37·057 | −58·311 | | | | |
| | $N_2$ | 28·02 | 1·933 | 0·26 | −0·32 | 14·082 | −17·332 | | | | |
| | $H_2$ | 2·01 | 26·145 | −0·03 | 0·04 | −1·577 | 2·102 | | | | |
| | $CO_2$ | 44·01 | 1·250 | −0·17 | 0·38 | −9·352 | 20·905 | | | | |
| | CO | 28·01 | 1·938 | −0·16 | 0·07 | −8·685 | 3·800 | | | | |
| | | | | | $\sum_j$ | 31·525 | −48·836 | | | | |

$F_{H,DIF}$ CALCULATED FROM $\sum_i \left( \frac{Nm_i}{\sum m_k X_k} \sum_{j, j \neq i} m_j D_{\ddot{u}} \text{ grad } X_j \right) \bar{C}_{p,i}(T-T_o)$

TABLE 3 EXAMPLE OF METHOD OF CALCULATION OF $F_{H,DIF}$

(METHANE FLOW RATE 650 $mls^{-1}$, y = 1·8 mm., z = 0·0 mm.)

side towards the visible flame sheet. Moreover, the results show that this positive diffusive flux contributes as much as 20% to the total heat flux along the inner edge of the visible flame sheet. Clearly, although the contribution to the total heat flux from molecular diffusion is small, compared with those from convection and thermal conduction, it is by no means insignificant. In addition, it can be seen that, on the oxidant side of the flame sheet, the positive flux due to thermal conduction is almost exactly balanced by the negative convective flux. In other words most of the heat conducted outwards is returned by the bulk flow to its point of origin in the flame sheet.

Considering now the z-flux components, it can be seen that on the unburnt-fuel side of the flame sheet there is a considerable degree of positive (upward) convection in the region close to the flame axis. This results in much of the heat liberated at the reaction zone being conveyed, via the central stream, to higher regions of the flame. Also, there is some downward diffusion of methane and products of combustion against the oxygen stream although the net heat energy conveyed by this process is small. This

downward diffusion results principally from the relatively high enthalpies of methane and water vapour compared with that of oxygen. As was the case for the y-flux components, the positive flux on the oxidant side of the flame sheet is almost exactly balanced by the negative flux due to conduction. Thus, at the extreme base of the flame, heat energy is used to pre-heat the inward flow of oxygen rather than be lost to the immediate surroundings.

Returning now to the diffusive fluxes, results show that the y- component of the positive diffusive heat flux contributes as much as 20% of the total heat flux along the inner edge of the visible flame sheet. Thus although, as inferred previously, the heat flux contribution from molecular diffusion is minor compared with those from thermal conduction and convection it is by no means insignificant. In this context it is interesting to note that the flame structure analysis of Pandya and Weinberg on a $C_2H_4$-$O_2$-$N_2$ counterflow diffusion flame ignores the possible contribution to heat transfer by molecular diffusion. Indeed, a closer examination of Figs. 30 to 43 of the results of this thesis shows that whilst

the gradients of the z-components of the diffusive heat fluxes are everywhere relatively small, and would not therefore be expected to contribute appreciably to the rates of heat release, those of the y-components show significant positive contributions on the unburnt-fuel side as well as significant negative contributions on the oxidant side of the flame sheet. This positive (exothermic) contribution to the heat release rate profile from molecular diffusion is of particular importance since there has been some debate recently as to whether methane decomposes due to pyrolysis-type reactions which would result in a net absorption of heat on the unburnt-fuel side of the flame sheet. In this context, it is interesting to note that in the only structural analyses of diffusion flames carried out to date, both Pandya and Weinberg, and Tsuji and Yamaoka, who ignored the contribution from molecular diffusion, found evidence of heat absorption on the unburnt-fuel side of the reaction zone, whilst Thomas, who included diffusive contributions, found no evidence of heat absorption. This aspect will be discussed further in section 1.5.7.

The previous discussion has centred on the relative importance of the various physical processes in effecting transfer of heat energy at the base of the flame. But, in order to show clearly the resultant heat flux pattern throughout the stabilising region of each flame, the results, given in Figs. 30 to 43, have been replotted in terms of heat flux vectors as shown in Figs. 44 and 45. Each vector represents, in addition to the direction of heat flow, the magnitude of the heat flux at the end of its tail according to the scale in the lower right hand corner of each figure. It can be clearly seen that, as mentioned previously, there is considerable transfer of heat energy from the flame base towards the upper regions of the flame. The vector patterns of Figs. 44 and 45 provide, also, direct intercomparison of the magnitudes of the heat fluxes lost to the burner head. At z=0.0 mm, corresponding to the level of the burner port, the local heat flux towards the burner head from the flame burning 142 $mls^{-1}$ is approximately 5 cal $cm^{-2}s^{-1}$ whereas the corresponding figure for the flame burning 650 $mls^{-1}$ is only about 2 cal $cm^{-2}s^{-1}$.

Thus, increasing the rate of supply of methane results in considerably less heat being lost from the system towards the burner head. But perhaps the most significant point to emerge from the results of fluxes of heat energy concerns the relative importance of the three major physical processes - convection, molecular diffusion and thermal conduction - in determining the resultant heat flow pattern. By comparing the heat flux patterns of Figs. 44 and 45 with the corresponding patterns of the isotherms (Figs. 3 and 4) it can be seen that, for the two flame systems examined, the heat flow, in the region encompassing the anchoring point of the flame, takes up an orientation approximately perpendicular to the isotherms. It would seem, therefore, that conduction of heat energy from the flame sheet to both the ambient surroundings and the unburnt-gas stream is the dominant heat transfer process in the region encompassing the anchoring point of the flame. Furthermore, it might reasonably be expected that conduction would be an important factor in shaping the distribution of heat release rates in the region of the anchoring point of each flame. This aspect is discussed in section 1.5.7.

1.5.6. Reaction Rates

Molar reaction rates of the six major stable species in the flames were estimated in terms of the individual contributions from convection and molecular diffusion according to equation (6). The derivative terms were evaluated graphically from the associated species flux profiles. Results, in the form of net molar reaction rates, are given in Figs. 46 to 49 at two levels in each flame. Figs. 46 and 48 give the profiles of the various reaction rates at a level which cuts through the stabilising region for flames burning 142 $mls^{-1}$ and 650 $mls^{-1}$ respectively. Figs. 47 and 49 give corresponding data at a level well above the anchoring point of each flame. These profiles are of considerable qualitative interest.

It can be seen from Figs. 46 and 48 that the molar rates of appearance and disappearance of the various species, at the base of each flame, are qualitatively similar to those obtaining in pre-mixed methane/oxygen flames (Fristrom and Westenberg). The flame may be considered to be composed of three spatially distinct regions. In the region adjacent

to the flame axis the transport of material by molecular diffusion and of heat energy by thermal conduction results in large changes of species concentrations and temperature but almost no reaction takes place in this region. In the central region, the main reaction zone, methane and oxygen combine in roughly stoichiometric proportions to form intermediate products (hydrogen and carbon monoxide) and final products (water vapour and carbon dioxide). In the third region, on the oxidant side of the main reaction zone, the intermediates, hydrogen and carbon monoxide, are oxidised to water vapour and carbon dioxide respectively. However, in contrast to the pre-mixed flames of Fristrom and Westenberg, where oxidation of carbon monoxide occurs out to the hot boundary, the molar reaction rates decrease rapidly as the temperature falls off in this region. Aside from this last point, however, the reaction rate profiles, at a level which cuts the anchoring region of the flame, are qualitatively similar to those for a stoichiometric methane-air flame, thus confirming the concept of a localised stoichiometric stabilising region discussed in section 1.5.3.

Higher up the flame a rather different pattern emerges. Here, as shown in Figs. 47 and 49 the maximum rate of disappearance of oxygen is displaced to the air side of that of methane. This confirms the evidence provided by the species profiles that the mixture becomes progressively fuel-rich with increasing distance above the flame base.

An equally significant point concerns the width of the reaction zone. For the levels examined, the width of the reaction zone lies between 1.8 mm and 2.6 mm indicating that combustion takes place over a relatively large proportion of the available mixing zone between the entraining methane stream and the refracted oxidant stream. This conclusion is at variance with the early work of Burke and Schumann and other subsequent investigators who considered, principally for mathematical convenience, that combustion occurs at an infinitesimally thin zone where the rates of supply of oxidant and reactant are in stoichiometric proportions. The results presented here clearly indicate a relatively broad reaction zone with stoichiometric combustion confined to a small localised region somewhat above the flame base.

1.5.7. Heat Release Rates

Volumetric heat release rates, throughout the stabilising region of each flame, were determined in terms of the individual contributions from convection, molecular diffusion and thermal conduction according to equation (8). The derivative terms were evaluated from the associated flux profiles. Results for five levels throughout the stabilising region are given in Figs. 50 to 54 for the flame burning 142 $mls^{-1}$ and in Figs. 55 to 59 for the flame burning 650 $mls^{-1}$.

Once again the results illustrate the relative importance of the three physical processes in determining the resultant heat release rate pattern. It can be seen that the major proportion of the heat, liberated by chemical reaction, arises from the contribution of the y-component of conduction. This means that heat leaves the reaction zone principally through conduction processes. Indeed, the conduction-y term accounts, on average, over the levels investigated, for 58% of the maximum total heat release rate in the case of the flame burning 142 $mls^{-1}$ and as much as 74%, on average, in the case of the flame burning 650 $mls^{-1}$. This conclusion supports the assumptions made in

earlier theoretical work where convection of heat energy and reactants in the reaction zone are ignored. Furthermore, since the bulk of the heat release arises principally from changes in the conduction flux profile, which in turn depend on changes in the temperature profile, it may be possible to estimate the rates of heat release from the temperature profile alone. This suggestion will be discussed later in the thesis.

Whilst these results give a reasonable indication of the resultant heat release rate pattern throughout the stabilising region, the picture is not so clear on the unburnt-fuel-side of the flame. The reason is not hard to see since, as shown in Fig. 55, the contributions from the conduction-y and convection-z terms are both large and in competition, and hence the resultant profile is prone to error. Additional difficulties arise in evaluating the convection-z term since, as was mentioned in section 1.5.2., very large gradients of velocity are present in the mixing region between the entraining methane stream and the refracted oxidant stream. For these reasons, the profiles of total heat release rate were not evaluated in the region immediately adjacent to the burner axis.

Nevertheless an important result which does emerge from the data, and which substantiates the evidence of the heat flux data, is the fact that the contribution from molecular diffusion provides a definite exothermic contribution to the total heat release rate profile in this region. This is particularly true for levels well above the extreme flame base (Figs. 57, 58 and 59) where the maximum contribution from the y-component of molecular diffusion may be as much as 25% of the total heat release rate peak, and considerably more as a proportion of the total heat release rate in the mixing region between the combustible streams. Clearly, this conclusion is at variance with the assumptions of both Pandya and Weinberg, and Tsuji and Yamaoka who ignored the contribution from molecular diffusion. In both these cases the systems studied were neat gas flames in which small negative heat release rate valleys, found in the mixing region between the combustibles, were attributed to pyrolysis of the fuel gas. Although such an explanation is not unreasonable, in view of the fact that the contribution from molecular diffusion would oppose the existence of negative heat

release rates, the amount of heat absorption, if any, is likely to be very small indeed.

The evaluation of the heat release rate pattern on the oxidant side of the flame sheet presents fewer problems. Here the contributions from conduction and convection compete to produce a gradual tailing-off in the total exothermic heat release rate profile whilst the contribution from molecular diffusion becomes negligible. This tailing-off in the total heat release rate profile would be expected since it was observed earlier that the maximum molar rates of disappearance of the intermediates, hydrogen and carbon monoxide, were displaced well to the oxidant side of the reaction rate profile for oxygen.

In order to show the pattern of total heat release rates, throughout the stabilising region of each flame, the results given in Figs. 50 to 59 have been replotted as iso-heat release rate lines. Those for the flame burning 142 $mls^{-1}$ are shown in Fig. 60 whilst those for the flame burning 650 $mls^{-1}$ are shown in Fig. 61. Also shown in these figures, as a broken line, is the locus of points of maximum heat release. A number of

interesting features emerge from these results.

Perhaps the first point to note concerns the width of the reaction zone. For both flames, the overall width, considered as the separation of the 10 cal $cm^{-3}s^{-1}$ iso-heat release rate lines, is approximately 2 mm. This confirms the conclusion of section 1.5.6. that reaction takes place over a relatively wide proportion of the available mixing zone between the combustibles. Moreover, as a consequence of the relatively broad reaction zone, there seems little doubt that diffusion flames at atmospheric pressure do offer an adequate flame thickness for the type of structural analysis attempted in this thesis. It should be pointed out that in all previous investigations of diffusion flames, the techniques associated with a flame structure study, have been applied to relatively thick or approximately one-dimensional flame systems. These simplifications make it easier to achieve the necessary degree of experimental precision.

The most striking feature, however, of the results given in Figs. 60 and 61 concerns the shape of the heat release rate patterns. Whilst, in general, the patterns are similar to those for the isotherms (Figs. 3 and 4), both flames exhibit a localised centre

of maximum heat release rate situated somewhat above the flame base along the inner edge of the visible flame sheet. Below this region the heat release rate falls off rapidly whilst with increasing distance up the flame sheet there is a more gradual decrease in heat release rate. Furthermore, intercomparison of Figs. 60 and 61 with the composition analyses shown in table 1 reveals that, for both flames, the localised centre of maximum heat release rate is situated where the combustible mixture attains stoichiometric proportions. This is shown more clearly in Fig. 62. In this way, the heat release rate profiles confirm the evidence provided by the species and reaction rate profiles that the anchoring point of a diffusion flame is situated somewhat above the extreme flame base where the mixture attains stoichiometric proportions.

Since the above mentioned results indicate a stoichiometric stabilising region the heat release rate patterns, evaluated in this thesis, have been contrasted with those for the corresponding pre-mixed flames of Datta, Hayward and Reed. It is interesting to note

that, in contrast to a localised centre of maximum heat release rate, the flames studied by these investigators (9.9% and 14% methane in air) showed, approximately, a line of constant maximum heat release rate along the inner edge of the visible flame. This pattern, of course, would be expected since it has been conclusively shown that little or no secondary air dilutes the combustible mixture at the base of these flames (Smith, 1971) and hence the composition field remains relatively invariant with distance along the flame front. This in turn reflects a constant heat release rate field. But quite a different situation arises for the flames of initially separated reactants studied in this thesis. Here the diffusive and convective flow of ambient atmosphere penetrates through the stabilising region producing a localised zone where the combustible attains stoichiometric proportions. It was confirmed in section 1.5.4. that the localised stoichiometric stabilising region results principally from diffusion of oxygen across the refracted stream tubes of oxygen into the base of the flame and hence this may be considered as a unique characteristic of diffusion flames or flames in which there is a substantial diffusive flux of ambient atmosphere into the stabilising region. Furthermore,

particle-track photographs indicate that the transition between flames controlled by the diffusive flow of ambient atmosphere and those controlled by the convective flow of primary mixture occurs at a methane concentration around the upper limit of inflammability. It follows that a localised stoichiometric stabilising region would be expected to characterise the structures of flames within the range 15-20% methane up to neat gas composition.

Regarding the magnitudes of the heat release rates, it is interesting to note that the maximum heat release rate found in this thesis (155 cals $cm^{-3}s^{-1}$) is in surprisingly good agreement with the maximum determined by Tsuji and Yamaoka (140 cals $cm^{-3}s^{-1}$), also on a methane diffusion flame. Both these values are significantly higher than that of Thomas (50 cals $cm^{-3}s^{-1}$) who studied a hydrogen-oxygen flame diluted with nitrogen and argon. But perhaps a more interesting comparison is provided when the maximum heat release rates of the diffusion flames studied in this thesis (155 cals $cm^{-3}s^{-1}$), which correspond to mixtures of stoichiometric proportions, are contrasted with the maximum heat release rates evaluated by Datta,

Hayward and Reed for a near-stoichiometric burner flame (160 cals $cm^{-3}s^{-1}$). Evidently there is again surprisingly good agreement which adds further weight to the concept of a localised stoichiometric stabilising region for diffusion flames. In addition it would be reasonable to suppose, from the results presented in this thesis and elsewhere, that the maximum heat release rate for any methane/air flame at atmospheric pressure would be unlikely to exceed 160 cals $cm^{-3}s^{-1}$.

At the extreme base of the visible flame sheet the results given in Figs. 60 and 61 indicate heat release rates of between 30 and 40 cals $cm^{-3}s^{-1}$. Although tailing-off, considerable heat energy is liberated beneath the base of the visible flame sheet. It was mentioned in section 1.5.3. that the flame base is extremely fuel-lean and combustion in this region is likely to be augmented by active species diffusing downward from the stoichiometric anchoring point which may be considered as a continuous ignition source. Further weight is added to this argument by the fact that considerable heat energy (30 to 40 cals $cm^{-3}s^{-1}$) is liberated in this region beneath the visible flame sheet.

Next, in considering the phenomenon of flame lift, the effect, on the overall heat release rate pattern, of increasing the supply of reactant to the burner may be seen by contrasting Fig. 60 with Fig. 61. Whilst the gradients of heat release rate steepen, as the flame base contracts, the maximum rate of heat release, present at the localised stoichiometric stabilising region, remains almost unchanged at around 155 cals $cm^{-3}s^{-1}$. It was mentioned earlier that the contribution to the total heat release rate from thermal conduction increases with increasing supply of reactant. However, at the same time, the contribution from the bulk flow decreases to maintain an approximately constant maximum heat release rate. Thus, in considering the phenomenon of flame lift, the limiting factor would seem to be the maximum rate of reaction or heat release, associated with the mixture prevailing at the stabilising point, which, as mentioned earlier is dependent predominantly on mass diffusion rather than mass flow or velocity.

Finally, comparison of the thermal and aerodynamic structures of the diffusion flames studied in this thesis with those of the corresponding pre-mixed flame

systems explains the greater stability of the former compared with the latter. It will be recalled that for stoichiometric and fuel-rich pre-mixed flame systems the stabilising mechanism has been examined in detail by Datta, Hayward and Reed. Structural analyses carried out on near-stoichiometric (9.9% methane) and fuel-rich (14% methane) flames illustrated a fundamental change in the stabilising mechanism when the flame becomes moderately fuel-rich. As mentioned earlier, the maximum heat release rate associated with the near-stoichiometric flame was found to be 160 cals $cm^{-3}s^{-1}$ whereas that for the moderately fuel-rich flame was significantly lower at 88 cals $cm^{-3}s^{-1}$. Nevertheless a 50% decrease in the maximum heat release rate was associated with a 50% increase in stability. In other words, for the 14% methane flame, the movement of the stabilising region away from the burner to a more favourable velocity field more than offset the drastic reduction in heat release rate, resulting in greater stability compared with the near-stoichiometric burner flame. But as recalled earlier, the stabilising region of very fuel-rich flames, such as diffusion flames, reverts to a

stoichiometric zone, in a localised form, with an associated heat release rate of 155 cals $cm^{-3}s^{-1}$ - much the same as the near-stoichiometric burner flame. Evidently, two effects combine to favour the stability of diffusion flames compared with the pre-mixed fuel-rich flames commonly encountered in practice. Admixture of the combustibles, by molecular diffusion, results in a stabilising region of more favourable velocity, for a given exit velocity of reactant. Second, a stoichiometric stabilising region provides substantially higher rates of heat release, compared with fuel-rich pre-mixed flames, which in turn engenders greater stability.

The results discussed in this section have shown that an analysis of the distribution of volumetric heat release rates gives considerable insight into the stability phenomena associated with diffusion flames. However, it will be appreciated, that the analysis involved, even for a single flame system, is extremely lengthy and as such is impracticable as regards the study of the many other flame systems which are currently of interest to the Gas Industry. Nevertheless,

an extremely important conclusion, resulting from the results discussed hitherto, concerns the relative importance of the various physical contributions to the total heat release rate. It will be recalled that the bulk of the heat release arises principally from changes in the conduction flux profile, which in turn depend on changes in the temperature profile. It follows that it should be possible, within certain limitations on precision, to estimate the pattern of heat release rates from the temperature profiles alone. However, as a rapid means of estimating the heat release rate patterns, obtaining in the stabilising region of various flame systems, this is easier said than done because a suitable technique for rapidly estimating temperature patterns is not readily available. For this reason the second part of this thesis centres on an attempt to develop a suitable technique capable of providing estimates of heat release rates for several flame systems.

1.5.8. Accuracy of Results

It was mentioned in section 1.4. that a full structural analysis in terms of rates of reaction and heat release depends on formal relations involving the experimentally accessible flame parameters and

their derivatives. Each parameter has, of course, been measured by a different experimental technique, each with its particular accuracy. In this context estimates of $\pm$ 1%, $\pm$ 3% and $\pm$5% have been placed on the accuracy of the magnitudes of temperature, velocity and species concentrations respectively.

In view of the critical dependence of the rates of reaction and heat release on the relations between the flame parameters and their derivatives, a most important consideration is to obtain reasonable congruence between the profiles from the various measurement techniques. This is easier said than done because invariably the sampling position is displaced from that of the probe. For example, a quartz micro-probe withdraws a sample a few millimetres upstream of the probe position whereas a thermocouple bead distorts the local mixture velocity and samples a temperature about four diameters downstream of its apparent position.

Several methods present themselves for assessing the effects of relative displacements between the experimental profiles. Perhaps the best would be to determine each profile in a number of independent ways, but this is generally impracticable. A second method

would be to utilise the conservation of species or heat energy as a criterion for best fit of the data. Unfortunately this is somewhat insensitive to misalignment of the experimental data. Nevertheless, in order to gain some idea of the effect of incongruence of the profiles, rates of reaction have been estimated with the species profiles displaced from the temperature profiles by $\pm$ one matrix unit ($\pm$ 0.01 cm) in each of the component directions. The resulting reaction rate profiles were found to be in error by $\pm$ 10% with a spatial error in the peak rate of $\pm$ 0.005 cm. It would seem, therefore, that the profiles of reaction rate are not particularly sensitive to misalignment of the experimental profiles. This results principally from the critical dependence of reaction rate profiles on species gradients rather than temperature.

However since absolute errors approximately double with each successive derivative, and the species profiles are less accurate than those of temperature, the reaction rate profiles are likely to be less accurate, overall, than those of heat release rate. Feeding in estimates of errors of the individual variables in the normal way into equation (6) the

reaction rates $q_i$ would be expected to be in error by at least $\pm$ 30% and for this reason these profiles have been analysed only qualitatively. However the profiles of heat release rate would be expected to be more accurate than those of reaction rate, $\pm$ 20% as estimated from equation (8), and indeed the internal consistency of the data suggests this to be the case.

## 1.6. CONCLUSIONS

The main conclusions to be drawn from the foregoing results of an investigation of the micro-structure of laminar diffusion flames of methane, may be summarised as follows:-

1. The results of this thesis show that, for diffusion flames, the limiting rate of supply of oxidant into the stabilising region is governed, not by the mass flow, as in premixed flames, but predominantly by diffusive flow across the stream tubes. At the stabilising region at least two thirds of the total species flux of oxygen emanates from molecular diffusion and there are indications that this increases with flow rate.

2. Contrary to earlier investigations (Robson and Wilson, Bellis) the results of this thesis suggest, strongly, that the magnitude of velocity at the flame base is, to some extent, incidental to the phenomenon of flame lift, extinction being limited by chemical reaction rate and mass diffusion rather than by the bulk flow.

3. Although the structural study carried out in this thesis has, of necessity, been restricted to flames operating some way from their limiting condition, a picture emerges of a maximum fuel consumption rate, for diffusion flames, of the same order as the maximum rate in a laminar stoichiometric pre-mixed flame, thereby supporting the "flame strength" approach of Spalding and Jain.

4. Despite the very dissimilar physical processes taking place in pre-mixed flames and diffusion flames, the reaction processes obtaining in the stabilising region of diffusion flames are qualitatively similar to those of the two-stage reactions occurring in pre-mixed hydrocarbon-air flames. The maximum rates of consumption of the intermediates, carbon monoxide and hydrogen, occur well to the air side of the main reaction zone.

5. The major proportion of heat liberated in the main reaction zone of diffusion flames arises, in mathematical terms, from changes in the conduction flux profile. It follows that

reasonable estimates of the rates of heat release in diffusion flames may be made from changes in the temperature profile alone.

6. On the unburnt-fuel side of the main reaction zone, transport of heat energy by molecular diffusion provides, in mathematical terms, a definite exothermic contribution to the total heat release rate. Any adequate analysis of the thermal picture in this region must take this fact into account.

7. Substantial heat energy is liberated at or below the base of the visible reaction zone, where the mixture is extremely fuel-lean. Chemical reaction, in this region, is likely to be augmented by a downward diffusive flux of high enthalpy active species from the stoichiometric stabilising region, which may be considered as a continuous ignition source.

8. The major proportion of the heat energy liberated at the reaction zone is conveyed by convection to higher regions of the flame. In comparison, the heat flux lost from the

system to the burner is comparatively small.

9. Last, but of no less importance, diffusion flames at atmospheric pressure do offer an adequate flame thickness for the type of detailed structural study carried out in part 1 of this thesis.

# PART II

# OPTICAL STUDY OF LAMINAR DIFFUSION FLAMES OF METHANE

## 2.1. INTRODUCTION

The results presented in part 1 of this thesis have shown that a full structural analysis can give considerable insight into the stability phenomena associated with flames of initially separated reactants. However, it will be readily appreciated that the analysis involved, even for a single flame condition, is extremely lengthy and as such impracticable as regards the study of the wide variety of flame conditions that are currently of interest to the Gas Industry.

Nevertheless, it will be recalled that the bulk of the heat released in diffusion flames arises principally from changes in the conduction flux profile, which in turn depend primarily on changes in the temperature profile. Indeed, for many flame systems the temperature profile provides, perhaps, the most valuable single characteristic of a flame. Although a rigorous analysis of flame structure, as carried out in part 1 of this thesis, requires sets of profiles of many interrelated variables, temperature

alone can, together with certain assumptions, be used to estimate velocity, rates of heat release and possibly the overall reaction rate.

An important first step, therefore, towards the application of flame structure analysis to a wider range of flame conditions would be the development of a sufficiently rapid and accurate method for measuring flame temperature. Although there are many existing methods of measuring flame temperature, those that possess sufficient reliability and spatial resolution, such as conventional probe methods, are quite unsuitable for accumulating a large volume of experimental data. Since rapidity of measurement is a prime consideration, optical methods, which yield instanteous photographic records of complete temperature fields, would seem eminently suitable for the purpose. Those that present themselves - namely shadowgraphy, schlieren and interferometry - are, however, complementary rather than competitive and primarily qualitative rather than quantitative. Nevertheless, although no one method is entirely suitable, the technique of interferometry would appear

to be the most promising. The technique itself is well established but the application to the yielding of quantitative data from flames is less well developed.

Thus, in the absence of a sufficiently rapid quantitative method for measuring flame temperature, the second part of this thesis attempts, first to develop a suitable experimental and analytical technique, utilising the principle of interferometry, and second to apply such a technique to elucidate the structures of the stabilising regions of several diffusion flames.

## 2.2. OPTICAL METHODS OF MEASURING TEMPERATURE

### 2.2.1. Introduction

Several optical methods are available for measuring flame temperature. A brief review of their merits and demerits is therefore pertinent to the present study. The methods may be subdivided into three groups:-

(i) Radiation thermometry methods; e.g. Optical pyrometry, Spectrum line reversal, Line intensity methods.

(ii) Methods of geometrical optics; e.g. Schlieren, Deflexion mapping, Shadowgraphy.

(iii) Methods of physical optics; e.g. Interferometry, Holography.

Each of these methods has its particular merits and demerits and the choice therefore depends on such factors as the range of temperature and temperature gradient to be measured, reliability, spatial resolution and rapidity of measurement.

### 2.2.2. Radiation Thermometry Methods

This is a very versatile group based on the emission or absorption of electromagnetic radiation. The energy of a system can be divided into a classical

part and a quantised part. The quantisation of internal energies results in light being absorbed or emitted only at discrete wavelengths, and the intensity of emission or absorption, for a given transition, is directly related to temperature. In principle, therefore, a single measurement of absorption or emission determines flame temperature.

The simplest method, utilising this principle, is optical pyrometry, which is essentially a measure of brightness. Temperature is measured by comparison of the flame emission with a light source of known temperature. However, in general, flames are not optically dense and require to be coloured with metal vapours which emit radiation in the region being studied. The most commonly used method, which utilises this principle, is the spectrum line reversal method due to Kurlbaum. Light from a suitable background source is focussed by a lens to give an image of the lamp in the flame. A second lens is then employed to focus the images of both the flame and the background source on to the slit of a spectroscope. The resolving power of the spectroscope should be such that on introducing sodium salts into the flame

the two NaD lines are separately visible. When viewed with the comparison source these lines appear brighter or darker according to whether the comparison source temperature is lower or higher than that of the flame (Kirchoff's law). At the reversal point the two temperatures are equal.

The great sensitivity of the method is due to the rapid variation of light intensity with temperature. This follows from Wien's law that the brightness of the metal radiation emitted from a flame increases exponentially with the temperature of the flame. However, aside from this advantage there are several important limitations . These are summarised below.

(i) In the region of normal applicability, the method is unsuitable for measuring steep temperature gradients. The"resolving power" of the method decreases rapidly with increase in temperature.

(ii) Reversal methods are of little use for temperatures below 1500$^{o}$K since metallic salts do not emit in this region. The method is limited, therefore,to high temperatures.

(iii) Spatial resolution is relatively poor (several mm) and not suitable for a study of the microstructure of the stabilising regions of laminar flames.

The first two disadvantages restrict the method to certain regions of the flame, in which its inherent advantages can be exploited. However, for the purpose of this thesis, the method seemed unsuitable for the determination of the temperature field in the stabilising region of laminar flames since it was mentioned in section 1.5.1. that temperature gradients in this region may be as high as $20{,}500^{\circ}K\ cm^{-1}$.

2.2.3. Methods of Geometrical Optics

In essence all the methods of geometrical and physical optics are designed to measure the distribution of the local velocity of light, caused by refractive index changes, by analysing the topography of a wavefront emerging from a test space. The methods of geometrical optics - notably deflexion mapping - deduce this by measuring the angles between the incident and emergent perpendiculars to the wavefront. They therefore record the slopes of

perturbations on the wavefront and for this reason are most sensitive for steep temperature gradients. On the other hand, the methods of physical optics - notably interferometry - shear the wavefront under examination with a reference wave and display its topography as contours or "fringes" at fixed phase increments. They therefore record the absolute heights of the perturbations and are less suited to measuring steep variations in temperature.

Of the methods of geometrical optics, the most suitable for quantitative measurement is deflexion mapping which portrays the first spatial derivative of optical path (the product of refractive index and geometric path length in the flame). In this method the distribution of deflexion of a light beam is deduced by measuring the distorted shapes of grids or other suitable reference patterns. The resulting image is a curved line whose vertical displacement from the straight line, obtained in the absence of a test field, is proportional to $(1/\rho)\frac{\partial \rho}{\partial x}$ or in special cases approximately $(1/T)\frac{\partial T}{\partial x}$.

This method has the unique advantage of measuring directly an important flame parameter, the temperature derivative, as well as the usual optical advantage of not disturbing the flame front. On the other hand there are several limitations and these are summarised below.

(i) To obtain a distribution of refractive index, a numerical integration has to be carried out with respect to some known state - usually ambient conditions.

(ii) In common with all the methods of geometrical and physical optics, the sensitivity of the method decreases at high temperatures.

(iii) Since the optical path gradient is integrated along the total light path, "end effects" can assume unwanted importance. The $1/T$ factor heavily weights the derivatives from the cooler end regions of the flame.

In spite of these difficulties the methods of geometrical optics have found extensive applications in combustion research - Dixon-Lewis (1953), Burgoyne and Weinberg (1954), Levy and Weinberg (1959), Dixon-

Lewis and Isles (1962) and Pandya and Weinberg (1963). In addition, the methods have been discussed definitively by Weinberg (1963). The problem of quantitative interpretation has been discussed by the individual authors. Two sources of error would seem to merit closer attention. These are the effects of composition variations on refractive index and the mathematical complexity of reducing the data, particularly for conical flames.

2.2.4. Methods of Physical Optics

The most extensively used method in this group is interferometry. This makes use of the fact that the velocity of light is a function of the density of a medium so that beams passing through gases of different density will have different traversal times. If the beams are initially coherent and in phase, the emergent wavefronts will exhibit a phase difference equal to the difference between the optical paths of the two beams.

An interferometer, utilising this principle, was developed as long ago as 1891 independently by Mach and Zehnder. Their design is still regarded today as the

most versatile form of interferometer. However, in the last decade or so, a second generation of interferometer has evolved with the advent of highly coherent monochromatic lasers as available light sources and these, in general, simplify interferometer design.

The great advantage of laser interferometry, lies in its simplicity and versatility. A single photograph is sufficient to provide full information regarding the refractive index distribution in a complete flame. Moreover, the exceedingly high monochromatic brightness of lasers makes it possible to "freeze" rapidly moving phenomena associated with combustion research.

However, despite the almost explosive proliferation of interferometer designs, associated with the advent of lasers, the quantitative interpretation of the resulting interferograms is much less well developed. The major difficulties are summarised below.

(i) In order to obtain the desired sensitivity, an interferogram must be interpreted to a fraction of a fringe. This is particularly important in applications involving steep refractive index gradients.

(ii) In order to interpret an interferogram it is necessary to specify the geometry of the refractive index field. In the case of an extended flat flame "end effects" can assume unwanted importance since the fringe pattern is integrated along the total light path. In the case of conical flames, the degree of symmetry must be as perfect as the desired resolution.

(iii) Because of the fact that refractive index depends both upon composition and temperature variations it is necessary to know the composition profile.

(iv) In the case of conical flames the techniques for reducing interferometric data (Raterink and Lamberts) are not entirely satisfactory. This difficulty principally arises from the need to solve non-linear differential equations.

For these reasons the method of interferometry has not been extensively employed for quantitative measurements in combustion research. One interesting application of interferometry, however, has been carried out by Pandya and Weinberg (1963) to yield the

thermal structure of counter-flow diffusion flames. In order to circumvent some of the difficulties, discussed above, the interferometric distribution was pegged to the maximum temperature attained in the flame, measured using the alternative method of spectrum line reversal, in order to effect corrections throughout the distribution.

2.2.5. Conclusions

The foregoing discussion highlights the fact that no one method, in its present form, is entirely suitable for measuring the range of temperature and temperature gradient which prevails in laminar diffusion flames. However, although no one method is entirely satisfactory, interferometry, which, in a single photograph, can furnish the temperature distribution in a complete flame, would seem to be the most suitable. The technique itself is well established but the application to yielding quantitative data, without recourse to employing additional methods for calibration, would seem to require further development. In particular:

(i) To develop suitable techniques for interpreting interferograms to a small fraction of a fringe.

(ii) To develop satisfactory data reduction techniques for conical flames, the most frequently encountered geometry in practice.

(iii) To make adequate allowance for the dependence of refractive index on the composition of the flame gases.

The general line of approach was therefore to attempt to fulfil these requirements and then to apply the technique to the stabilising region of several diffusion flames of methane.

## 2.3. DETAILS OF APPARATUS

The previous discussion highlights the fact that despite the almost explosive proliferation of interferometer design, associated with the advent of lasers, quantitative interpretation of the resulting interferograms is much less well developed. For this reason the choice of burner geometry, suitable for use in interferometric studies, is limited to either the slot-type burner which produces a flat flame, of the type examined in part 1 of this thesis, or a cylindrical burner which produces an axisymmetric flame.

In the case of a flat flame "end effects" can assume unwanted importance since the phase changes are integrated along the total light path. This disadvantage stems from the inverse dependence of refractive index on temperature (Gladstone and Dale's law), thereby heavily weighting the phase contributions from the cooler end regions of the flame. On the other hand, in the case of axisymmetric flames no such problems exist concerning end effects. Here, however, the degree of symmetry must be as perfect as the desired resolution and furthermore it must be assumed that the isotherms and isopleths do lie accurately

parallel to one another such that the flame front properties are independent of lateral position. It would seem that only for flames of axial symmetry can the optical path equations, involved in interferometry, lead to unambiguous solutions for refractive index. For this reason a cylindrical burner was adopted for the present study, thus alleviating the need to correct for edge effects which can contribute disproportionately to the observed fringe shift values. The choice of a cylindrical burner as opposed to the flat flame burner studied in part 1 of this thesis might at first sight be construed as an apparent inconsistency. However it was felt that the fundamental conclusions drawn from part 1 of this thesis would be largely independent of burner geometry and would be applicable to other simple flame geometries, such as the axisymmetric case.

Three steady state diffusion flames of methane were selected for study, covering the stable flow rate spectrum between the instability limits of extinction and lift. The flames selected are shown in Fig. 63.

2.3.1. Burner and Flow System

The flames were supported on a cylindrical burner of internal diameter 1.5 mm, external diameter 3.1 mm and length 10.5 cm - sufficient to ensure a Poiseuille flow distribution at the burner port. The burner was housed in a vertical wind tunnel of cross section 100 cm.sq. and length 100 cm. Air for combustion entered through flow-straightening honeycomb thereby providing an essentially streamline flow. Ignition was provided by a battery-operated Platinum/Rhodium hot-wire igniter and was effected remote from the wind tunnel to minimise thermal and aerodynamic disturbances.

Pure methane for combustion was taken from a high pressure cylinder through a rotameter at constant pressure and thence to the burner. A simple by-pass arrangement, incorporating two magnetic solenoid valves, enabled a pre-selected gas rate to be switched to the burner almost instantaneously, thus preventing any contamination of the combustion air by unburnt methane prior to ignition. It is particularly important, when utilising the technique of interferometry,

to maintain unvitiated air for combustion since the method is essentially self calibrating and dependent on an accurate knowledge of ambient conditions. A schematic diagram of the entire system is shown in Fig. 64.

## 2.4. DEVELOPMENT OF AN INTERFEROMETRIC METHOD

### 2.4.1. Choice of Interferometer

An interferometer for use in combustion research must possess certain special features. Since large differences of temperature exist between the combustion phenomenon under study and the ambient environment, the two beams should be thermally separated. Furthermore, since it is necessary to transluminate the flame with a plane wavefront, the beam should be parallel and collimated in all directions (i.e. effectively the source should approximate to a point).

An interferometer which adequately fulfils these requirements is the four mirror Mach-Zehnder in which the beam is split and recombined using half silvered plates. Its major disadvantage is its initial cost and the difficulty of adjustment.

In the last decade or so, however, a second generation of interferometer has evolved with the advent of lasers as available light sources. Their high degree of monochromaticity and coherence have offered a new range of opportunities in interferometer design. Perhaps the first of these new freedoms is

that, in superimposing reference and test beams, it is no longer required to maintain point-to-point correspondence of rays originating from different parts of an extended light source. Since all parts of a plane and coherent wave can now be regarded as identical, superimposition of two beams may be achieved in a variety of ways; e.g. inversion, rotation or overlapping of the beams. Such methods have been reviewed in detail by Tanner (1966) and more recently by Schwar and Weinberg (1969). Furthermore, for small test objects, such as domestic-scale laminar flames, it may not be necessary to designate separate reference and test beams at all since an unperturbed part of the wavefront can be folded, at a convenient point, over the perturbed part which traverses the test space. An additional freedom, afforded by the extremely high degree of monochromaticity and coherence, permits large path differences between the two beams. Prior to the advent of lasers, interference of very high orders was difficult to achieve owing both to a lack of monochromaticity and coherence of available light sources. This new attribute

therefore makes it unnecessary to match geometric path lengths closely, allows the use of windows in one beam without requiring compensators in the other and makes possible the folding and overlapping of a beam using, for example, the front and rear reflections from an inclined glass slab of a few mm. thickness. It is not surprising, therefore, that these new freedoms have produced a very large number of possible designs; e.g. Murty (1964), Dyson (1957), Hariharan and Sen (1959), Tanner (1965) and Oppenheim, Urtiew and Weinberg (1966). This proliferation in design is extremely useful because investigations in fluid mechanics are very varied and a final choice depends on the exact system under consideration.

Probably the simplest method for the study of domestic-scale laminar flames is that due to Murty in which the beams are superimposed using the front and rear reflections from an inclined glass slab. Furthermore this alleviates the need to designate separate beams, a single broad beam sufficing for both reference and test arms of the interferometer. For

these reasons the principles outlined by Murty have been utilised in this thesis.

2.4.2. Principle of Single Beam Interferometer

In this design of interferometer, highly coherent and monochromatic light from a laser is split and recombined at the points of focus of two schlieren mirrors. The principle is best illustrated by reference to Fig. 65. The narrow collimated beam emanating from a laser (L) is expanded by lens $L_1$ to fill exactly the aperture of schlieren mirror $M_1$. The resulting single broad parallel beam between the two schlieren mirrors, $M_1$ and $M_2$, serves conveniently for both the reference and test arms of the interferometer. Lens $L_2$ reduces the divergence of the beam from the second schlieren mirror $M_2$ and interference fringes are produced in the overlapping region $II'$ of the beams reflected from the front and rear surfaces of an inclined glass slab, G. Lens $L_3$ focusses the test space on a receptor (photographic plate) at $PP'$. A pinhole (P) located at the focus of lens $L_1$ is sufficient to remove unwanted diffraction effects which may result from imperfections on the surfaces of the mirrors of the laser. The main advantage of this

system is that it is not necessary to designate separate reference and test beams in the conventional sense because the wavefront is conveniently folded and the two parts superimposed after traversing the test space.

Choice of adjustment lies between the infinite fringe condition or a finite fringe condition. The infinite fringe condition may be achieved by adjusting lens $L_2$ such that a parallel beam is incident on the glass slab, G. In this case the relation between beam diameter, d, slab thickness, a, angle of incidence, $\beta$, and the extent of overlap, n, in terms of fraction of the beam diameter, is given by:

$$n = w/D = 2a/d\sin\beta$$

It follows that the greatest working space (W/2) is achieved with n set to $\frac{1}{4}$ and $a/d\sin\beta = \frac{1}{4}$. If, however, the beam incident on the glass slab, G, is now made slightly non parallel, by adjustment of lens $L_2$, a set of finitely spaced fringes, located at infinity, are observed at PP'. The observed fringes are strictly hyperbolic in shape but their deviation from straight evenly spaced fringes is negligible over the usual working section of the interferometer.

In practice the choice of operating mode depends on the size and nature of the refractive index field under study. The infinite fringe condition is ideally suited to the study of large test objects but for small test objects, such as the flames examined in this thesis, the resulting phase shifts are relatively small ($\sim \lambda$'s) and would give insufficient data for quantitative interpretation. For this reason adjustment to a finite fringe condition is preferred for phase objects such as domestic-scale laminar diffusion flames.

It should be stressed that in the absence of partial silvering of G, fringe legibility decreases with increasing $\beta$ since illumination of the two beams will be unequal. However provided $\beta$ is restricted to $\lesssim 45^{\circ}$ the system gives adequate fringe legibility without recourse to partial silvering of G. It should be noted also that the present optical system can be used only with a laser source since one part of the beam traverses G twice while the other part is reflected from its front surface, the path difference between the two beams being very large indeed.

2.4.3. Construction of Interferometer

The layout of the optical system employed is set out in Fig. 65. $M_1$ and $M_2$ are two schlieren mirrors of aperture 20 cm and focal length 243 cm. Each mirror was fitted with tangent screws enabling rotation to be effected about horizontal and vertical axes. Each mirror was claimed, by the manufacturer, to be optically flat to $\lambda/10$ across the field of view.

Highly monochromatic and coherent light was provided by a He/Ne gas laser (Scientifica and Cook Electronics) at a wavelength of 6328 Å. The Laser was operated in $TEM_{oo}$ mode at an output of 4 mW (about 40% of its maximum output) to ensure good fringe legibility.

The optical components - laser, schlieren mirrors, lenses and the wind tunnel - were mounted on a 3/16 inch steel bench to ensure adequate rigidity. The bench itself was suspended on four airmounts (Firestone Airide) thereby isolating the entire system from the wide range of vibrational frequencies encountered in the research laboratory.

The wind tunnel was fitted with a thin water jacket on the side adjacent to the unperturbed part of the beam to thermally separate the reference beam from the combustion system under study (Fig. 64).

2.4.4. Experimental Procedure

A number of preliminary adjustments were first made to the interferometer. With the laser operating in $TEM_{oo}$ mode the expanded beam between $M_1$ and $M_2$ was adjusted to be perfectly parallel. The burner was then adjusted to be vertical and the fringes orientated parallel to the burner by careful adjustment of the orientation of G. Lens $L_3$ and the orientation of G were then further adjusted to give a fringe frequency of $3\lambda$ per mm of test space. This figure provides a compromise between an optimum wavelength resolution (small fringe frequency) and an optimum spatial distribution of fringes (large fringe frequency). The interferometer was now in full adjustment.

Ambient conditions in the vicinity of the reference beam (humidity, temperature and pressure) were noted prior to photography of several reference interferograms. A pre-set flame condition was then

switched to the burner using a magnetic solenoid valve arrangement and remote ignition effected using a platinum/rhodium hot-wire igniter. After sufficient time had elapsed for the flame to reach thermal equilibrium with its burner head (about 2 minutes) a number of interferograms were photographed in rapid succession. Finally, ambient conditions were re-measured to check their constancy over the time scale of the experiment.

2.4.5. Diffusion Flame Interferograms

The above mentioned process was carried out at three flow rates covering the flow rate spectrum between the instability limits of extinction and lift. A typical interferogram is displayed in Fig. 66.

The introduction of a diffusion flame into the test space produced a sideways fringe shift which at each point represented the decrease in optical path length through the flame compared with the unperturbed reference beam. It was readily apparent, from the interferogram, shown in Fig. 66, that the lateral fringe shift profiles, at a level which cut the flame close to the burner port, were relatively complex since part

of the region traversed by the test beam comprised a fuel core at near ambient temperature surrounded by an envelope of burning gases at high temperatures. It was necessary, therefore, to have a sufficiently versatile analytical procedure that would be capable of coping with a variety of relatively complex lateral fringe shift profiles.

## 2.5. ANALYSIS OF A DIFFUSION FLAME INTERFEROGRAM

### 2.5.1. Existing Methods of Analysis

A fringe shift results from the difference in optical path of two light beams, one of which passes through the refractive index disturbance and the other through a reference refractive index field. If the disturbance shows axial symmetry about, say, the z axis, the fringe shift, which is the difference, in wavelengths, of the optical paths of the two light beams, is given by:

$$S(y) = \frac{1}{\lambda} \int_{X_1}^{X_2} \left[N(x) - N_o\right] \, dx \qquad (25)$$

where x is in the direction of the light beam. In polar co-ordinates equation (25) becomes

$$S(y) = \frac{2}{\lambda} \int_{y}^{R_o} \frac{\left[N(r) - N_o\right]}{(r^2 - y^2)^{\frac{1}{2}}} \, r dr \qquad (26)$$

where, Fig. 67, $r = (x^2 + y^2)^{\frac{1}{2}}$ and $R_o$ is the radius of the disturbance, i.e. where $N(r) = N_o$. Equation (26) is one form of Abel's integral equation and inverts analytically into

$$N(r) - N_o = -\frac{\lambda}{\pi} \int_{r}^{R_o} \frac{(dS/dy)dy}{(y^2 - r^2)^{\frac{1}{2}}} \qquad (27)$$

In practice interferograms yield S(y) as a set of numerical data and not as an analytic function.

Several methods have been proposed for performing the integral in equation (27), the attainable accuracy of each depending in a different way of the size of random experimental errors.

Numerical solutions to equation (27) have been used, e.g. Bockasten (1961) and Nestor and Olsen (1960), but they all suffer necessarily from the fact that noise in the data is magnified when the derivative of S(y) is evaluated. For this reason, therefore, there should be an advantage in reversing the order of differentiation and integration and applying smoothing techniques after integration but before differentiation.

If the functions are suitably well behaved, then by Abel's transformation (Pearce (1960)) equation (26) becomes

$$N(r) - N_o = -\frac{\lambda}{\pi r} \frac{d}{dr} \int_r^{R_o} \frac{S(y)ydy}{(y^2-r^2)^{\frac{1}{2}}} \qquad (28)$$

and in the case where the data can be fitted by least squares to a function of the form

$$S(y) = \sum_{i=0}^{m} C_i(R_o^2 - y^2)^i \qquad (29)$$

then the solution to equation (28) may be written simply as

$$N(r) - N_o = \lambda \sum_{i=0}^{m} A_i C_i (R_o^2 - r^2)^{i-\frac{1}{2}} \qquad (30)$$

where

$$A_i = (2^{2i}/\pi)\left[(i!)^2/(2i)!\right] \qquad (31)$$

Freeman and Katz (1963) have used this approach for analysing radiance profiles in plasma discharges. The possibility of a singularity developing in equation (30), should i take a value less than $\frac{1}{2}$, has been discussed fully by Freeman and Katz. If i is restricted to a value greater than $\frac{1}{2}$, to preclude such a singularity developing, then this requires that the observed lateral profiles be known, or extrapolated to zero, before commencing a least squares fit of the data. For this reason it is simpler to include an i = o term in the summation and simply not compute any solutions beyond the edge of the observed distribution. This approach has the additional merit that the part of the fringe shift distribution near the boundary of the disturbance, where experimental errors tend to be large, can be omitted without impairing the accuracy at the centre. Bradley (1968) used a similar approach in which the observed fringe shift distribution is represented in the unit interval by a cubic and the coefficients are determined by a least squares fit of the observed fringe shift values.

The solutions discussed above and the forerunners of these have been applied to a variety of problems, such as the determination of density distributions in the region surrounding a moving projectile (Bennet, Carter and Bergdolt (1952)), the determination of the rate of mass diffusion from a laminar jet (Ladenberg, Van Voorhis and Winckler (1949)), the measurement of temperature in a one-dimensional flat flame (Pandya and Weinberg (1963)), and for the determination of radiance distributions in plasma discharges (Freeman and Katz (1963)). All of these applications have in common a relatively simple lateral observed distribution, of the form shown in Fig. 68 (curve 1) from which the density or temperature is ultimately derived. However, the solutions that have been discussed in the analysis of axisymmetric interferograms are not very satisfactory when the fringe shift distribution is more complex, as is the situation with which this thesis is concerned, namely the interferogram from an axisymmetric diffusion flame stabilised on a cylindrical burner. In this case part of the region traversed by the test beam is composed of a fuel core

at room temperature surrounded by an envelope of burning gases at high temperatures. This situation gives rise to a lateral fringe shift pattern of the form shown in Fig. 68 (curve 2).

The distinction between the distributions shown in Fig. 68 may seem trivial at first sight. However the distinction is readily clarified when an attempt is made to represent the complete observed fringe shift distribution, Fig. 68, by a polynomial of sufficiently low order and within the experimental error of the data. Even if the fitted representation is artificially weighted and forced to lie close to the observed data, a situation will eventually arise where a single curve of sufficiently low order will not be capable of representing the observed data adequately. Moreover an important prerequisite of a method of analysis of axisymmetric interferograms is that the method shall be sufficiently versatile to cope with the different forms of lateral fringe shift profile which characterise the wide variety of flames of interest to the Gas Industry. It was apparent that the solutions of previous workers, were not particularly suitable or sufficiently versatile, in their present

form, for the analysis of axisymmetric diffusion flame interferograms, where the observed fringe shift profile is a relatively complex function of lateral distance.

2.5.2. Extension to Existing Methods

In order to circumvent the above mentioned difficulties, an extension to the existing approaches is proposed which is suitable for cases, such as the interferograms of axisymmetric diffusion flames, where the complete observed lateral fringe shift distribution cannot adequately be represented by a single curve of sufficiently low order. To be acceptable, a representation of the observed fringe shift data should be reasonably low-ordered, correlate the data within experimental error, and introduce no unwarranted inflection points.

One way to fulfil these requirements is to use the spline fit technique, discussed originally by Landis and Nilson (1962), and extended by Klaus and Van Ness (1967) to permit some smoothing of experimental data. Using the extended approach the observed lateral fringe shift distribution may be represented in sections, the sectional boundaries or "knots" being determined arbitrarily such that each interval may

contain a number of data points. A cubic may be used to represent the data within each section, constraints being placed upon the cubics such that at each knot the adjacent cubics give the same values for the dependent variable (observed fringe shift) and its first two derivatives. In addition some smoothing of the experimental data may be achieved by applying the usual constraint that the sum of the squares of the deviations between the observed data and the analytical representation be minimised.

Utilising these principles, consider a section p, p + 1 such that $R_{p+1} < r < R_p$ and let the observed lateral fringe shift distribution be represented by a function of the form

$$S(y) = \sum_{i=0}^{3} C_i (R_p^2 - y^2)^i \qquad (32)$$

Substitution into equation (28) then yields

$$N(r)-N_o = -\frac{\lambda}{\pi(r} \frac{d}{dr} \left[ \int_r^{R_p} \frac{S(y)_{p,p+1}\, ydy}{(y^2-r^2)^{\frac{1}{2}}} + \sum_{n=1}^{p} \int_{R_n}^{R_o} \frac{S(y)_{n-1,n}\, ydy}{(y^2-r^2)^{\frac{1}{2}}} \right] \qquad (33)$$

where $S(y)_{p,p+1}$ is the analytical representation of data within section p,p+1. Equation (33) then becomes

(South (1970))

$$N(r)-N_o = \lambda \left\{ \left[ \sum_{i=0}^{3} A_i C_i \, (R_p^2 - r^2)^{i-\frac{1}{2}} \right] + \sum_{h=1}^{p} \sum_{i=0}^{3} C_i \left( A_i \left[ (R_{n-1}^2 - r^2)^{i-\frac{1}{2}} - (R_n^2 - r^2)^{i-\frac{1}{2}} \right] - \sum_{j=1}^{i+0} \frac{(R_{n-1}^2 - R_n^2)^{i-j+1} (R_n^2 - r^2)^{j-\frac{3}{2}} \, 2^{2(j-1)} \, i! \, (j-1)!}{\pi \, (i-j+1)! \, (2j-2)!} \right) \right\} \quad (34)$$

The first term in equation (34) represents the contribution to N(r) from the interval adjacent to r and the second and third terms represent the summation of the contributions to N(r) from the remaining intervals.

2.5.3. Final Flame Temperature

As mentioned in section 2.2. optical methods, such as deflexion mapping and interferometry, measure, essentially, the distribution in the local velocity of light and this leads to distributions of the refractivities (N-1) of the burning mixture of gases. If combustion takes place at constant pressure, then refractivity may be related to flame temperature through

$$T = \left[ (N_o - 1) / (N - 1) \right] T_o \quad (35)$$

where $N_o$ and N denote the refractive indices of the mixture of gases at $T_o$ and T respectively. This last stage of the analysis presents some problems because in

the case of laminar diffusion flames, the temperature rise is accompanied by diffusion induced changes in the composition of the flame gases. In order to quantify the temperature rise, from interferometric data, it is necessary, therefore, to separate the refractivity associated with the temperature rise from that associated with the accompanying composition changes.

An indication of the extent of the problem may be seen by contrasting the refractivity of the final products of combustion against those of the reactant and oxidant. Employing equation (41) for the refractivity of a mixture of gases and pure component refractivities from table 4, then at $\lambda = 6328\text{Å}$, p = 1 atmosphere and T = 298°K

$$(N-1)_{PRODUCTS} = \frac{(N-1)_{CO_2} + 2(N-1)_{H_2O} + 7.52(N-1)_{N_2}}{10.52}$$

$$= 276.8 \times 10^{-6}$$

$$(N-1)_{AIR} = \frac{(N-1)_{O_2} + 3.76(N-1)_{N_2}}{4.76} = 266.6 \times 10^{-6}$$

$$(N-1)_{CH_4} = 402.5 \times 10^{-6}$$

Thus complete combustion would lead to a change of

refractivity, due to composition changes alone, from an initial $266.6 \times 10^{-6}$ on the air side of the flame to a final $276.8 \times 10^{-6}$, a difference of only $10.2 \times 10^{-6}$. The corresponding change of refractivity on the methane side of the flame, however, would be $125.7 \times 10^{-6}$. Thus, it may be seen that diffusion induced changes in composition present difficulties only on the unburnt-fuel side of the flame sheet but since, with increasing concentration of fuel towards the jet core, flame temperature decreases and because refractivity is inversely proportioned to temperature, even a relatively large diffusion-induced composition component of refractivity results in a temperature correction of second order dependence compared with the final flame temperature. It may be concluded, therefore, that in diffusion flames at atmospheric pressure, most of the refractive index variation is caused by temperature changes rather than by composition changes and the effect of diffusion induced changes in composition becomes pronounced only in the early part of the temperature rise itself where temperature is only a fraction of the final flame temperature.

Whilst temperature is the main variable, the diffusion induced composition variation should be taken into account in a rigorous treatment of the problem. In the absence of experimental data, although the general form of the composition profiles is known from the results of part 1 of this thesis, two methods for overcoming this difficulty were tested. First, despite the rather unrealistic assumptions of Burke and Schumann, their simple mathematical approach was employed to estimate radial concentrations of reactant, oxidant and products. However this proved unsuccessful principally because the mathematically defined reaction zone of Burke and Schumann was located well inside the inner edge of the visible flame sheet and any further corrections to their already simplified assumptions seemed unjustified. A second method was then tried utilising the assumptions underlying the theories of diffusion flame structure viz. the equality of diffusion coefficients with thermal diffusivity. It can be seen from equation (7) that the thermal conduction term in the enthalpy balance always represents

a negative flux whilst the diffusion term is always positive; i.e. high enthalpy reactants diffusing outwards against low enthalpy products of combustion. The net effect of these two terms then determines the specific enthalpy profile. In the case of accidental cancellation of the conduction and diffusion fluxes throughout the flame, the specific enthalpy, h, would be constant everywhere. The requirement for this to occur is that the Lewis number, $\rho \overline{c}_p D_{ij}/\lambda$, is equal to unity. Although a gross simplification in practice, for an idealised flame, characterised by an overall reaction scheme, the assumption of a unit Lewis number has been shown to be a reasonable approximation (Fristrom and Westenberg) and would seem suitable for the second order correction required in this thesis. Under these conditions it can be shown that, for a constant enthalpy requirement, the fraction of reaction completed, $\phi$, must be linearly related to the temperature rise

$$\text{i.e. } \phi = \frac{1-X_{CH_4}}{X_{CH_4,0}} = \frac{T-T_o}{T_b-T_o} \qquad (36)$$

where $T_b$ is the temperature at which the fuel mole

fraction has been reduced to zero and $X_o$ denotes the unburnt state. Furthermore utilising equation (41), $N_o$ may be expressed in terms of the component contributions from reactant (suffix R) and products (suffix P).

$$\text{i.e. } N_o = (1 - \emptyset)N_{R,O} + \emptyset N_{P,O} \qquad (37)$$

Elimination of $\emptyset$ and $N_o$ between equations (35) to (37) then yields a solution for flame temperature

$$\text{i.e. } T = \frac{(N_{R,O}-1) + \left[(N_{R,O}-N_{P,O}) \Big/ \left(\frac{T_b}{T_o} - 1\right)\right]}{(N-1) + \left[(N_{R,O}-N_{P,O}) \Big/ \left(\frac{T_b}{T_o} - 1\right)\right]} \qquad (38)$$

Equation (38) was used, therefore, for determining flame temperature from refractivities (N-1) calculated from equation (34). The reference refractive indices, $N_o$, were calculated from the Gladstone-Dale equation:-

$$N_o - 1 = k\rho_o \qquad (39)$$

where k denotes the Gladstone-Dale constant and

$$\rho_o = \frac{m(1+\alpha)}{22.414\times10^3} \; \frac{P}{760} \; \frac{273.15}{T_o} \left(\frac{P-0.378P_v}{P}\right) \qquad (40)$$

In equation (40) $\alpha$ denotes the degree of imperfection of a component gas and the term in brackets represents a humidity correction, valid only for air, where $P_v$

denotes the pressure of water vapour in air (Kaye and Laby). The Gladstone-Dale constants, k, of the component gases were calculated from component refractivities taken from the International Critical Tables. A full table of the values employed is listed below:

| SPECIES | k ($ml g^{-1}$) | $(N-1)\times10^6$ $\lambda$=6328Å, T=298°k, P=1At. |
|---|---|---|
| $O_2$ | 0.18920 | 247.7 |
| $N_2$ | 0.23707 | 271.6 |
| Air | 0.22509 | 266.6 |
| $CH_4$ | 0.61290 | 402.5 |
| $H_2O$ | 0.22980 | 229.8 |
| $CO_2$ | 0.22665 | 410.5 |

Table 4. Component Gladstone-Dale Constants and Refractivities

Finally, the refractivity of a mixture of components was calculated from the equation given by Dixon-Lewis

$$(N_o-1)_{MIXTURE} = \sum_i (N_o-1)_i X_i \qquad (41)$$

2.5.4. Analysis Procedure

It was mentioned in section 2.2.4. that in order to obtain the desired sensitivity, a laminar flame interferogram must be interpreted to a small fraction of a fringe. This is particularly important in the case of domestic-scale laminar flames because this application involves relatively steep refractive index gradients and integrated fringe shifts along the light beam add up to no more than several wavelengths at $\lambda = 6328\text{Å}$. Hence, in order to exploit, quantitatively, the data furnished by an interferogram, each photograph was enlarged, on average, to a magnification of X50 on high contrast, high stability lithographic film (Agfa-Gevaert type R1pM). Fringe co-ordinates (y, z) from the magnified interferogram were then digitised on to paper tape, for subsequent processing by computer, using the Pencil Follower (d-Mac Ltd.) employed for measuring up the particle track photographs of part 1 of this thesis. In this way fringe shifts were capable of being resolved to $\lambda/100$, the resolution of the Pencil Follower being set by the spatial resolution of the shaft encoders

of the measuring system (0.1mm). Of course, spatial resolution depends also on fringe legibility, and by using a long photographic exposure time (1s) together with underdeveloping on printing, a set of narrow dark fringes, capable of measurement to $\lambda/50$ by the unaided eye, were produced on the resulting interferogram enlargements. In this way a Pencil Follower proved eminently suitable for analysing laminar diffusion flame interferograms.

Prior to commencing measurements, a given pair of interferograms (reference and test) were matched up using a pair of marker pins, attached to but well removed from the burner. A convenient origin was then chosen which fixed the congruence of the two interferograms. The Pencil Follower was then employed to record, on paper tape, the co-ordinates (y, z) of both the reference and test interferograms for up to 16 pre-selected levels encompassing the stabilising region of a flame. Employing a fringe frequency of about $3\lambda\,mm^{-1}$, the stabilising region was represented by up to 50 fringes so that the complete temperature distribution in each flame was contained in about 800 data points of the form (y, z).

2.5.5. Organisation of Programs for Computing Refractivity and Final Flame Temperature

The evaluation of the expressions, given in the preceding sections, for calculating refractivity, $N(r)-1$, and final flame temperature $T(r)$, involves numerous repetitive calculations. For this reason some time was spent in evolving a two-part computer program to analyse completely the interferograms of axisymmetric laminar diffusion flames. The first part computes and plots out fringe shift profiles throughout the stabilising region of the flame. At this stage the output may be checked for any erronious data resulting from human or machine errors. The second part then computes, from equations (34) to (41), the radial distributions of refractivity and final flame temperature. The stages involved in each program may be set out as follows:-

A) Computation of Fringe Shifts, $S(y)$

(i) Input of co-ordinates $(y, z)$ of reference and test interferograms at a number of specified levels, each level lying perpendicular to the axis of the interferogram.

(ii) Input of number of specified levels, number of fringes per level, magnification of interferogram, approximate co-ordinate of axis of interferogram, $y_c$, co-ordinates of origin $(y_o, z_o)$ and coefficients of a first order equation describing the dependence of reference fringe spacing, $\Delta y$, on fringe number.

(iii) Calculation at each specified level, z, of profiles of S(y) from $S(y)\big|_z = (y_T - y_R)/\Delta y$ where the subscripts T and R denote test and reference co-ordinates respectively.

(iv) Calculation of the co-ordinate of the axis of the interferogram, $y_c$, by orthogonal polynomial fitting of the "long" sides of the lateral fringe shift profile (Fig. 68).

(v) Output, at each selected level of:-

1. Listings of S(y), $(y-y_c)$ and $(y-y_c)^2$
2. Computer graph of $S(y-y_c)$ against $(y-y_c)^2$ to allow checking for erronious data.

B) Computation of Refractivities, N(r)-1, and Final Flame Temperatures, T(r).

(i) Input of tables of pure component properties k, $(N_o-1)$, M, $\alpha$ and $T_b$.

(ii) Input of ambient reference conditions $T_o$, $P_o$ and $H_o$.

(iii) Input of numerical fringe shift data $S(y-y_c)$, $(y-y_c)^2$.

(iv) Input of spline boundaries, $R_p(p=1,10)$, selected from a computer graph of $S(y-y_c)$ against $(y-y_c)^2$.

(v) Calculation of reference refractivities, $N_o-1$, at $T_o$, $P_o$ and $H_o$ using equations (39) and (40).

(vi) Calculation of the coefficients, $C_i$, of the spline cubics to yield a piecewise analytic function for S(y) as set out in equation (32).

(vii) Calculation of the radial distribution of refractivity, N(r)-1, using equation (34).

(viii) Calculation of the radial distribution of final flame temperature, T(r), using equation (38).

(ix) Output of N(r) and T(r) in the range $o<r<R_o$ in radius increments of 0.1 mm.

2.5.6. Assessment of Method of Analysis

The merit of the approach, discussed in the foregoing sections, is that the method of analysis lends itself to situations where the complete observed lateral fringe shift profile cannot adequately be represented by a single polynomial of sufficiently low order. It may be noted that the extended approach retains the advantage of existing methods that the part of the fringe shift distribution near the boundary of the disturbance can be omitted without impairing the accuracy of the computed values nearer the centre. A sectional method, such as the spline technique, has however a limitation that the higher derivatives will, to some degree, be unsmooth. Nevertheless, it has been found that a careful selection of the necessarily arbitrarily chosen knots can lead to an adequate representation of the data with minimum discontinuities at the knots.

In order to test its merits, the extended approach, developed in this thesis, has been contrasted against the best of the existing methods, namely that of Freeman and Katz. The lateral fringe shift distribution of Fig. 68 (curve 2), typical of an

axisymmetric laminar diffusion flame in which the refractivity of the jet core is significantly different from that of the oxidant and burnt gases at the same temperature, was analysed in three separate ways for refractive index. The resulting refractive indices were then related to final flame temperature using equation (38).

Curve 1, Fig. 69, was computed using the extended approach, developed in this thesis, in which the observed fringe shift data are represented in sections using the extended spline technique. Curve 2 was computed using a complete representation of the observed fringe shifts by the method of Freeman and Katz with i set equal to 10 in equation (30). Curve 3 was computed by restricting the method of Freeman and Katz to the less complicated distribution over the outermost parts of the flame where the method might be expected to be valid. A comparison between curves 1 and 3 shows that the extended spline method and the existing method of Freeman and Katz show good agreement, indeed as expected, over the outermost part of the flame. Curve 2, however, shows a breakdown in the adequacy of a single curve representation of the observed fringe shift data.

Curve 3 shows a shape close to that to be expected.

The question then arises as to whether any of these representations adequately represents the data. Unfortunately there is no entirely satisfactory method which could, in the present situation, be regarded as a primary standard. However some measure of cross-checking was provided by contrasting the temperature profile determined interferometrically with the profile measured by fine-wire thermocouple thermometry, probably the closest method to a primary standard. The thermocouple measurements were carried out, as discussed in section 1.3.2., using a couple constructed by butt-welding 0.0025 cm. diameter wires of Pt/20%Rh and Pt/40%Rh and coating with silica. A radiation correction was applied in the normal way using equation (2). As may be seen in Fig. 70 the agreement between the temperature profiles obtained by thermocouple and by the extended spline analysis of an interferogram is remarkably good. It should be noted that the temperature difference across the thermocouple in the part of the flame where the temperature gradient was steepest was as high as 80°K. For this reason and also because the very small thermocouple

may disturb the flame, a more precise comparison is not possible between the two quite independent methods.

It has been shown that an extended Spline technique can be adapted for the analysis of axisymmetric interferograms of laminar diffusion flames. Indeed the method, developed in this thesis, would seem particularly suitable for situations, such as the lateral fringe shift profile of axisymmetric diffusion flames, where the observed data are a relatively complex function of lateral distance.

2.5.7. Estimation of Conductive Heat Energy Fluxes and Heat Release Rates

It will be recalled, from the results of part 1 of this thesis, that the bulk of the heat released in diffusion flames arises principally from changes in the conduction flux profile which in turn depends on changes in the temperature profile. It follows that it should be possible, within certain limitations on precision, to estimate the pattern of heat release rates from the temperature profiles alone. The final chapters of this thesis attempt first to estimate the conductive heat flux pattern from interferometrically

determined temperatures using the equation

$$\underline{F}_{H,CND} = -\lambda \, \text{grad } T \qquad (42)$$

and second to estimate the rates of heat release from the equation

$$Q = \text{div}_y \, (-\lambda \, \text{grad } T) \qquad (43)$$

In the absence of species data, $\lambda$, in equations (42) and (43), was taken as $\lambda(N_2)$ since, as was shown in Figs. (13) and (20), nitrogen is the dominant species (64% to 75% by volume) within the reaction zone of diffusion flames.

## 2.6. RESULTS AND DISCUSSION

### 2.6.1. Diffusion Flame Interferograms

It was mentioned earlier that, in general, in order to quantitatively interpret an interferogram it is necessary to specify precisely the geometry of the refractive index field. In the case of the simplest flame geometry - namely that of an extended flat flame - end effects can assume unwanted importance since the fringe pattern is integrated along the total light path. Furthermore, even if the device of subtractive interferometry is employed to minimise end effects (Sandhu and Weinberg (1972)) difficulties arise from the extremely high sensitivity of the method to differential disturbances particularly in the indeterminate boundary layers in the end regions. Of course in the case of the conical flames, studied in this thesis, difficulties arising from end effects and differential disturbances are largely removed but the ensuing analysis for density and temperature is mathematically more complex. Thus, diffusion flame interferograms, in general, and those of conical flames in particular cannot be readily interpreted in terms of flame temperature. Nevertheless, the inter-

ferogram itself exhibits a number of important features which largely dictate the ensuing analysis for final flame temperature.

A typical conical flame interferogram is shown in Fig. 66 for a diffusion flame of methane burning 7.81 $mls^{-1}$. Perhaps the first point to note is that the maximum fringe shift for phase objects such as domestic-scale laminar flames is no more than a few $\lambda$'s (e.g. 3 $\lambda$'s in Fig. 66). Clearly, in this situation, an infinite fringe interferogram would give an insufficient spatial distribution of data points for quantitative interpretation whereas finite fringe interferometry is more suited to phase objects of this scale. The shape of the lateral fringe shift profile resulting from an interferogram depends, to a large extent, on the refractivity of the fuel-gas under examination. In the case of a fuel-gas of relatively high refractivity, such as methane, the refractive index field consists of a core of fuel-gas of high refractivity surrounded by an envelope of burning gases and products of lower refractivity, even at the same reference temperature and significantly lower at elevated flame temperatures.

In this situation, the resulting lateral fringe shift profile tends to exhibit a characteristic valley at the interferogram axis, of the form shown in Fig. 68 (curve 2), and this, as mentioned in section 2.5., gives rise to considerable difficulties in the subsequent analysis. This situation is in contrast to that of a fuel-gas of relatively low refractivity, such as hydrogen, where the lateral fringe shift profile would tend to assume a simpler gaussian shape of the form shown in Fig. 68 (curve 1). It should be mentioned also that in the case of fuel-gases of relatively high refractivity, such as methane, the observed lateral fringe shift profiles may vary considerably between a relatively simple profile of the form shown in Fig. 68 (curve 1) at a distance well above the flame port to a more complex profile of the form shown in Fig. 68 (curve 2) at a level close to the burner port. Clearly, the shape of the observed profile depends not only on the refractivity of the fuel-gas under examination but also on the particular level in the flame.

The foregoing discussion shows that diffusion flame interferograms, in general, and conical flame interferograms in particular cannot directly be interpreted in terms of temperature. Furthermore, the above discussion emphasises that any analytical procedure that leads to flame temperature must possess sufficient versatility to cope with the wide range of fringe shift profiles which characterise interferograms of the stabilising region of laminar diffusion flames.

2.6.2. Temperature Profiles

The distributions of temperature for the three flames examined, namely diffusion flames of methane burning 0.42 $mls^{-1}$, 3.72 $mls^{-1}$ and 7.81 $mls^{-1}$, were obtained using the method of interferometric analysis outlined in section 2.5. Radial distributions of flame temperature were computed for up to sixteen levels in each flame and the results plotted out in the form of isotherms (Figs. 71, 72 and 73). As mentioned in part 1 of this thesis, measurements of the extent of the visible flame sheet are partly subjective but, nevertheless their approximate positions

are superimposed on Figs. 71 to 73 for reference purposes.

The shapes of the temperature patterns for the flames examined are much as expected. In the case of the flame burning 0.42 $mls^{-1}$, the reaction zone assumes a shape such that combustion occurs over a hemispherical flame front, inclined vertically at the flame base. With increasing supply of reactant it can be seen from Figs. 72 and 73 that the flame sheet becomes inclined away from the axis of the flame with increasing distance above the burner port, a similar pattern to that shown in Figs. 3 and 4 where the temperature profile was measured using a thermocouple probe method.

For the flame burning 0.42 $mls^{-1}$ the locus of the points of maximum temperature lies within the visible flame sheet at the extreme base of the flame but on the unburnt-fuel side of the flame sheet at levels above the flame base. Those for the flames burning 3.72 $mls^{-1}$ and 7.81 $mls^{-1}$ lie along the inner edge of the visible sheet (Figs. 72 and 73) which, considering the partly subjective nature of the location of the

visible flame sheet, are in good agreement with the results of part 1 of this thesis (Figs. 3 and 4). It was mentioned in section 1.5.7. that substantial heat energy may be liberated at or below the visible flame sheet and indeed the interferometrically determined temperatures in this region (1100°K at 0.42 $mls^{-1}$ and 1300°K both at 3.72 $mls^{-1}$ and 7.81 $mls^{-1}$) are fairly high which would in turn reflect liberation of heat energy through conduction processes. The maximum flame temperature for the flame burning 0.42 $mls^{-1}$ is little more than 1600°K whereas those for the flames burning 3.72 $mls^{-1}$ and 7.81 $mls^{-1}$ are close to 1900°K, within 2.5% of the peak temperatures determined in part 1 of this thesis using the method of thermocouple probe thermometry.

The foregoing discussion shows clearly that an extended spline analysis of an interferogram provides not only an extremely versatile method of measuring flame temperature but also the resolution and precision compatible with the more conventional probe methods

that are normally associated with flame structure studies. Of course the technique would have additional merit if it could be utilised to provide estimates of the fluxes of heat energy and the rates of heat release within the all important stabilising region of laminar diffusion flames.

2.6.3. Conductive Heat Energy Fluxes

Fluxes of conductive heat energy for the flame burning 7.81 $mls^{-1}$ were estimated from equation (42) using the interferometrically determined temperature profiles of Fig. 73. An example of the method of calculation is shown in table 5, the derivative terms being evaluated using a simple graphical method. Results for six levels encompassing the flame base have been plotted out in the form of heat flux vectors as shown in Fig. 74.

Fig. 74 shows that the conductive heat flux pattern in the region encompassing the base of diffusion flames is qualitatively similar to the total heat flux pattern of part 1 of this thesis (Figs. 44 and 45) where the total flux was evaluated as the sum of the component contributions from molecular diffusion, thermal convection, and thermal conduction. Clearly,

| $\tau$ | T | $\lambda_{N_2} \times 10^6$ | $-\frac{\partial T}{\partial y}$ | $-\frac{\partial T}{\partial z}$ | $F_{H,CND,y} = -\lambda \frac{\partial T}{\partial y}$ | $F_{H,CND,z} = -\lambda \frac{\partial T}{\partial z}$ |
|---|---|---|---|---|---|---|
| mm | °k | cal $cm^{-1}$ $s^{-1}$ $°k^{-1}$ | °k $cm^{-1}$ | °k $cm^{-1}$ | cal $cm^{-2}$ $s^{-1}$ | cal $cm^{-2}$ $s^{-1}$ |
| 1·2 | 1010 | 160·2 | −14,000 | 0,100 | −2·24 | 0·02 |
| 1·6 | 1480 | 217·5 | −7,400 | 0,100 | −1·61 | 0·02 |
| 2·0 | 1730 | 244·3 | −6,200 | −0,450 | −1·51 | −0·11 |
| 2·4 | 1800 | 251·7 | −0,100 | −1,000 | −0·03 | −0·25 |
| 2·8 | 1745 | 246·0 | 3,600 | −1,400 | 0·89 | −0·34 |
| 3·2 | 1535 | 223·7 | 6,900 | −1,900 | 1·54 | −0·42 |
| 3·6 | 1240 | 189·2 | 7,700 | −3,000 | 1·46 | −0·57 |
| 4·0 | 930 | 150·0 | 7,000 | −3,200 | 1·05 | −0·48 |
| 4·4 | 660 | 114·5 | 5,000 | −2,600 | 0·57 | −0·30 |
| 4·8 | 505 | 93·5 | 2,900 | −1,700 | 0·27 | −0·16 |

TABLE 5 EXAMPLE OF METHOD OF CALCULATION OF $F_{H,CND}$

(METHANE FLOW RATE 7·81 $mls^{-1}$, z = 1·5 mm.)

as suggested earlier, conductive flux profiles determined from interferometric data do give a reasonable indication of the heat flow pattern at the base of diffusion flames. The magnitudes of the fluxes, shown in Fig. 74, are in good agreement also with the more rigorously determined fluxes of Figs. 44 and 45. At a level in the region of the burner port the local heat flux towards the burner is approximately 2 cals $cm^{-2}s^{-1}$, similar to the corresponding figure from Fig. 45. Of course not shown in Fig. 74 are the heat flux vectors in the central stream from where a large proportion of the heat liberated in the reaction zone would be expected to be conveyed by convection to higher levels in the flame. Nevertheless, conductive heat flux vectors, evaluated from interferometrically determined temperature profiles, give a reasonable indication of the heat flow pattern within the all important stabilising region of diffusion flames.

2.6.4. Heat Release Rates

The approximate rates of volumetric heat release throughout the stabilising region of the flame burning 7.81 $mls^{-1}$ were estimated from the associated flux

profiles of Fig. 74 using equation (43). Results for 6 levels have been plotted out in the form of iso-heat release rate lines as shown in Fig. 75. Several points emerge.

First, it can be seen that the heat release rate pattern of Fig. 75 assumes an overall shape similar to that derived from the more rigorous studies of part 1 of this thesis (Fig. 61), thus lending further support to the conclusion that the heat release rate pattern arises principally from changes in the conduction flux profile. The peak rate of heat release of Fig. 75, namely 45 cals $cm^{-3}s^{-1}$, is, however, significantly less than the corresponding rate (155 cals $cm^{-3}s^{-1}$) of Fig. 61. Of course part of this discrepancy originates from the fact that changes in the conduction flux profile would be expected to account for about 70% and not all of the peak rate of heat release. If allowance is made for this, the peak rate of heat release in the flame burning 7.81 $mls^{-1}$ would be expected to be about 75 cals $cm^{-3}s^{-1}$. However, this is still some 50% lower than and well outside the experimental error limit of the corresponding figure

from part 1 of this thesis (155 $\pm$ 31 cals $cm^{-3}s^{-1}$). This sort of discrepancy illustrates well the great difficulty of providing reasonable estimates of the rates of heat release in laminar flames. Clearly, although the internal consistency of each of the different experimental methods is reasonably good, there must be some doubt as to their absolute accuracy particularly since heat release rate depends critically on the second derivative of flame temperature. A major problem, here, is that no one method of measuring flame temperature may be regarded as a primary standard. Thermocouples, in common with other probe methods, tend to perturb the flame front under examination to an indeterminate degree and furthermore, with temperature gradients within diffusion flames of up to $20,000^{o}K\ cm^{-1}$, a temperature difference of up to $100^{o}K$ may prevail across the bead of fine-wire thermocouples. Optical methods, too, are not without their problems. Although they have a very definite advantage in not disturbing the flame front under examination they suffer from reduced sensitivity at high temperatures as a result of the

inverse dependence of refractivity on flame temperature.

In this sort of situation heat release rates determined from temperature data cannot be quoted to better than a factor of two accuracy although the internal consistency of each method, as shown both here and elsewhere, is likely to be considerably better than this. Indeed the results presented in this thesis offer encouragement, that the technique of laser interferometry coupled with an extended spline analysis of an interferogram can provide a powerful tool for estimating the complete thermal picture (temperature, fluxes of heat energy and rates of heat release) of laminar diffusion flames.

## 2.7. CONCLUSIONS

The following conclusions may be drawn from the foregoing results of an optical investigation of the structures of laminar diffusion flames of methane.

1. It has been shown that an extended spline technique can be successfully adapted for the quantitative interpretation of conical flame interferograms. The analysis developed has particular merits for situations, such as laminar diffusion flames, where the observed fringe shift distributions are a relatively complex function of lateral distance.
2. The foregoing discussion shows that an extended spline analysis of a conical flame interferogram provides not only a versatile method of measuring flame temperature but also the resolution and precision compatible with the more conventional probe methods that are normally associated with flame structure studies.
3. Finally, the results offer encouragement that a method similar to that described can provide a complete picture of the thermal structure (temperature, fluxes of heat energy and rates of heat release) of laminar diffusion flames.

## 2.8. FUTURE WORK

Much of the work that has been carried out on flame structure relates to monoport burner flames whereas in practice there is interaction between adjacent main flames on multiport burners and between main and retention flames on retention flame burners. Whilst the work on monoport flames is an essential and logical step towards the development of burner design procedures more quantitative information is required on the process of flame interaction. The empirical work carried out so far, mainly on retention flames (Heller), has met with limited success and there is a very real need to establish the factors controlling the extent of flame interaction, particularly the effects on stability of interaction of heat energy, aerodynamic and species fields, before real progress can be made in improving the use that is made of flame interaction in burner design.

With natural gas likely to be supplemented, in the near future, by substitute gases, particularly at peak loading times, a knowledge of the structures of flames burning multicomponent fuel gases containing hydrogen and higher hydrocarbons will be essential to the burner design engineer. The technique developed

in part 2 of this thesis, namely laser interferometry coupled with an extended spline analysis of a conical interferogram, could provide a powerful tool for estimating the complete thermal structures of flames burning multicomponent fuel-gas mixtures.

REFERENCES


| | |
|---|---|
| Anagostou, E. and Potter, A.E., | Ninth Symposium (International) on Combustion, Academic Press, p.1. |
| Andersen, J.W. and Fein, R.S., | J. Chem Phys., 18, p.441, 1950. |
| Barr, J., | Fourth Symposium (International) on Combustion, Williams and Wilkins, p. 765, 1953. |
| Barr, J., | Fuel, p. 51, 1954. |
| Barr, J., | A.G.A.R.D. Memo. No. AG 11/M7, 1954. |
| Barr, J. and Mullins, B.P., | Fuel, pp. 181-188, 225-228, 1949. |
| Bellis, R.J., | Ph.D. Thesis, University of Leeds, 1968. |
| Bennet, F.D., Carter, W.C. and Bergdolt, V.E., | J. Appl. Phys., 23, No. 4, p. 453, 1952. |
| Bockasten, K., | J. Opt. Soc. Amer., 51, No. 9, p. 943, 1961. |
| Bradley, J.W., | A.I.A.A. Journal, 6, No. 6, p. 1190, 1968. |
| Bradley, D. and Entwistle, A.G., | Brit. J. Appl. Phys., 17, p. 1155, 1966. |

| | |
|---|---|
| Burgoyne, J.H. and Weinberg, F.J., | Proc. Roy. Soc., A. 224, p. 286, 1954. |
| Burke, S.P. and Schumann, T.E.W., | Ind. Eng. Chem., 20, p. 998, 1928. |
| Craven, A.D. and Foster, M.G., | Comb. and Flame, 10, p. 95, 1966. |
| Datta, P., Hayward, B.M. and Reed, S.B., | Comb. and Flame, 17, No. 3, p. 399, 1971. |
| Datta, P. and Reed, S.B., | Comb. and Flame, 19, p. 89, 1972. |
| Dixon-Lewis, G., | Proc. Roy. Soc. (London), A. 307, p. 111, 1968. |
| Dixon-Lewis, G., | Proc. Roy. Soc. (London), A. 308, p. 517, 1969. |
| Dixon-Lewis, G. and Isles, G.L., | Eighth Symposium (Int.) on Combustion, p. 448, 1962. |
| Dyson, J., | J. Opt. Soc. Amer., 47, p. 386, 1957. |
| Fay, J.A., | J. Aero. Sci., 21, p. 681, 1954. |
| Forsythe, G.E., | J. Soc. Indust. Appl. Math., 5, No. 2, 1957. |

Freeman, M.P. and Katz, S., J. Opt. Soc. Amer., 53, No. 10, p. 1172, 1963.

Friedman, R., Fourth Symposium (Int.) on Combustion, p. 259, 1953.

Fristrom, R.M., Prescott, R. and Grunfelder, C., Comb. and Flame, 1, p. 102 1957.

Fristrom, R.M. and Westenberg, A.A., Flame Structure, McGraw-Hill: New York, 1965.

Gaydon, A.G. and Wolfhard, H.G. Flames, Their Structure, Radiation and Temperature, Chapman and Hall: London, 1960.

Gunther, R. and Janisch, G., Comb. and Flame, 19, No. 1, p. 49, 1972.

Hariharan, P. and Sen, D., J. Opt. Soc. Amer., 49, p. 1105, 1959.

Heller, M., J. des Usines a Gaz, 82, No. 6, p. 225, 1958.

Hirshfelder, J.O., Curtiss, C.F. and Bird, R.B., Molecular Theory of Gases and Liquids, Wiley and Sons, 1954.

Hottel, H.C. and Hawthorne, W.R., Third Symposium (Int.) on Combustion, Williams and Wilkins, p. 254, 1949.

Johnston, H.L. and Grilly, E.R., J. Chem. Phys., 14, p. 233, 1946.

Jost, W., Explosion and Combustion Processes in Gases, McGraw-Hill: New York, 1946.

Kaskan, W.E., Sixth Symposium (Int.) on Combustion, Reinhold: New York, p. 134, 1957.

Kaye, G.W.C. and Laby, T.H., Physical and Chemical Constants, Longmans, 1966.

Klaus, R.L. and Van Ness, H.C., A.I.Ch.E.J., 13, p. 1132, 1967.

Kurlbaum, F., Phys. Z., 3, p. 187, 1902.

Ladenburg, R., Van Voorhis, C.C. and Winckler, J., Physical Review, 76, No. 5, p. 662, 1949.

Lamb, H., Hydrodynamics, Cambridge University Press: Cambridge, 6th ed., p. 614, 1932.

| | |
|---|---|
| Landis, F. and Nilson, E.N., | Progress in International Research on Thermodynamic and Transport Properties, Academic Press: New York, p. 218, 1962. |
| Levy, A. and Weinberg, F.J., | Comb. and Flame, 3, p. 229, 1959. |
| Lewis, B. and Von Elbe, G., | Combustion, Flames and Explosions of Gases, Academic Press, 1961. |
| Linan, A., | O.S.R./B.O.A.R. T.N. 62-24, Madrid, 1961. |
| Lindsay, A.L. and Bromley, L.A., | Ind. Eng. Chem., 42, p. 1508, 1950. |
| Linnett, J.W. and Simpson, C.J.S.M., | Sixth Symposium (Int.) on Combustion, Reinhold: New York, p. 20, 1957. |
| Melvin, A., Moss, J.B. and Clarke, J.F., | Comb. Sc. and Tech., 6, p. 135, 1972. |
| Murty, M.V.R.K. | Appl. Optics, 3, p. 531, 1964. |
| Nestor, O.H. and Olsen, H.N., | S.I.A.M. Review, 2, No. 3, p. 200, 1960. |
| Oppenheim, A.K., Urtiew, P.A. and Weinberg, F.J., | Proc. Roy. Soc. (London), A. 291, p. 279, 1966. |

| | |
|---|---|
| Pandya, T.P. and Weinberg, F.J., | Proc. Roy. Soc. (London), A. 279, p. 544, 1964. |
| Pearce, W.J., | Optical Spectrometric Measurement of High Temperatures, Univ. of Chicago Press, 1960. |
| Potter, A.E. and Butler, J.N., | Am. Rocket Soc. J., 29, p. 54, 1959. |
| Potter, A.E., Heimel, S. and Butler, J.N., | Eighth Symposium (Int.) on Combustion, p. 108, 1960. |
| Raterink, H.J. and Lamberts, C.W., | Ninth Int. Congress on High-Speed Photography, Denver Colorado, Aug. 1970. |
| Robson, K. and Wilson, M.J.G., | Comb. and Flame, 13, p. 626, 1969. |
| Sandhu, S.S. and Weinberg, F.J., | J. Sci. Instrum., 5, p. 1018, 1972. |
| Schwar, M.J.R. and Weinberg, F.J., | Comb. and Flame, 13, p. 335, 1969. |
| Simmonds, W.A. and Wilson, M.J.G., | Gas Research Board Communication No. 61, p. 378, 1948. |

| | |
|---|---|
| Smith, R.A. , | J. Inst. Gas Engrs., 11, p. 318, 1971. |
| Smith, S.R. and Gordon, A.S. , | J. Chem. Phys., 60, p. 759, 1956. |
| South, R. , | A.I.A.A.J., 8, No. 11, p. 2057, 1970. |
| Spalding, D.B. , | Fuel, 29, pp. 2 and 25, 1950. |
| Spalding, D.B. , | Am. Rocket Soc. J., 31, p. 763, 1951. |
| Spalding, D.B. , | Fourth Symposium (Int.) on Combustion, Williams and Wilkins, p. 847, 1952. |
| Spalding, D.B. , | Fuel, 32, p. 169, 1953. |
| Spalding, D.B. , | Some Fundamentals of Combustion, Butterworths: London, 1955. |
| Spalding, D.B. , | Am. Rocket Soc. J., 31, No. 6, p. 763, 1961. |
| Spalding, D.B. and Jain, V.K. , | Comb. and Flame, 6, p. 265, 1962. |

| | |
|---|---|
| Spiers, M.H., | Technical Data on Fuel, British National Committee World Power Conference, 6th ed., 1962. |
| Svehla, R.A., | N.A.S.A., TR R-132, Lewis Research Centre, Cleveland, Ohio, 1962. |
| Tanner, L.H., | J. Sci. Instrum., 42, p. 834, 1965. |
| Tanner, L.H., | J. Sci. Instrum., 43, p. 878, 1966. |
| Tewari, G.P. and Weinberg, F.J., | Proc. Roy. Soc. (London), A. 296, p. 546, 1967. |
| Thomas, J.R., | Ph.D. Thesis, University of Leeds, 1968. |
| Tsuji, H. and Yamaoka, Z., | Thirteenth Symposium (Int.) on Combustion, p. 723, 1970. |
| Walker, R.E. and Westenberg, A.A., | J. Chem. Phys., 29, No. 5, p. 1139, 1958. |
| Walker, R.E. and Westenberg, A.A., | J. Chem. Phys., 29, No. 5, p. 1147, 1958. |
| Walker, R.E. and Westenberg, A.A., | J. Chem. Phys., 32, No. 2, p. 436, 1960. |
| Wassiljewa, A., | Phys. Z., 5, p. 737, 1904. |

Westenberg, A.A. and de Haas, N., Phys. of Fluids, 5, No. 3, p. 266, 1962.

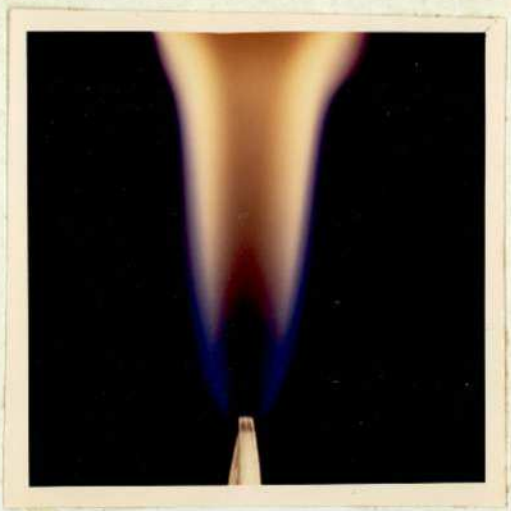
Wohl, K., Kapp, N.M. and Gazley, C., Third Symposium (Int.) on Combustion, Williams and Wilkins, p. 3, 1949.

Wolfhard, H.G. and Parker, W.G., Proc. Phys. Chem. Soc., 65A, p. 2, 1952.

Zeldovich, Y.B., Zh. Tech. Fiz., 19, p. 1199, 1949. Translated by N.A.S.A., T. Memo 1296.



(a) SIDE VIEW



(b) END VIEW

FIG.1 TWO-DIMENSIONAL METHANE DIFFUSION FLAME BURNING 142 $ms^{-1}$

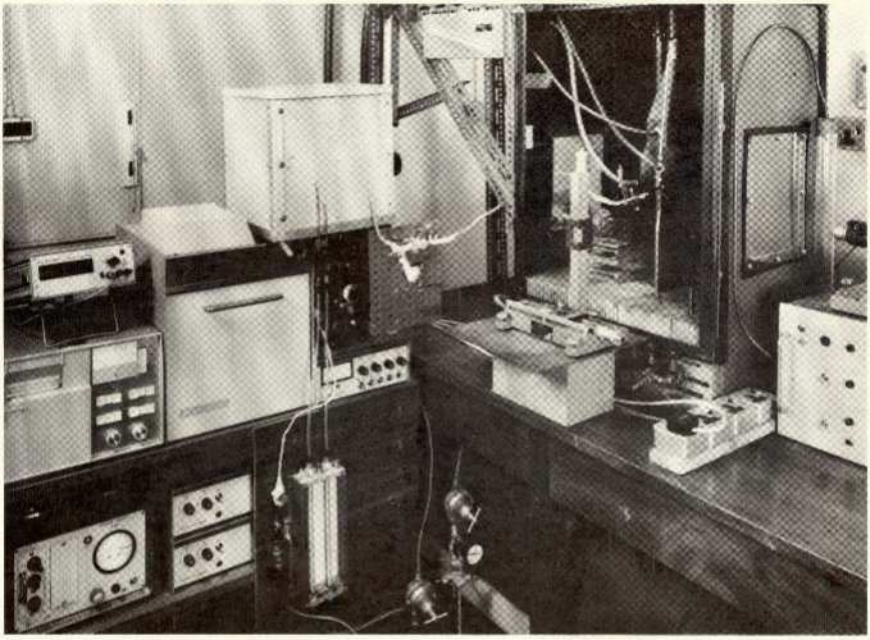


FIG. 2 GENERAL VIEW OF EXPERIMENTAL RIG.

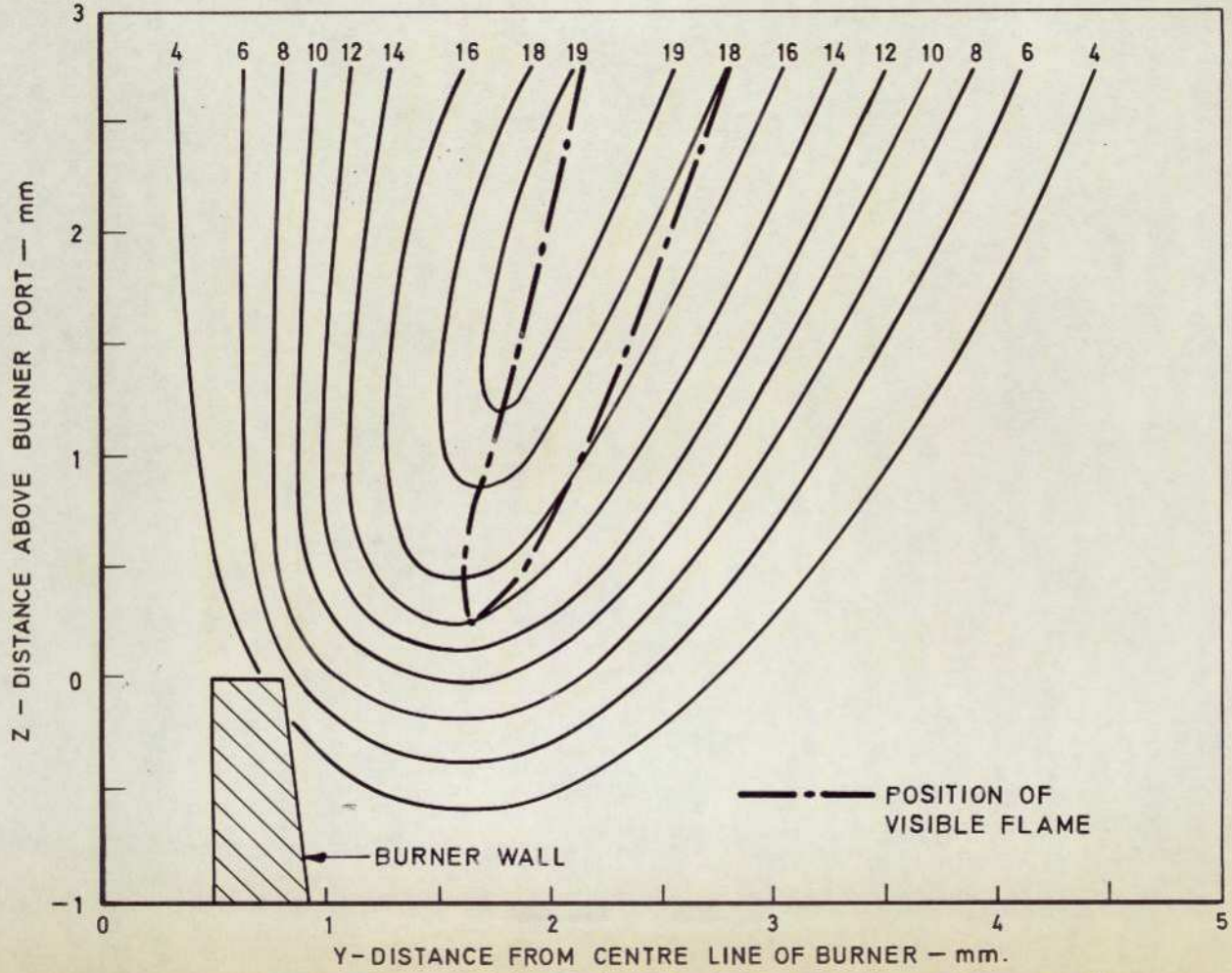



FIG. 4 ISOTHERMALS (°K) x $10^{-2}$ FOR FLAME BURNING 650 mls $^{-1}$

3053/48/3

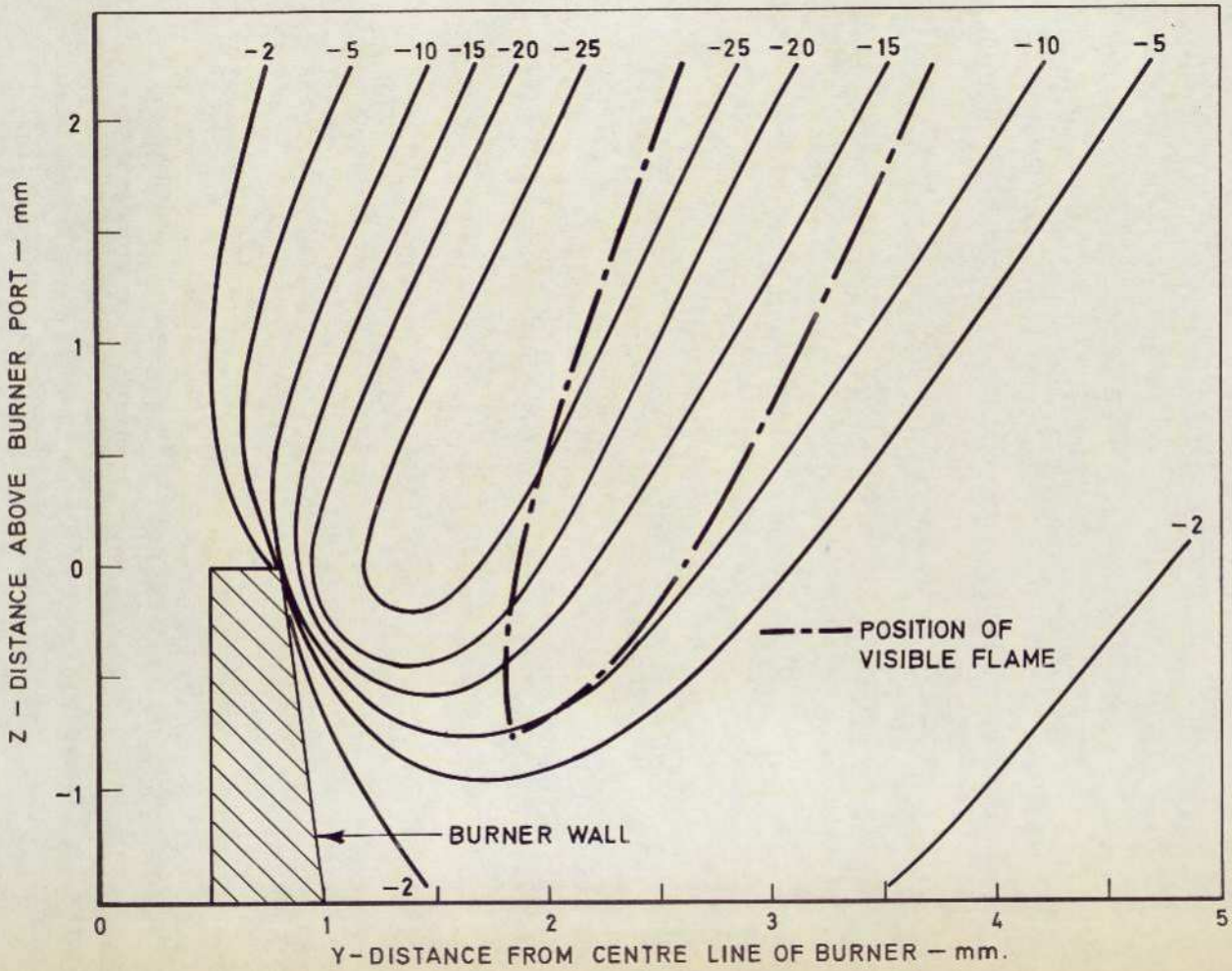



FIG. 5 ISOVELS OF COMPONENT $V_y$ (cm. $s^{-1}$) FOR FLAME BURNING 142 mls $^{-1}$

305348/4.

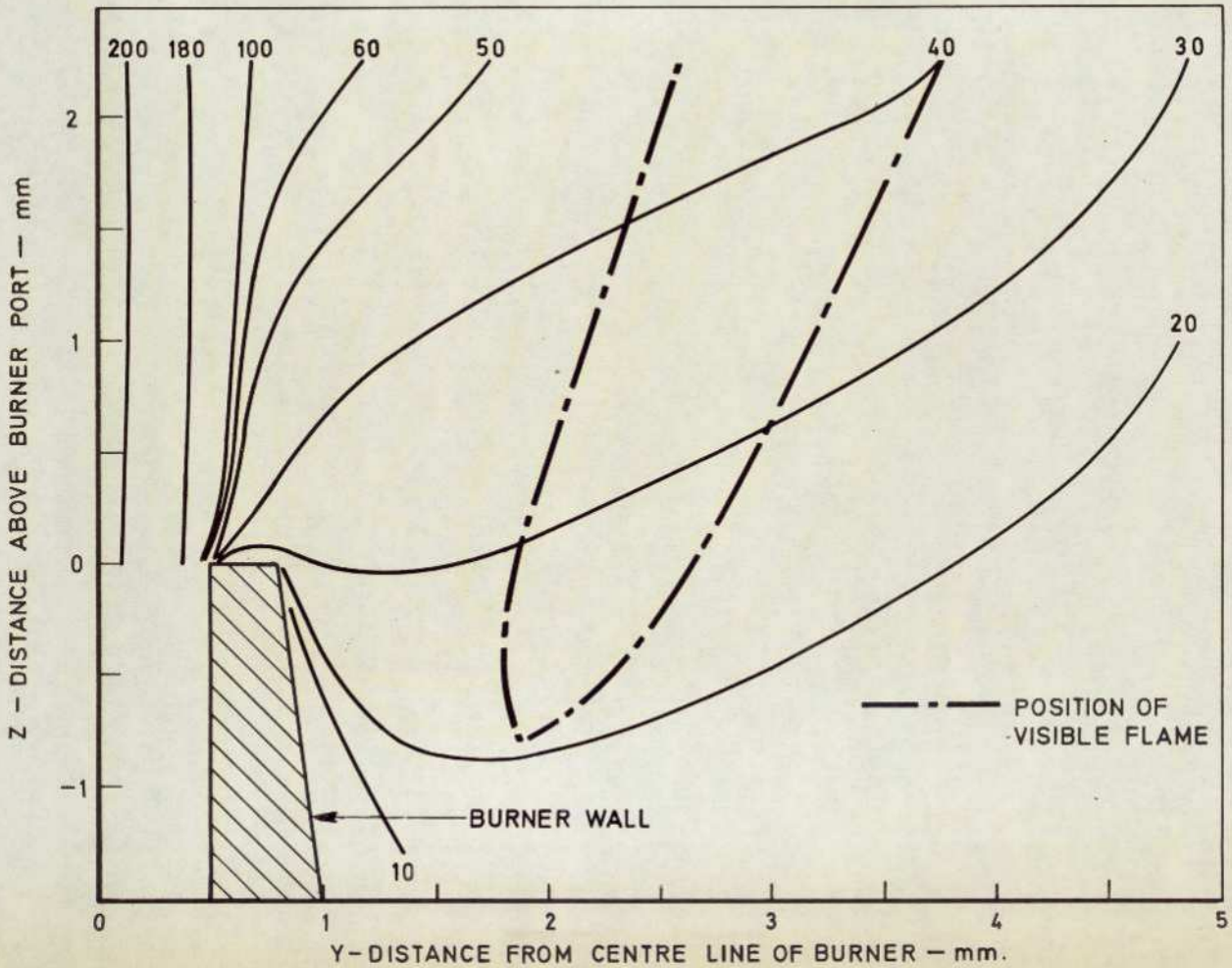



FIG. 6 ISOVELS OF COMPONENT $V_z$ (cm.s$^{-1}$) FOR FLAME BURNING 142 mls$^{-1}$

305348/5

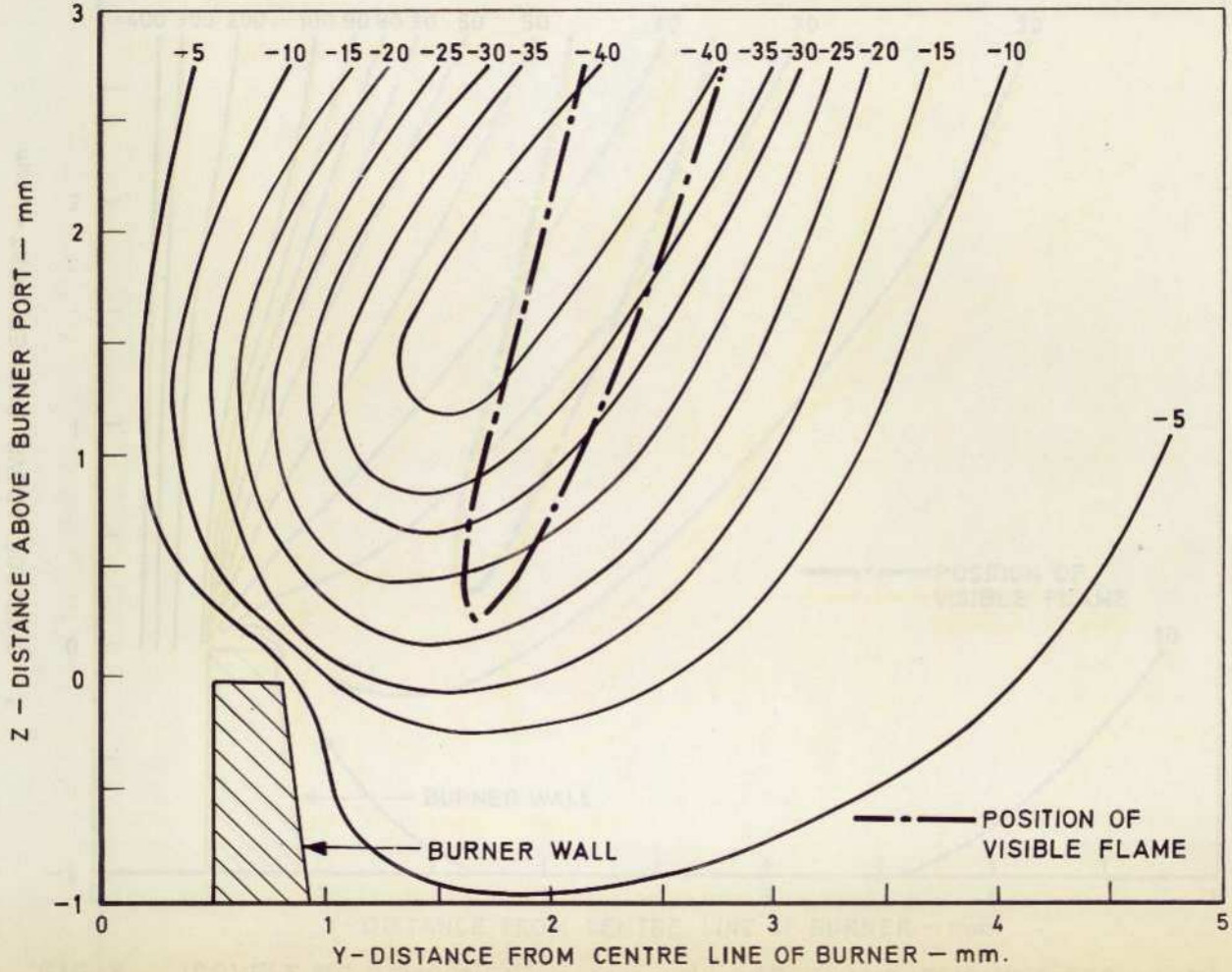



FIG. 7 ISOVELS OF COMPONENT $V_y$ ( $cm.s^{-1}$ ) FOR FLAME BURNING 650 $mls.^{-1}$

305348/6

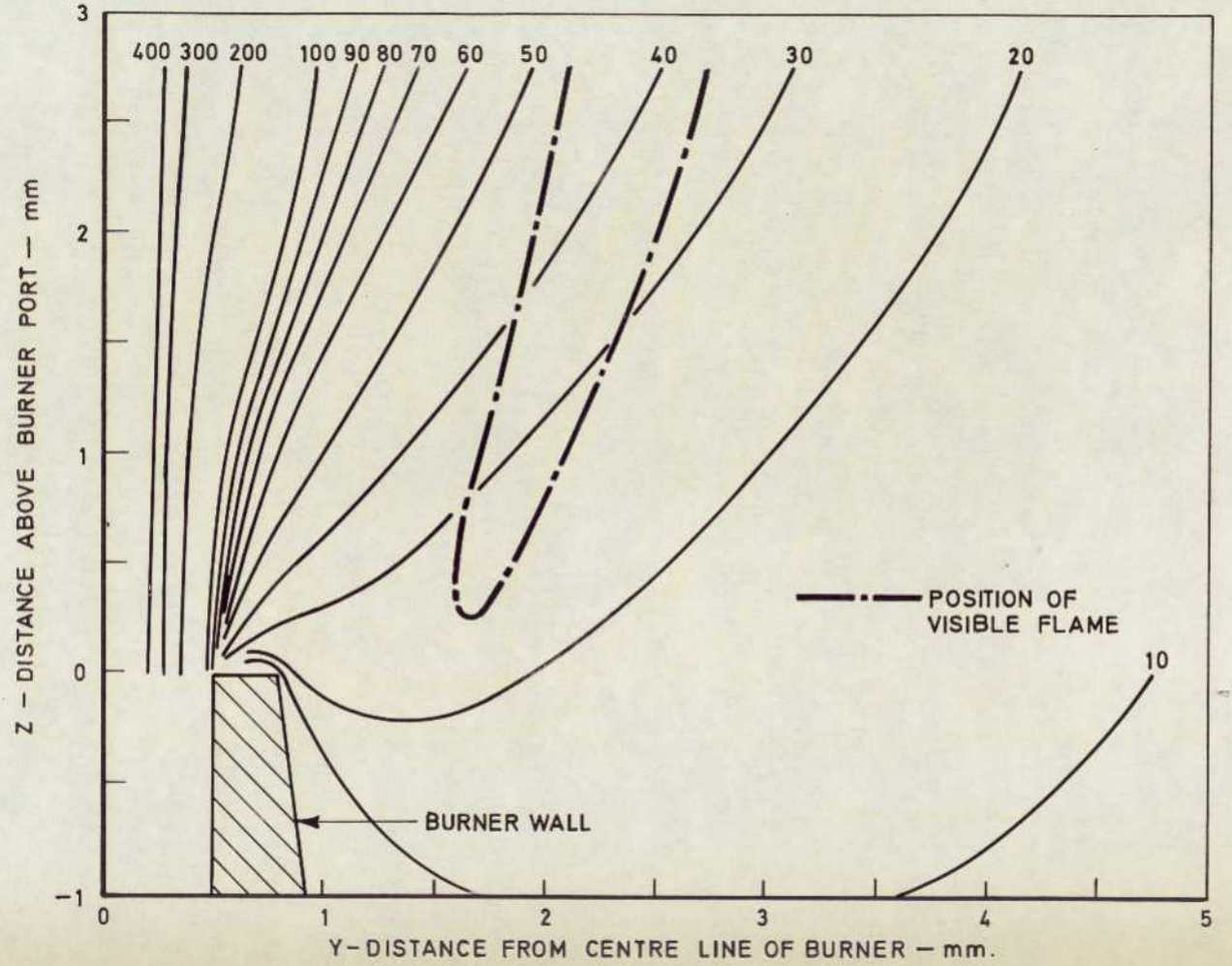
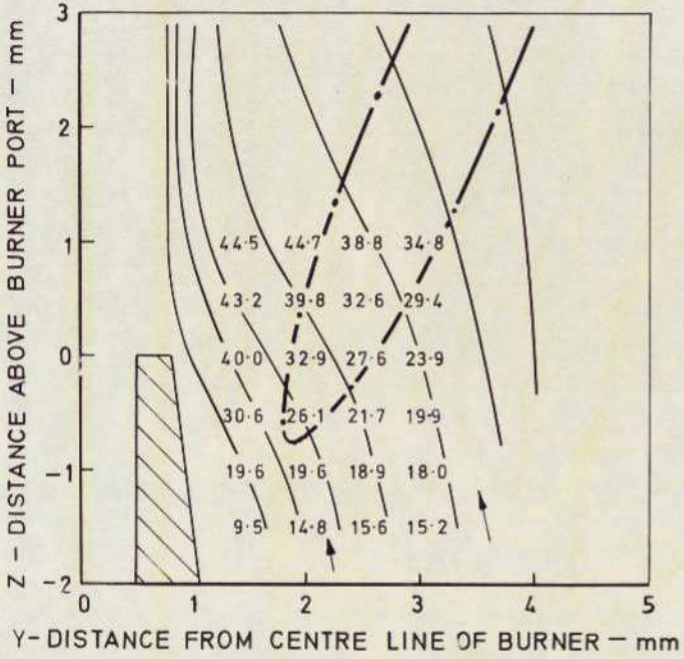
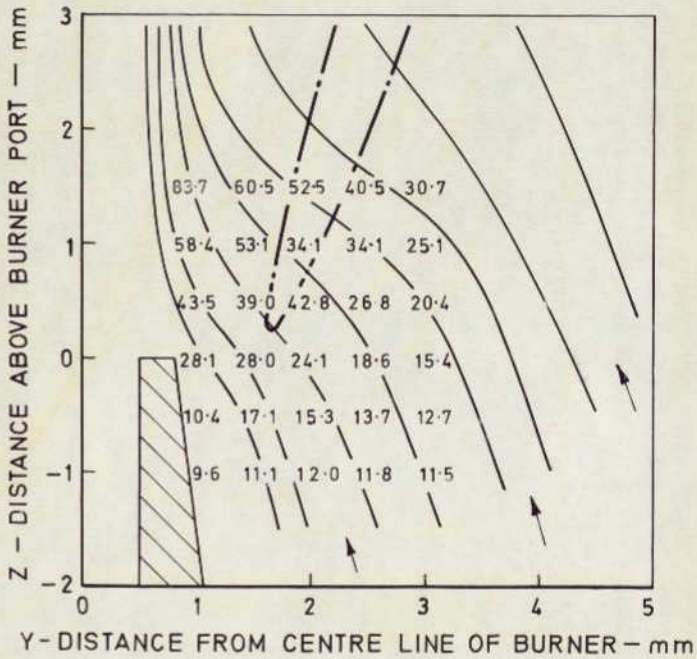



FIG. 8 ISOVELS OF COMPONENT $V_z$ (cm.s$^{-1}$) FOR FLAME BURNING 650 mls$^{-1}$

3053/48/7




FLAME BURNING 142 mls$^{-1}$




FLAME BURNING 650mls$^{-1}$

FIG. 9 FLOW STREAMLINES - VELOCITIES IN cms$^{-1}$

305348/8

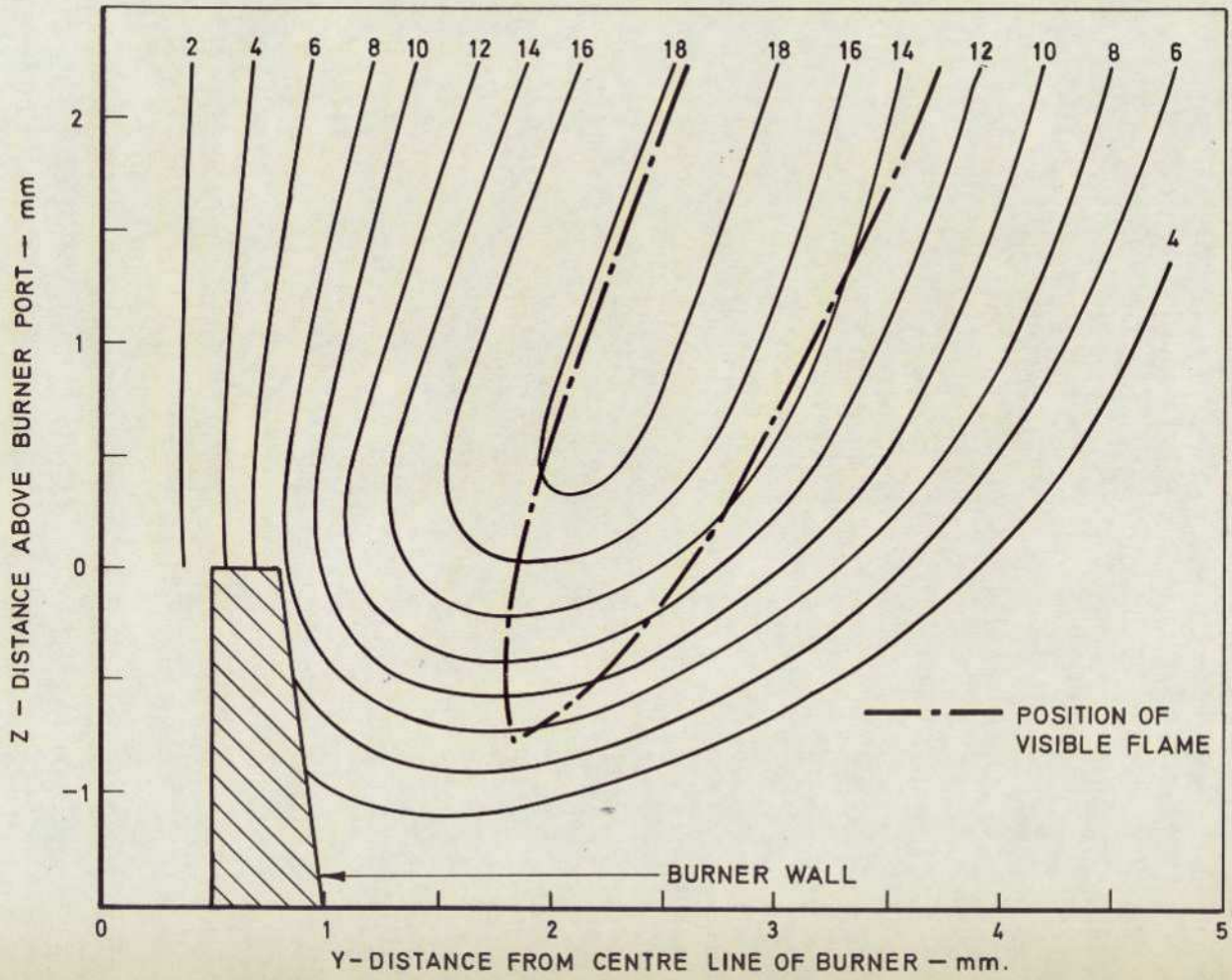



FIG. 10 ISOPLETHS OF $H_2O$ (mole %) FOR FLAME BURNING 142 mls$^{-1}$

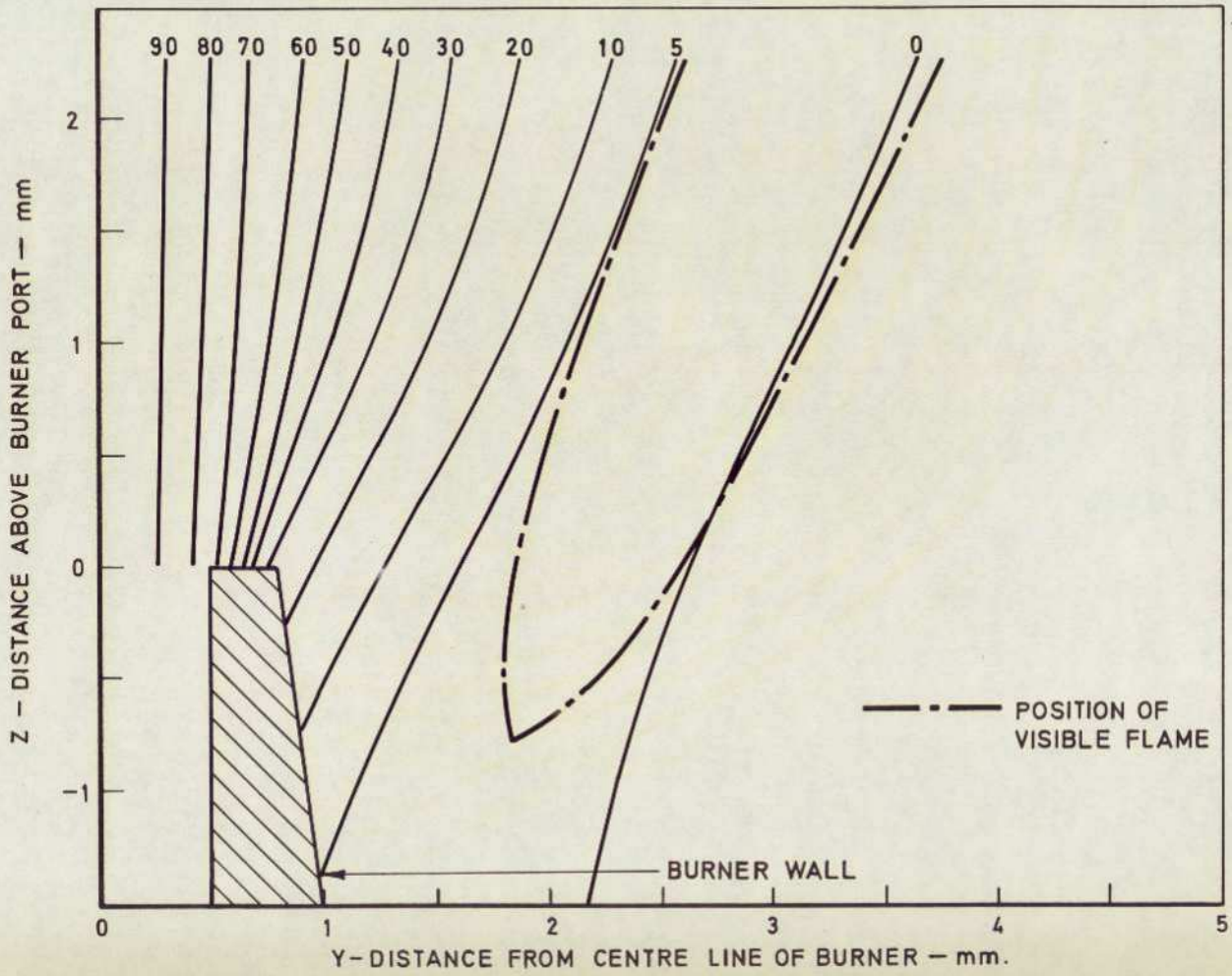



FIG. 11 ISOPLETHS OF $CH_4$ (mole %) FOR FLAME BURNING 142 mls $^{-1}$

305348/10

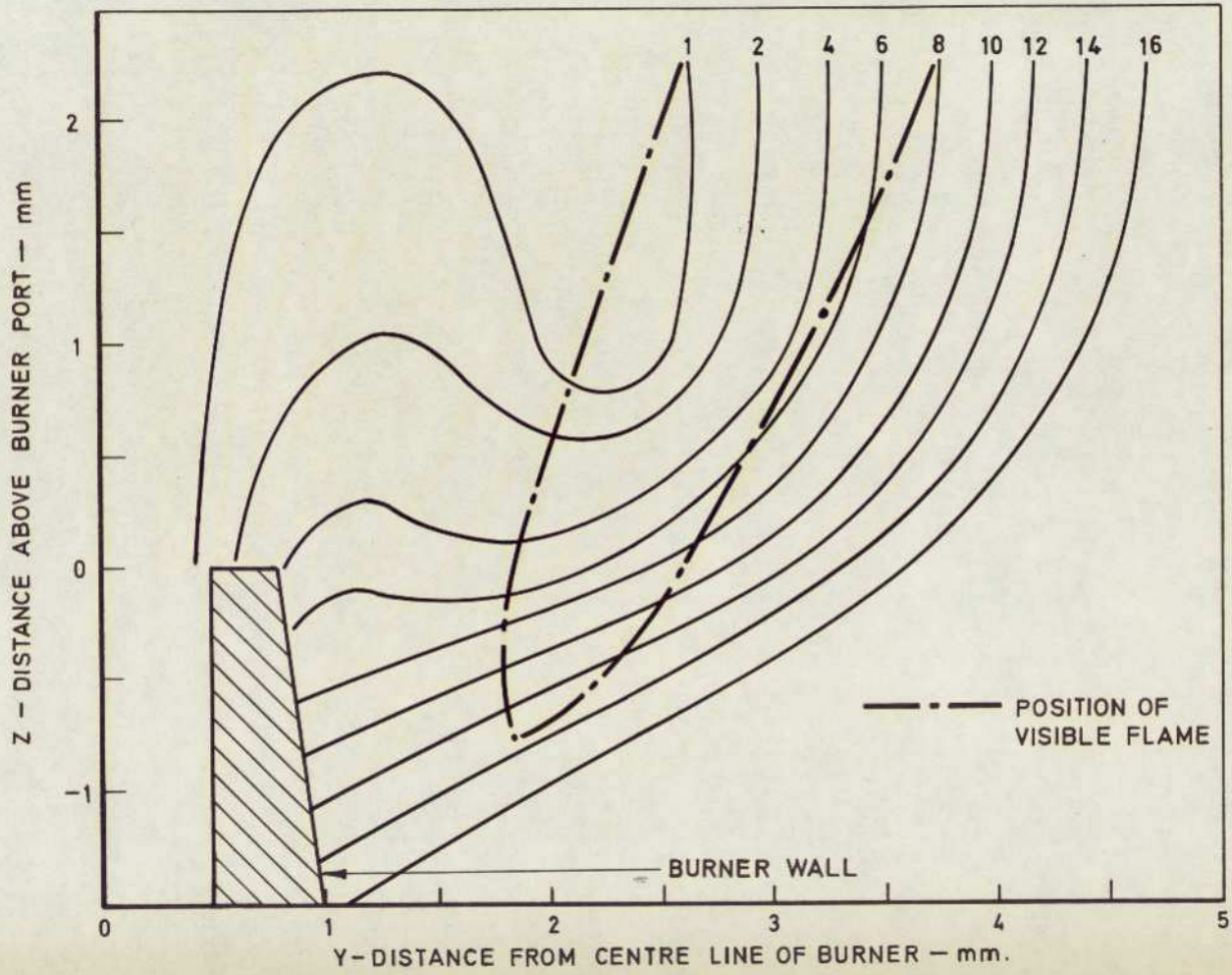



FIG. 12 ISOPLETHS OF $O_2$ (mole %) FOR FLAME BURNING 142 mls $^{-1}$

305348/11

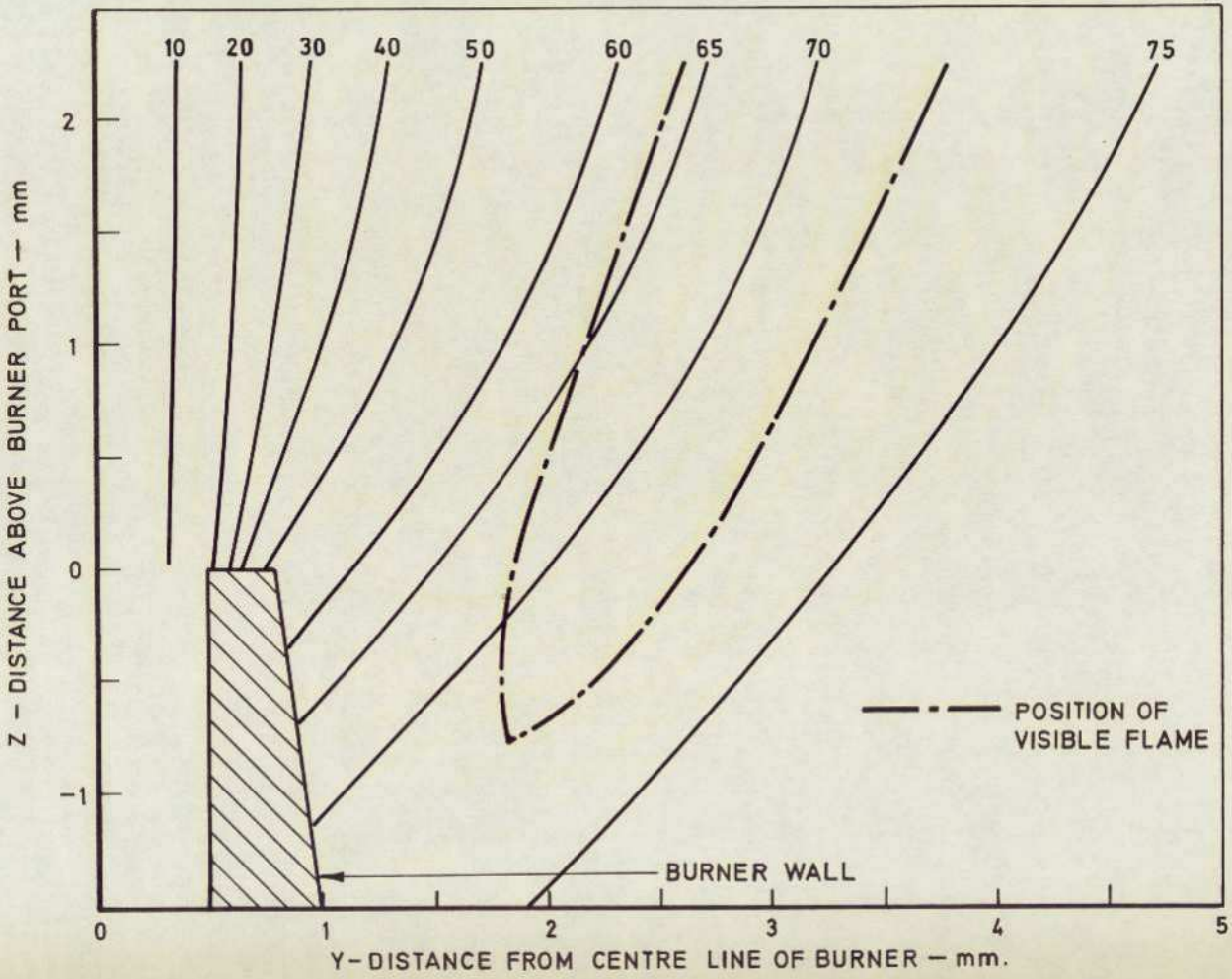



FIG. 13 ISOPLETHS OF $N_2$ (mole %) FOR FLAME BURNING 142 mls $^{-1}$

305348/12

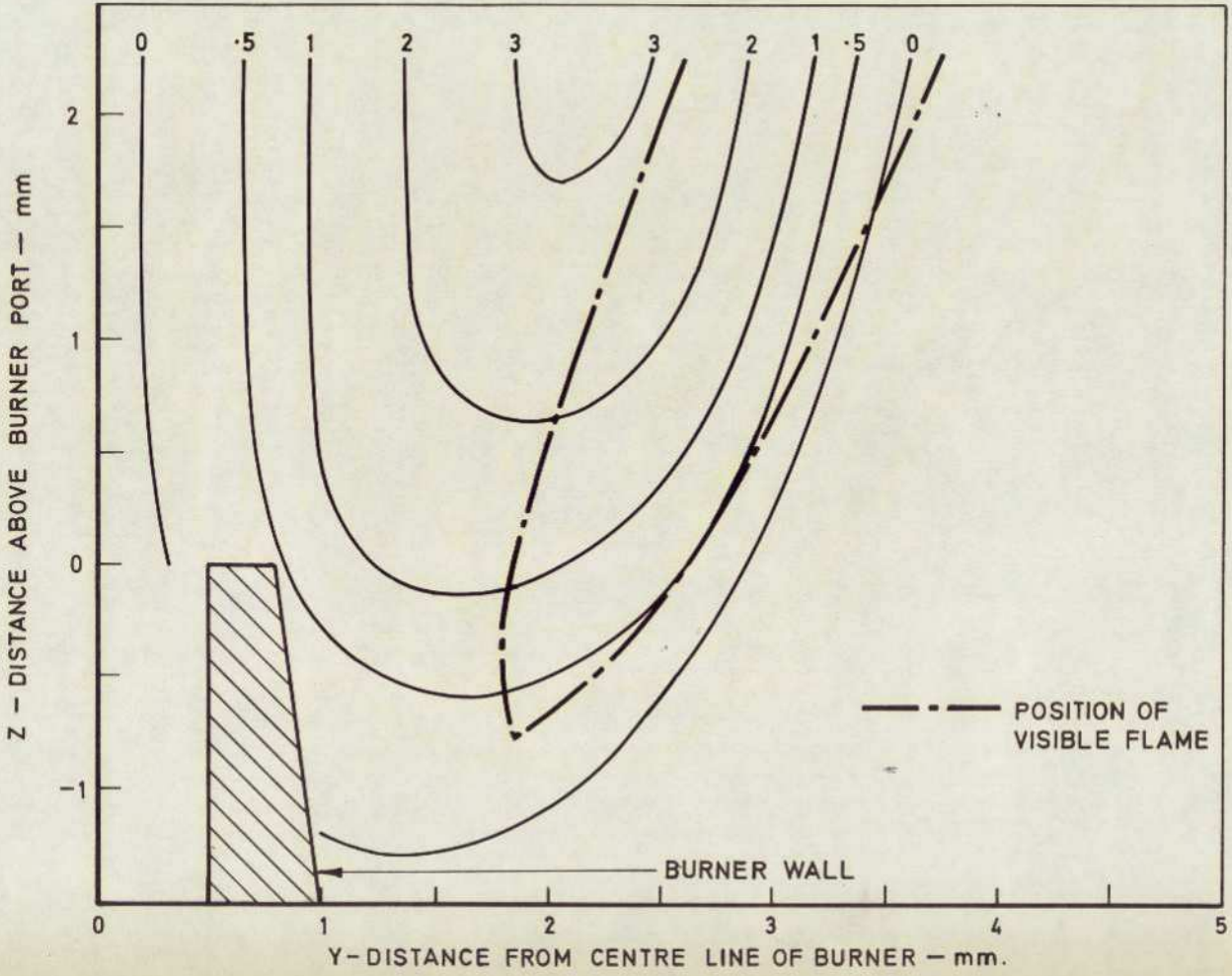



FIG. 14 ISOPLETHS OF $H_2$ (mole %) FOR FLAME BURNING 142 mls $^{-1}$

305308/13

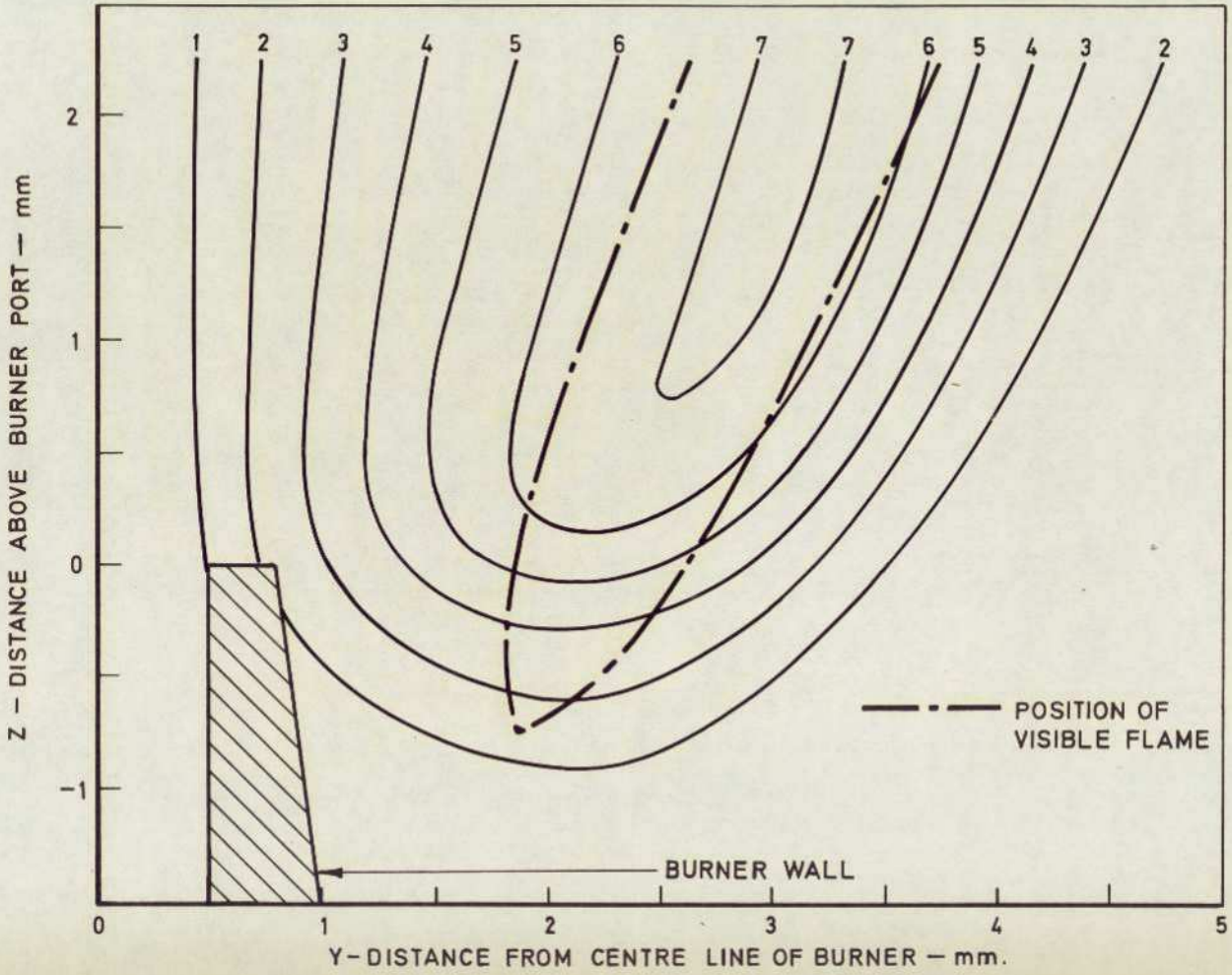



FIG. 15 ISOPLETHS OF $CO_2$ (mole %) FOR FLAME BURNING 142 mls $^{-1}$

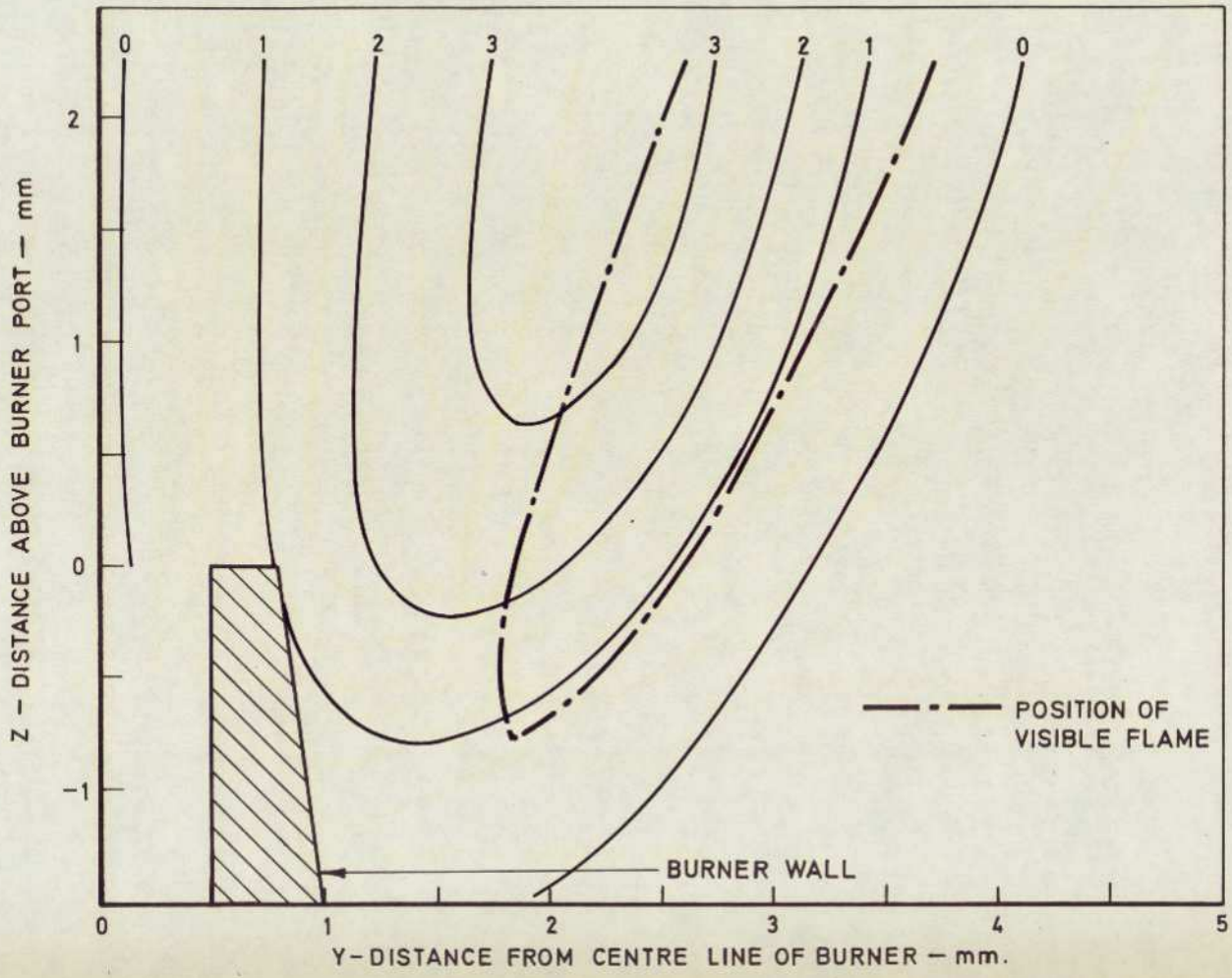



FIG. 16 ISOPLETHS OF CO (mole %) FOR FLAME BURNING 142 mls $^{-1}$

305348/15

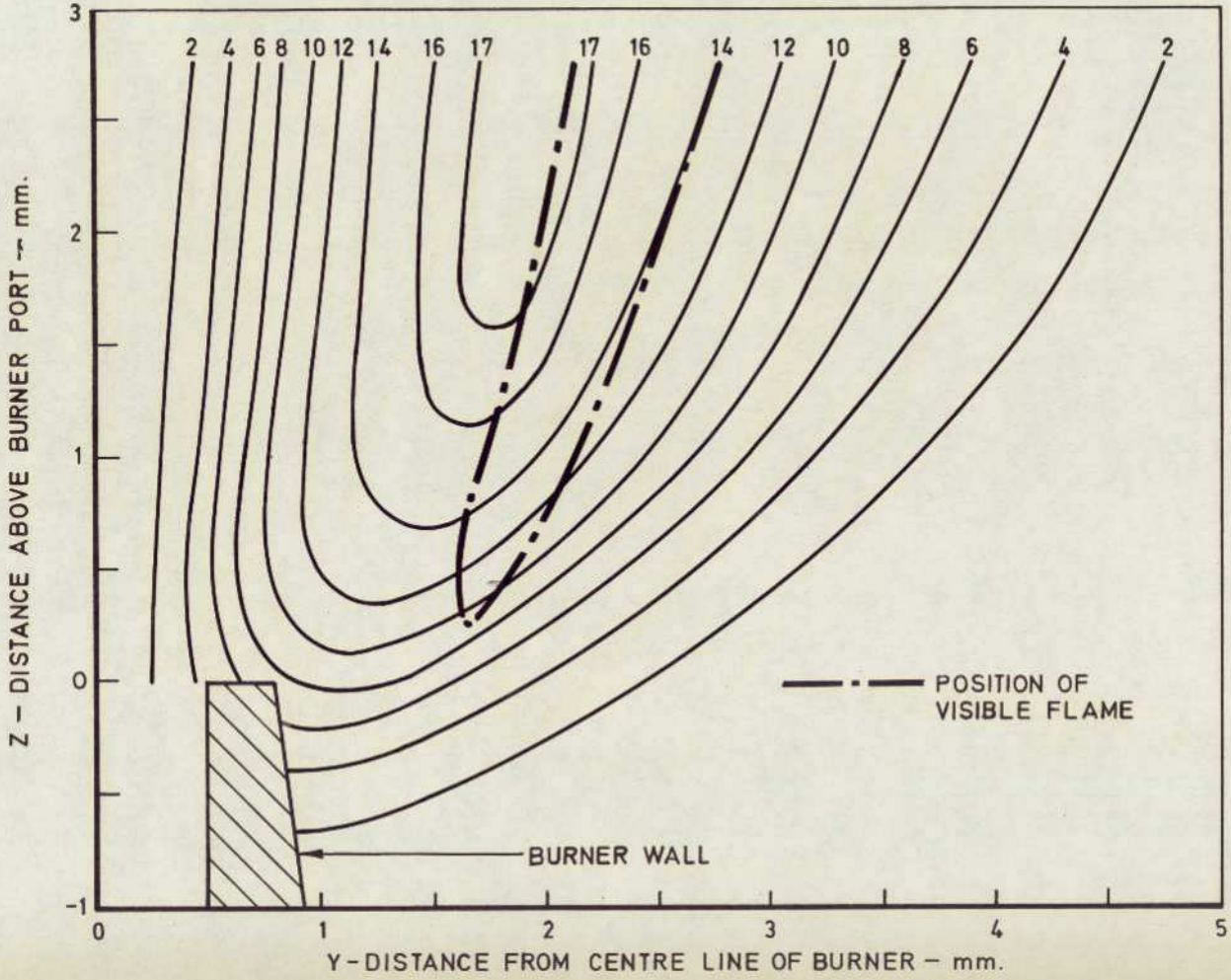



FIG. 17 ISOPLETHS OF $H_2O$ (mole %) FOR FLAME BURNING 650 $mls^{-1}$

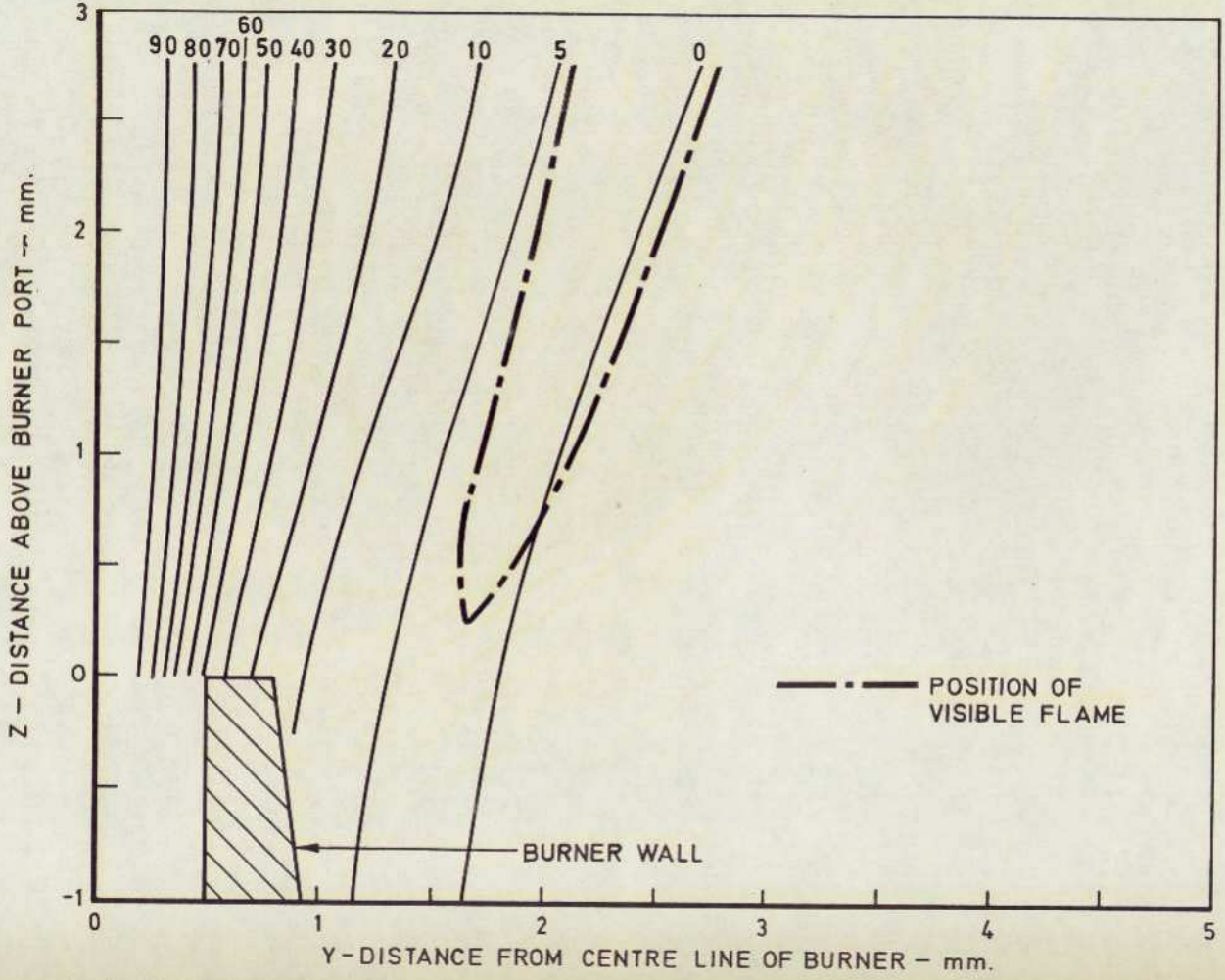



FIG. 18 ISOPLETHS OF $CH_4$ (mole %) FOR FLAME BURNING 650 $ml s^{-1}$

305348/17

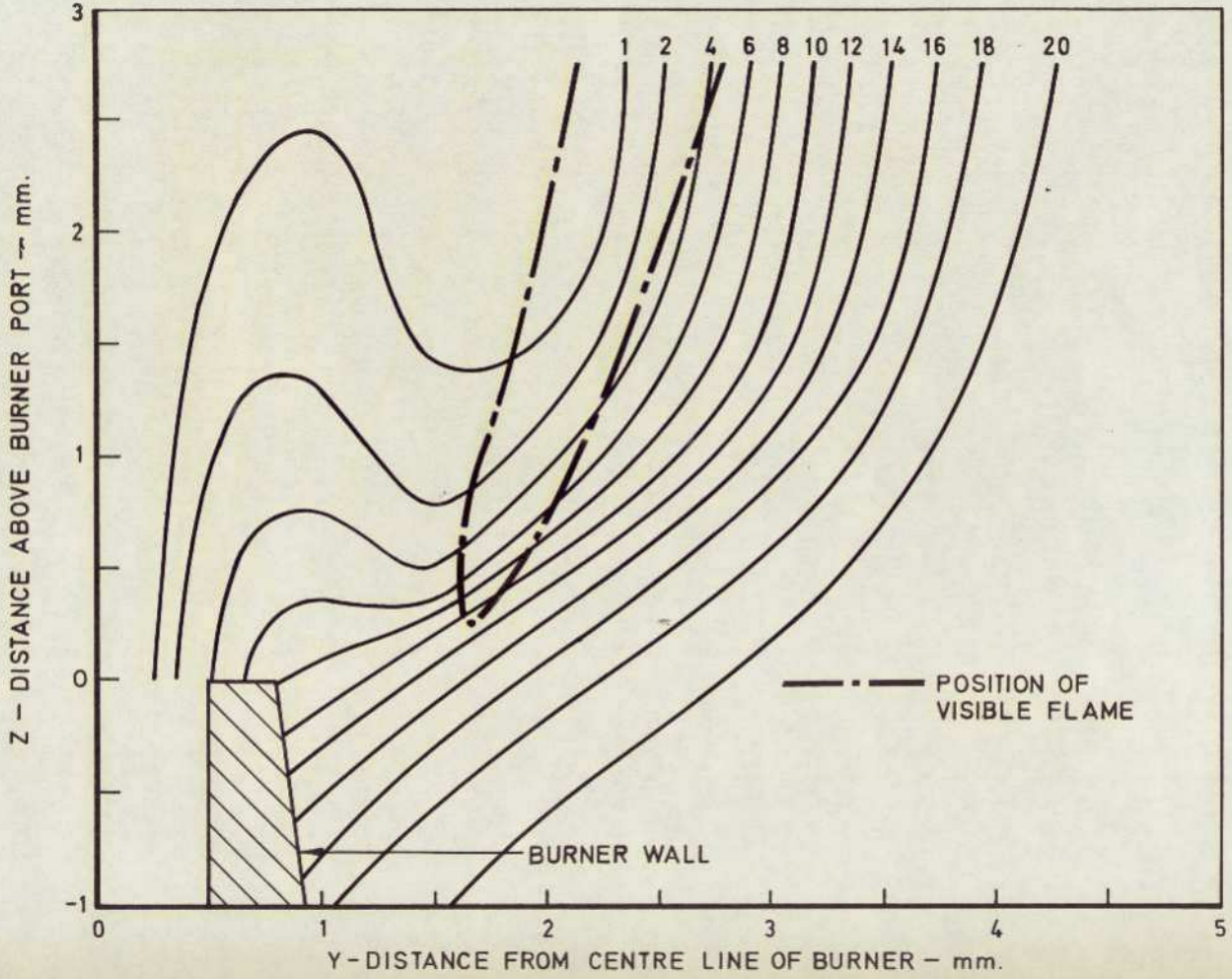



FIG.19 ISOPLETHS OF $O_2$ (mole %) FOR FLAME BURNING 650 $mls^{-1}$

305348/18

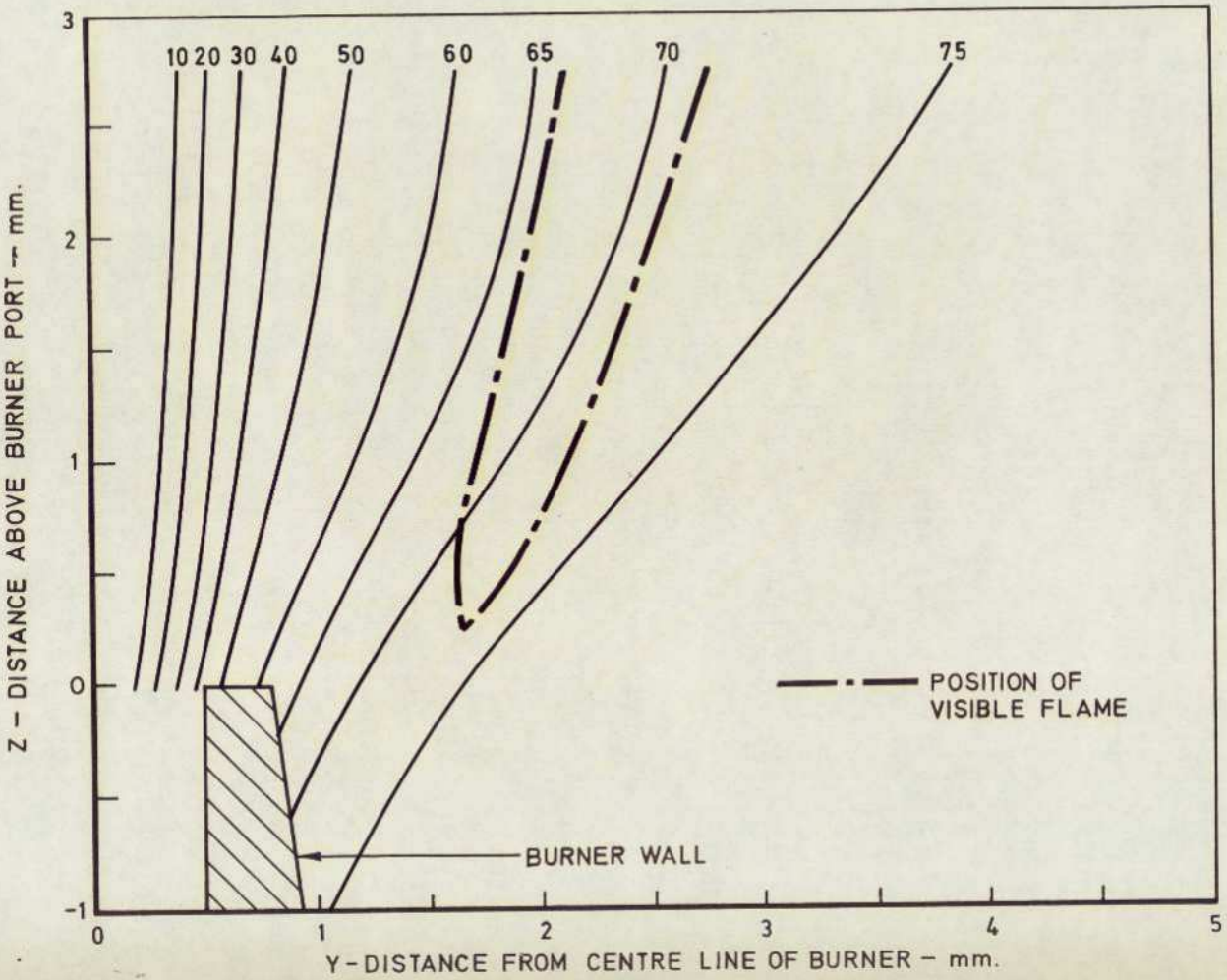



FIG. 20 ISOPLETHS OF $N_2$ (mole %) FOR FLAME BURNING 650 mls$^{-1}$

305348/19

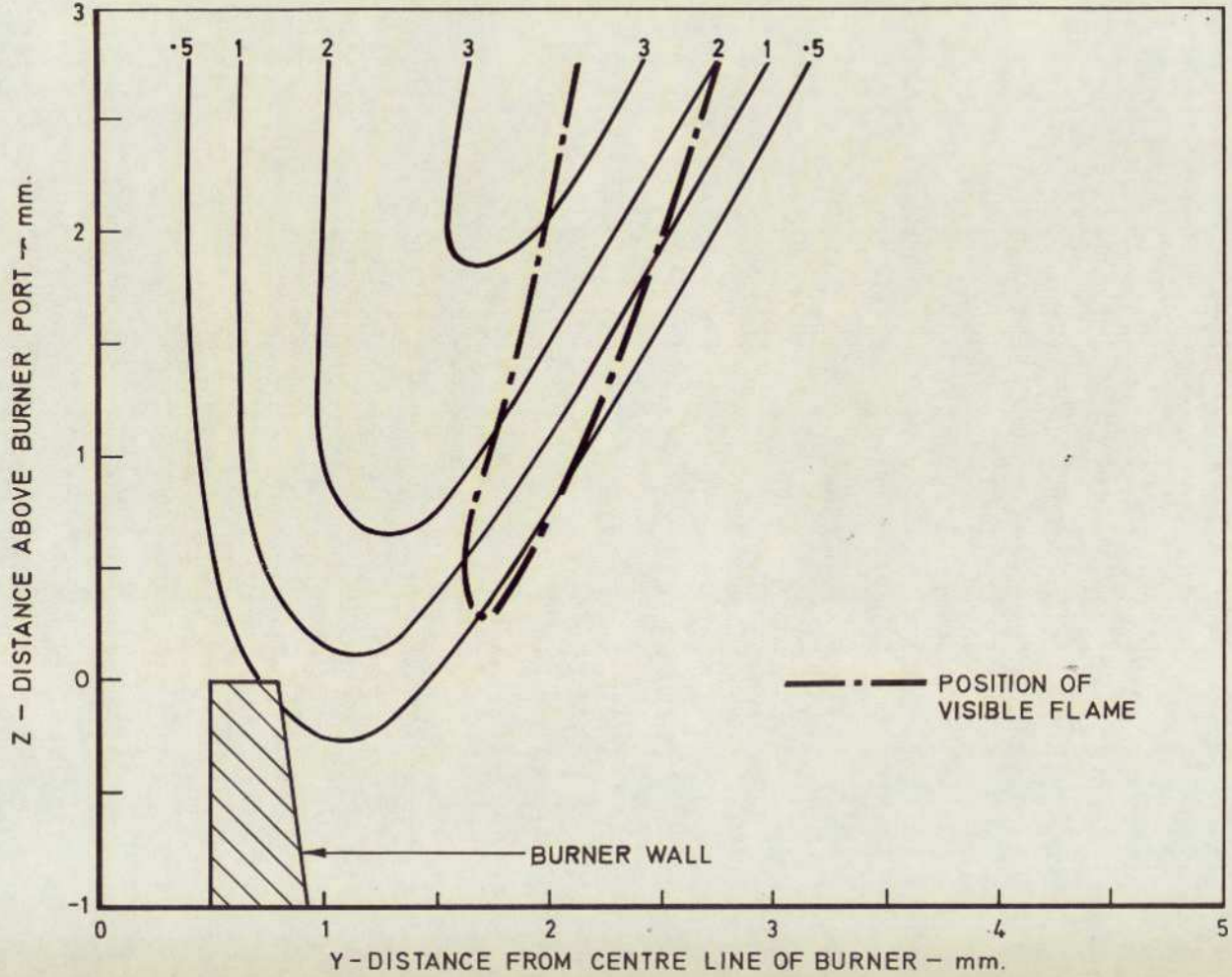



FIG. 21 ISOPLETHS OF $H_2$ (mole %) FOR FLAME BURNING 650 mls$^{-1}$

3053/48/20

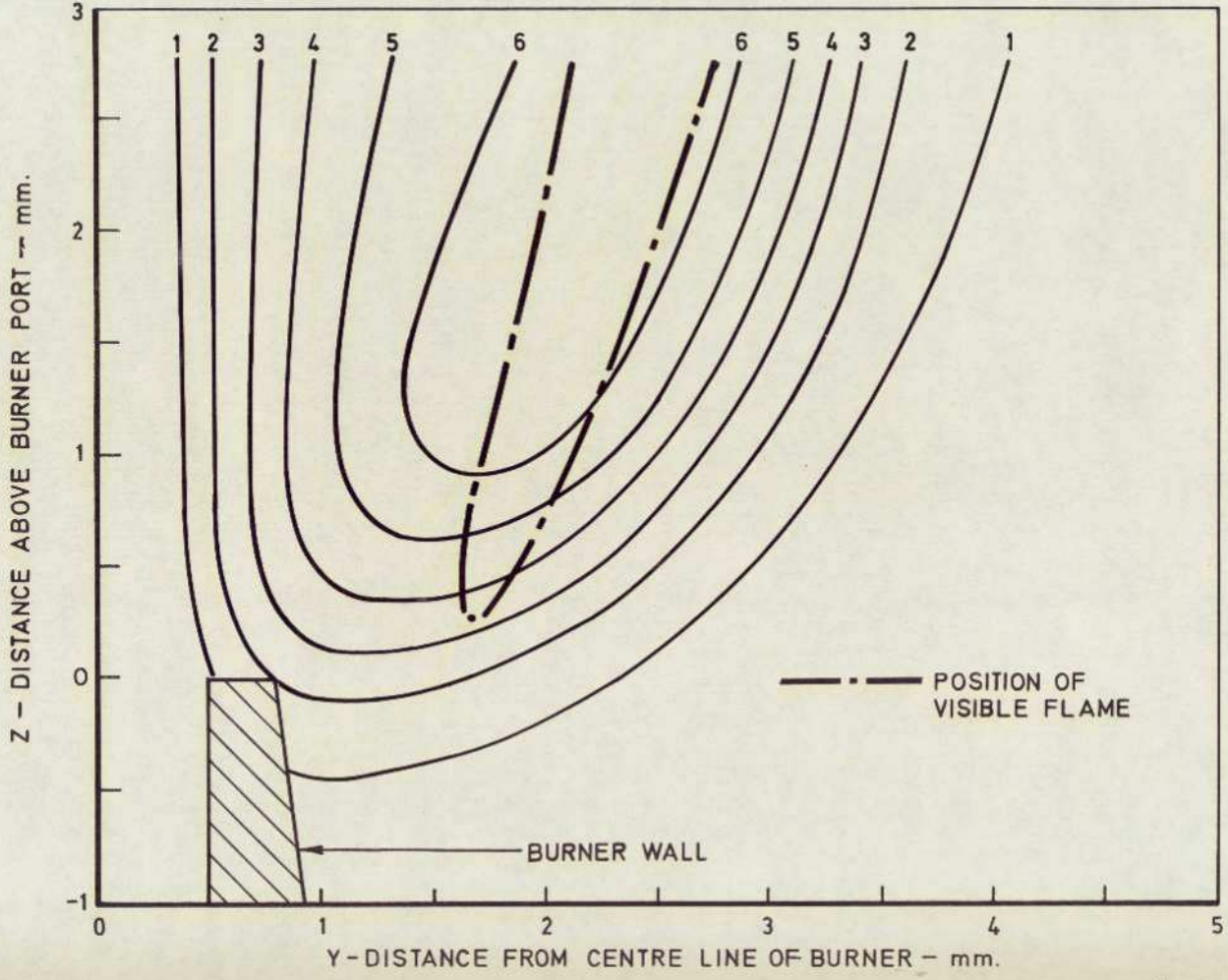



FIG. 22 ISOPLETHS OF $CO_2$ (mole %) FOR FLAME BURNING 650 $mls^{-1}$

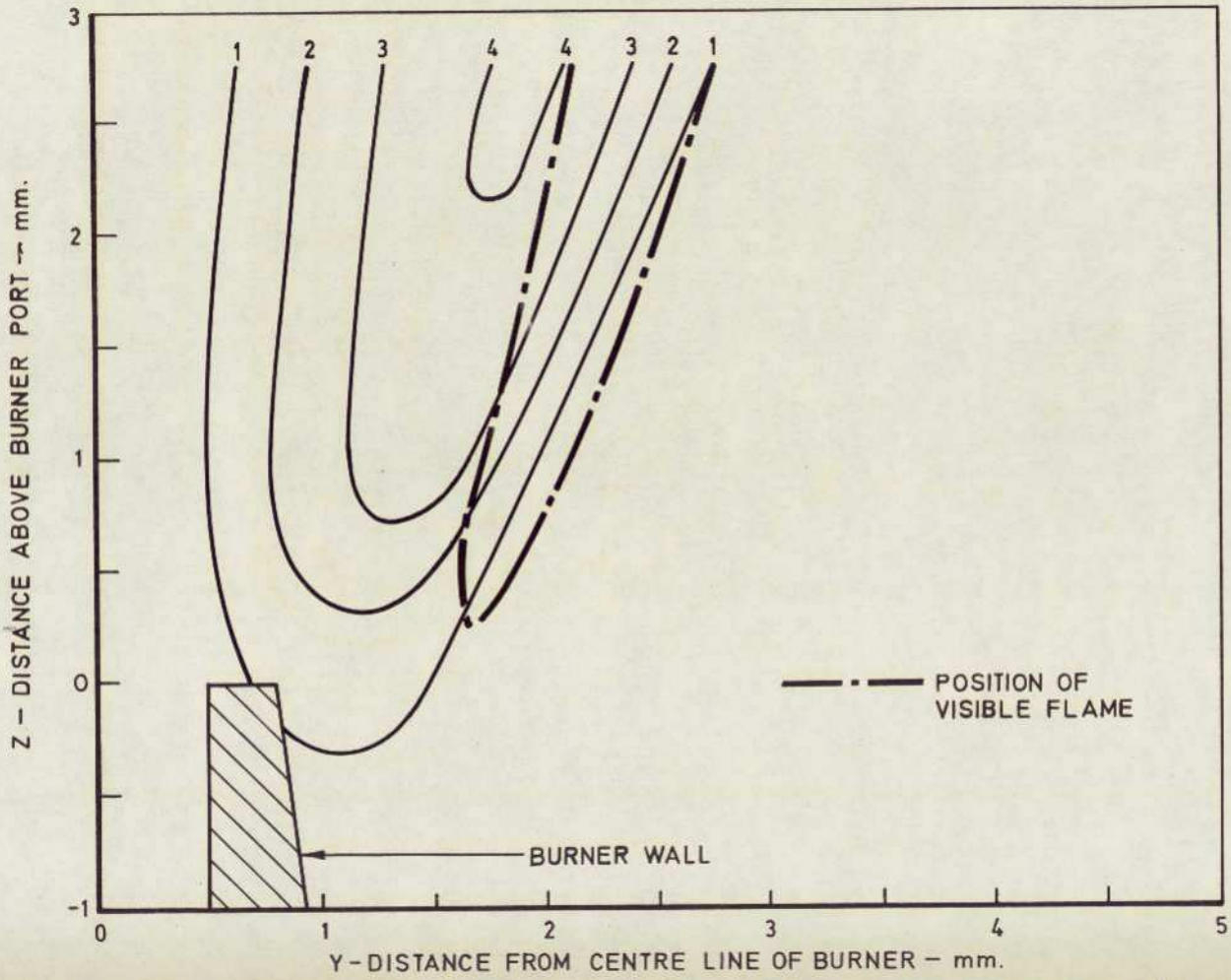



FIG. 23 ISOPLETHS OF CO (mole %) FOR FLAME BURNING 650 $mls^{-1}$

305348/22

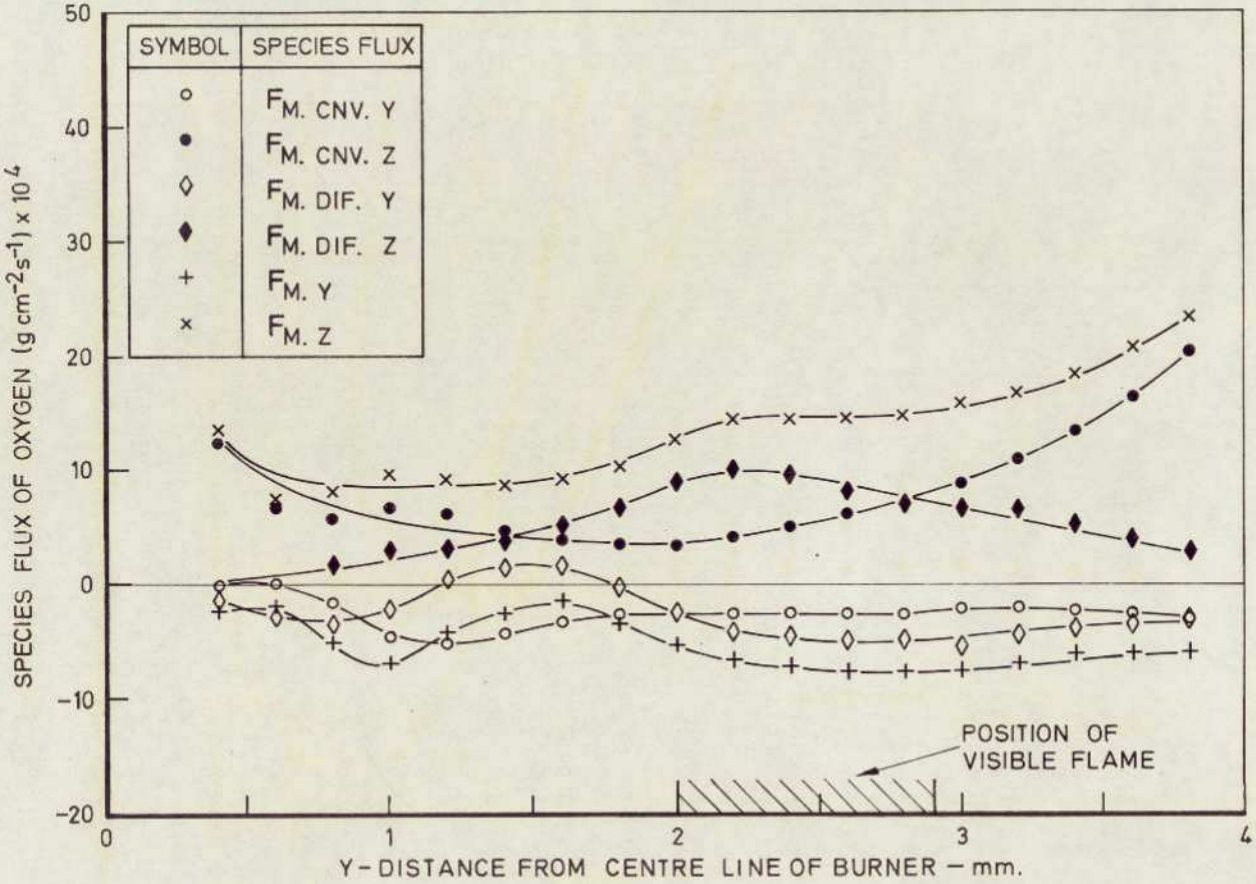



FIG. 24 SPECIES FLUXES OF OXYGEN AT A PLANE 0·0mm ABOVE THE BURNER PORT METHANE FLOW RATE 142mls$^{-1}$

305348/23

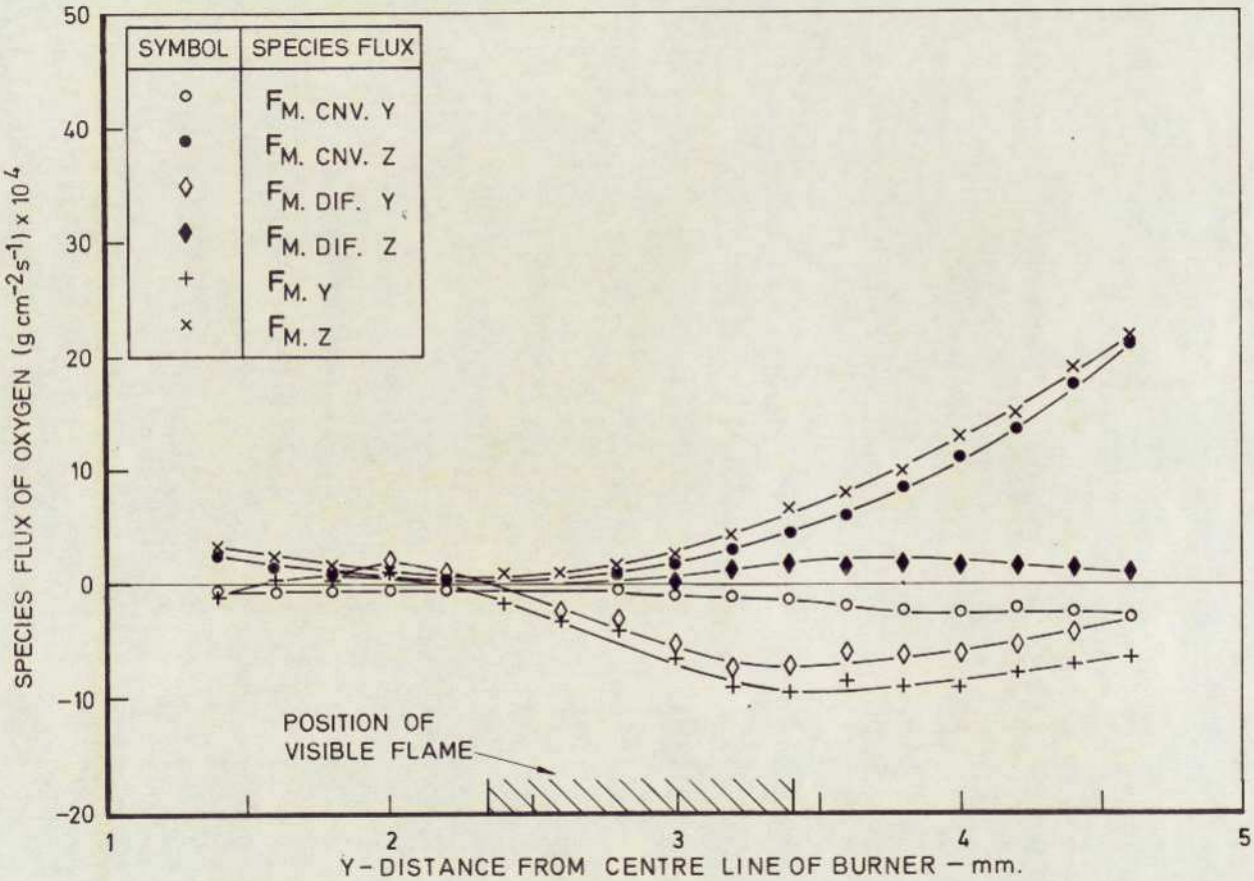



FIG. 25 SPECIES FLUXES OF OXYGEN AT A PLANE 1·5mm ABOVE THE BURNER PORT
METHANE FLOW RATE 142mls $^{-1}$

305348/24

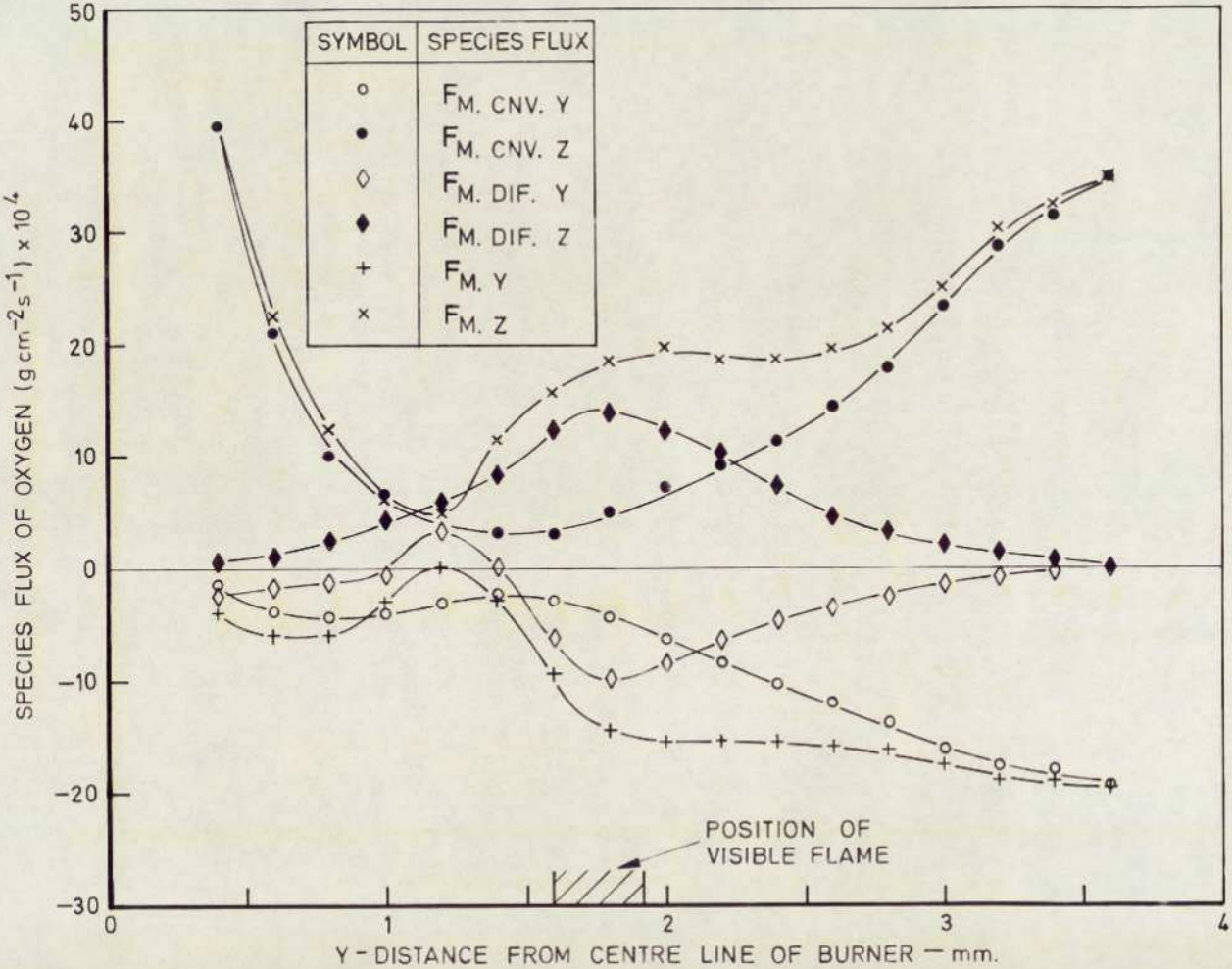



FIG. 26 SPECIES FLUXES OF OXYGEN AT A PLANE 0·5 mm ABOVE THE BURNER PORT METHANE FLOW RATE 650 $mls^{-1}$

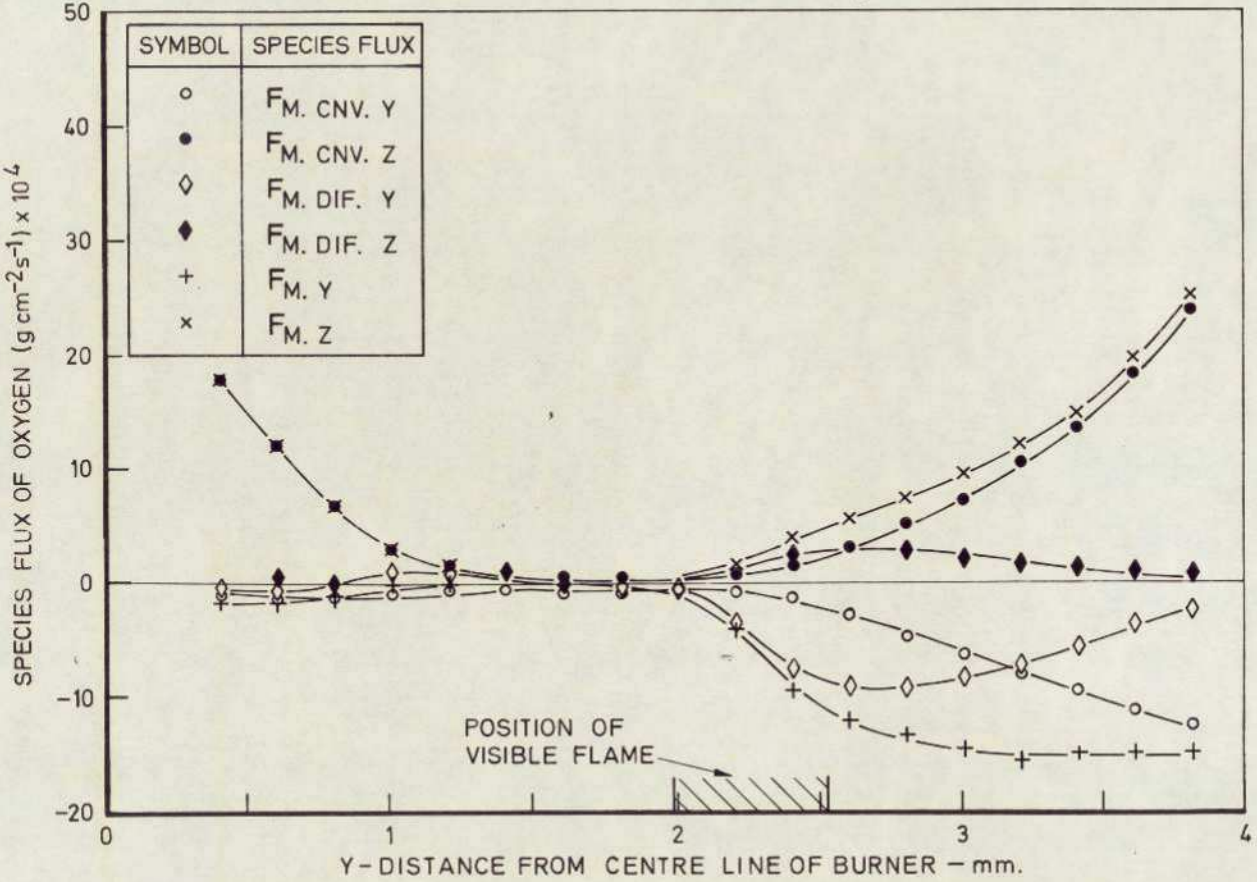



FIG. 27 SPECIES FLUXES OF OXYGEN AT A PLANE 2·0mm ABOVE THE BURNER PORT METHANE FLOW RATE 650mls $^{-1}$

305348/26

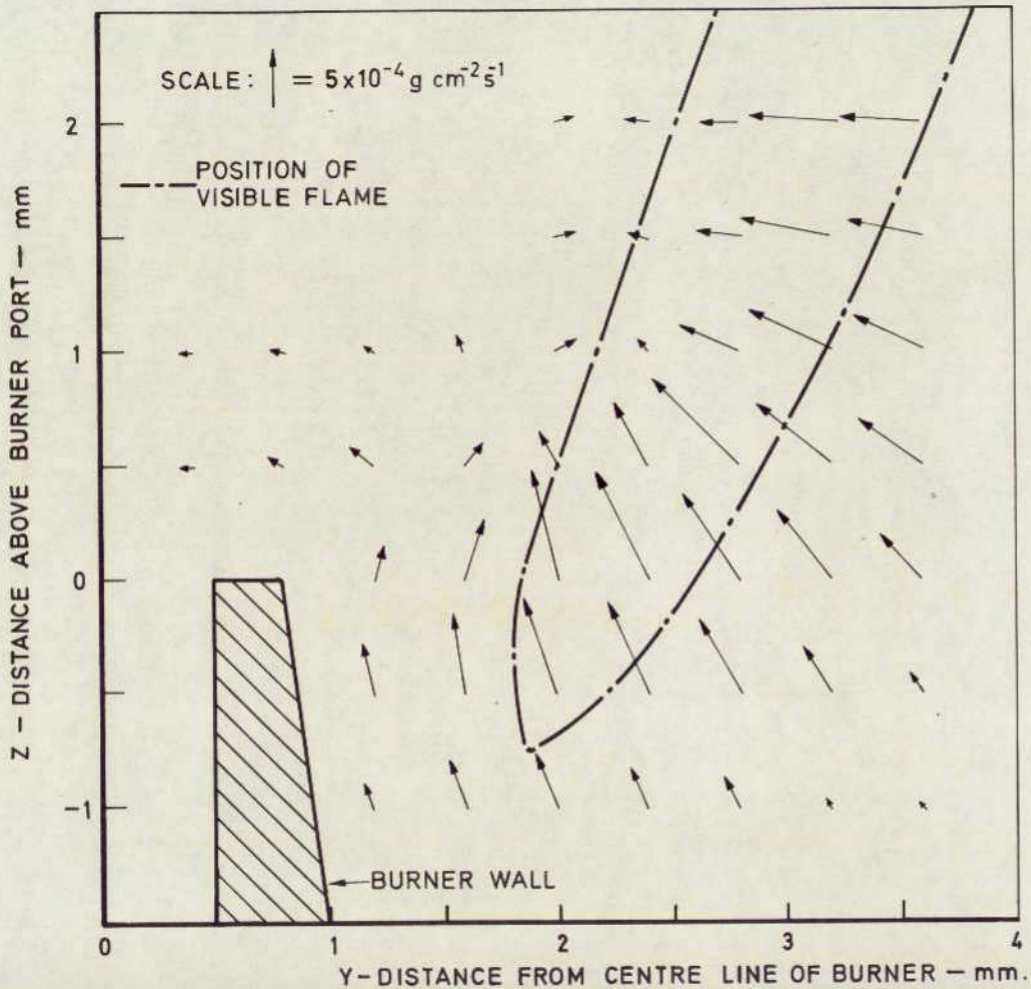



FIG. 28. LOCAL DIFFUSIVE FLUXES OF $O_2$ IN FLAME BURNING 142 mls$^{-1}$

305348/27

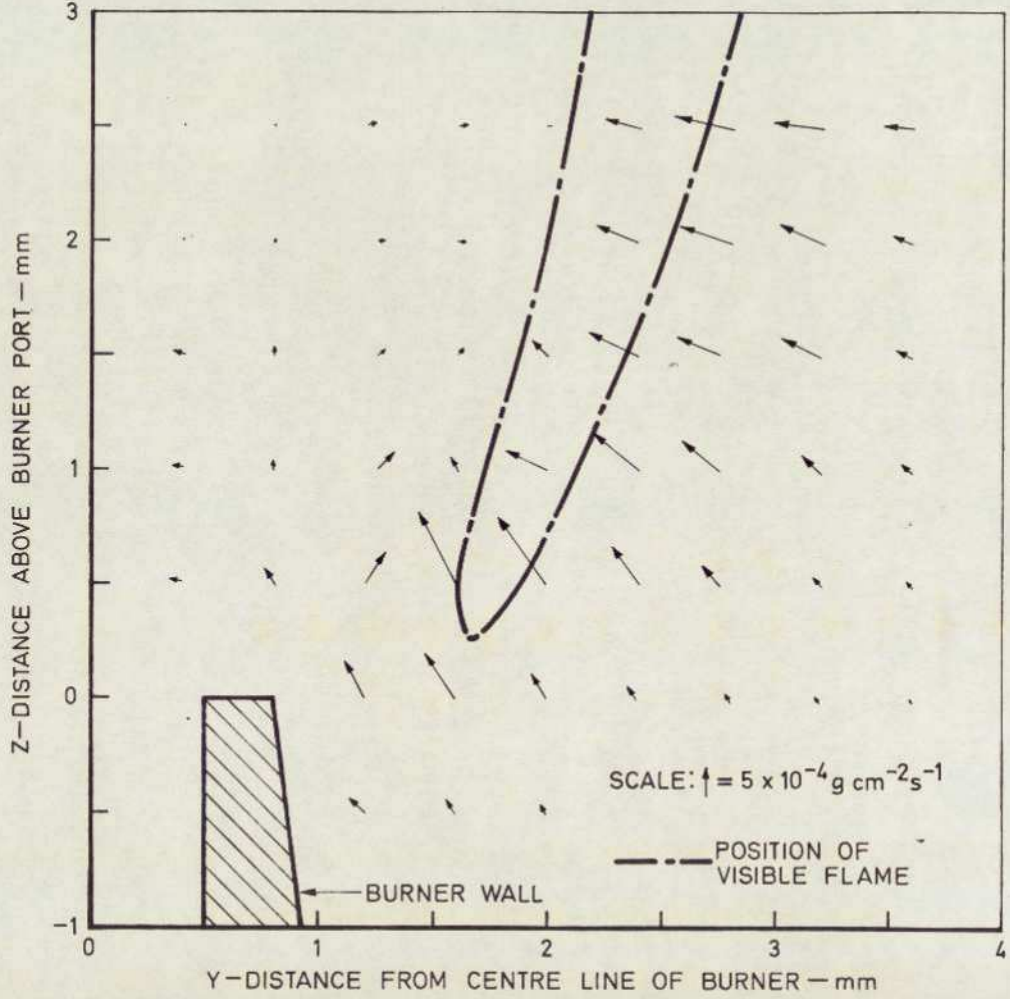



FIG. 29 LOCAL DIFFUSIVE FLUXES OF $O_2$ IN FLAME BURNING 650 mls$^{-1}$

305348/28

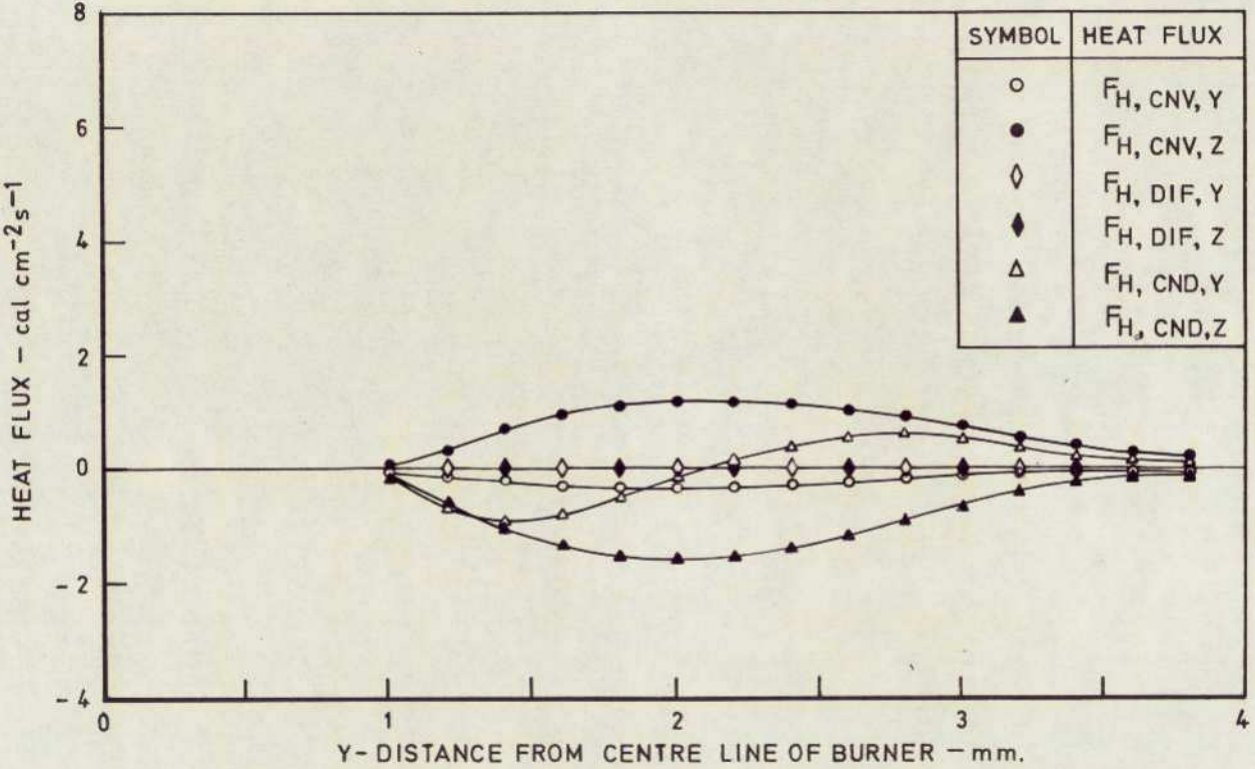



FIG.30 HEAT FLUXES AT A PLANE 1·0 mm BELOW THE BURNER PORT

METHANE FLOW RATE 142 mls $^{-1}$

305348/29

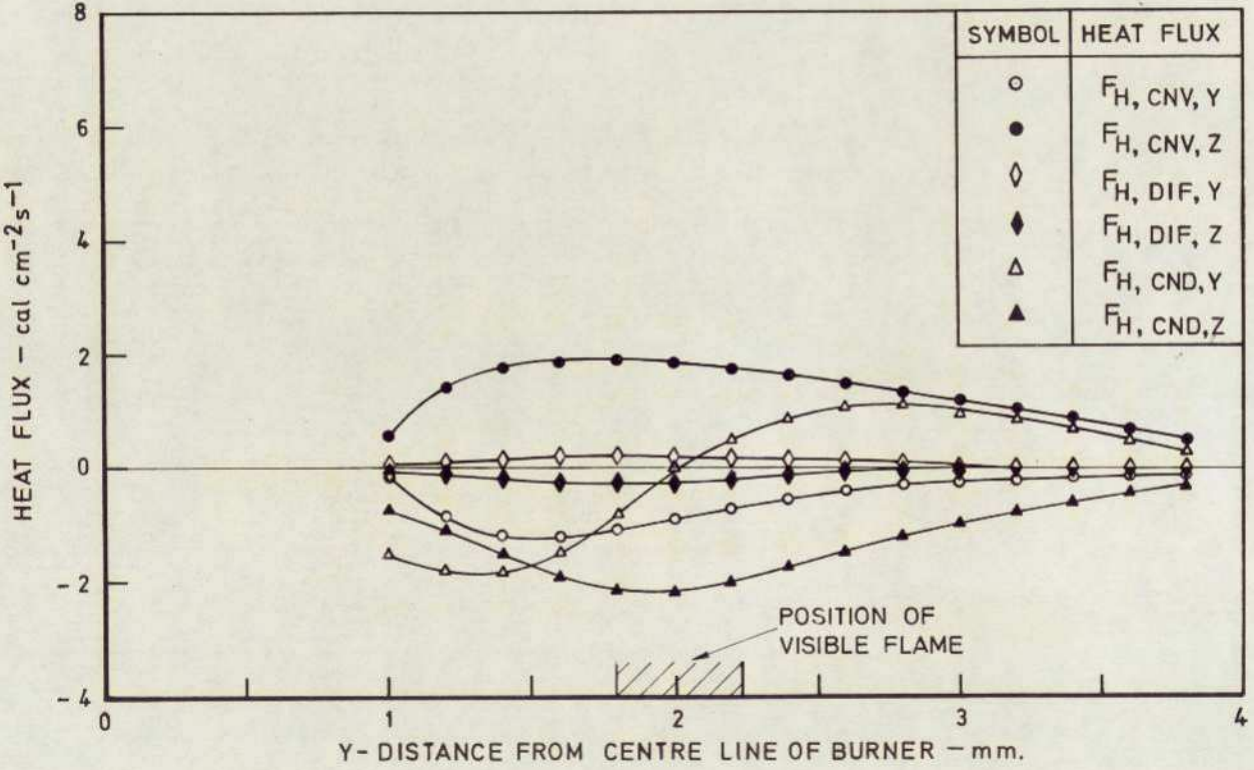



FIG. 31 HEAT FLUXES AT A PLANE 0·5mm BELOW THE BURNER PORT

METHANE FLOW RATE 142 ml $s^{-1}$

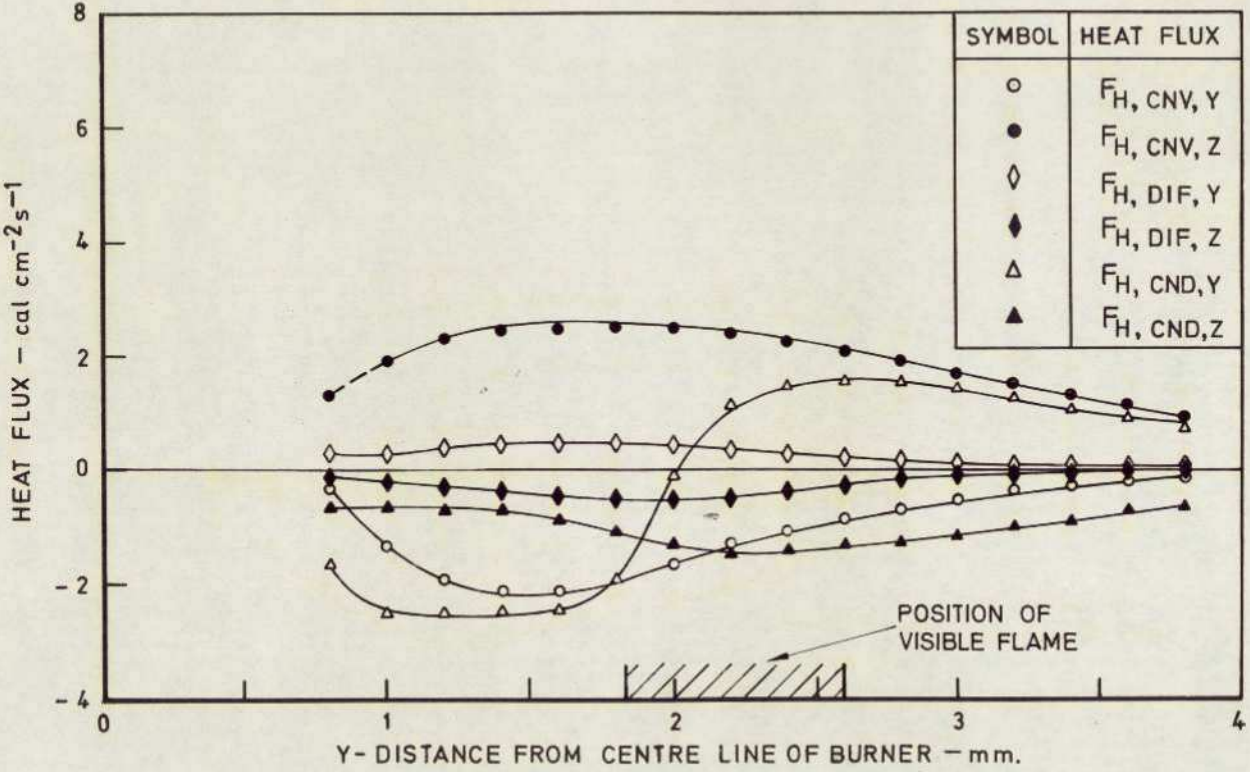



FIG.32 HEAT FLUXES AT A PLANE 0·0mm ABOVE THE BURNER PORT

METHANE FLOW RATE 142 mls $^{-1}$

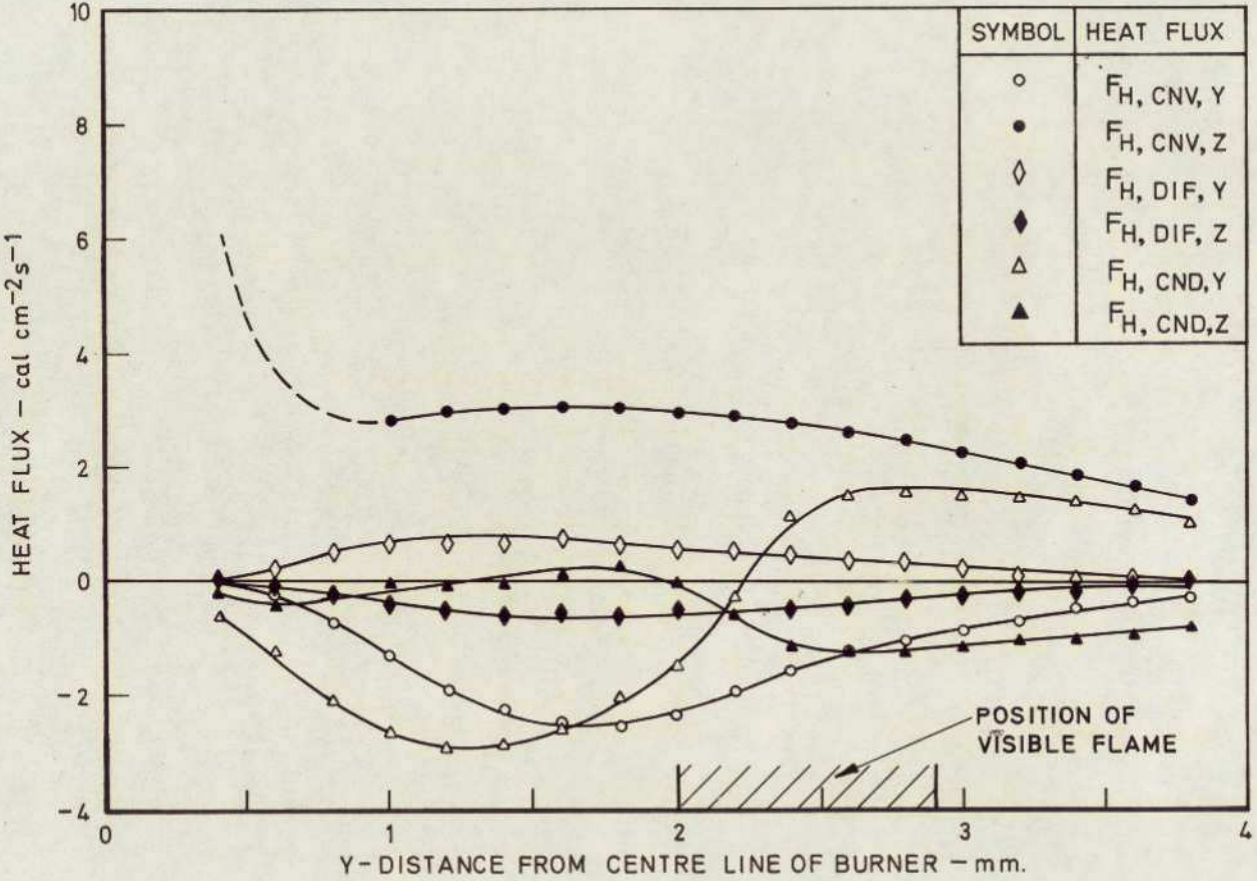



FIG. 33. HEAT FLUXES AT A PLANE 0·5mm ABOVE THE BURNER PORT METHANE FLOW RATE 142 mls $^{-1}$

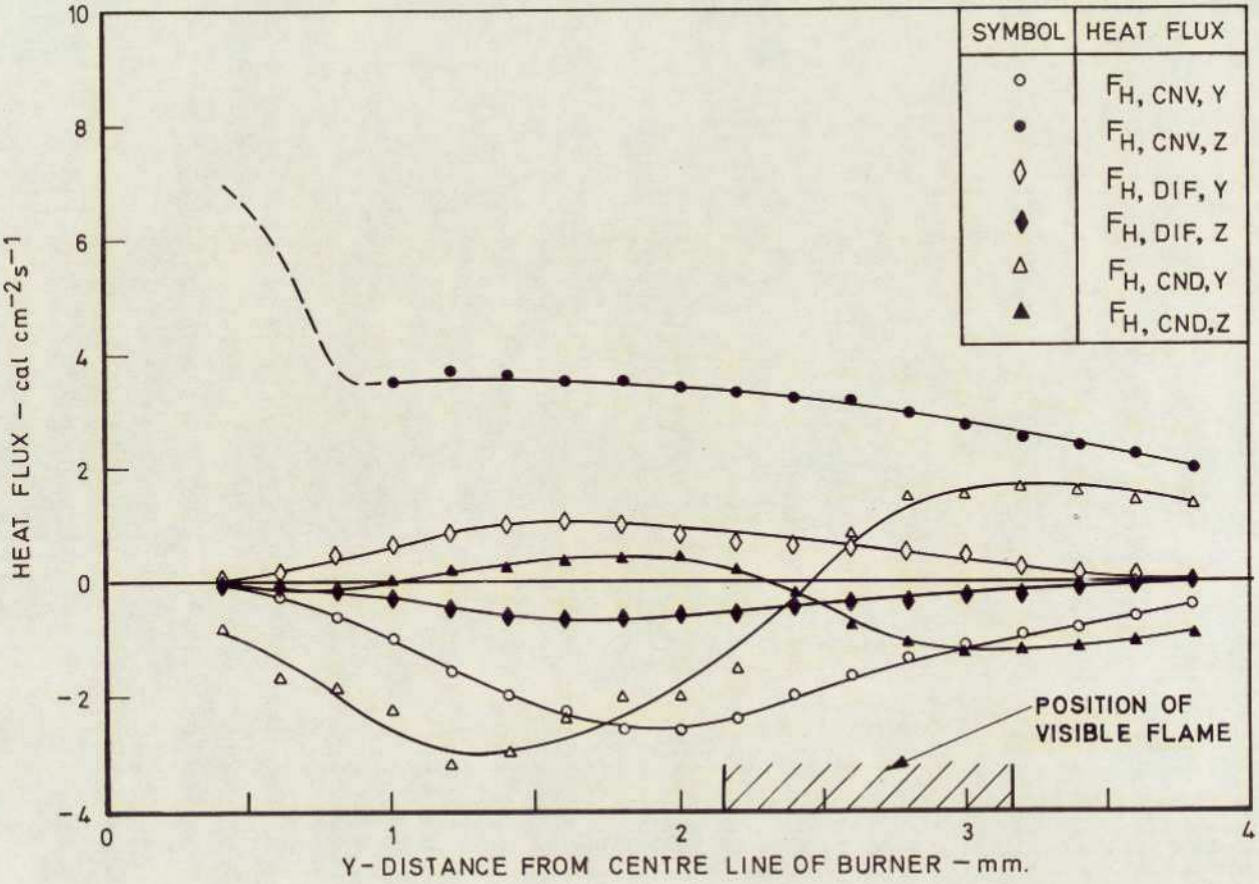



FIG. 34. HEAT FLUXES AT A PLANE 1·0mm. ABOVE THE BURNER PORT

METHANE FLOW RATE 142mls $^{-1}$

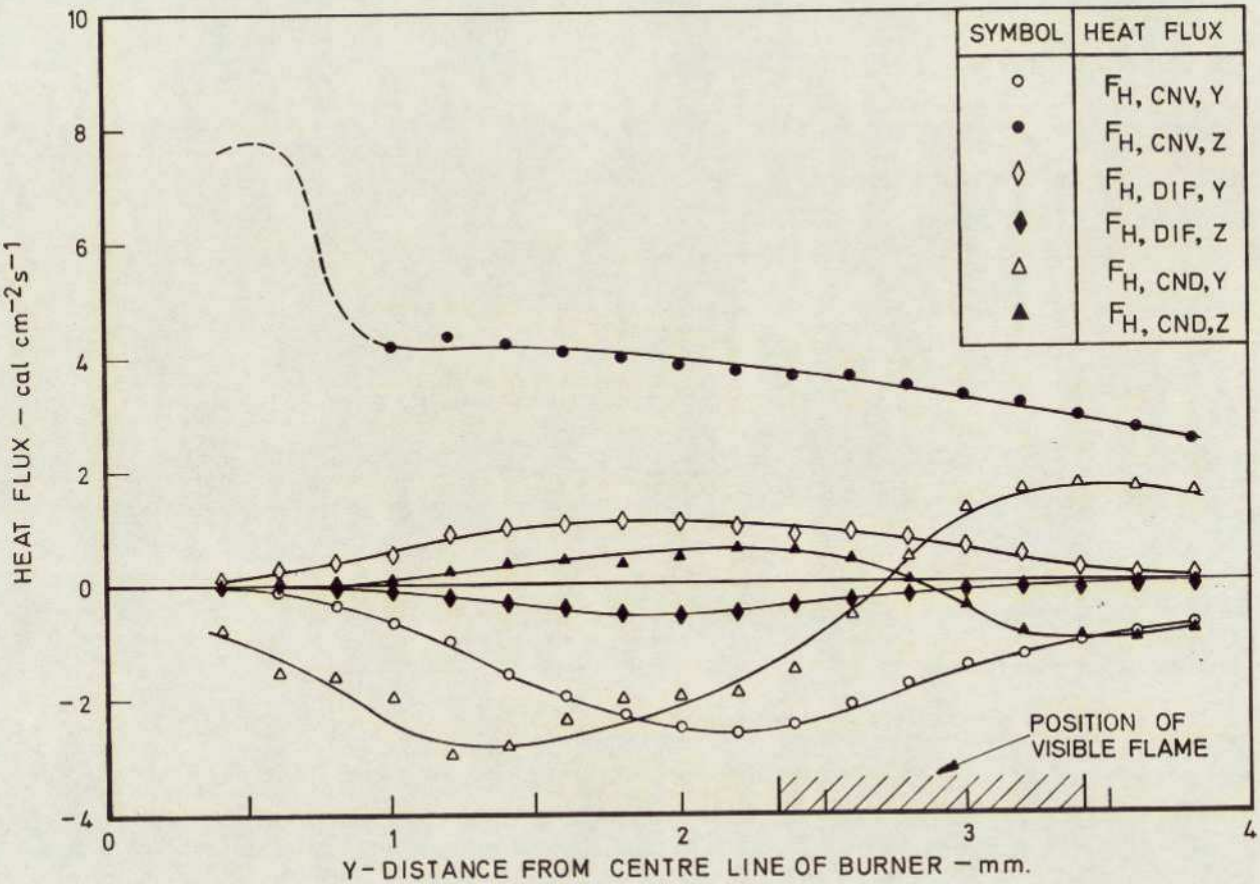



FIG. 35 HEAT FLUXES AT A PLANE 1·5mm ABOVE THE BURNER PORT
METHANE FLOW RATE 142 mls $^{-1}$

305348/34

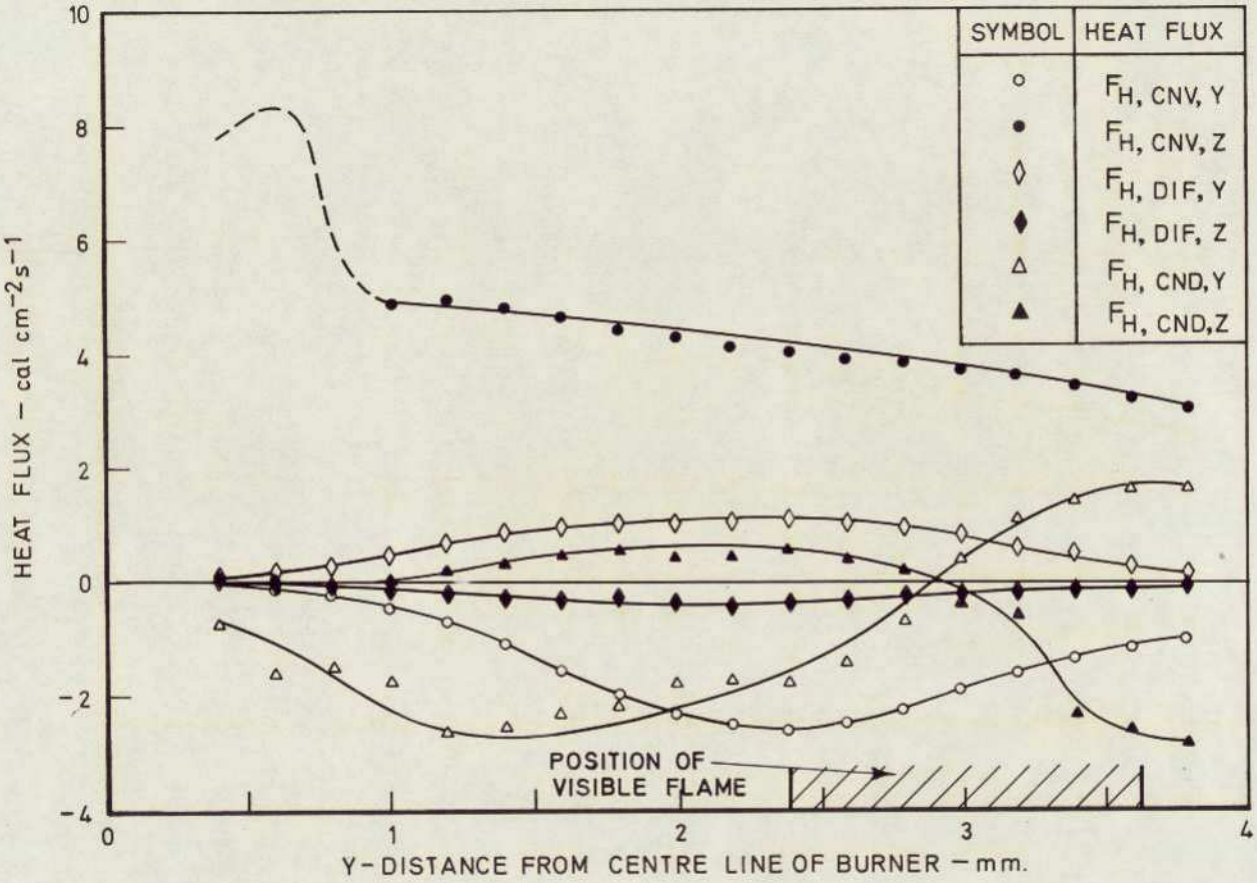



FIG. 36 HEAT FLUXES AT A PLANE 2·0mm ABOVE THE BURNER PORT METHANE FLOW RATE 142 mls $^{-1}$

305348/35

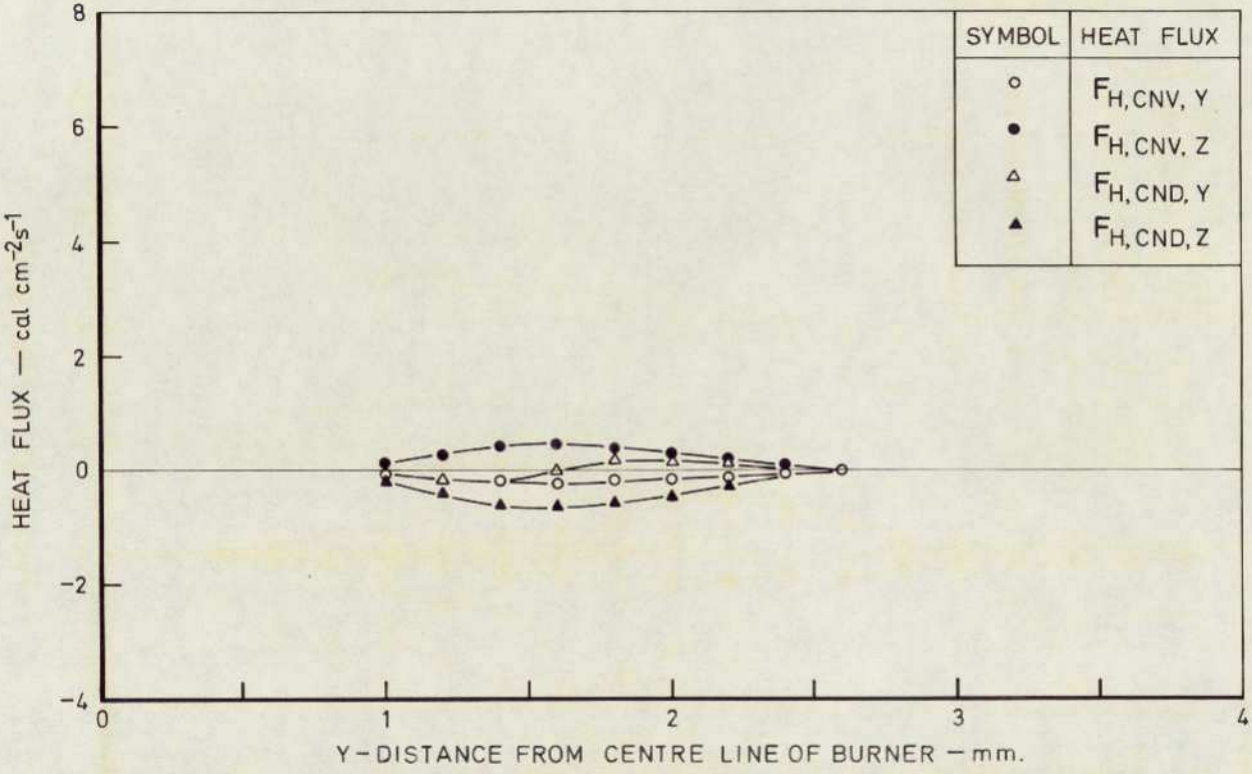



FIG. 37 HEAT FLUXES AT A PLANE 0·5 mm BELOW THE BURNER PORT

METHANE FLOW RATE 650 $mls^{-1}$

305348/36

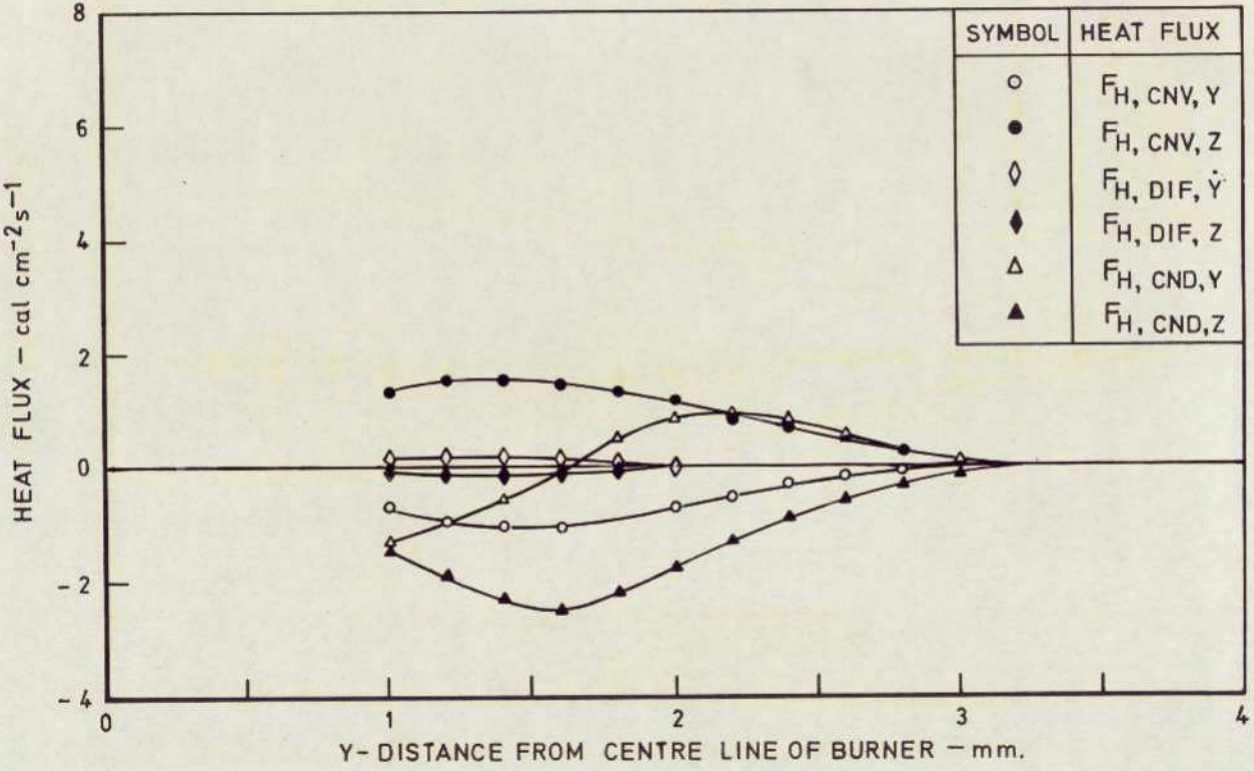



FIG. 38 HEAT FLUXES AT A PLANE 0·0 mm ABOVE THE BURNER PORT METHANE FLOW RATE 650 mls $^{-1}$

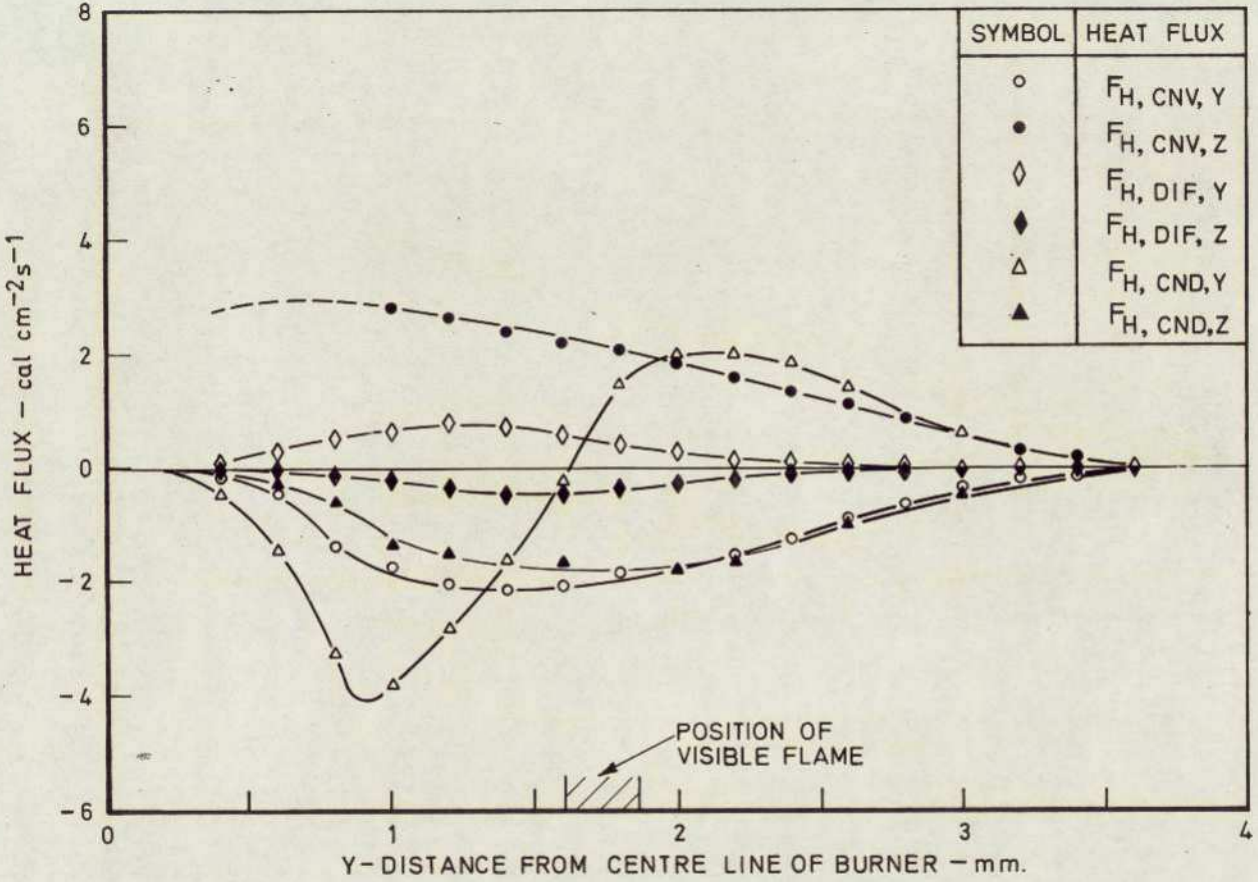



FIG. 39. HEAT FLUXES AT A PLANE 0·5 mm ABOVE THE BURNER PORT
METHANE FLOW RATE 650 mls $^{-1}$

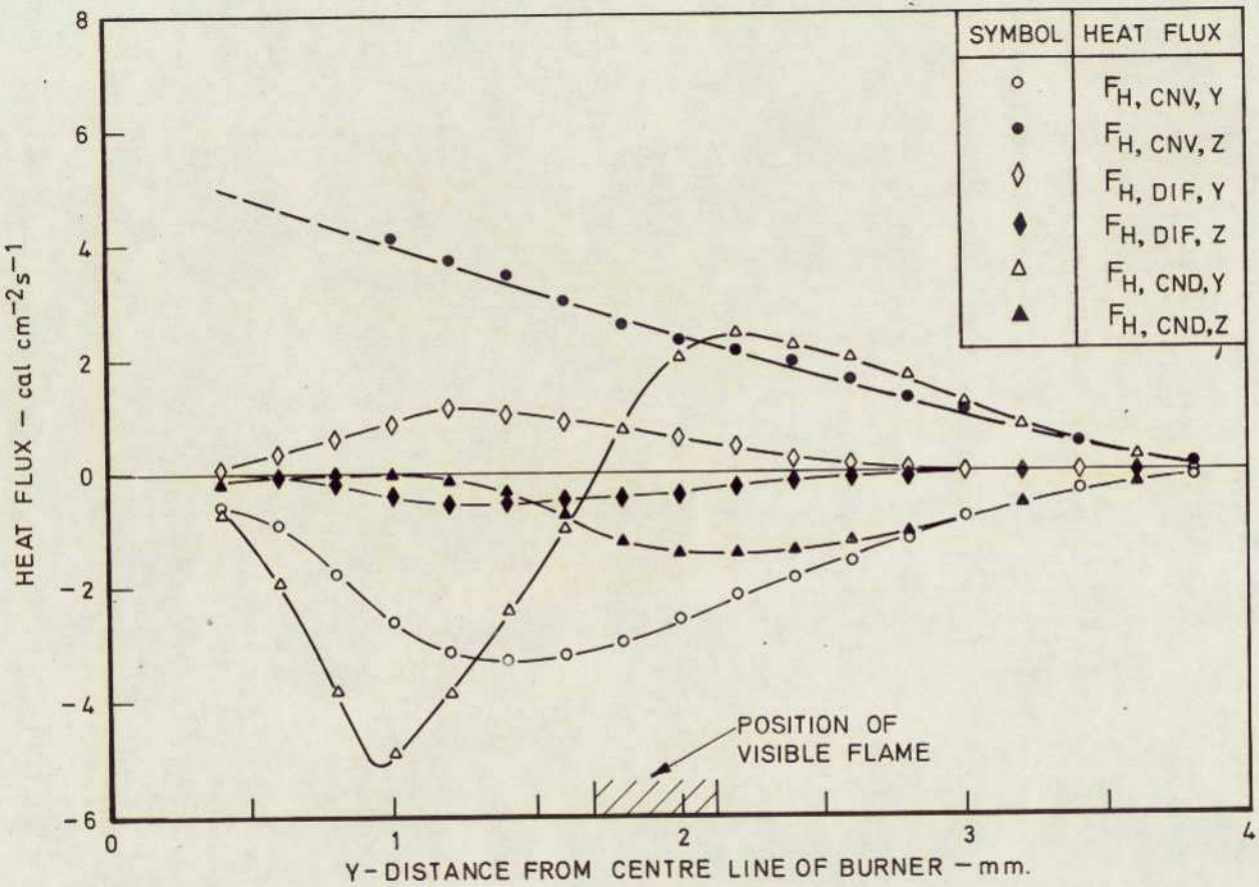



FIG.40 HEAT FLUXES AT A PLANE 1·0mm ABOVE THE BURNER PORT METHANE FLOW RATE 650 mls $^{-1}$

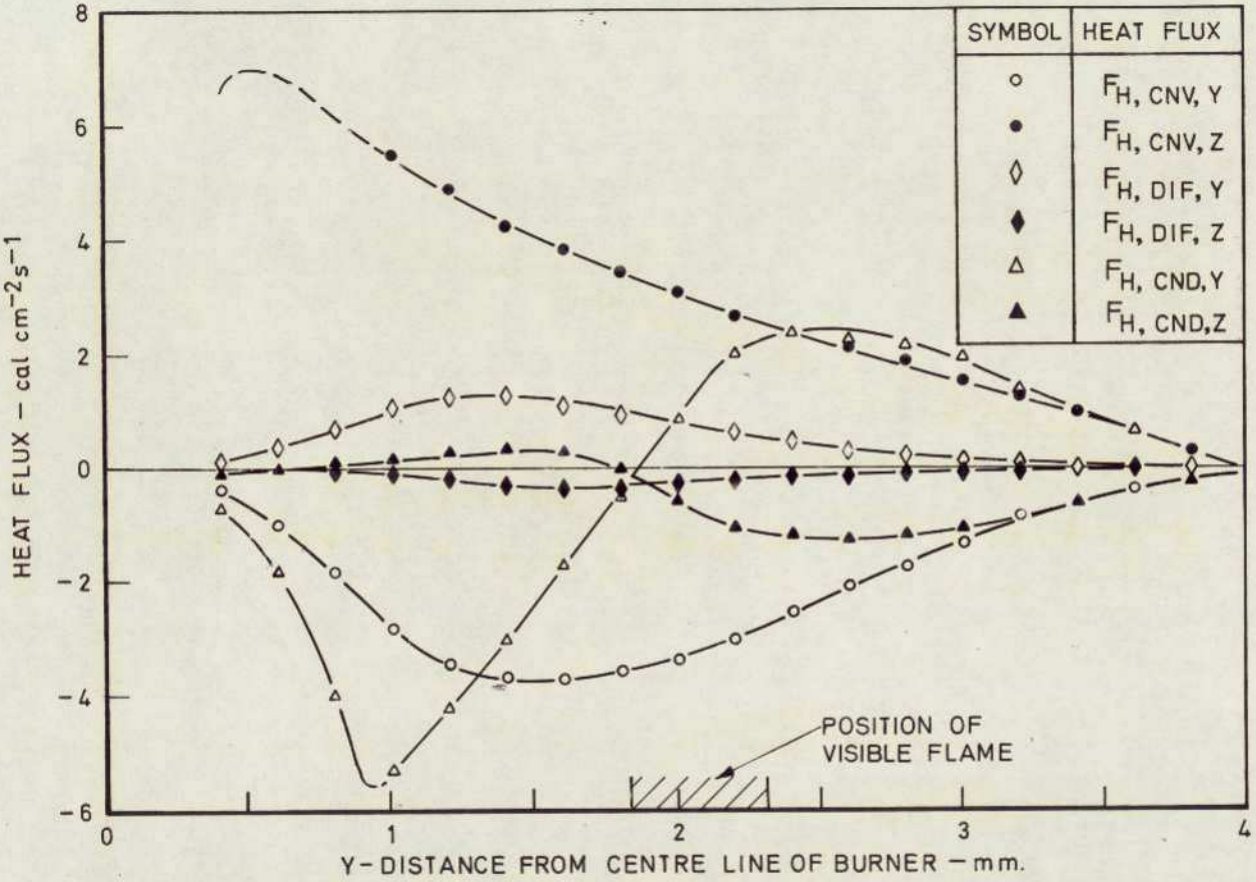



FIG. 41 HEAT FLUXES AT A PLANE 1·5mm ABOVE THE BURNER PORT METHANE FLOW RATE 650 mls $^{-1}$

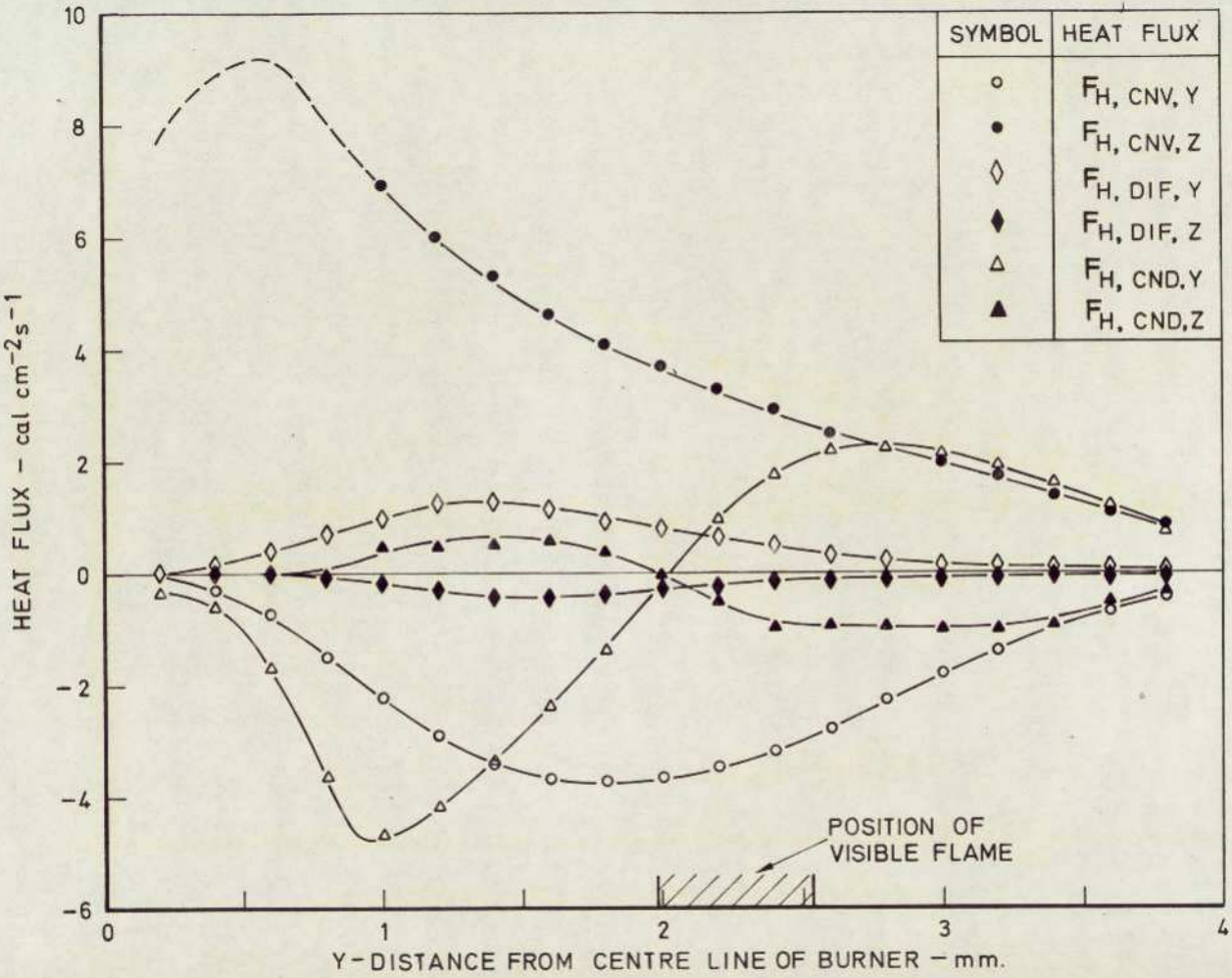



FIG. 42 HEAT FLUXES AT A PLANE 2·0mm ABOVE THE BURNER PORT METHANE FLOW RATE 650 mls $^{-1}$

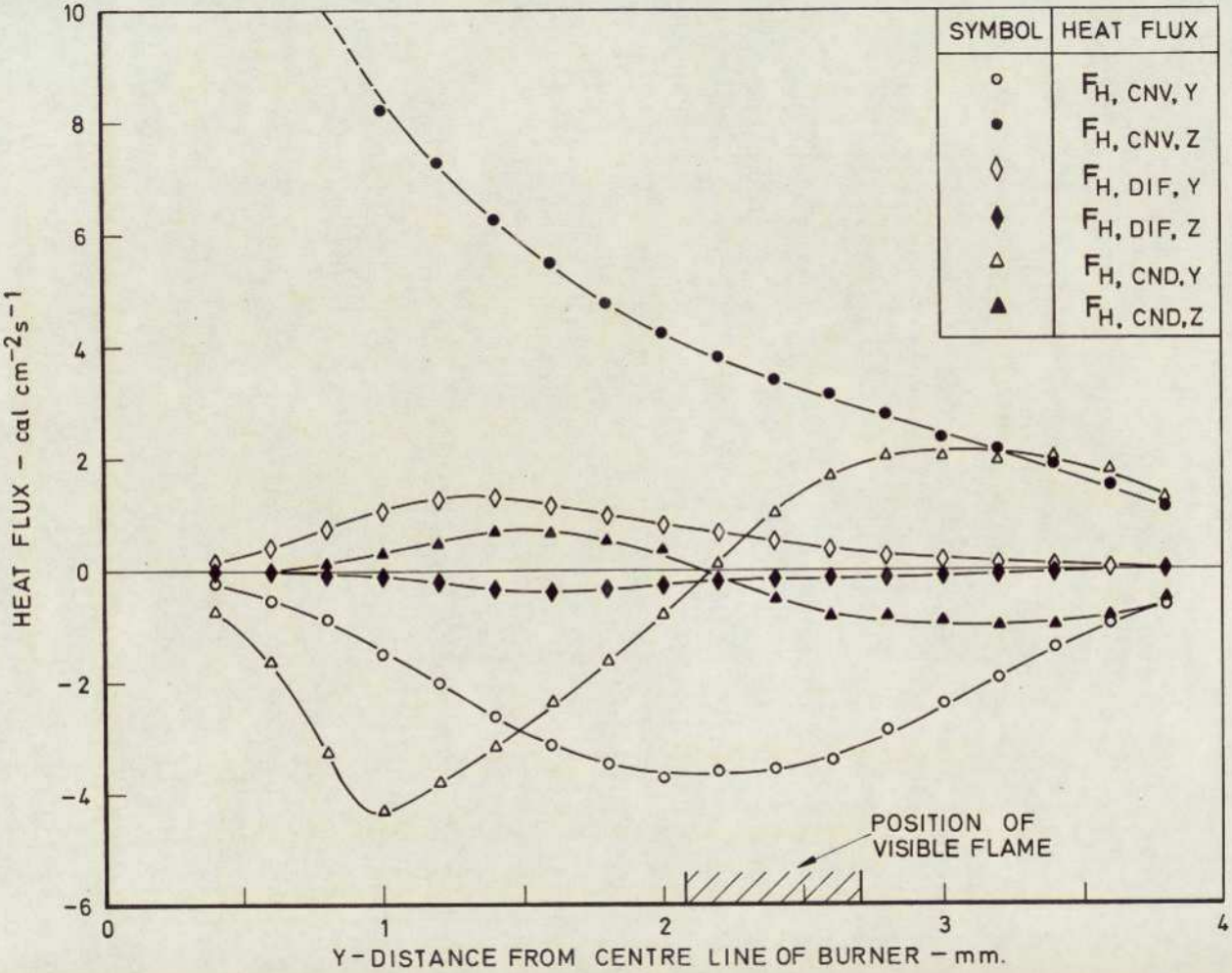



FIG. 43 HEAT FLUXES AT A PLANE 2·5mm ABOVE THE BURNER PORT METHANE FLOW RATE 650 mls $^{-1}$

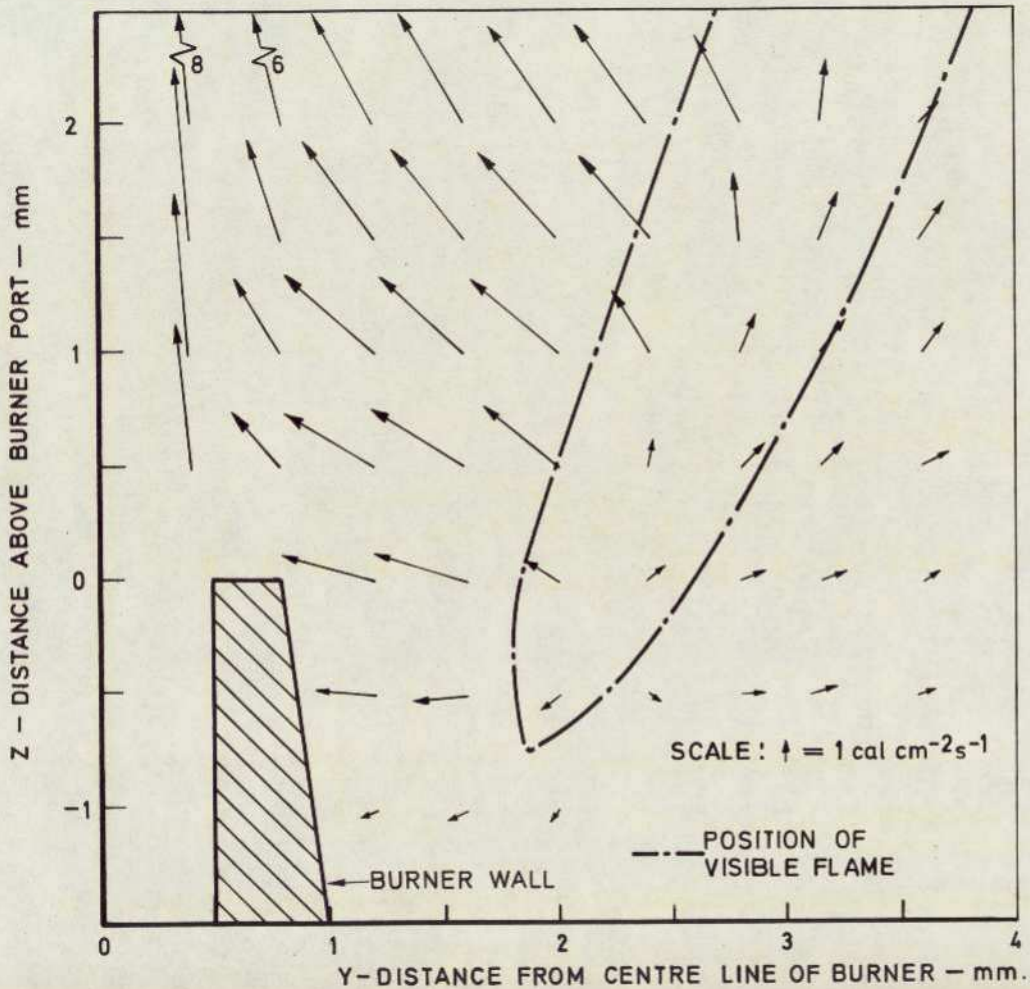



FIG. 44 LOCAL HEAT FLUX VECTORS IN FLAME BURNING 142 mls$^{-1}$

305348/43

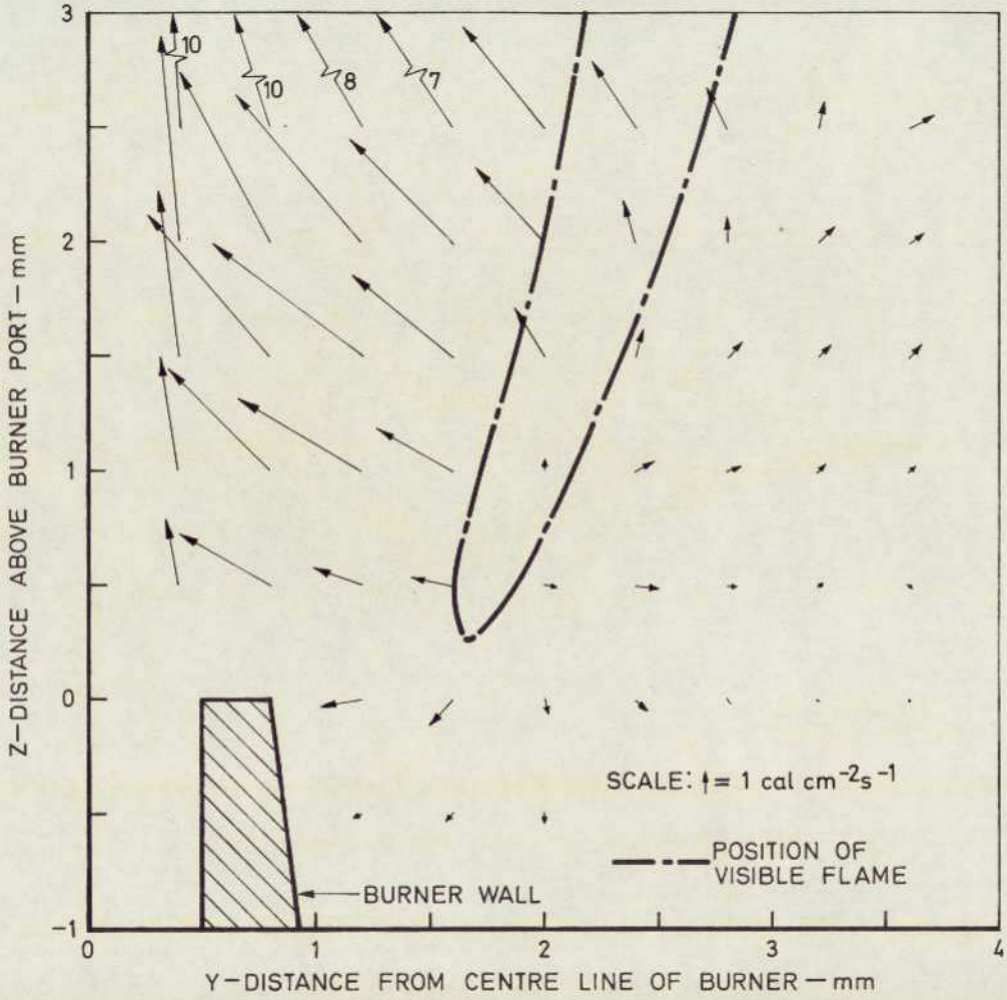



FIG. 45 LOCAL HEAT FLUX VECTORS IN FLAME BURNING 650 mls$^{-1}$

305348/44

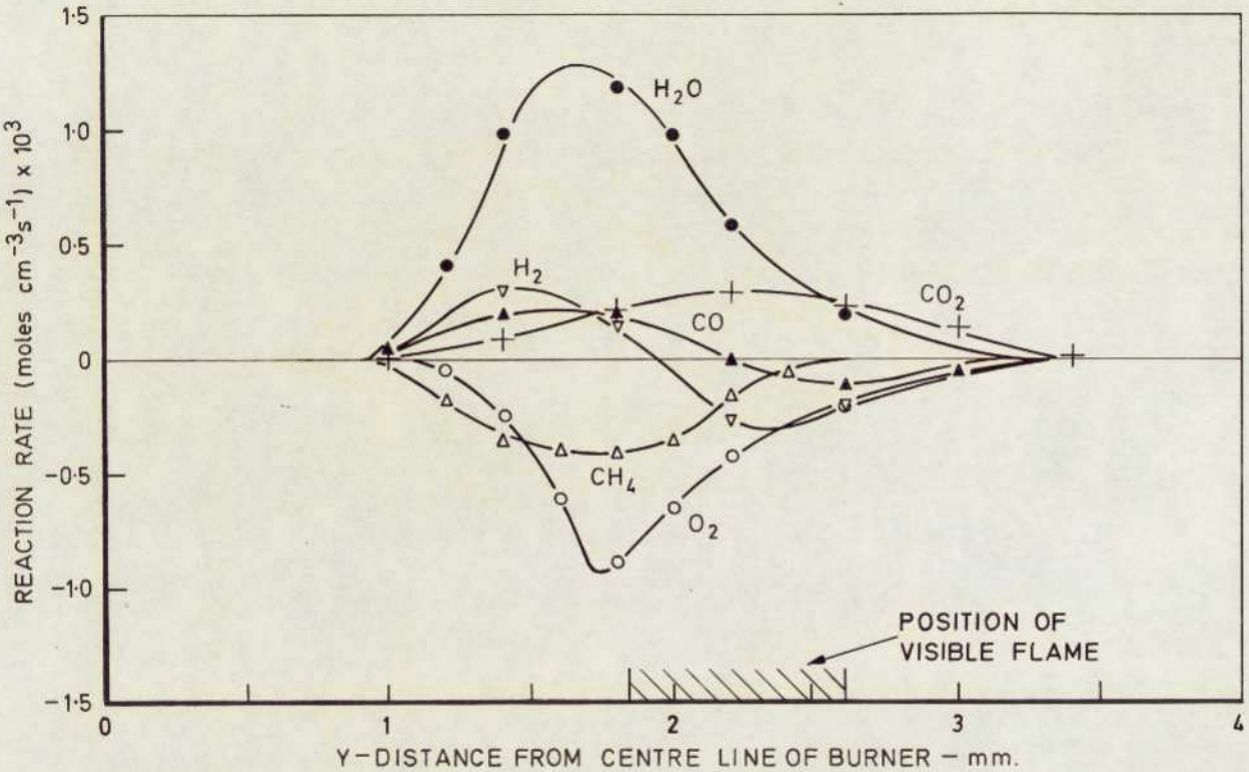



FIG. 46 NET REACTION RATES AT A PLANE 0·0 mm ABOVE THE BURNER PORT

METHANE FLOW RATE 142 mls$^{-1}$

305348/45

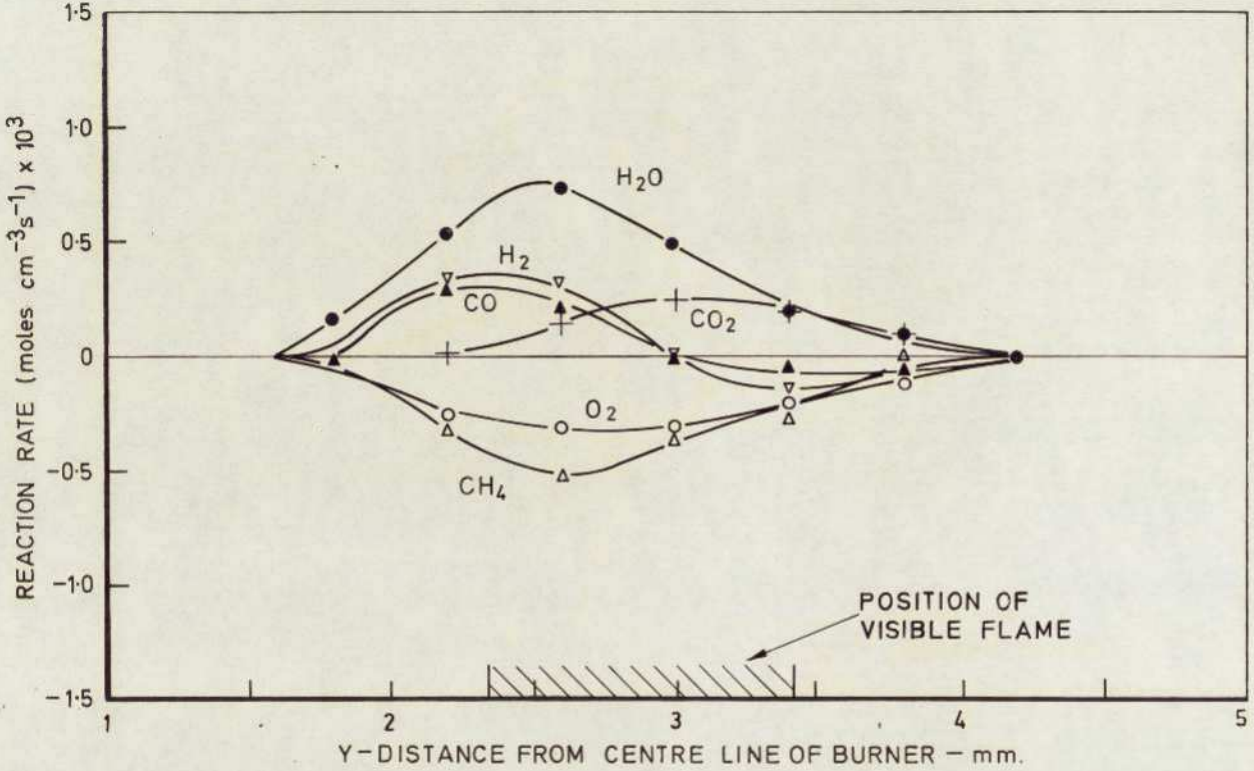



FIG. 47 NET REACTION RATES AT A PLANE 1·5 mm ABOVE THE BURNER PORT

METHANE FLOW RATE 142 mls$^{-1}$

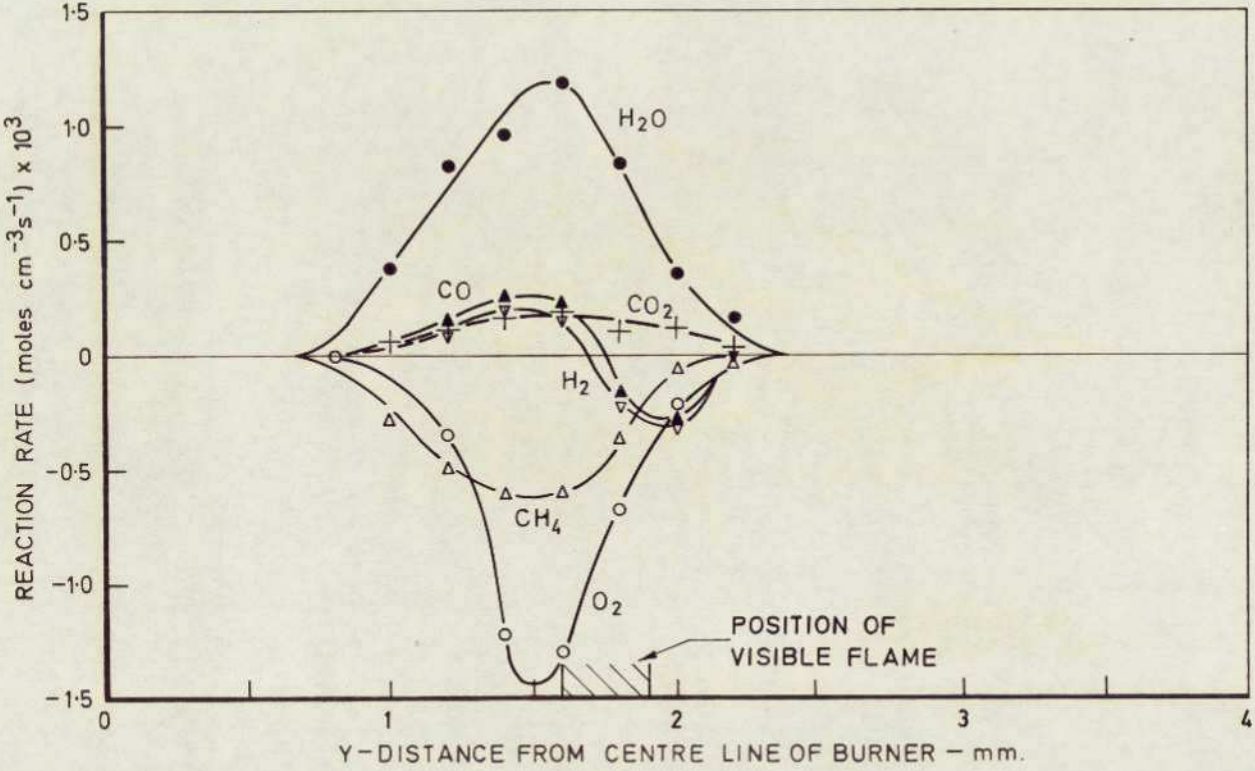



FIG. 48 NET REACTION RATES AT A PLANE 0·5 mm ABOVE THE BURNER PORT

METHANE FLOW RATE 650 mls$^{-1}$

305348/47

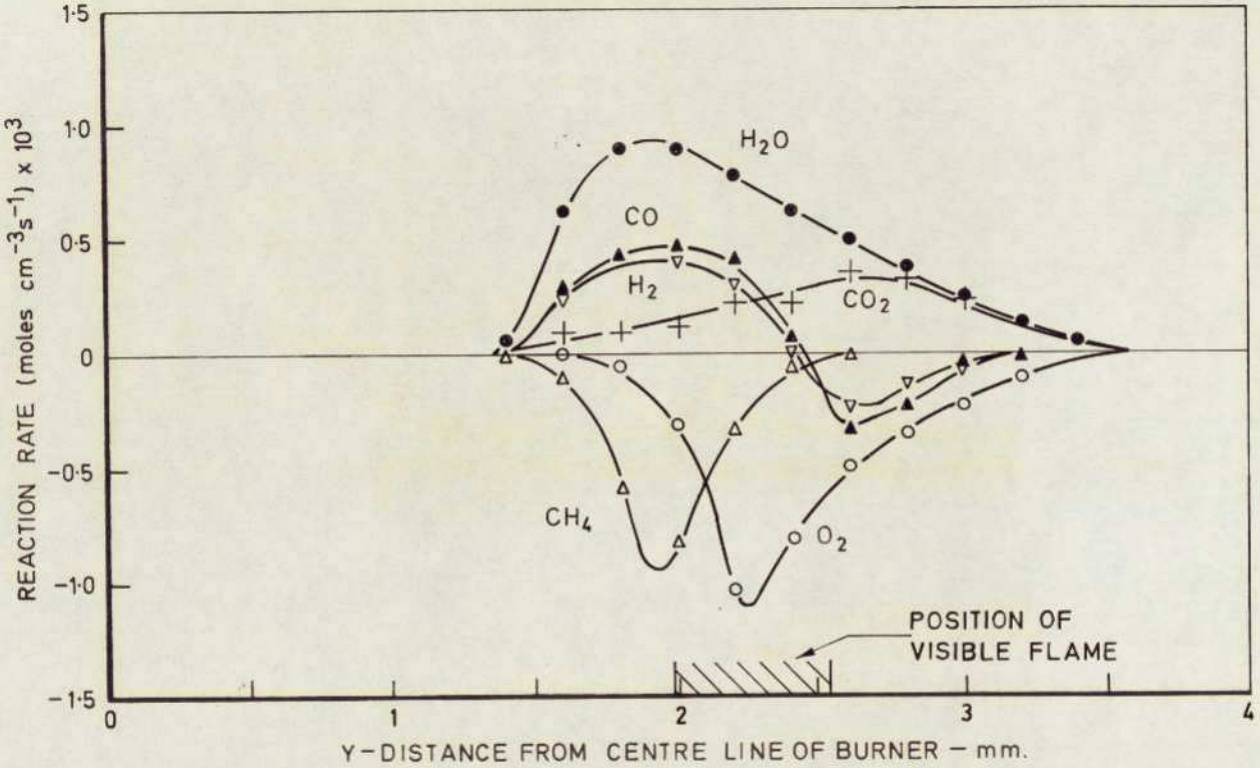



FIG. 49 NET REACTION RATES AT A PLANE 2·0 mm ABOVE THE BURNER PORT

METHANE FLOW RATE 650 mls$^{-1}$

305348/48

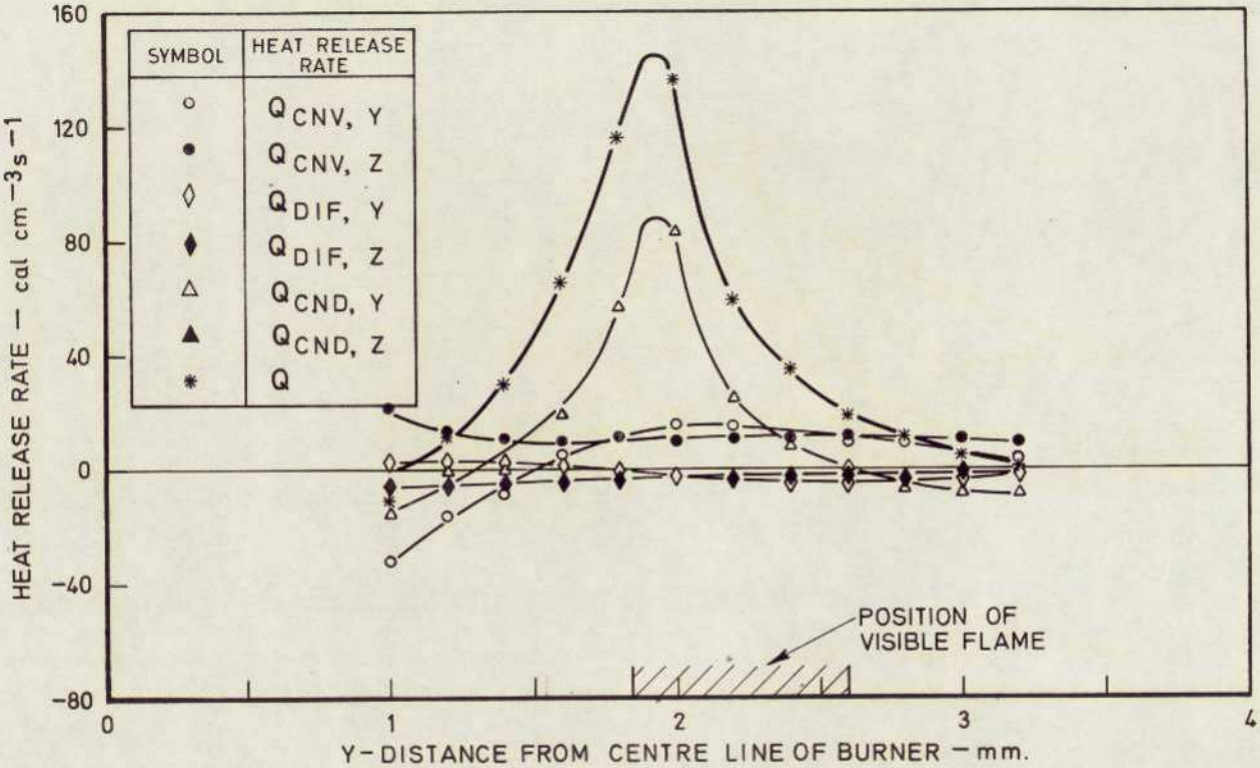



FIG. 50 HEAT RELEASE RATES AT A PLANE 0·0mm ABOVE THE BURNER PORT

METHANE FLOW RATE 142 mls $^{-1}$

305348/49

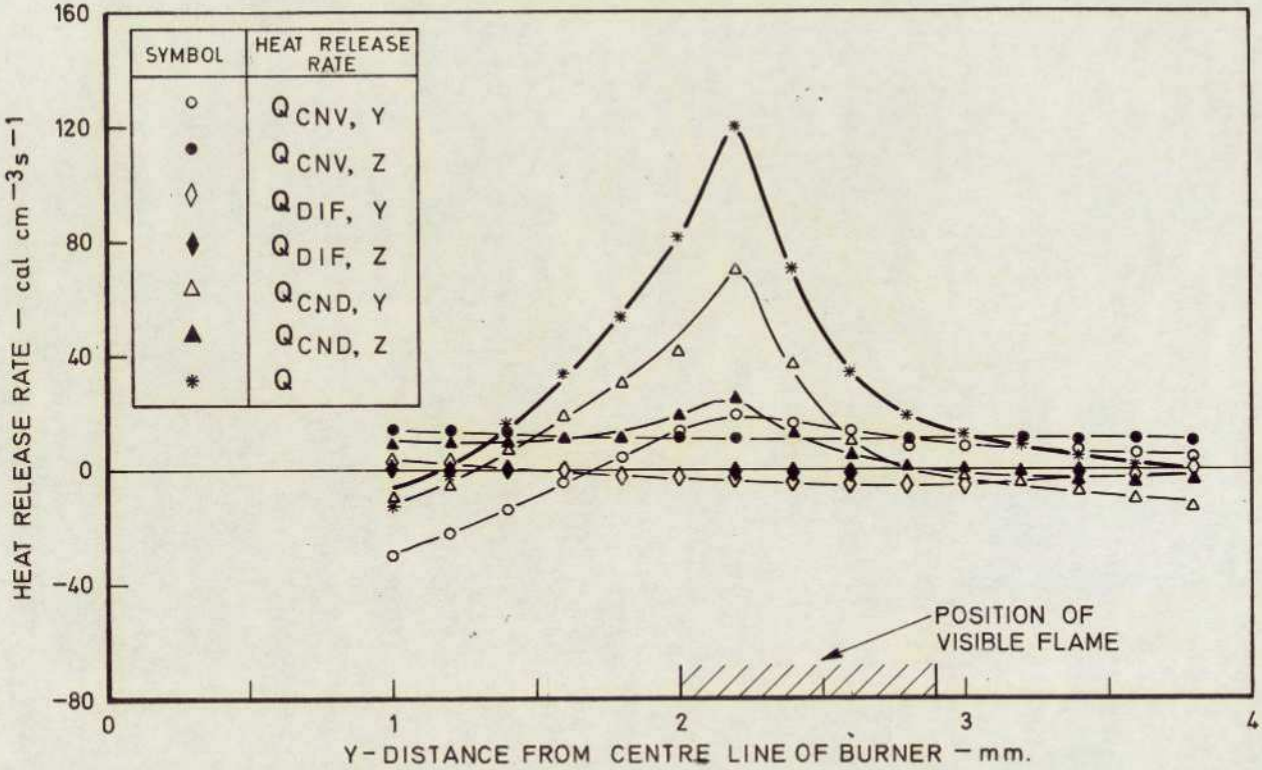



FIG. 51 HEAT RELEASE RATES AT A PLANE 0·5mm ABOVE THE BURNER PORT

METHANE FLOW RATE 142 mls $^{-1}$

305348/50

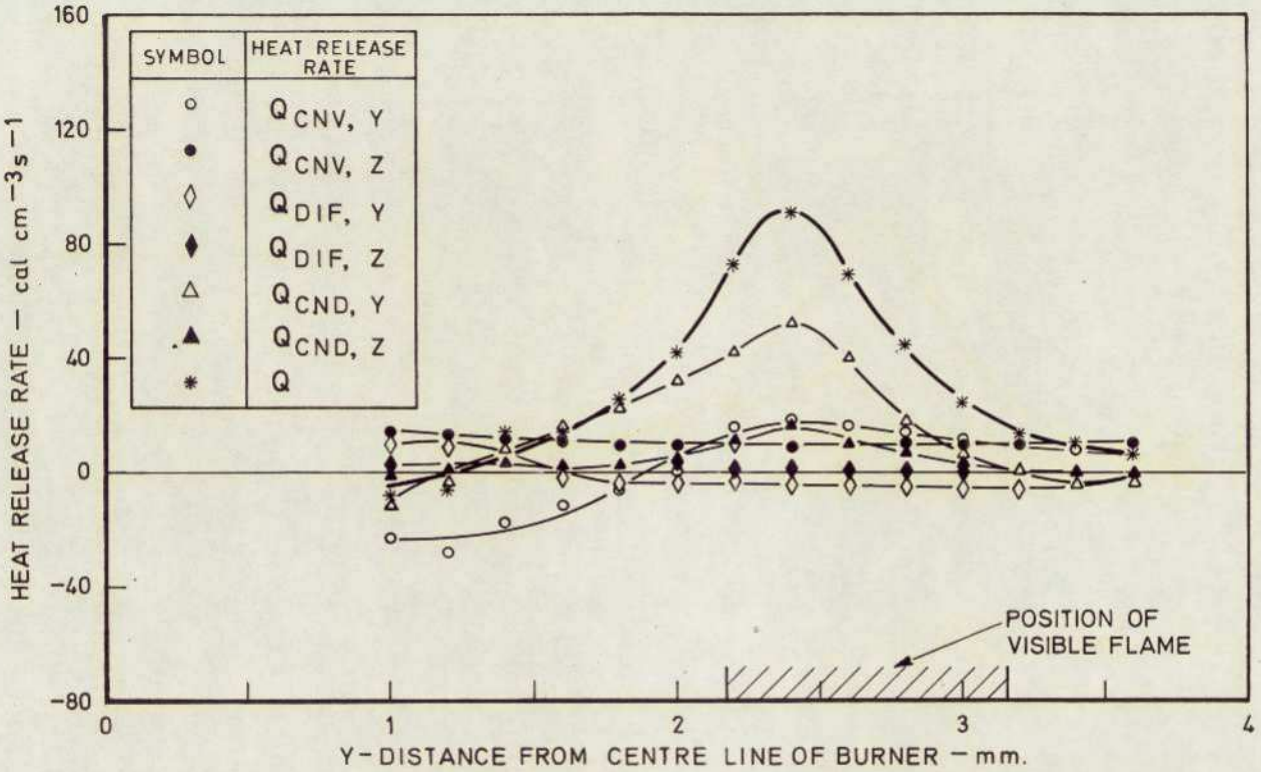



FIG. 52 HEAT RELEASE RATES AT A PLANE 1·0mm ABOVE THE BURNER PORT

. METHANE FLOW RATE 142 mls $^{-1}$

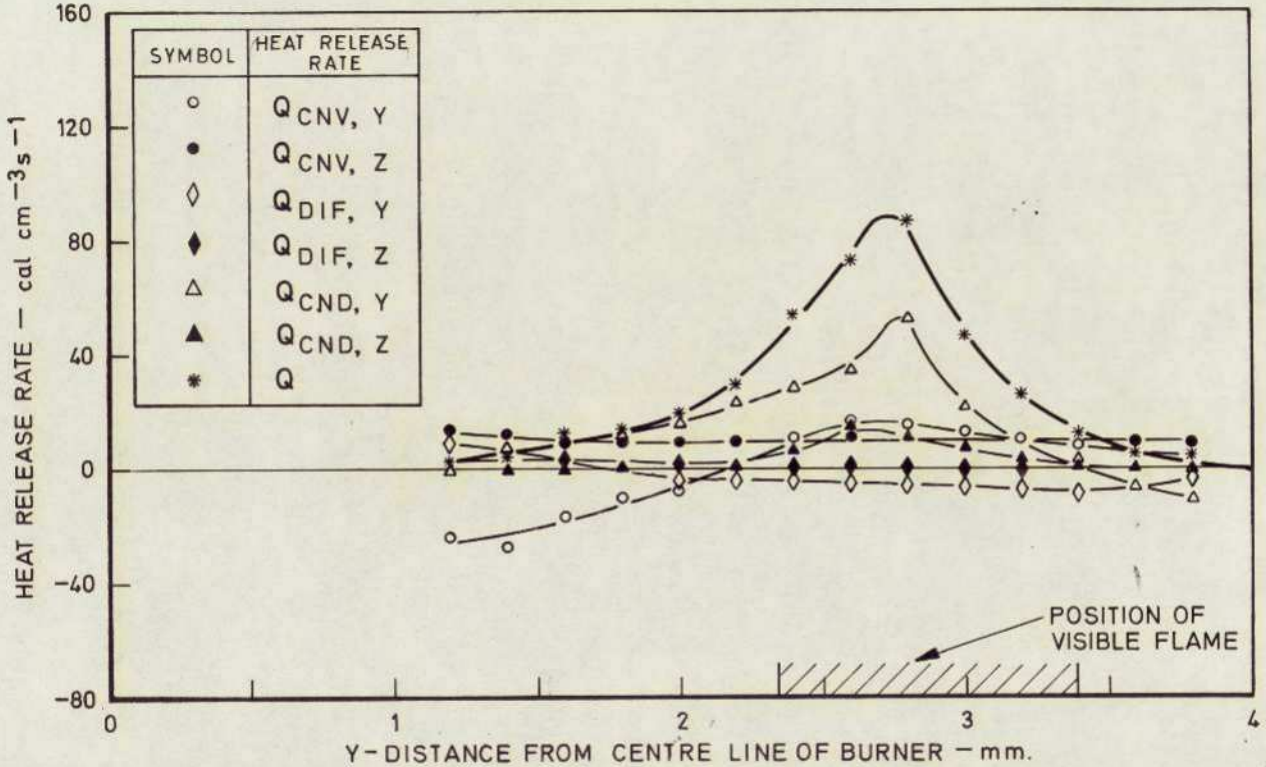



FIG. 53 HEAT RELEASE RATES AT A PLANE 1·5mm ABOVE THE BURNER PORT

METHANE FLOW RATE 142 mls $^{-1}$

305348/52

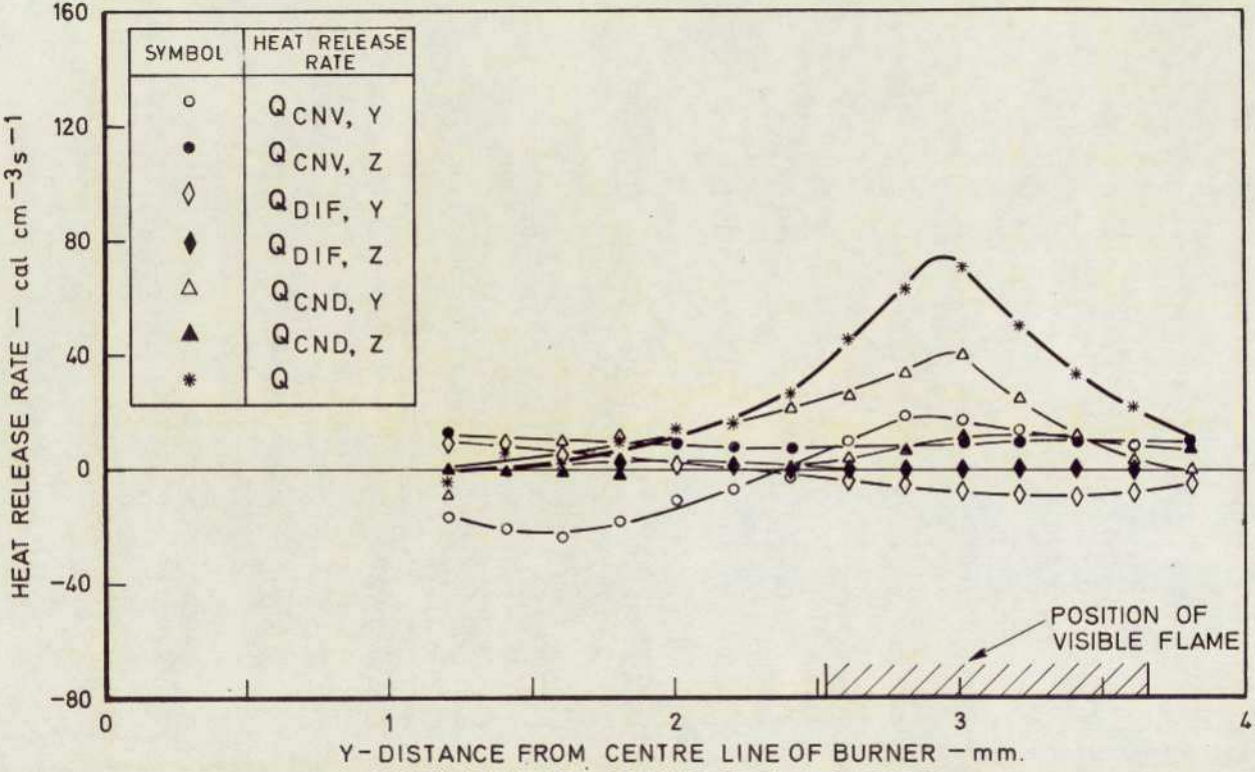



FIG. 54 HEAT RELEASE RATES AT A PLANE 2·0mm ABOVE THE BURNER PORT

METHANE FLOW RATE 142 mls$^{-1}$

3053/48/53

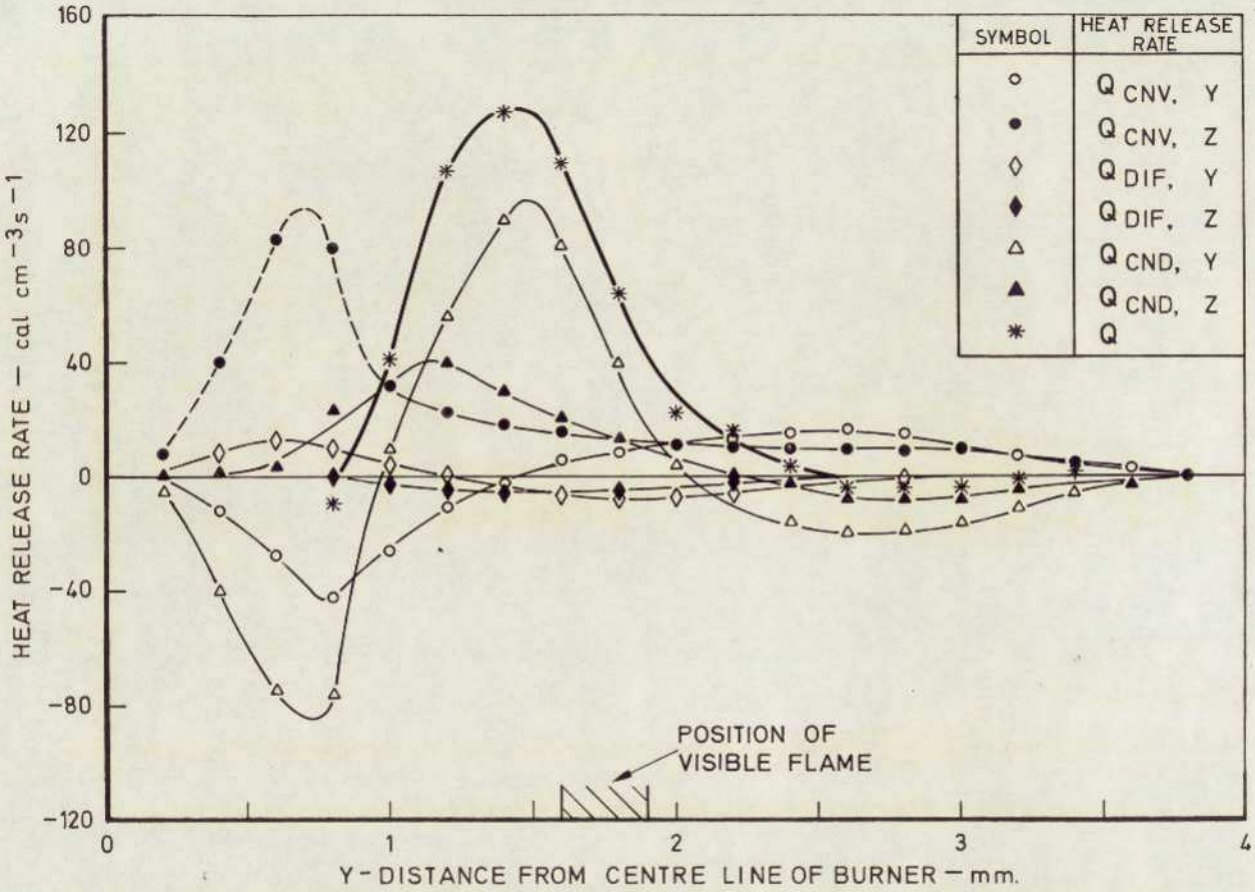



FIG. 55 HEAT RELEASE RATES AT A PLANE 0·5mm ABOVE THE BURNER PORT

METHANE FLOW RATE 650mls $^{-1}$

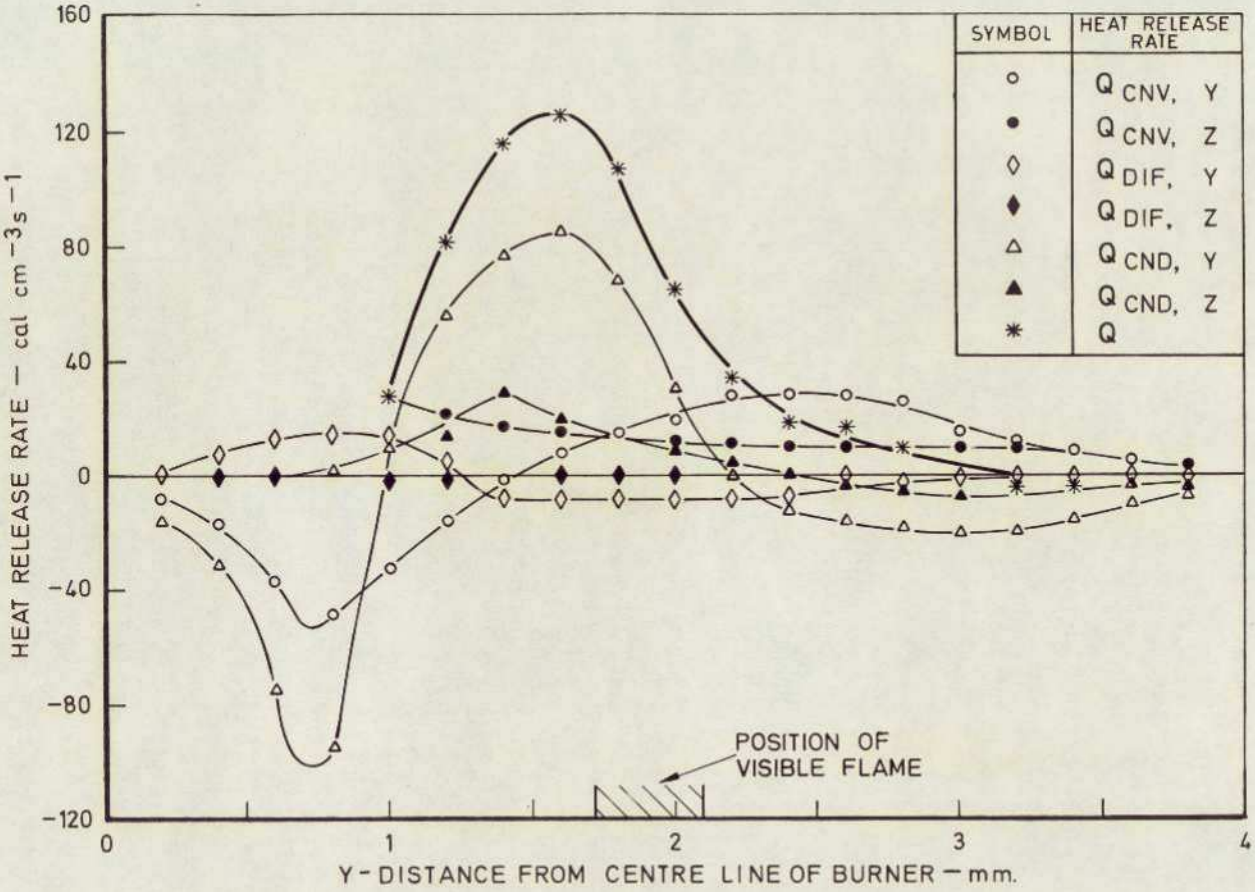



FIG. 56 HEAT RELEASE RATES AT A PLANE 1·0mm ABOVE THE BURNER PORT

METHANE FLOW RATE 650mls $^{-1}$

305348/55

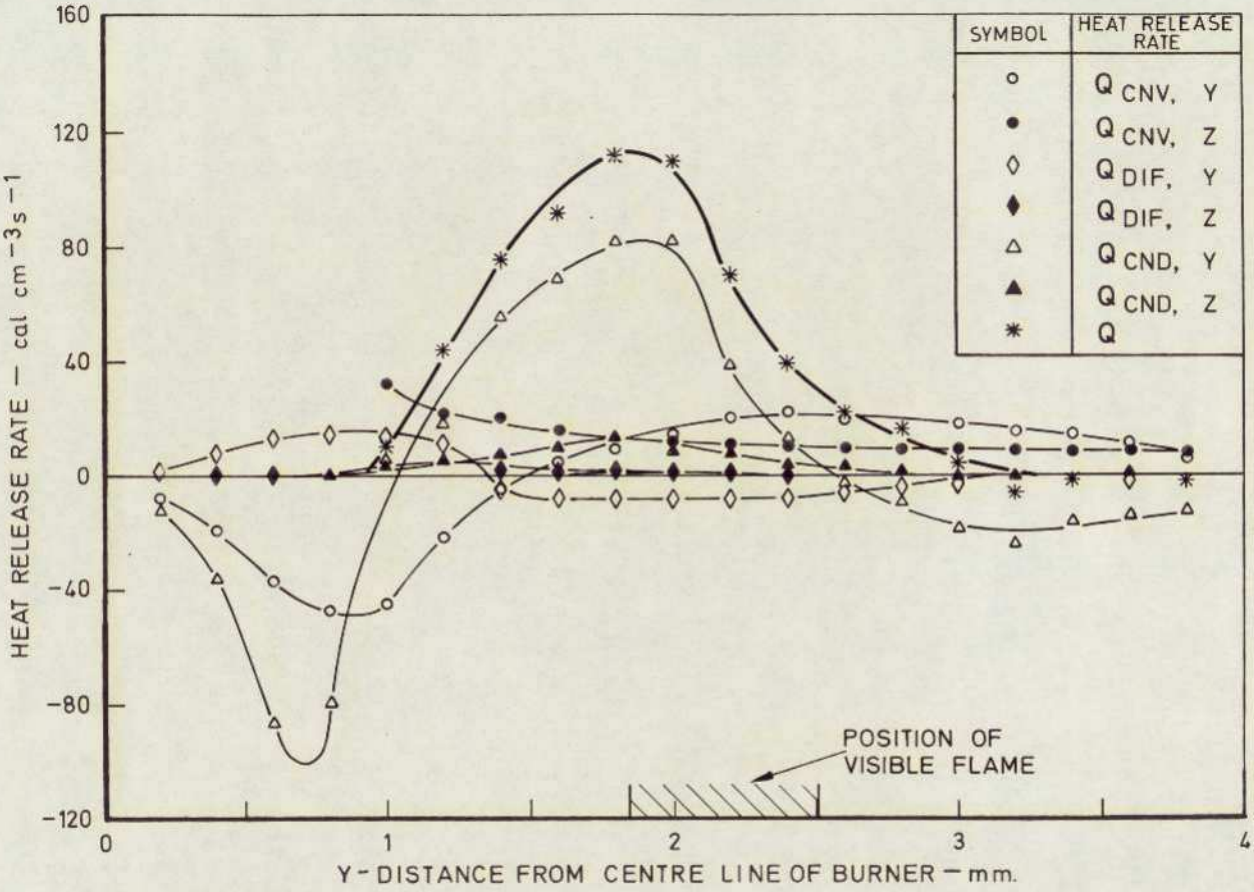



FIG.57 HEAT RELEASE RATES AT A PLANE 1·5mm ABOVE THE BURNER PORT

METHANE FLOW RATE 650 mls $^{-1}$

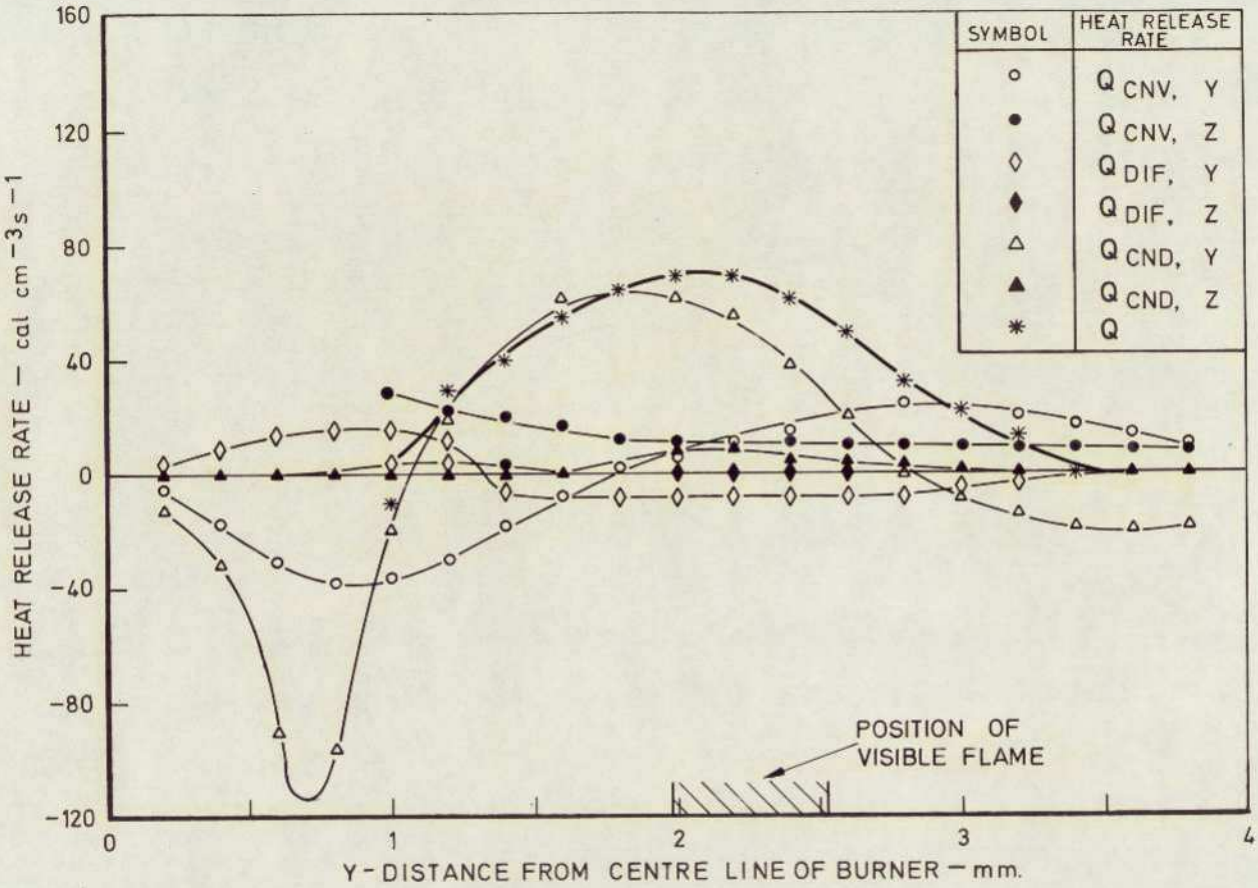



FIG. 58 HEAT RELEASE RATES AT A PLANE 2·0mm ABOVE THE BURNER PORT

METHANE FLOW RATE 650mls $^{-1}$

305348/57

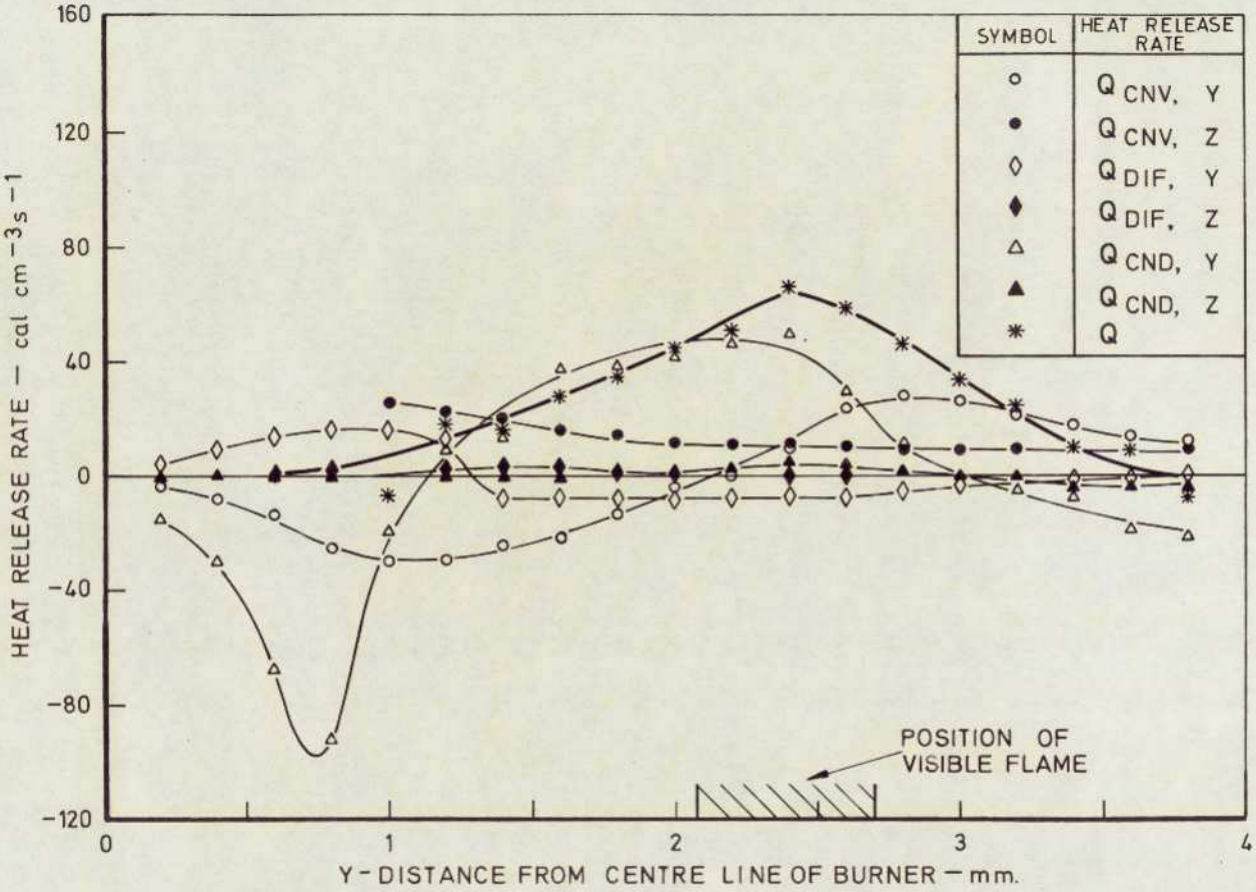



FIG. 59 HEAT RELEASE RATES AT A PLANE 2·5mm ABOVE THE BURNER PORT

METHANE FLOW RATE 650mls $^{-1}$

305348/58

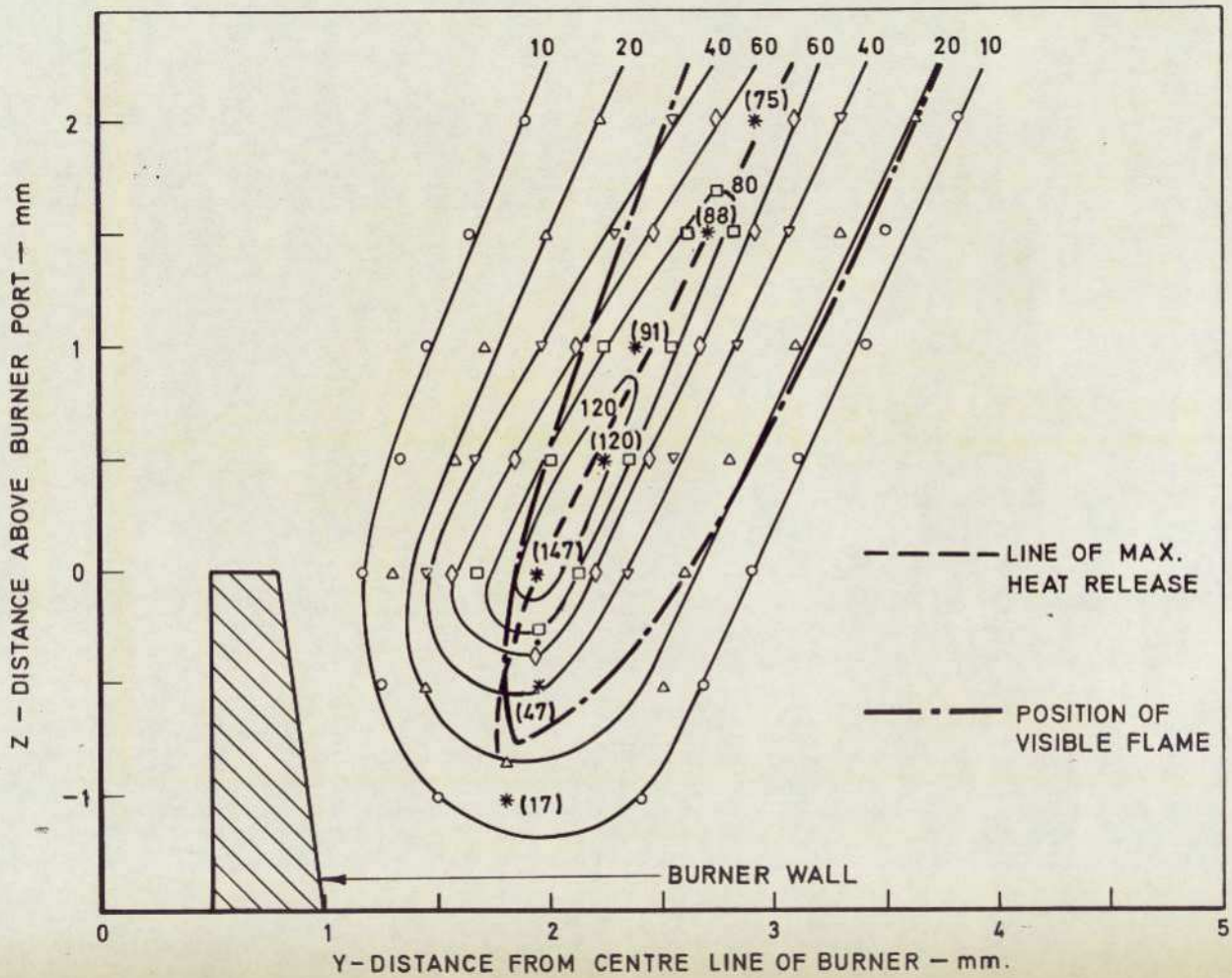



FIG. 60 LINES OF CONSTANT HEAT RELEASE RATE (cal $cm^{-3}s^{-1}$) FOR FLAME BURNING 142 $mls^{-1}$

305348/59a

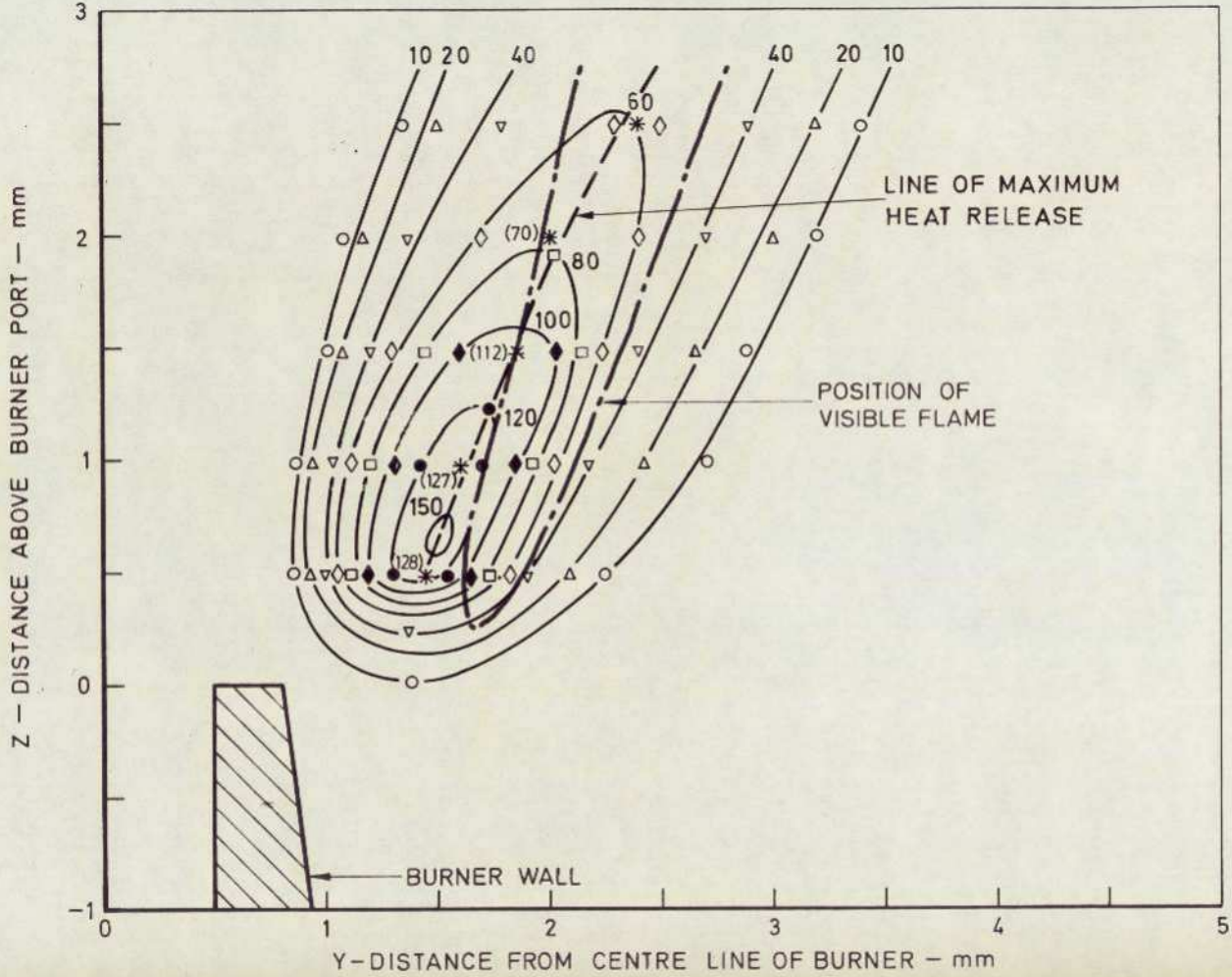



FIG.61 LINES OF CONSTANT HEAT RELEASE RATE (cal $cm^{-3}s^{-1}$) FOR FLAME BURNING 650 $ml s^{-1}$

3053348/60a

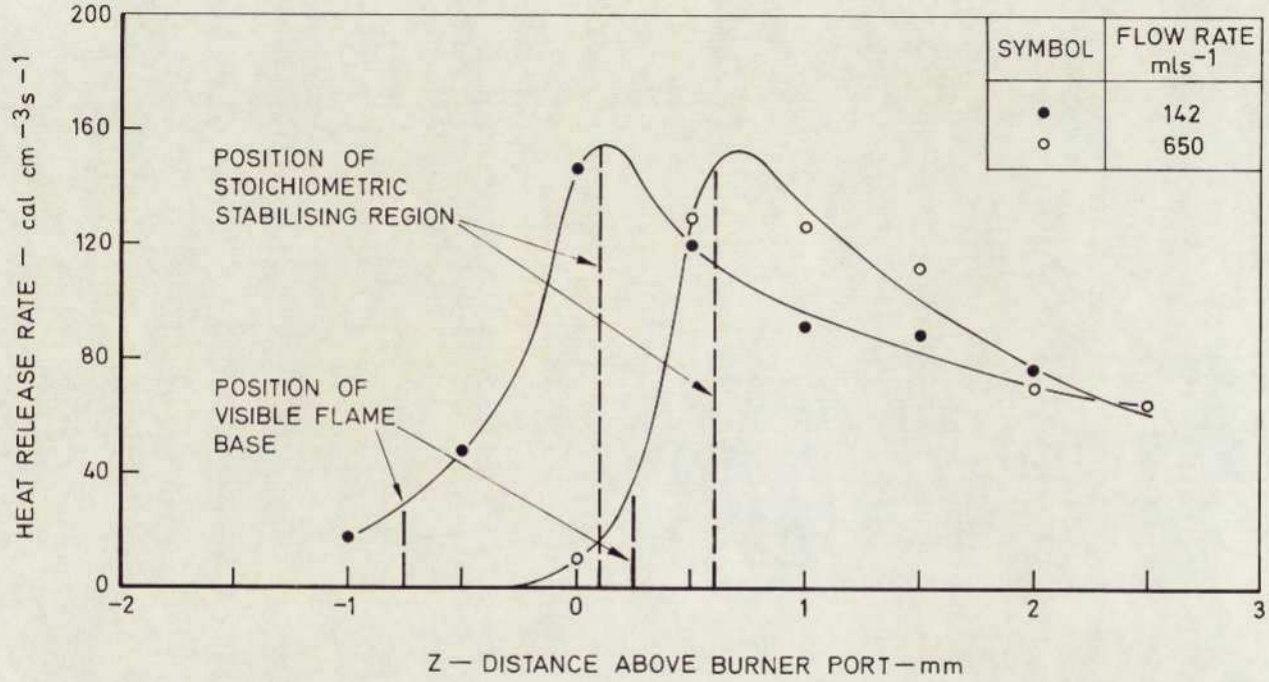
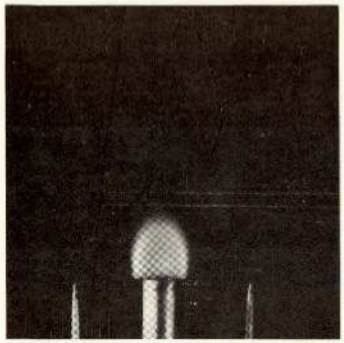
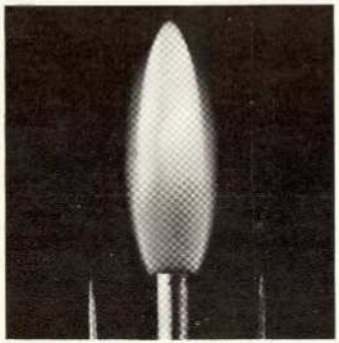



FIG.62 MAXIMUM HEAT RELEASE RATES



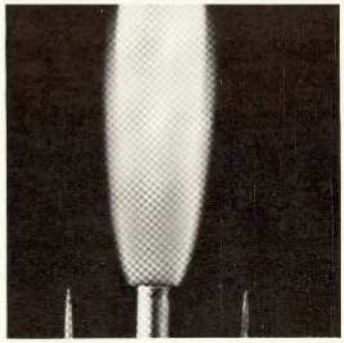
FLOW RATE

$0 \cdot 42\ ms^{-1}$



FLOW RATE

$3 \cdot 72\ ms^{-1}$



FLOW RATE

$7 \cdot 81\ ms^{-1}$

FIG. 63 AXISYMMETRIC METHANE DIFFUSION FLAMES

305348/62

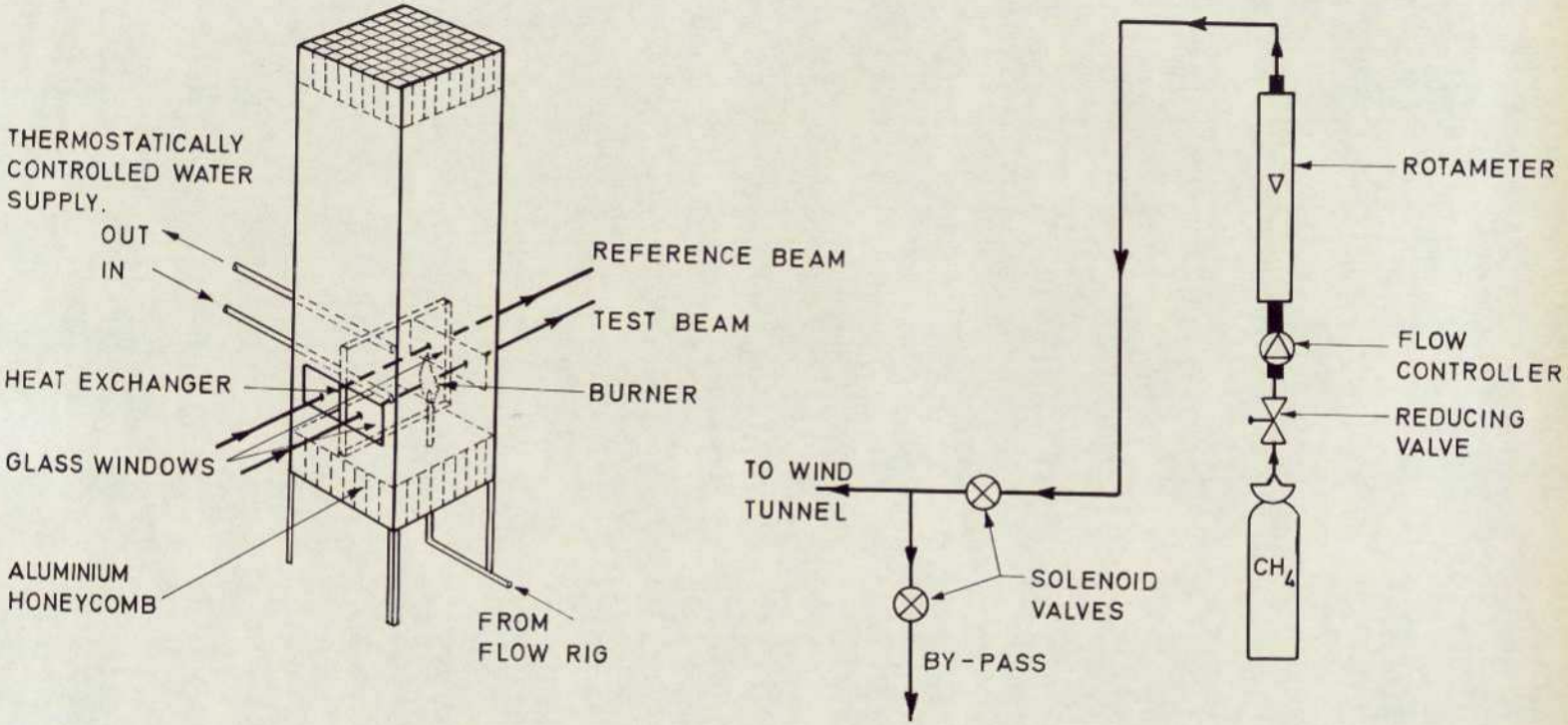



FIG. 64 WIND TUNNEL AND FLOW SYSTEM

305348/63

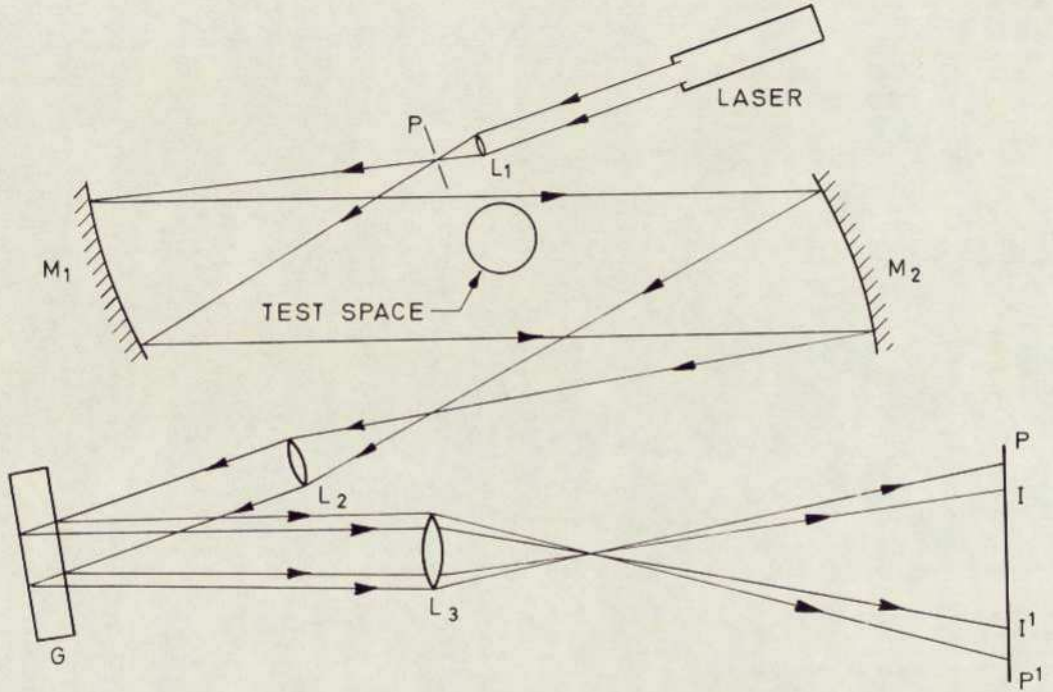



FIG. 65 SINGLE BEAM LASER INTERFEROMETER

305348/64

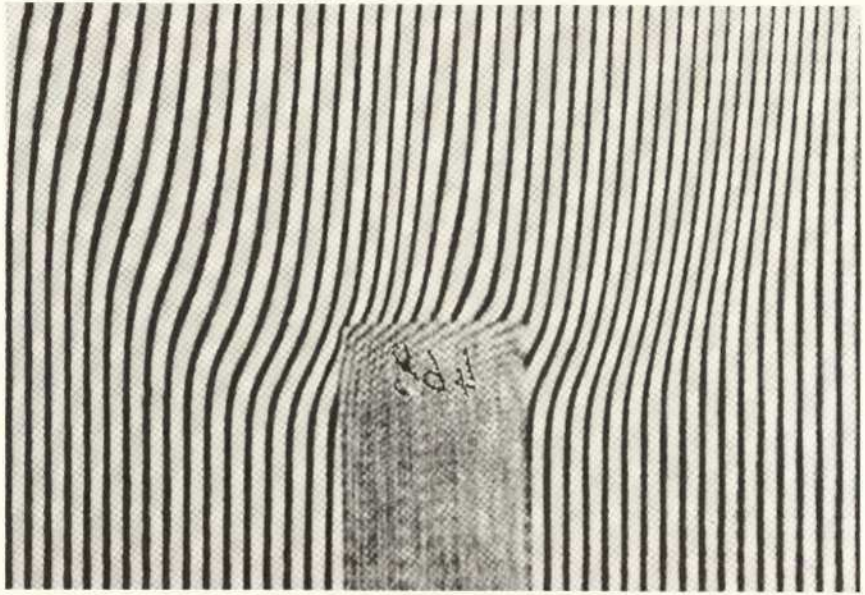


FIG. 66 DIFFUSION FLAME INTERFEROGRAM

METHANE FLOW RATE 7·81 $ml s^{-1}$

305348/65

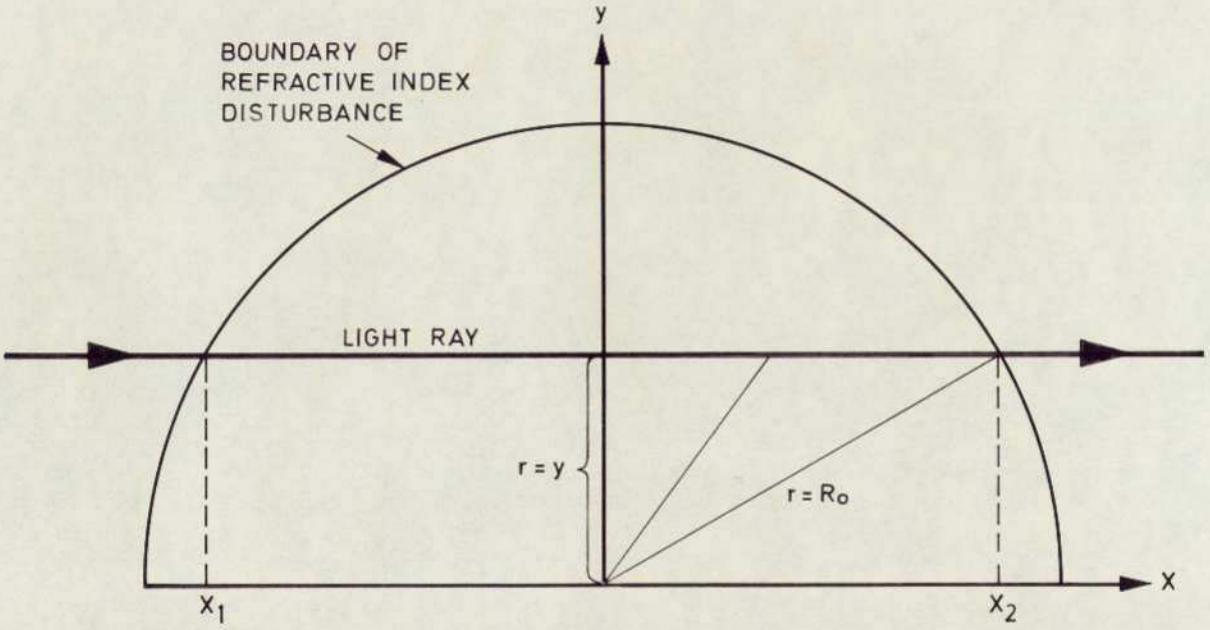



FIG. 67 AXISYMMETRIC REFRACTIVE INDEX DISTURBANCE TRAVERSED BY A LIGHT BEAM

305348/66

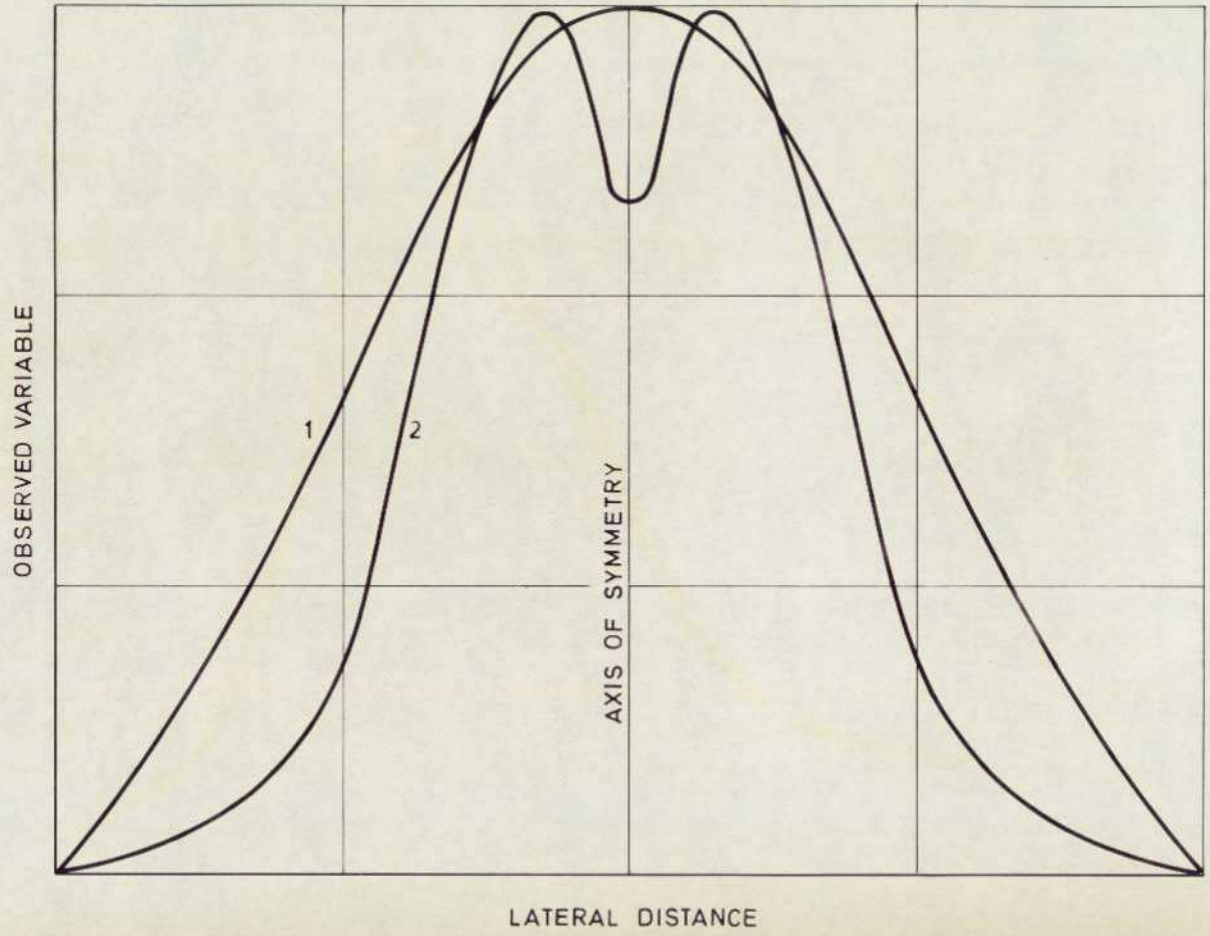



FIG. 68 TYPICAL OBSERVED LATERAL PROFILES

305348/67

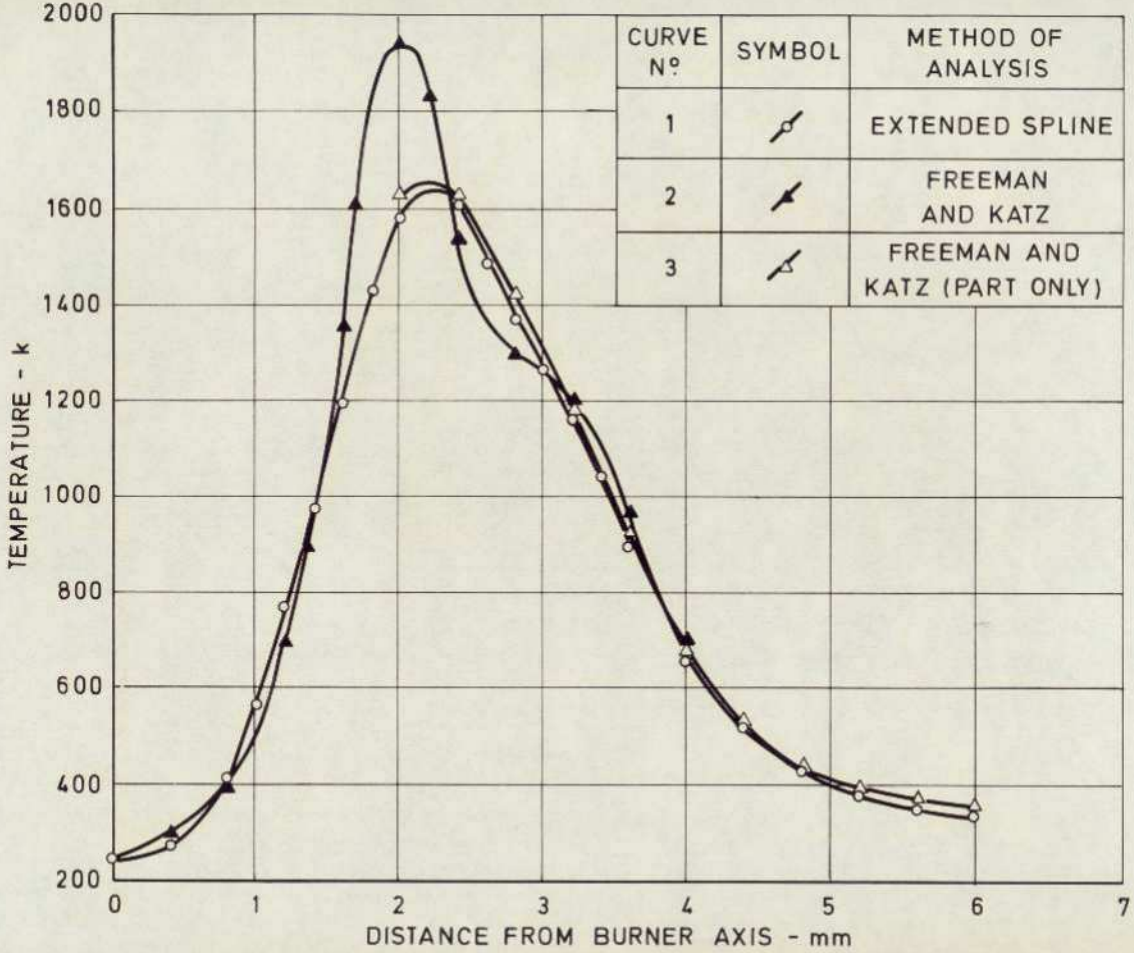



FIG. 69 RADIAL TEMPERATURE DISTRIBUTIONS.
COMPARISON BETWEEN THE EXTENDED SPLINE APPROACH
(CURVE 1), AND THE FREEMAN AND KATZ APPROACH (CURVES 2 AND 3)

305348/68

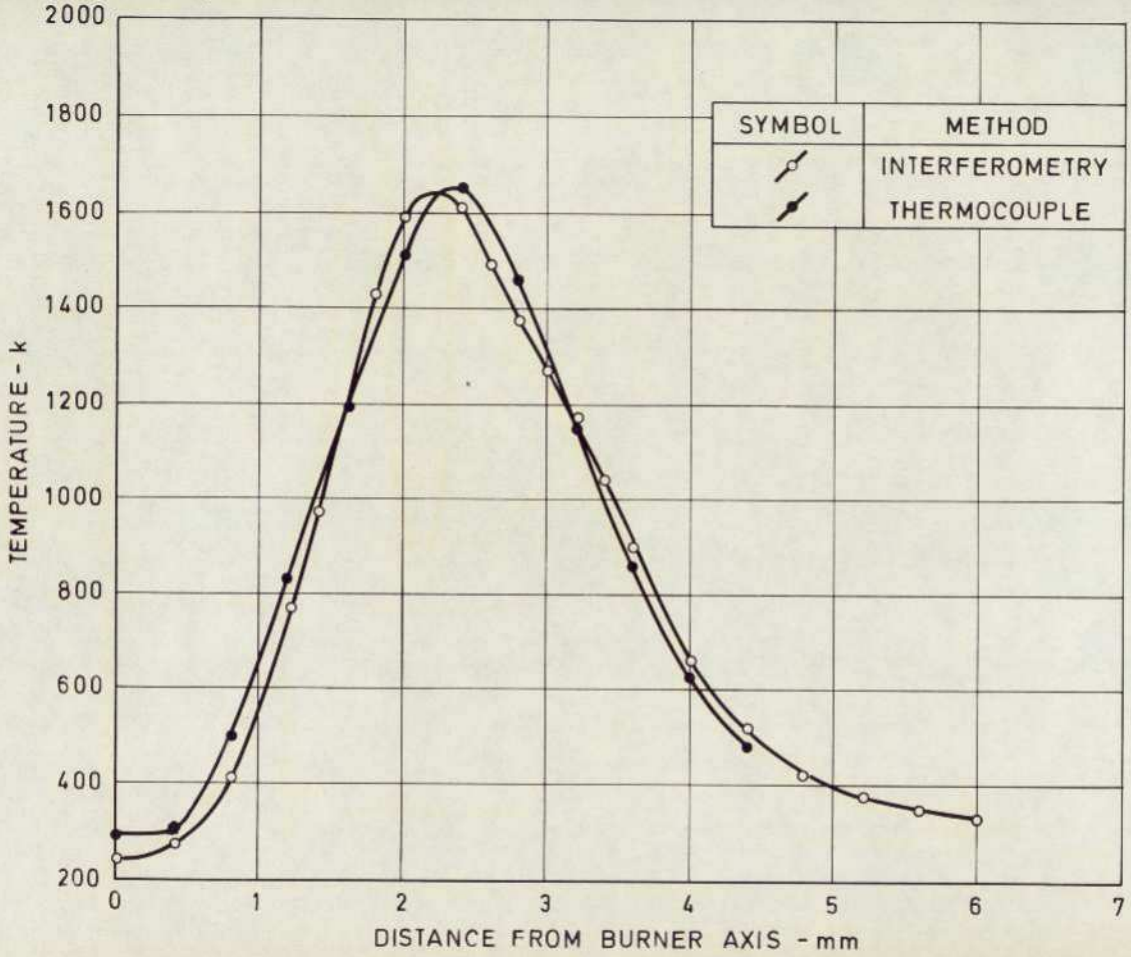



FIG. 70 RADIAL TEMPERATURE DISTRIBUTIONS.
COMPARISON BETWEEN THE EXTENDED SPLINE APPROACH
AND A THERMOCOUPLE PROBE METHOD.

305348/69

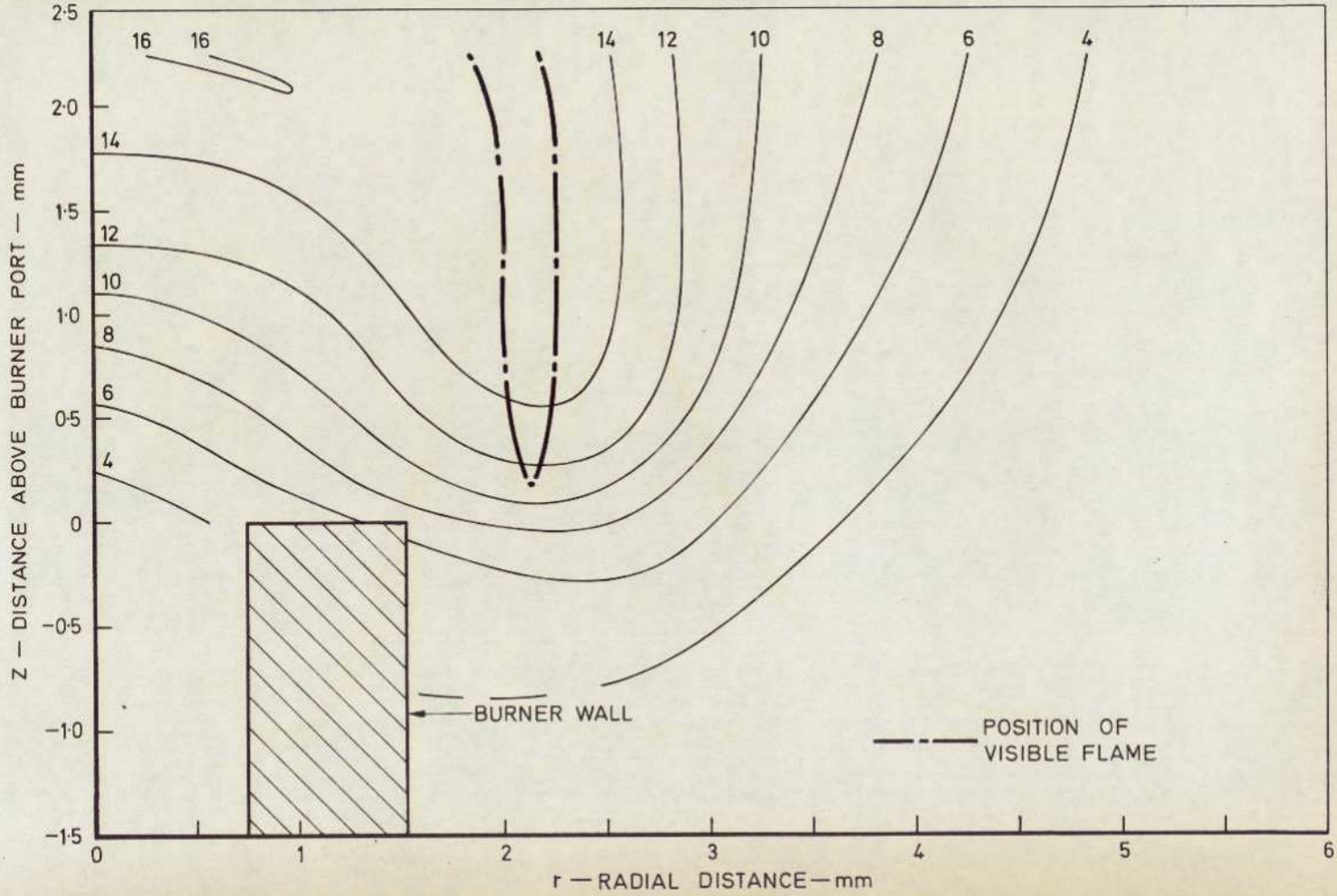



FIG. 71 ISOTHERMALS (°k) x $10^{-2}$ FOR FLAME BURNING 0·42 mls$^{-1}$

305348/70

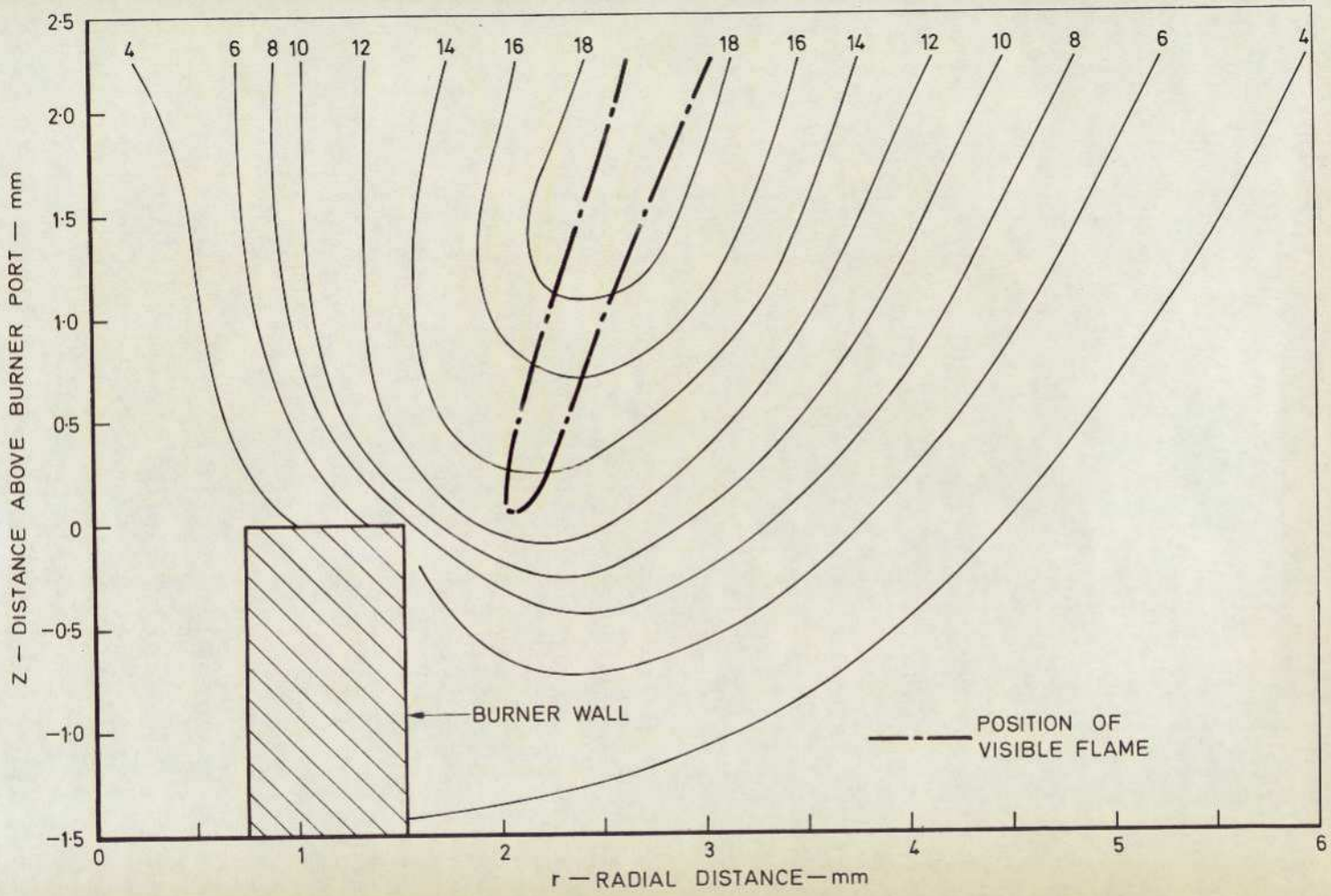



FIG. 72 ISOTHERMALS (°k) x $10^{-2}$ FOR FLAME BURNING 3·72 mls$^{-1}$

305348/71

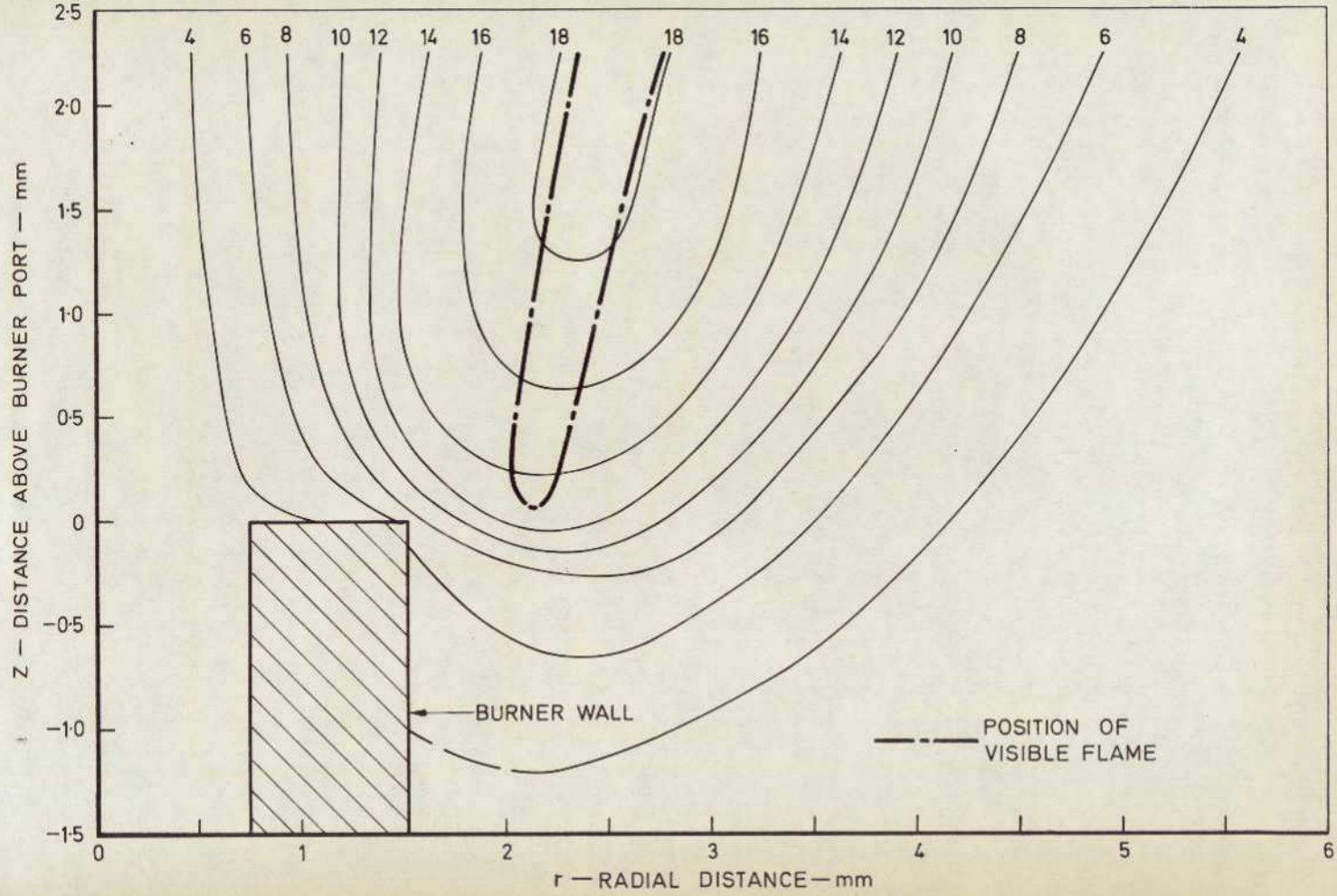



FIG. 73 ISOTHERMALS (°k) x $10^{-2}$ FOR FLAME BURNING 7·81 mls$^{-1}$

305348/72

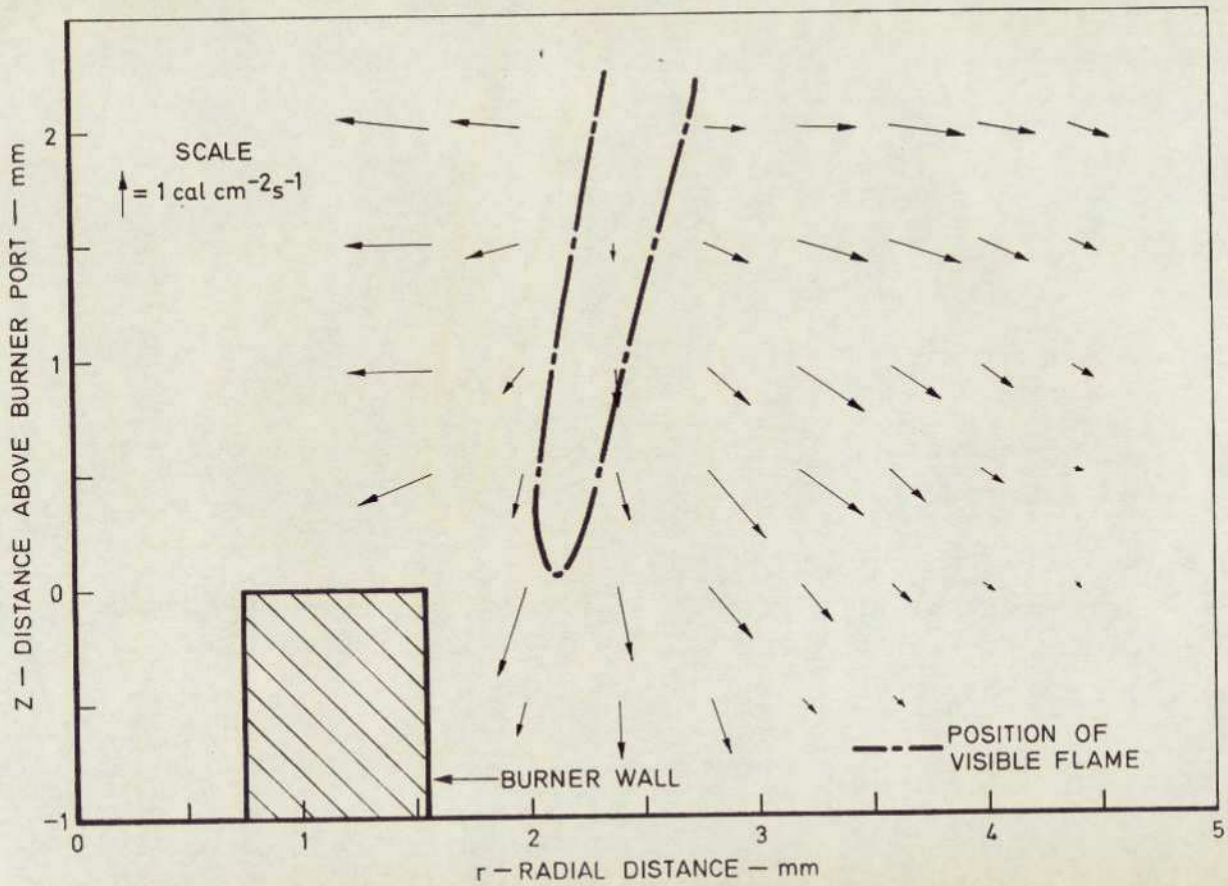



FIG. 74 LOCAL CONDUCTIVE HEAT FLUX VECTORS IN FLAME BURNING 7·81 mls$^{-1}$

305348/73

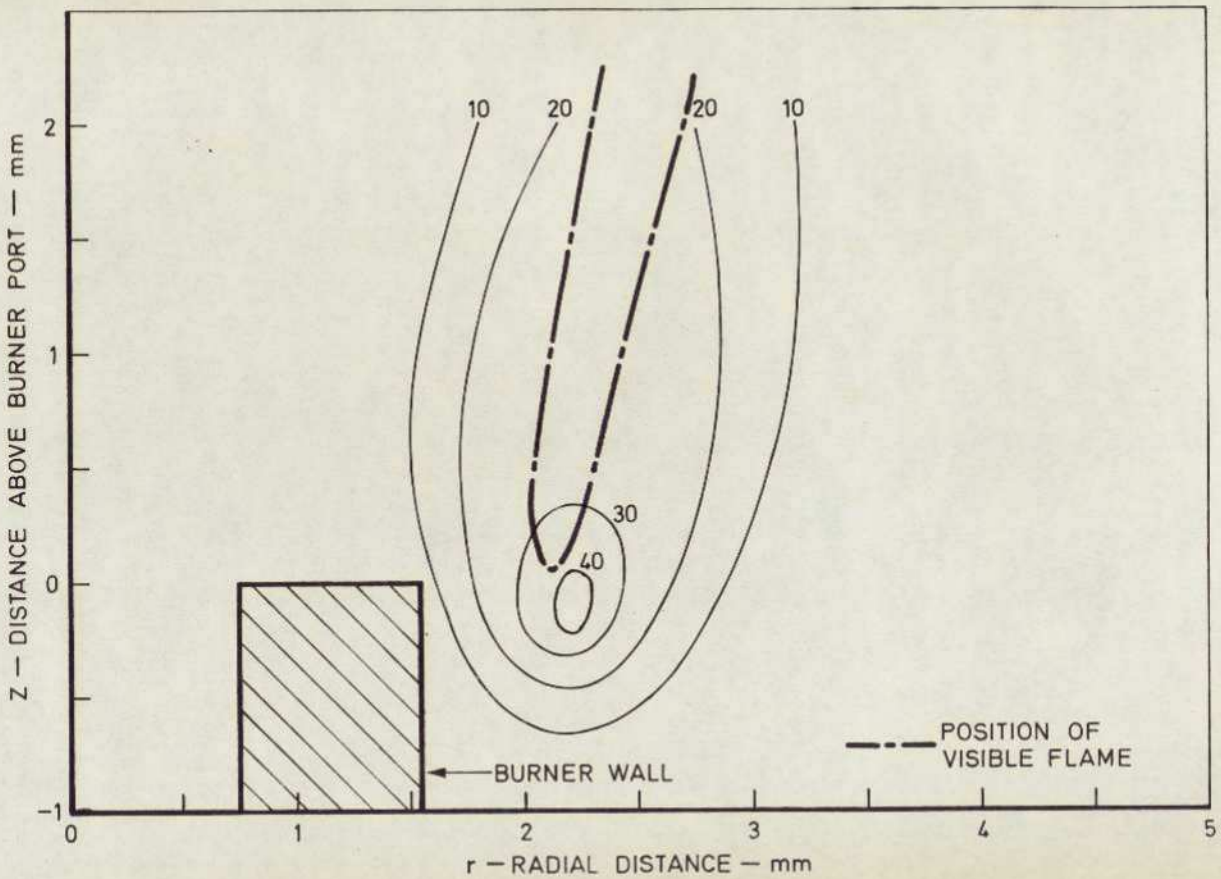



FIG. 75 LINES OF CONSTANT HEAT RELEASE (cal $cm^{-3}s^{-1}$) FOR FLAME BURNING 7·81 $mls^{-1}$

305348/74